Etude numérique et expérimentale de l'enrobage en voie sèche dans un mélangeur à fort taux de cisaillement

Akira Sato

NNT : 2012 EMSE 0658

THÈSE

présentée par

Akira SATO

Pour

obtenir le grade de
Docteur de l'École Nationale Supérieure des Mines de Saint-Étienne

Spécialité : Génie des Procédés

Etude numérique et expérimentale de l'enrobage en voie sèche dans un mélangeur à fort taux de cisaillement

soutenue à Saint-Etienne, le 14 Septembre 2012

Membres du jury

Président :	Pierre TCHORELOFF	Professeur, Université Paris-Sud, Châtenay-Malabry
Rapporteurs :	Mojtaba GHADIRI	Professeur, University of Leeds, Leeds
	Fumio SAITO	Professeur, Tohoku University, Sendai
Examinateurs :	Philippe GROSSEAU	Directeur de recherche, ENSMSE, Saint-Etienne
	Laurence GALET	Maître-assistant, EMAC, Albi
	Eric SERRIS	Ingénieur de recherche, ENSMSE, Saint-Etienne
Directeurs de thèse :	Gérard THOMAS	Professeur, ENSMSE, Saint-Etienne
	Michel BARON	Professeur, EMAC, Albi
Invité éventuel:	Alain CHAMAYOU	Maître-assistant, EMAC, Albi

Spécialités doctorales :

SCIENCES ET GENIE DES MATERIAUX
MECANIQUE ET INGENIERIE
GENIE DES PROCEDES
SCIENCES DE LA TERRE
SCIENCES ET GENIE DE L'ENVIRONNEMENT
MATHEMATIQUES APPLIQUEES
INFORMATIQUE
IMAGE, VISION, SIGNAL
GENIE INDUSTRIEL
MICROELECTRONIQUE

Responsables :

J. DRIVER Directeur de recherche – Centre SMS

F. GRUY Professeur – Centre SPIN
B. GUY Maître de recherche – Centre SPIN
J. BOURGOIS Professeur – Fayol
E. TOUBOUL Ingénieur – Fayol
O. BOISSIER Professeur – Fayol
JC. PINOLI Professeur – Centre CIS
P. BURLAT Professeur – Fayol
Ph. COLLOT Professeur – Centre CMP

Enseignants-chercheurs et chercheurs autorisés à diriger des thèses de doctorat (titulaires d'un doctorat d'État ou d'une HDR)

AVRIL	Stéphane	MA	Mécanique & Ingénierie	CIS
BATTON-HUBERT	Mireille	MA	Sciences & Génie de l'Environnement	Fayol
BENABEN	Patrick	PR 1	Sciences & Génie des Matériaux	CMP
BERNACHE-ASSOLLANT	Didier	PR 0	Génie des Procédés	CIS
BIGOT	Jean-Pierre	MR	Génie des Procédés	SPIN
BILAL	Essaïd	DR	Sciences de la Terre	SPIN
BOISSIER	Olivier	PR 1	Informatique	Fayol
BORBELY	Andras	MR	Sciences et Génie des Matériaux	SMS
BOUCHER	Xavier	MA	Génie Industriel	Fayol
BOUDAREL	Marie-Reine	PR 2	Génie Industriel	DF
BOURGOIS	Jacques	PR 0	Sciences & Génie de l'Environnement	Fayol
BRODHAG	Christian	DR	Sciences & Génie de l'Environnement	Fayol
BURLAT	Patrick	PR 2	Génie industriel	Fayol
COLLOT	Philippe	PR 1	Microélectronique	CMP
COURNIL	Michel	PR 0	Génie des Procédés	SPIN
DAUZERE-PERES	Stéphane	PR 1	Génie industriel	CMP
DARRIEULAT	Michel	IGM	Sciences & Génie des Matériaux	SMS
DECHOMETS	Roland	PR 1	Sciences & Génie de l'Environnement	Fayol
DESRAYAUD	Christophe	MA	Mécanique & Ingénierie	SMS
DELAFOSSE	David	PR 1	Sciences & Génie des Matériaux	SMS
DOLGUI	Alexandre	PR 1	Génie Industriel	Fayol
DRAPIER	Sylvain	PR 2	Mécanique & Ingénierie	SMS
DRIVER	Julian	DR 0	Sciences & Génie des Matériaux	SMS
FEILLET	Dominique	PR 2	Génie Industriel	CMP
FOREST	Bernard	PR 1	Sciences & Génie des Matériaux	CIS
FORMISYN	Pascal	PR 1	Sciences & Génie de l'Environnement	Fayol
FRACZKIEWICZ	Anna	DR	Sciences & Génie des Matériaux	SMS
GARCIA	Daniel	MR	Sciences de la terre	SPIN
GIRARDOT	Jean-Jacques	MR	Informatique	Fayol
GOEURIOT	Dominique	MR	Sciences & Génie des Matériaux	SMS
GRAILLOT	Didier	DR	Sciences & Génie de l'Environnement	Fayol
GROSSEAU	Philippe	MR	Génie des Procédés	SPIN
GRUY	Frédéric	MR	Génie des Procédés	SPIN
GUY	Bernard	MR	Sciences de la Terre	SPIN
GUYONNET	René	DR	Génie des Procédés	SPIN
HERRI	Jean-Michel	PR 2	Génie des Procédés	SPIN
INAL	Karim	PR 2	Microélectronique	CMP
KLÖCKER	Helmut	DR	Sciences & Génie des Matériaux	SMS
LAFOREST	Valérie	CR	Sciences & Génie de l'Environnement	Fayol
LERICHE	Rodolphe	CR CNRS	Mécanique et Ingénierie	SMS
LI	Jean-Michel	EC (CCI MP)	Microélectronique	CMP
MALLIARAS	George Grégory	PR 1	Microélectronique	CMP
MOLIMARD	Jérôme	MA	Mécanique et Ingénierie	SMS
MONTHEILLET	Frank	DR 1 CNRS	Sciences & Génie des Matériaux	SMS
PERIER-CAMBY	Laurent	PR 2	Génie des Procédés	SPIN
PIJOLAT	Christophe	PR 1	Génie des Procédés	SPIN
PIJOLAT	Michèle	PR 1	Génie des Procédés	SPIN
PINOLI	Jean-Charles	PR 0	Image, Vision, Signal	CIS
STOLARZ	Jacques	CR	Sciences & Génie des Matériaux	SMS
SZAFNICKI	Konrad	MR	Sciences & Génie de l'Environnement	Fayol
THOMAS	**Gérard**	PR 0	Génie des Procédés	SPIN
TRIA	Assia		Microélectronique	CMP
VALDIVIESO	François	MA	Sciences & Génie des Matériaux	SMS
VIRICELLE	Jean-Paul	MR	Génie des procédés	SPIN
WOLSKI	Krzysztof	DR	Sciences & Génie des Matériaux	SMS
XIE	Xiaolan	PR 1	Génie industriel	CIS

Glossaire :

PR 0	Professeur classe exceptionnelle
PR 1	Professeur 1ère classe
PR 2	Professeur 2ème classe
MA(MDC)	Maître assistant
DR	Directeur de recherche
Ing.	Ingénieur
MR(DR2)	Maître de recherche
CR	Chargé de recherche
EC	Enseignant-chercheur
IGM	Ingénieur général des mines

Centres :

SMS	Sciences des Matériaux et des Structures
SPIN	Sciences des Processus Industriels et Naturels
Fayol	Institut Henri Fayol
CMP	Centre de Microélectronique de Provence
CIS	Centre Ingénierie et Santé

Remerciements

En préambule à ce mémoire, je souhaite adresser mes remerciements les plus sincères aux personnes qui m'ont apporté leur aide et qui ont contribué à l'élaboration de ce mémoire ainsi qu'à la réussite de ces formidables années.

Tout d'abord, j'exprime mes profonds remerciements à mes directeurs de thèse, le professeur Michel BARON et le professeur Gérard THOMAS pour m'avoir accueilli gentiment dans leur groupe de travail, pour les aides précieuses qu'ils m'ont apportées, pour leurs patiences et leur encouragement durant ma thèse.

Mes sincères remerciements s'adressent également à mes encadrants : Dr. Alain CHAMAYOU, Dr. Eric SERRIS, Dr. Laurence GALET et Dr. Philippe GROSSEAU. Merci beaucoup de m'avoir fait confiance et d'avoir pris le temps pour m'encadrer. Vos remarques et conseils ont été indispensables à l'avancement de cette thèse.

Je tiens à remercier le professeur Fumio SAITO, et le professeur Mojtaba GHADIRI d'avoir accepté d'examiner et de juger ce travail de thèse. Je profite de cette occasion pour vous remercier à l'encadrement pendant mes études universitaires. En particulier, Prof. SAITO qui m'a enseigné et encadré durant mes années universitaires à l'université de TOHOKU.

Un grand merci pour le professer Pierre TCHORELOFF de m'avoir fait l'honneur de présider le jury.

J'exprime ma gratitude à tous les consultants et internautes rencontrés lors des recherches effectuées et qui ont accepté de répondre à mes questions avec gentillesse. Surtout pour nos excellents techniciens Marie-Claude de Saint-Etienne, Laurent, Philippe, Sylvie, Christine et Didier ADE d'Albi, pour nos secrétaires formidables, Carole de Saint-Etienne et Anne-Marie d'Albi, et pour Yamina qui m'a aidé sur les points scientifiques.

Enfin, j'adresse mes plus sincères remerciements à tous mes proches et amis qui m'ont toujours soutenu et encouragé au cours de la réalisation de ce mémoire.

Merci à tous et à toutes.

25 Septembre 2012

Akira SATO

Table of contents

Introduction

The surface modification of particles is widely used in many fields such as paints, ceramics, cosmetics and pharmaceutics in order to give particles new functionalities or improvement of properties. It is an essential operation to aim the desired properties for powders, such as the production of pharmaceutical materials in a drug delivery system, dry ink (toner) particle for laser printer, powder foundation for skin cosmetic and so on. Traditionally, those surface modifications are generally done by wet coating methods, for instance fluidized bed and pan coater. However, this method has certain disadvantages, especially, from the environmental point of view since it tends to produce waste products, which may be hazardous due to the use of volatile solvents.

Meanwhile, the dry coating that emerged recently has attracted considerable attention as an alternative coating method because of its simplicity and environmental friendliness since it does not require any binder or solvent. In such processes, the fine particles called ‘guest particles’ and relatively large size particles called ’host particles’ are mixed together with mechanical actions such as shear or impact forces so that guest particles can be attached firmly on the surface of host particles and change their properties (Alonso et al. 1988, Pfeffer et al. 2001). There are many successful research works found on dry particle coating (Linsenbühler et al. 2005, Lefevre et al. 2011, Klar et al. 2009, Mujumdar et al. 2004, Zhou et al. 2010, Young et al. 2005).

However, less research works have been done for the understandings of process controlling of dry coating. Since the coating process is generally done only by the dry mixing, it can be easily estimated that operating conditions of the mixing, such as rotational speed ω, filling ratio of samples J and processing time t, should strongly affect the performance of dry coating (Thomas et al. 2009).

Another issue of dry coating is that even though a lot of experimental works of the dry particle coating can be found in the literature (Alonso et al. 1989 Honda et al. 1994, Watano et al. 2000, Ouabbas et al. 2009a, Lefevre et al. 2010, Lefevre et al. 2011) this technique is not yet in commercial use. This is because they are still try and error states due to the lack of the

understanding of particle behavior inside a mixer. In other words, it is difficult to predict the optimal process operation for the commercial use or/and to scale up to the industrial scale. While, there are few researchers that have studied the theoretical approaches for dry coating mechanism so that better understandings of dry coating which may be able to optimize the process operation could be obtained. For instance, Mei et al. (Mei et al., 1997) developed an extended Johnson-Kendall-Roberts (JKR) particle model to include the effect of particle coating on the force-displacement relationship due to surface energy and elastic deformation. The method for determining the optimum operating conditions of equipment on dry coating processes based on the energy requirement for immobilizing the guest particles on the surface of host particles was established (Iwasaki et al., 2002). The theoretical modeling for such a process is very important to optimize or to design new geometry of the coating apparatus.

To try to solve those issues of dry coating, the objectives of this research work are the experimental and numerical investigations on dry coating to have better understandings so that the best method of process controlling could be established. Experimental part of this research work will be dedicated to investigate the effects of operation condition as mentioned above, on dry coating using a high shear mixer called Cyclomix supplied by the firm Hosokawa micron by experiment. The properties of the coated products such as flowability, wettability, morphology and a defined conversion ratio of guest particles will be characterized to understand the phenomena of dry coating, and to obtain a general method to estimate the dry coating efficiency.

The other objective is to simulate the particle motion inside the coating apparatus. This work is devoted to reveal by a numerical approach the effect of operating conditions, such as rotation speed of the mixer or the filling ratio, on the particles coating. Discrete Element Method (DEM), proposed by Cundall and Strack (Cundall and Strack, 1979), is one of the most popular techniques for simulating and analyzing the solid particle behavior and has been successfully applied in many fields (Kano et al., 1997, Machett et al. 2000, Cleary and Sawley 2002). This method allows us to obtain the trajectory of every single particle inside a mixer.

Since dry coating is generally done by mechanical forces originated from mixing, the particle motion would be the most important factor for dry coating. This method would be one of the most suitable ways to investigate the dry coating. DEM has already been applied in several coating devices such as Hybridizer (Mujumbar 2003), Mechanofusion system (Dave et al. 2003), Magnetically Assisted Impaction Coating system (MAIC) (Dave et al. 2003). Those researches have contributed to provide valuable information and understandings of the dry coating process and devices. Hence, in this research work the DEM will also be applied to investigate the particle motion in a high shear mixer. To compare the simulated and real particle motion, the real particle motion will be derived from by a high speed camera with a transparent vessel of a high shear mixer. Both simulated and experimental motions will be compared by means of the Particle Image Velocimetry (PIV) method. First, only the host particle motion will be simulated for sake of simplicity. From this simulation, the valuable information related to the dry coating performance, such as collision frequency, rotational kinetics of particles and force distributions on different operating conditions are intended to be calculated and compared to the experimental results when possible. Secondly the behavior of host and guest particles during a mixing based on a simple model of adhesion will be investigated.

The manuscript is divided in five main chapters.

The first chapter describes the synthesis of the bibliography on the dry coating processes and also the numerical and theoretical approaches for the dry coating. The history, mechanism and fundamental theory of dry coating will be presented in this chapter. The experimental works on diverse coating apparatus, different host-guest particles couple and their applications in different domain found from literatures will be introduced. The numerical and theoretical approaches on dry coating will also be presented.

The second chapter explains the experimental details of this research work. The host and guest particles, which have been chosen as the model couple in this research work will be

introduced. The detail of coating device, its operation conditions and the principals of characterization methods will be presented.

The third chapter will present the fundamental theory of DEM and its application to a high shear mixer. The procedure of the numerical investigation, as well as the model of interaction forces among particles carried out in this research work will be presented.

The forth chapter mentions the experimental results of characterizations of coated particles with various operating conditions. The process will be first followed thanks to a new macroscopic parameter of the dry coating process, the conversion ratio. The changes of flowability, wettability versus the conversion ratio will be reported. The evaluation of the dry coating efficiency, newly obtained from this research work, will also be presented.

The fifth chapter presents the results of numerical experiments in a high shear mixer, whose dimensions are identical to that of the real mixer Cyclomix. The comparison of real and simulated particle motions by PIV will be shown. The analysis of valuable information mentioned above on various operating conditions in the high shear mixer and their relations to the experimental results will also be presented. The modeling of dry coating behavior based on simple model, that is to say, the investigation of host and guest particle behavior will be presented in this chapter.

Finally **the general conclusion** presents the discussion from those obtained results.

Chapter I Bibliography on the dry particle coating: Process, applications and modelling

I. 1. Bases of the process

1.1 Introduction

Recently, the demand for powder products has been increasing more and more with the advancements of technology and science. For example, in the foods and pharmaceutical industries, more and more the powder products have been replacing the liquid products as the alternative or advanced products. Especially, it is said that more than 80 % of the products have been produced in form of powders in pharmaceutical industries. These tendencies are due to interesting characteristics of powders such as simplicity to deal with, easy handling, stability of qualities and capacity to add new functions.

Nowadays the powders are also required to fulfill various functions. Then, in several key industries, such as pharmaceutical, cosmetic and food, surface modification processes are routinely used to change /add the physical and chemical surface properties of particles.

Particle coating, that can give the multi-functions to powders, has been generally done by wet coating methods such as fluidized beds, pan coaters, or by wet chemistry based techniques such as coacervation, interfacial polymerization and so on. However, these techniques have several disadvantages, especially in terms of environmental effects. As these techniques often use organic phases as coating materials, they are prone to produce toxic wastes of solvent (VOC emissions (Ramlakhan et al. 2000)) which could cause hazardous phenomena.

Dry coating processes emerged recently and have attracted considerable attention as an alternative coating method because of their simplicity and environmental friendliness. In such processes, fine particles called ‘guest particles’ and relatively large size particles called ’host particles’ are mixed together with mechanical actions such as shear or impact forces without any binder so that guest particles can be attached firmly on the surface of host particles and change their properties (Alonso et al. 1989 a, Pfeffer et al. 2001). There are many successful research works found on dry particle coating. For instance, Honda et al. (Honda et al. 1987, 1991, 1994 and 1998) have done the researches that should be the first step for the dry particle

coating by using the dry impact blender. The improvement of humidity resistance of ground magnesium by coating with carnaubawax has been shown by Mujumber et al. (2004) by using three dry coating systems, Magnetically Assisted Impaction coating (MAIC), Hybridizer and Mechanofusion. The dry coating of Silica gel powder with magnesium stearate (MgSt) by a high shear mixer 'Cyclomix' has been done by Ouabbas et al. (2009 a). It shows the improvement of flowability and humidity by the dry coting treatment. Ouabbas et al. (2009 b) has also investigated the stability and ageing of coated particles (Silica gel and MgSt). This study made clear the influence of storage conditions, in particular, the relative humidity on the stability of the coated surfaces.

1.2 Principles

Fig. I. 1 shows the schematic diagram of the dry particle coating. Generally, the dry particle coating could be roughly classified as following: discrete coating and continuous coating. In contrast to wet particle coating, the guest particles are brought directly into close contact with the host particles through the application of mechanical forces such as shear and impact forces. The particles are forced to collide with each other as well as with the system walls, since the size of the guest particles is small, adhesion forces are strong enough to keep them firmly attached onto the host particles. Thus, either a discrete or continuous coating of guest particles can be achieved depending on a variety of operating conditions, including processing time, mass fraction of guest to host particles and particle properties.

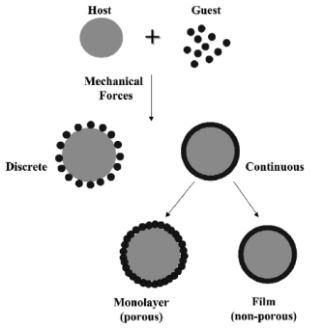

Fig. I. 1 Schematic of dry particle coating (Pfeffer et al. 2001)

1.3. Origin of the process

The idea of dry particle coating is originally derived from the ordered mixing named by Hersey (Hersey, 1975). In the ordered mixing, the adhesion force between a smaller particle and a larger particle is greater than the weight of the smaller particle, and then it is not easily removed from the larger particles. Consequently, the surface of the larger particles are loosely coated or covered with smaller particles (**Fig. I.2**). In the dry particle coating, the same thing happens even though the surface covering is more permanent due to a stronger physical (or chemical) bonding. Thus it is important to look back the literature on ordered mixing which precedes the dry coating method.

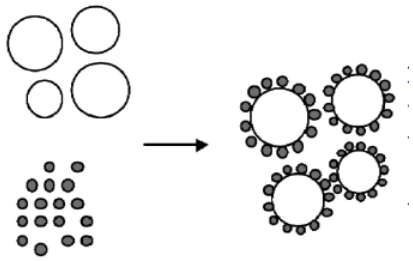

Fig. I. 2 Ordered mixing (Pfeffer et al. 2001)

The advantage of ordered mixture is that it provides a much better level of homogeneity than random mixing as long as the particle size distribution of the larger size particles is not too wide (Hersey, 1977, Bannister et al. 1983). Thus, in terms of subsequent segregation, ordered mixtures are more stable than random mixtures (Hersey, 1975, Yip et al. 1977 and Alonso et al. 1989 b). It was also shown by early researchers that having a very wide size distribution of the large size particles may lead to “ordered unit segregation”, because of the nature of the poly-disperse coarse particles (Hersey, 1977, Yip et al. 1977 and Thiel et al. 1982). Egermann et al. (1983) called the term “regimented” mix or “interactive mix” for this phenomenon. Staniforth (1985) also studied ordered mixtures applicable to the pharmaceutical industry.

Bannister and Harnby (1983) explained the ordered mixing process qualitatively. They

identified that ordered mixing proceeds in three stages. It starts with the separation of agglomerates of fine particles into their primary particles. Then the bonding of these fines with coarse particles undergoes. It ends with a re-distribution and exchanges of fine particles among the carrier particles until a random distribution is achieved. The real process may not take place exactly in that order but it is sure that the de-agglomeration of fine particles must occur in order to get the ordered mixture. Therefore in order to achieve ordered mixing, sufficient mechanical energy to promote de-agglomeration of fine particles must be used, which means to create particle collisions by mechanical impact and shearing forces. The apparatus that can be used for this purpose are high shear mixers and grinding machines. Yeung and Hersey (1977) showed that it is easier to break up fine agglomerates into primary particle size in the presence of coarser particles in the mix when processed in a high shear mixer, than having fine particle agglomerates alone. Therefore, the host particles act as the media and help the de-agglomeration of the fine particles in this phenomenon.

1.4 Advantages and drawbacks

Dry particle coating can be used to modify the properties of the surface such as flowability, solubility, dispersibility, wettability, electric, electrostatic, magnetic, optical, colour, flavour, taste, shape, and solid phase reactivity. These can find many applications into the research or commercial uses. Another advantage of the dry particle coating process is that they are environmentally benign, producing none of the organic (neither gas nor liquid) or aqueous waste streams, which usually occurs in wet coating processes (Honda et al. 1994, Sreejith et al. 2000, Pfeffer et al. 2001). These advantages attract various industries in many fields such as food, pharmaceutical, herbal/cosmetic, agricultural, chemical, powder processing and so on. Many interesting applications of dry particle coating have been also reported (Alonso et al. 1989 a and 1989 b, Watano et al. 1998, Ramlkhan et al. 2000).

However, due to the lack of a general rule governing the coating process, the optimizations of the coating process have to be carried out mostly by experimental try and error method. As the characterization of these powders often takes a long time and money, the try and error method is not the ideal way to choose the processing parameters for coating. In addition, controlling of the product quality is also a crucial issue for the coating process. For instance, if the particles coated with fine particles by relatively weak adhesive forces such as electrostatic and liquid bridge forces are used in the processes such as mixing, pneumatic transport and compression forming where relatively strong forces are applied to the particles, the fine particles are prone to be peeled off from the surface of host particles during those transport and compression forming because of insufficient adhesive strength given by dry coating (Iwasaki et al. 2002). Moreover, a try and error method does not allow us to determine the ideal process conditions for obtaining the optimal quality. Therefore, the development of optimization methods is necessary for industrial uses.

I. 2. Experimental devices and applications

2.1 Devices

There are various devices available for the dry particle coating such as Mechanofusion, Magnetically Assisted Impaction Coater (MAIC), Rotating Fluidized Bed Composer (RFBC), and Hybridizer, Theta composer and Cyclomix. Although the methods are different to give the necessary forces, they all try to efficiently promote the de-agglomeration of the invited particles and their adhesion onto the surface of the host particles.

2.1.1 Mechanofusion

Fig. I. 3 shows a mechanofusion device. It is a batch system, composed mainly of a rotating outer vessel, a stationary inner piece and a stationary scraper. Host and guest particles are placed into the rotating vessel. As the vessel rotates at speeds from 200 to 1600 rpm, the powder is forced outward towards the walls of the vessel. The gap between the inner piece and the rotating drum is controlled, and as a result, the particles passing through the gap are exposed to intense shearing and compressive forces. These forces generate sufficient energy to fuse the guest particles onto the surface of the host particles. The gap size between the inner piece and the walls of the vessel is very important to control the thickness of the desired coating. The clearance between the scraper blade and the chamber is much smaller, usually around 0.5 mm. Those clearances are adjustable and are determined by many factors, such as powder properties, particle size, requirements for final products (Naito et al. (1993), Pfeffer et al. (2001)). The scraper breaks up and prevents from any build-up or caking of the particles on the walls of the vessel. There are several advantages in using the mechanofusion system. First of all, the shape of the inner piece, the small gap, and the high rotation speed of the drum allow the particles to be given a very high shear stress and compression. Second, there is a local temperature build up due to these forces acting on the particles, which can result in the fusion of the surface of host and guest particles. This could cause very strong physical and/or

chemical bonds, which enhances the coating process.

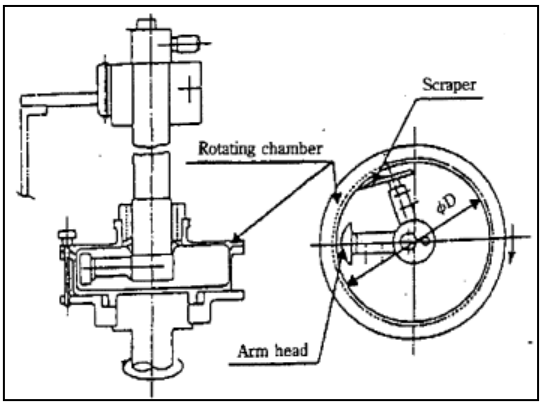

Fig. I. 3 The mechanofusion system (Pfeffer et al. 2001)

Jiang et al. (2006) coated micro-size PMMA particles with nano-size TiO_2, Al_2O_3 and SiO_2 particles in mechanofusion in order to study the effect of treatment in mechanofusion on the particle-wall interactions of the composite particles. The particles after treatment were dispersed on a flat metal surface and an experiment on particle entrainment was carried out in an airflow channel to evaluate particle-wall interactions. Relationships between particle entrainment efficiency and air velocity, which controls the distribution of the particle-wall interaction forces, were obtained under various conditions, showing that the particle-wall interaction force tends to decrease with the increase in the concentration of added nano-particles.

2.1.2 Hybridizer

The schematic design of the hybridizer is shown in **Fig. I. 4**. This device consists of a very high-speed rotating rotor with six blades, a stator and a powder recirculation circuit. The powder placed in the processing part of the vessel is given high impaction and dispersion due to the high rotating speed of rotor. The particles should be submitted to many collisions, and then this behaviour allows de-agglomerations of fine particles and particle coating due to the embedding or filming of the guest particles onto the surface of the host particles. The rotational speed of the rotor ranges from 5000 to 16000 rpm that can make a powerful mixing of the powder. Due to the applied force on the materials at these high rotational speeds, very short processing time is required to have the coated products. In addition, the device consists

in a recirculation unit that continuously moves the particles in and out of the processing vessel and against the rotor blades. At last, similarly to the mechanofusion, there is a temperature build-up due to the high impaction forces caused by the high rotational speed, which could encourage the guest particles to attach firmly on the surface of the host particles

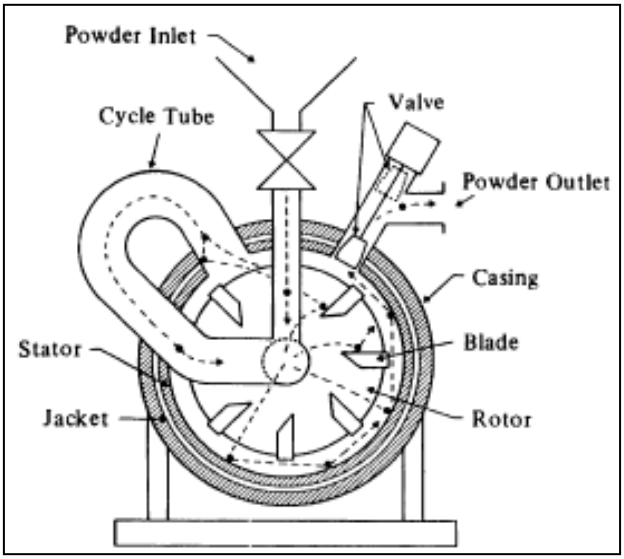

Fig. I. 4 The hybridizer

Ouabbas et al. (2009 a) and Galet et al. (2010) studied the surface modification of silica particles by dry coating with magnesium stearate (MgSt) in hybridizer. Visual analysis showed that MgSt was softened and smeared over host particles after treatment in hybridizer. The flowability of the silica particles was not strongly affected by coating. They also observed that the coating of silica gel particle by hydrophobic MgSt improved the compressibility and moisture resistance of the composite particles. One main field of application for hybridizer is pharmaceutical research. In the pharmaceutical area, there are some examples of major concern, like the controlled release of an active pharmaceutical ingredient (API), the change of the mechanical and physical character of a drug as well as the improvement of the properties of the drug and its functionability. Ishizaka et al. (1989) coated starch particles in hybridizer with various active principles (oxyphenbutazone, prednisolone, theophylline, indometacin, phenacetin, aspirin, particle sizes< 100 μm), which are sparingly soluble in water, in order to increase the dissolution kinetics of these solid forms of API. They observed

that after the process, these drugs dissolved very rapidly. In order to have a long dissolving time or controlled release the hybridizer products were coated by carnauba wax as a monolayer at first, and then a multilayer. They observed that the dissolution is very quick after the API is coated on the starch. Moreover, the dissolution time is much longer when the composite particles are coated by monolayer and even more when coated by two carnauba wax layers.

As an interesting application of the hybridizer, Pieper and Mattern (2004) coated potato starch with praziquantel in order to mask the taste of this drug. Analysing the content of praziquantel composite powders with respect to drug content showed that it did not decrease due to processing compared to the weight ratio of the material at the start. Moreover, they observed that the release of praziquantel in water is very fast after hybridizing it with potato starch. On the other hand, although the initial dissolution of the composite particles is rather fast there is tremendous difference in taste compared to the initial states of the particles.

2.1.3 Magnetically assisted impaction coater (MAIC)

Fig. I. 5 shows the schematic diagram of the magnetically assisted impaction coater. Both host and guest particles are placed into a processing vessel. The oscillating magnetic field generated by the external coil surrounding the processing vessel is used to accelerate and spin the relatively large magnetic particles mixed with the host and guest particles promoting collisions between particles and with the walls of vessel. Since the magnetic particles fluidize the host and invited particles, the coating should be relatively gentle, that is to say, the host particles are not to be easily broken or worn. Hence, softer or more fragile materials could be chosen as host particles by using the MAIC.

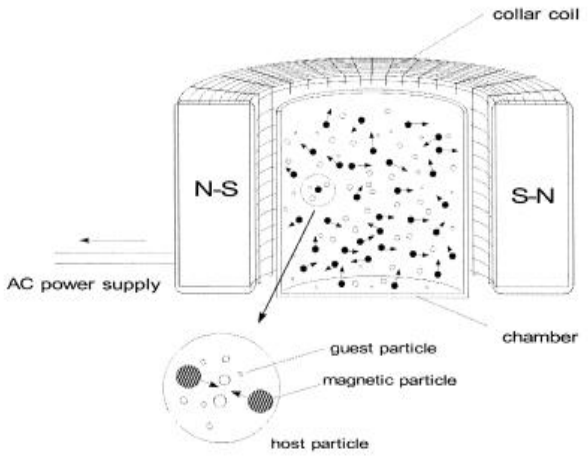

Fig. I. 5 Schematic diagram of the magnetically assisted impaction coater (Ramlakhan et al. (2000)).

Several applications of MAIC have been reported mainly from American research groups. For instance, Yang et al. (2005) performed dry coating of corn starch by the Aerosil R972 silica and EH-5 silica, and then measured the angle of repose to evaluate the efficiency of the dry coating. **Fig. I. 6** indicates the angle of repose of the products as a function of the processing time. The angle of repose decreases with an increase in the processing time. In other words, the flowability of the products has been improved by the dry coating using MAIC, which indicates that MAIC is capable to carry out the dry coating.

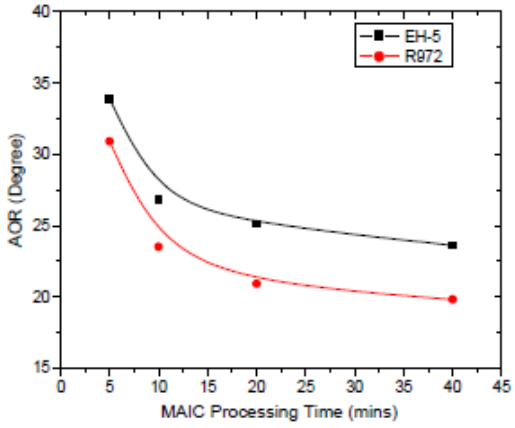

Fig. I. 6 Angle of repose of samples of corn starch coated with silica EH-5(1.0 wt.%) or aérosil R972(1.0wt.%) using the MAIC technique for each processing time (Yang et al. (2005)).

2.1.4 Theta composer

The Theta composer, shown **Fig. I. 7,** is a high-speed rotor mixer with an elliptical vessel and an elliptical rotor. As the rotor rotates inside the vessel, the powder mixture consisting of host and guest particles is exposed to shear and compressive stresses as it is forced into the small clearance between the vessel and the rotor. As the rotor continues to move and the clearance between the vessel wall and the rotor becomes larger, a bulk mixing of the host and guest particles occurs (Pfeffer et al. 2001).

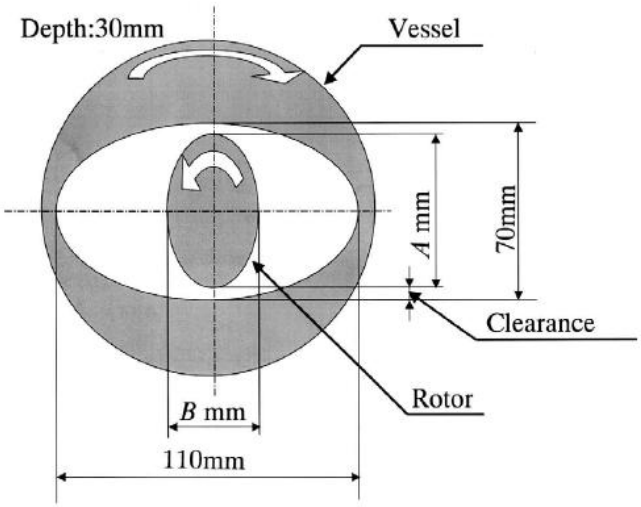

Fig. I. 7 Schematic diagram of the theta composer.

Another noticeable dry particle coating study with theta composer has been done by Coowanitwong et al. (2003). They coated Al_2O_3 particles with nano-sized CuO particles in the theta composer and studied the effect of mass percentage of guest particles and operating conditions on the coating obtained. They observed that the product surface area increased with higher nano-particle loadings. They also found that the degree of dispersion and homogeneous distribution of CuO nano-particles on the surface of Al_2O_3 particles increased with the processing time.

2.1.5 Cyclomix

The Cyclomix is defined as a high shear mixer/granulator, manufactured by Hosokawa Micron B.V..

As it can be seen in **Fig. I. 8**, it consists of a conical shaped vessel and a rotor in the centre of the vessel equipped with an impeller and four sets of blades. It applies high mechanical impact, shearing forces on the particles in order to break the fine agglomerates and coat them on the host particles. In this study, the Cyclomix has also been used as a device for dry particle coating. The properties and the working principle of the Cyclomix will be explained in detail in the following chapter.

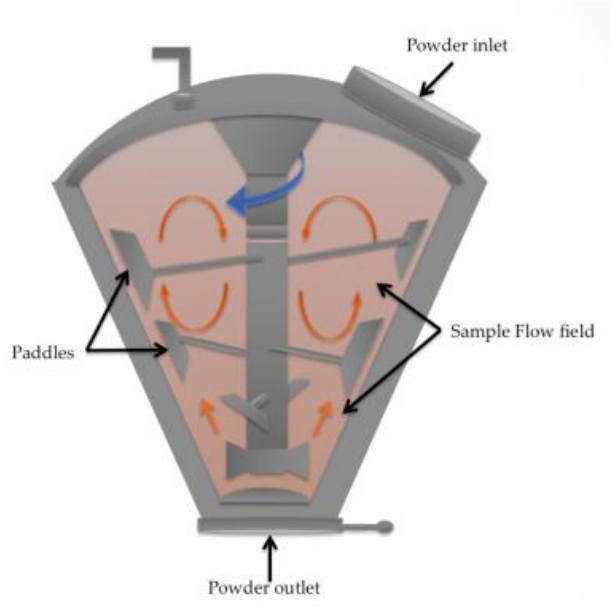

Fig. I. 8 Schematic diagram of the Cyclomix

Kwan et al. (2005) worked on the effect of the volume of Cyclomix on the structure, properties and strength of the granules. They treated glass beds particles in two different capacities (1 L and 5 L) of the Cyclomix vessel. They observed that the different configurations of the impeller in the 5 L and 1 L Cyclomix affected considerably the flow field of the particles. Ng et al. (2007, 2008) studied the particle motion inside a mixer by Positron Emission Particle Tracking Method (PEPT). Hassanpour et al. (2009) compared the simulated particle motion given by DEM to PEPT results and obtained quite well agreement. . Ng et al. (2009) also investigated the particle motion in Cyclomix by CFD and compared the

experimental data obtained by PEPT. It was shown that the CFD model is capable of capturing the particle distribution in the vessel at various rotational speeds and with different materials and fill levels.

Another granulation study with the Cyclomix has been done by Rahmanian et al. (2008, 2009 and 2011). They studied the influence of operation scale and impeller speed of high shear mixer granulators on the strength of granules. Calcium carbonate particles were granulated in four scales of a geometrically similar high shear granulator (Cyclomix) with 1, 5, 50 and 250 L capacities. They observed that the granulation operations produce granules with a similar strength of the particles for all four cases.

Ouabbas et al. (2009 a) coated silica particles with different mass percentages of magnesium stearate in Cyclomix, in order to understand the effect of coating on surface properties of the particles. They observed that the flowability of the silica gel powder significantly decreased after treatment by the Cyclomix mixer with 5% of MgSt.

Lefebvre et al (2011 a) showed the coating of Talc particles with hydrophobic silica (Aerosol R972®). It is observed that the wettability and dispersibilty in aqueous solution were dramatically modified.

2.2 Applications

Dry particle coating is applicable to solve a great variety of industrially important problems. This is due to its ability to create engineered and tailored particles with substantial improvement of certain physical and/or chemical properties. In this section, the applications of dry particles coating will be shown from the surface property approach.

2.2.1 Flowability

The improvement of the flowability of the product is a very important issue, especially in pharmaceutical industries. The die-filling process is affected by the cohesiveness of the powder, which determines the capability for the powder to be fed into the die (Guerin et al. 1999). Cohesiveness also causes the non-uniformity of the API mass in the tablets (Lindberg et al. 2004). Powder bulk properties and its compressibility also impact the pre-compaction and compaction processes. For the purpose of flow improvement, the dry coating method has been successfully used to coat different types of cohesive powders and improve their flow. For instance, a mixture using mechanofusion of 5 μm polymethylmethacrylate (PMMA) particles coated with 10 % by weight of 0.015 μm TiO_2 particles, flowed freely and had a near zero angle of repose. In contrast, both original PMMA and TiO_2 particles did not flow so well and had an angle of repose greater than 30^o (Yokoyama et al. 1987). Another example is that flowability of a series of cohesive lactose powders was substantially improved after mechanofusion with small quantities of magnesium stearate (MgSt). The non-flowing cohesive lactose monohydrate powder with a median diameter size approximately 20 μm achieved the same free-flowing characteristic as that of the lactose monohydrate powder with 120 μm, which is already a free-flowing powder (Jallo et al. 2011). Many other research work on the improvement of flowability have also been reported (Ramlakhan et al. 2000, Yang et al. 2005, Han et al. 2012, Zhou et al. 2011, Lecoq et al. 2011, Mullarney et al. 2011).

2.2.2 Wettability

Improvement of wettability is also a crucial issue for the product quality. Especially the powders that are highly hydrophilic can be easily decayed by the moisture in the air.

Mujumdar et al. (2004) used mechanofusion to enhance the moisture resistance of ground magnesium powder (primary size 75 µm) by coating its surface with carnauba wax (primary size 15 µm). As a result, dry coating of magnesium powders with carnauba wax by using mechanofusion generated a material which is much hydrophobic compared to ground magnesium particles. Lefebvre et al. (2011 b) has investigated the effect of coating on the wettability of the coated Talc particles with different concentrations of hydrophobic Silica (Aerosil R972®), using Cyclomix. The wettability of coated particle was measured by the sessile drop method depositing a small drop of 10 µl of pure water on tablets formed from coated products. The contact angle increased from 53° to 133°, which confirms the increase in hydrophobicity of the composite particles caused by the presence of hydrophobic silica (**Fig. I. 9**).

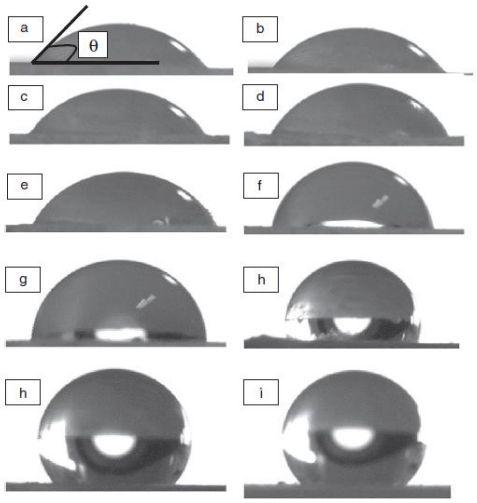

Fig. I. 9 Pictures at initial time t_0 of water sessile drops on uncoated Talc tablets (a) and coated talc tablets with different concentration of silica: 0.5 % (b), 1 % (c), 1.5 % (d), 2 % (e), 3 % (f), 4 % (g), 5 % (h), 7 % (i), 10 % (j). (Lefebvre et al. (2011 b))

2.2.3 Other property modifications

Due to the large possibilities of the surface modification, many other applications of dry coated materials can be found. Liu and Kamat (1995) produced nanocrystalline thin films of

metal oxides such as TiO_2 and SnO_2 with a highly porous structure to use in photo-electrochemical cells.

The improvement in biocompatibility of artificial bone material hydroxyapatite (HAP) by coating with partially stabilized zirconia to provide high fracture toughness while preserving the original surface properties of HAP was also done by Kawashima et al. (1997).

Kangwabtrakool et al. (2001, 2002, 2003) coated WC particles first with TiC and then with Al_2O_3 in order to modify the hot hardness of the particles. They observed that the hot hardness of the composite particles increased with higher amount of TiC whereas increasing Al_2O_3 additions reduced the hardness.

I. 3. Modelling studies on dry coating

Even though many applications of the dry coating have been reported as shown in the previous section, this technique is not yet in the commercial use. This is because they are still in the try and error state. In other words, it is difficult to predict the optimal process operation for the commercial use or/and to scale up to the industrial scale. Anyway, there are several researchers that have studied theoretical approaches for elucidating dry coating mechanisms so that a better understanding and optimization of the process operation could be obtained.

3.1 Particle-particle interaction forces

It is quite important to know the driving forces causing the adhesion of guest particles on host particles. That should be a fundamental knowledge for the theoretical approach to the dry coating process.

The nature and degree of particle interactions determine the surface properties of the composite particles (Podczeck et al. 1996). There are two major interaction mechanisms between the particles: adhesion and friction. Adhesion is the result of the inter-particular forces between the particles or a particle and a surface that are in contact. It may occur between the particles and surfaces with different chemical nature or with the same chemical nature, called cohesion. With respect to single particle interactions, the term cohesion is applicable only when the particles are as close as an atomic distance between each other. Friction is the force preventing the tangential displacement of two solid or particle surfaces in contact (Podczeck et al. 1997).

Adhesion between particles and between particles and surfaces are primarily due to Van der Waals Forces, capillary forces, electrical forces and electrostatic Coulomb forces. They usually arise because of the interactions dipole-dipole, charge-dipole, charge-charge, covalent, charge-non-polar, dipolar-non-polar, non-polar-non-polar and also hydrogen bonding (Seville et al. 1997). The inter-particular forces depend on the particle size and the distance between

the two acting particles and on the other hand on the shape including surface properties and deformations, as well as the chemical identity of the particles.

The predominance of these depends on environmental conditions during experiment and the physicochemical properties of the materials that are in contact (Podczeck et al. 1996). The total adhesion force is assumed to be the sum of several forces, as illustrated in **Eq. (I. 1)**.

$$F_{\mathrm{ad}} = F_{\mathrm{vdw}} + F_{\mathrm{liq}} + F_{\mathrm{es}} \qquad \textbf{I. 1}$$

where:

F_{ad} is the total adhesion force;

F_{vdw} is the Van der Waals force;

F_{liq} is the liquid bridge force;

F_{es} is the electrostatic force.

3.1.1 The Van der Waals force

The Van der Waals force is an interaction which outcomes in dipole moment of atoms and molecules. As in the attraction forces in chemical bonding, the Van der Waals force results from the attraction of opposite electric charges. Areas of the molecule with electron abundance lead to a partially negative charges and are attracted by areas deficient of electrons (partially positive) of other molecules. These Van der Waals forces are secondary bond forces and are much weaker than the primary bonds (covalent, ionic and metallic). Van der Waals interaction between two particles is calculated by the sum of interaction between all molecules of these two particles (Fröberg et al. 1999). This is performed by integration, known as the macroscopic model. Hamaker (1937) proposed **Eq. (I. 2)**, the following expression of the Van Der Waals potential energy, V_{A} of two spherical particles of radius *a* and *b* separated *in vacuum* by a distance *D*.

$$V_{\mathrm{A}} = -\frac{A}{6}\left[\frac{2ab}{D^2 - (a+b)^2} + \frac{2ab}{D^2 - (a-b)^2} + ln\frac{D^2 - (a-b)^2}{D^2 - (a-b)^2}\right] \qquad \textbf{I. 2}$$

Where, *A* denotes the Hamaker constant that depends on the material characteristics. When the radius of two particles is much bigger than the separated distance, the expression of above

equation could be simplified to:

$$V_{\mathrm{A}} = -\frac{A}{6D}\left[\frac{ab}{a+b}\right] \qquad \textbf{I. 3}$$

Thus, the van der Waals force can be given by the following equation:

$$F_{\mathrm{vdw}} = -\frac{dV_{\mathrm{A}}}{dD} = \frac{A}{6D^2}\left[\frac{ab}{a+b}\right], \quad if\ a,b \gg D \qquad \textbf{I. 4}$$

The minimum separation D_{min} between two particle surfaces is assumed to be 4 Å (Krupp, 1967).

3.1.2 The liquid bridge force

The liquid bridge is formed in the gap between particles (**Fig. I. 10**). Generally, there are two kinds of forces caused by the liquid bridge.

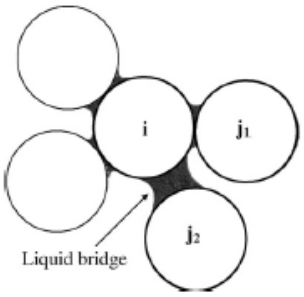

Fig. I. 10 Liquid bridges formed between particles

One is the adhesive force, which arises from capillary and surface tension effects. The other is a viscous force, which is dependent on the viscosity of the liquid and it is always opposed to the motion of the particles. Based on the assumption that the shape of the liquid bridge between two particles may be approximated by an arc of a circle, this approximation gives the adhesive capillary force is given as follows (Fisher, 1926);

$$F_{\mathrm{L}} = \pi r_2^2 \gamma \left(\frac{1}{r_1} - \frac{1}{r_2}\right) + 2\pi r_2 \gamma \qquad \textbf{I. 5}$$

Where γ is the liquid surface tension and r_1, r_2 are the radii of curvature of the liquid bridge surfaces. The first term on the right hand side is due to the pressure drop across the air-liquid interface. The second term arises from the surface tension of the liquid.

Muguruma et al. (Muguruma et al. 2000) provided the numerical solution of the Young-Laplace equation of the liquid bridge. The contact angle was assumed to be zero. Curvature of the liquid bridge could be determined if the volume of the bridge and the length of the gap between particles are known. It should be noted that there is a limit to the length of the gap between particles in which the liquid bridge is formed. Calculation of this limit is also provided by Muguruma et al (2000). In addition to the capillary force, wet particles also encounter a resisting viscous force in their motion. Viscous force can be predicted using the lubrication theory (Adams and Perchard (1985), Goldman et al. (1967)). There are two components of the viscous force, one in the normal and the other in the tangential direction. The expression of the viscous force in the normal direction between two particles was given by Nase et al. (2001):

$$F_{v_n} = 6\pi\mu R^* v_n \frac{R^*}{D} \qquad \textbf{I. 6}$$

Where R^* is defined as:

$$\frac{1}{R^*} = \frac{1}{a} + \frac{1}{b} \qquad \textbf{I.7}$$

Here μ is the viscosity of the interstitial fluid, v_n is the relative normal velocity of the spheres, a and b are the radii of the two particles, respectively, and D is the separation between particles. The viscous force in the tangential direction could be predicted by the following equation (Lian et al. 1998):

$$F_{v_t} = \left(\frac{8}{15} ln \frac{R^*}{D} + 0.9588\right) * 6\pi\mu R^* v_t \qquad \textbf{I.8}$$

Where v_t is the relative tangential velocity of the particle. Thus, the resulting force exerted on the liquid bridge could be obtained from adding these forces.

3.1.3 The electrostatic force

Electrostatic forces (Coulomb forces) (F_{es}) emerge between charged particles. When both of the particles are either positively or negatively charged, the force is repulsive. When they are of opposite charge, it is attractive. The force can result from friction or even by contacting solid surfaces and building up an electric potential. Because electron transfers between the particles a potential emerges. The particle, which needs less energy to release the electrons, delivers them to the other particle. The charging of isolators and electronic conductors depends on the electron surface density (Visser, 1995). The force acting on one charged particle having charge q_1 by another charged particle having charge q_1 is given by Coulomb's law as:

$$F_{\text{es}} = \frac{1}{4\pi\epsilon_0}\frac{q_1 q_2}{z^2} \qquad \textbf{I. 9}$$

Where, ε_0 is the permittivity of vacuum.

3.1.4 Other driving forces

In the specific couples of host and invited particles, a chemical reaction driven by the mechanical action could occur for bonding each other. This phenomenon is called mechanochemistry. Generally, mechanochemical reactions required high enough mechanical energy to cause the chemical reaction such as the planetary ball mill grinding (Mizukami et al. 2004, Kano et al. 2006). In the dry coating, there are a few publications mentioning the mechanochemical bonding between host/invited particles. For instance, Watanabe et al. (2002, 2003) studied the mechano–chemical reaction by mixing indometacine with silica nano-particles. Watano et al. (2000) worked on changing the properties of some special type of food powder by coating them with hydrophilic silica (SiO_2). They have done investigations on the mechanochemical reaction in dry particle coating processing. They have observed that reaction between hydrophilic OH groups of food fibre and silanol groups -Si(OH)- results in dehydration (**Fig. I. 11**), which leads to suppression of the hygroscopic properties of the food fibre.

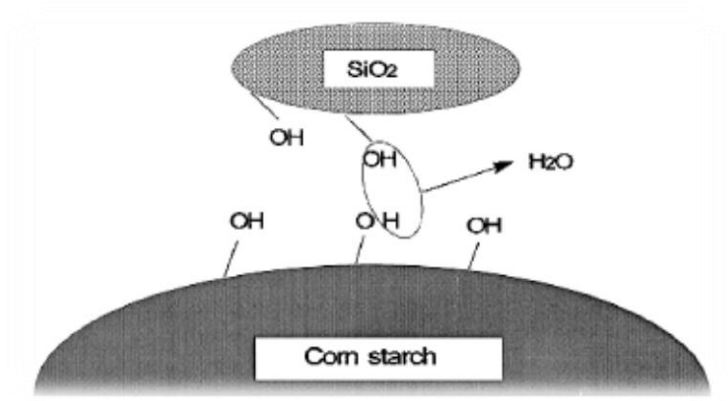

Fig. I. 11 Mechanochemistry effect occurring on the surface of corn starch to form hydrophobic groups (Watano et al. 2000).

3.2 Modelling study of the dry coating

Modelling works on the dry coating are generally classified into 2 categories: microscopic modelling and macroscopic one. The former one focuses on the interaction forces between particles, using often theories mentioned in the previous sections.

The latter one generally focuses on the whole process of the dry coating such as the energy given by the coating devices to the particles, the motion of the particles inside the coating devices and so on. Both approaches are quite important for the multi-scale understandings of the dry coating, even though few research works can be found in literature.

3.2.1 Microscopic modelling

The microscopic modelling reported in literature is mostly based on the earlier work on ordered mixing. Based on the experimental observations and the concepts of statistical modelling, Alonso et al. (1989 a) explained the basic mechanisms of dry coating. Initially, the coating consists of loose agglomerates of guests particles adhering to the host particles in their immediate vicinity. This occurs rather quickly and is followed by the dispersion and rearrangement of guests spread over the surface due to collisions between a coated host and a non-coated host.

Mei et al. (1997) developed an extended Johnson-Kendall-Roberts (JKR) particle model to include the effect of particle coating on the force-displacement relationship due to surface

energy and elastic deformation.

The theoretical force values of dry coating products treated by the hybridizer have been estimated as follows. Host silica gel (SG) and invited magnesium stearate (MS) have been mixed, and the contact interaction force between a MS grain stuck on the cantilever and the surface (point where either a SG grain or a MS grain is present) has been measured by the atomic force microscopy (AFM) (Thomas et al. 2009). The MS- SG force (or MS-MS force) are quite different. The theoretical mean interaction force MS-MS or MS-SG was derived from the following approach. It is assumed that particles are spherical with an uniform radius For the multilayer coating structure (semi-ordered system model), the number of free sites for the invited particles after having placed at random p invited particles on a host particles, q_p could be estimated by following equation:

$$q_p = N(1-\frac{1}{N})^p \qquad \textbf{I. 10}$$

Where, N is initial number of free sites on host surface. Then the free surface fraction is given by :

$$S_{\mathrm{H}} = (1-\frac{1}{N})^p \qquad \textbf{I. 11}$$

N can be expressed very simply as follows. Dividing the overall surface of contact between host and invited particles by the effective area occupied by one invited particle on the surface, the maximum coordination number, equal to N, is obtained. The effective area is considered as the area of invited particle projected vertically to the host surface, divided by the packing fraction.

$$N = 4C_{2\mathrm{D}}(k_{\mathrm{H}}+1)^2 \qquad \textbf{I. 12}$$

Where, C_{2d} is the 2D packing fraction (for a compact hexagonal structure: $C_{2d} = 0.906$, a random arrangement $C_{2d} = 0.82$ and a quadratic loose packing structure $C_{2d} = 0.785$) and k_{H} is a fraction of radius ratio. The value of number p of invited particles on the surface of one host particle can be expressed as:

$$p = {k_{\mathrm{H}}}^3 \frac{\rho_{\mathrm{H}}}{\rho_{\mathrm{I}}} \frac{w_{\mathrm{I}}}{1 - w_{\mathrm{I}}}$$

I. 13

Where, ρ_{H} and ρ_{I} denote the density of the host and invited particles respectively and w_{I} expresses the mass fraction of invited particles.

Assuming that the probability for an invited particle placed on the tip of the cantilever of AFM to encounter a free surface site is proportional to the available free surface fraction and also that invited particles are placed at random on the surface of host particle, the probability to reach the invited – invited particles interactions force f_{i} or invited – host particles interactions force f_{H} would be proportional to the analysed corresponding area. Hence, the mean interaction force f is expressed by the equation below:

$$f = (1 - S_{\mathrm{H}}) f_i + S_{\mathrm{H}} f_{\mathrm{H}}$$

I. 14

Substituting the equation (**I. 12**) and (**I. 13**) into eq. (**I. 11**) and then eq. (**I. 11**) into (**I. 14**), the expression of the mean interaction force becomes:

$$f = \left\{1 - \left(1 - \frac{1}{4C_{2\mathrm{D}}(k_{\mathrm{H}} + 1)^2}\right)^{{k_{\mathrm{H}}}^3 \frac{\rho_{\mathrm{H}}}{\rho_{\mathrm{I}}} \frac{w_{\mathrm{I}}}{1 - w_{\mathrm{I}}}}\right\} f_i + \left(1 - \frac{1}{4C_{2\mathrm{D}}(k_{\mathrm{H}} + 1)^2}\right)^{{k_{\mathrm{H}}}^3 \frac{\rho_{\mathrm{H}}}{\rho_{\mathrm{I}}} \frac{w_{\mathrm{I}}}{1 - w_{\mathrm{I}}}} f_{\mathrm{H}}$$

I. 15

The curves $f(w)$ given by the SOC model have been compared to the experimental results (**Fig. I. 12**).

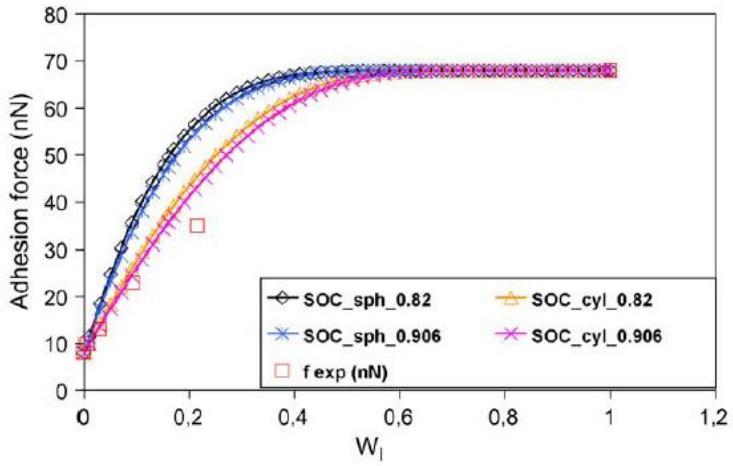

Fig. I. 12 semi-ordered coating: evaluation of the averaged force of interactions between a MS particle attached to the tip of the cantilever and the surface of spherical (or cylindrical) host particles covered by spherical invited particles MS, for different surface packing fraction (Thomas et al. 2009)

The calculated curves have a good agreement with the experimental results, especially when C_{2d} is supposed to be 0.906 and the shape of the host particles is assumed to be cylindrical.

The other example on the microscopic modelling is an analysis of the coating process in the hybridizer. In this research (Honda et al. 1994) the energy of adhesion for formation of a monolayer under the assumption that Coulomb and London-Van Der Waals interactions works together. This makes possible predicting the qualitative effect of two important factors of the coating process, namely, the size of the particles, and the size ratio between the host and guest.

3.2.2 Macroscopic modelling

The approaches for macroscopic modelling are found in rather recent works. The method for determining the optimum operating conditions of equipment on dry coating processes based on the energy required for immobilizing the guest particles on the surface of host particles was established by Iwasaki et al. (2002).

The model for estimating the coating time in a magnetically assisted impact coating device (MAIC) has been developed by Singh et al. (1997). This model has been achieved by assuming that the particles collide randomly with each other in the system, and the system is

in homogeneous statistical equilibrium state. This work indicated that the optimum coating time is shown to depend on several parameters including the number density of host particles, the diameter ratio of the host and guest particles, the height of the fluidized particles bed and the material properties such as density, stiffness and particle size of host and guest particles.

Davé et al. (2003) has done the numerical analysis of the Hybridizer by the Discrete Element Method (DEM) to understand the particle motion. The exact modelling of the whole hybridization system including the recirculating pipe is extremely complicated. Hence only the mixing chamber is modelled. As shown in **Fig. I. 13**, the outer circle represents the outer wall of the mixing chamber. The blade mounted on the rotor is approximated as three overlapping cylinders.

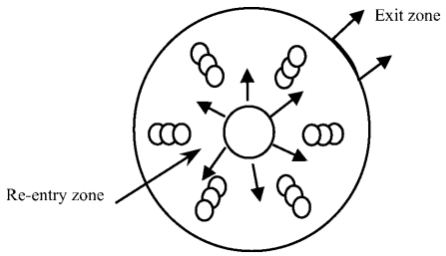

Fig. I. 13 Simplified diagram of the simulation model of the hybridizer system

They have studied several values that could be related to the dry coating performance, for example, frequency of collisions as a function of the rotating speed of Hybridizer (**Fig. I. 13**).

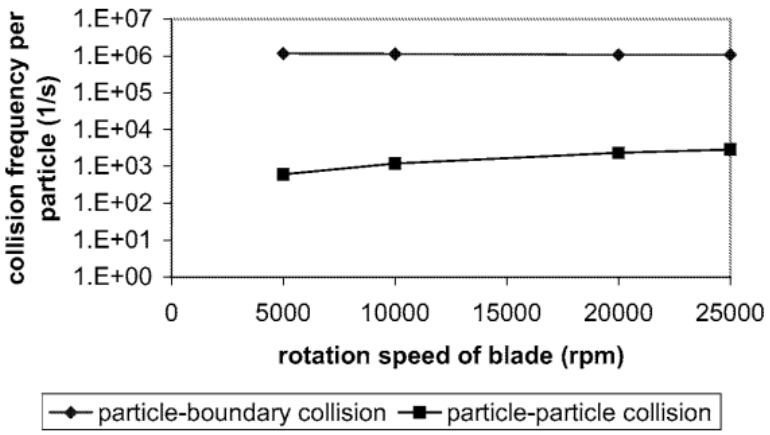

Fig. I.14 Particle–particle and particle–walls collision frequency (1/s) (averaged per particle) as a function of the rotation speed of the blade for a loading of 1000 particles

As seen in **Fig. I.14**, the number of collisions increases with an increase in loading as well as an increase in the rotational speed of the rotor. However, the increase in frequency of particle –walls collisions is not as significant as the loading or the rotation speeds increase. Nonetheless, particle collisions with the walls of the system, which include the blades as well, are dominant as compared to inter-particle collisions. As shown in the example, the DEM simulation could give the important information which can't be obtained by the experiments. That could help to optimize the process operation of the dry coating and to predict the performance.

Conclusion

Dry particle coating process, which originally came from the concept of ordered mixtures, is expected to be the alternative method for the surface modification of the particles from the previous wet coating method due to its simplicity, low cost operation and environmental friendliness. Since some decades, diverse dry coating devices have been developed and used for the surface modification even though the type of coating produced and its application would be also different. Many research papers on the application of the dry coating processes are found: They indicate that this process has large possibilities for application in various industrial purposes, not only for a viable alternative to wet coating but also for certain application where wet coating processes are not adequate

However, the current state of art to determine the operating conditions is still a try and error method that may be inadequate, because it is very time consuming and does not allow determining the conditions for obtaining optimal coating quality. The current try and error approaches imply that the coating processes are not yet well optimized, which is one of the reason why this process has not yet become commercially successful.

Though, a theoretical predictive capability is necessary to scale-up and to optimize the operating conditions to obtain the best possible coated particles for industrial needs, there are very few studies about the modelling of the dry particle coating process. Hence, in this research work, those facts strongly motivate us to establish a new method to optimize the operating condition of the dry coating process and to try to understand the general rules which govern the coating phenomena. Especially, simulating the particle motion, which was introduced in section 3.2.2, would be one of the possible ways to accomplish this work.

Chapter II: Materials and Experimental Methods

II. 1. Introduction

In this study, a Cyclomix high shear mixer has been used to generate composite materials by dry coating method. The reason why this device has been chosen is that there are few publications for dry coating with this apparatus and it has a large potential to be capable of industrial application due to its large capacity, which can treat large quantities of powders in one operation. The Cyclomix device (available until 500 L) can be used at an industrial scale after an appropriate process scaling-up. This apparatus uses different mechanical forces (mechanical impact, compression, shearing etc) that are able to break up the agglomerates and coat the particles. Different characterization methods have been used, in order to compare the quality of coating obtained by different process conditions. In this chapter, the powders, the dry coating device, and different characterization methods that have been used for the dry coating experiments in order to analyse different properties of the particles will be presented in details. To analyse the particle motion in a high shear mixer, the PIV (Particle Image Velocimetry) that allows us to investigate the velocity field of the particle flow has been used and introduced in this chapter.

II. 2. Materials

In this study, the Suglets and magnesium stearate have been chosen as host and guest particles respectively. The characteristics of those materials and rational reasons to use them will be shown in this section.

2.1 Suglets^{TM} (Host particles)

Suglets, a product of Colorcon®, is a sugar core composed of mainly sucrose and remainder is maize starch. This material is mainly used as critical excipients in capsule and tablet formulation, particularly in multiparticulate formulations. They are the core upon which a

drug is coated, usually used for controlled or sustained release drug delivery technologies. The use of such sugar spheres in multiparticulate drug delivery system is an area of increasing interest in the pharmaceutical industry. This is largely due to the clinical and formulation advantages of sugar spheres that have over single-unit dosage form, including the ease of processing in modified release applications. Especially, Suglets have a low friability and an ability to withstand the process of drug loading with an accurate amount of the Active Pharmaceutical Ingredient (API). The suglets are obtained through the granulation processes and sieved to desired particle size. **Fig. II. 1** shows the SEM image of the Suglets. The particles observed are not exactly spheres despite relatively high sphericity and the surface seems to have crystal-like form.

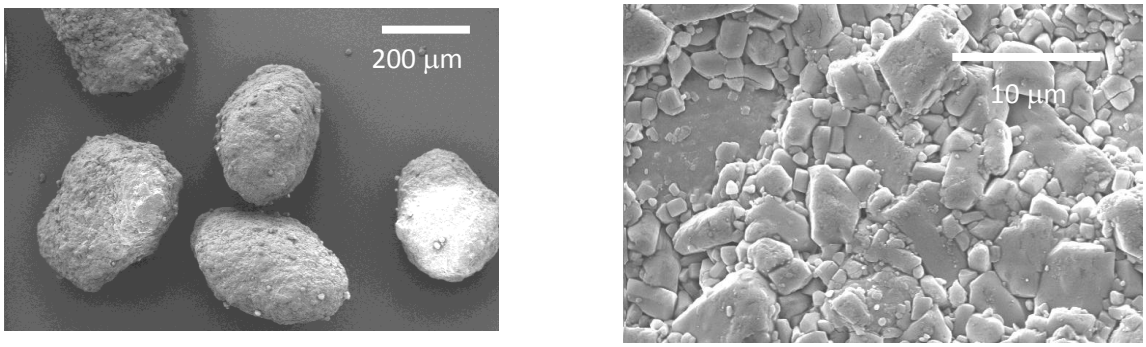

Fig. II. 1 SEM images of Suglets

The particle size distribution measured by laser diffraction technique (shown in later section) is shown in **Fig. II. 2**. As it seen, this powder has sharp population from 180 to 500 μm. The volume median diameter (D_{50}) is 250 μm.

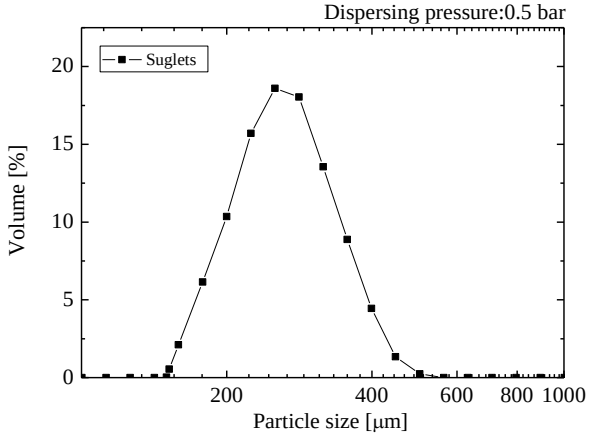

Fig. II. 2 Particle size distribution of Suglets

The density measured by the Helium Pycnometer (detail also shown in later section) is 1.58 g/cm^3. Since the density of the sucrose found in literature is about 1.6 g/cm^3, this granule product should be non-porous. The properties of Suglets are summarized in **Table II. 1**.

2.2 Magnesium Stearate (guest particles)

For the guest particles, Magnesium Stearate (MgSt) has been chosen. This material is a fine, white, greasy, cohesive and hydrophobic powder widely used in pharmaceutical formulation as a lubricant due to its capacity to reduce the friction between sliding surfaces, for instance during tablet formation and ejection, or during capsule filling. (Lerk et al. 1982). Melting point is between 125^{o}C and 145^{o}C. SEM shows that shapes of MgSt are relatively random including plate and flake-like forms, and it is also seen that aggregates of MgSt (**Fig. II. 3**).

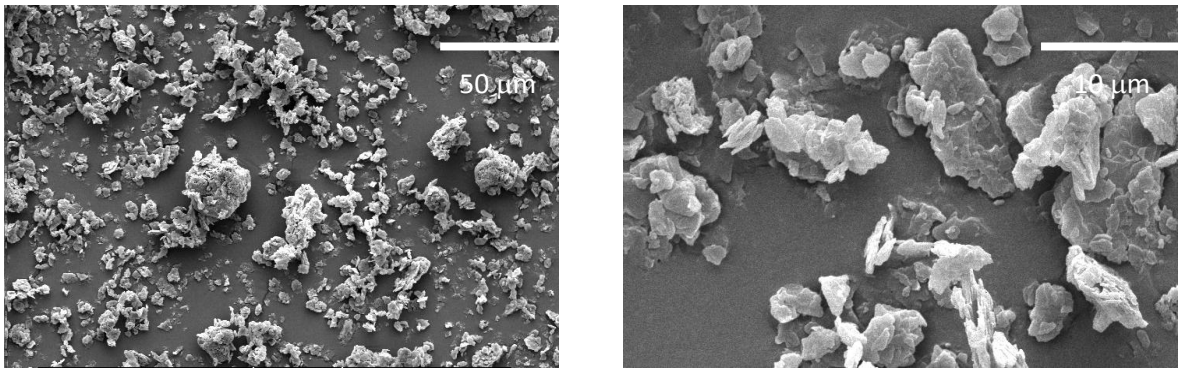

Fig. II. 3 SEM images of Magnesium Stearate

The particle size distribution is shown in **Fig. II. 4**. As seen in this figure, this powder exhibits a large size distribution from submicron to 20 μm, due to the presence of the fine particles and those aggregates. The median diameter of MgSt is 5 μm. Some properties of MgSt are summarized in **Table II. 1**.

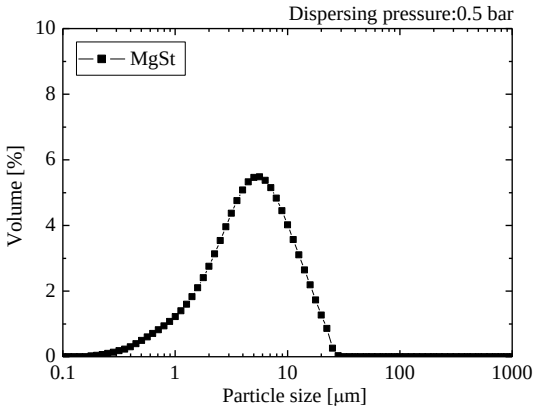

Fig. II. 4 Particle size distribution of MgSt

Table II. 1 Properties of materials

	D_{50} (μm)	density (g/cm^3)	water resistance
Suglets	250	1.58	hydrophilic
MgSt	5	1.14	hydrophobic

II. 3. Coating device: High shear mixer (Hosokawa Cyclomix)

The Cyclomix, a high shear mixer/granulator, manufactured by Hosokawa Micron B.V., has been chosen as a dry coating device in this research work. The Cyclomix used this research work has a conical shaped vessel with 1 L in capacity. The vessel is surrounded with a cooling/heating jacket in order to control the temperature in the vessel. At the bottom of the vessel there is a valve in order to recover the powders at the end of the treatment. There is a rotor in the centre of the vessel consisting of a vertical rotor with four sets of impellers (**Fig. II. 5**). The angle of the flat impeller is 30° to the vertical axis; the angle of the first (bottom) and the third pairs of the impellers is opposite to that of the second and fourth (top) pairs in such a way that when the shaft is turned clockwise, the first and the third pairs give upwards agitation while the second and fourth pairs give downwards agitation. The gaps between the impellers and the vessel wall are 5 mm at the side and 2 mm at the bottom. Due to the features of this high shear mixer, there are several advantages as following:

- Conical shape vessel provides easy discharge and cleaning
- No bearings or seals in the product zone
- High level of temperature control
- Suitable for a wide range of applications
- Suitable for coating or mixing application

The details of the geometry are presented in **Appendix 1**.

Fig. II. 5 High shear mixer 'Cyclomix' lab-scale device used in this research work

This high shear mixer is 416L stainless-steel made. To visualize the particle motion in the

mixer, the transparent acrylate vessel was toll manufactured by Hosokawa Micron as seen **Fig. II. 13**.

3.1 Operating parameters

The major operating parameters which can be considered for using this device are as follows:

- Rotation speeds of impellers, ω
- Operating time, t
- Filling ratio of the samples, J

The rotation speeds of impellers ω can vary from 200 rpm to 3000 rpm. Since the dry coating is generally done by the mechanical forces induced by mixing of the powder, this parameter should have large influences on the dry coating. For example, the lower speed operation may not be able to give enough mechanical forces for the guest particles to attach firmly on the surface of host particle. On the contrary, even though the higher speed operating could give the sufficient forces, there are risks to break host particles. However, few literatures mentioning the effect of rotation speed of this device is found (Otles, 2008). Then, the investigation of the effect of rotation speed should be an interesting issue.

Operating time t, could also be a crucial issue for the dry coating. From the literature, generally the operating time was fixed at around 240 - 600 s (Ouabbas et al. 2009 a, Otles et al. 2009) However, the operating time could also have a big influence on the dry coating performance as indicated by Lefebvre (Lefebvre et al. 2011 b)

The filling ratio of the sample J influences the process probably less than other operating parameters. It is also recommended to use about 60 % by its manufacturer Hosokawa micron B.V. However, the filling ratio also may affect the particle motion inside the mixer, and then it could change the coating performance. In addition, the filling ratio effect is hardly found in the literature. It is worth investigating the effect of the filling ratio as well.

The filling ratio of sample is obtained from the capacity of the mixer V and the total apparent volume of host particles V_p:

$$J = \frac{V_p}{V} = \frac{m}{\rho} \cdot \frac{1}{V} \qquad \textbf{II. 1}$$

m and ρ are the mass and density of host particles respectively.

V_p is measured by putting the host particles graduated cylinder without tapping.

3.2 Mass fraction of MgSt, *w*

The mass fraction *w* of guest particles added to the host particles in the experiments was calculated with reference to an ideal 100 % surface coverage of host particles. Supposing that all particles are homogeneous and spherical and do not deform during the coating treatment, the mass fraction *w* can be obtained by the following equation with the size ratio of host/guest particle k_H (Thomas et al. 2009) for perfectly ordered systems:

$$w = \frac{4C_{2D}(k_H+1)^2}{4C_{2D}(k_H+1)^2 + \frac{\rho_H}{\rho_I}{k_H}^3} \qquad \textbf{II. 2}$$

$$k_H = \frac{R_H}{R_I} \qquad \textbf{II. 3}$$

C_{2D} is the surface packing fraction in two dimensions of the guest particles on the surface of host particle. ρ_H and ρ_I: densities of host and guest particle. R_H and R_I: the radius of host and guest particles, respectively.

Supposing that C_{2D} is that of a hexagonal compact structure with C_{2D} = 0.906, the mass fraction of guest particles for 100 % coverage is estimated to be 4.8 %. This theoretical value may be subject to variations according to the type of particles (densities, radius ratio…). In real experiments, a part of the materials may also be stick on the walls of the mixer, and it would be better to choose a higher value like 5% minimum. On the contrary, a large particle size distribution of fine particles would rather induce lower values for the critical mass fraction *w* by increasing the mean size ratio k_H.

In the following, the mass fraction of guest particles introduced in the chamber at the beginning of the process w_0 will be fixed at 5 % to see clearly the effects of process conditions, even if a smaller value could be more realistic and efficient enough for modifying surface properties.

II. 4. Characterization methods

Different characterization methods have been used after treatments. The surface morphology of the particles have been analysed by scanning electron microscopy (SEM) techniques. The SEM allows us to analyse the surface morphology of the particles and also to identify the guest particles on the surface of the host particles. Malvern Mastersizer 2000 laser diffraction granulometer has been used in dry method, in order to analyse the different size distributions of the particles and also to evaluate qualitatively the interactions between the guest and host particles by changing dispersing air pressures. Modification of different surface properties of the particles has been analysed by using different techniques. Freeman technology powder rheometer (FT4) has been used in order to analyse the flowability properties of the powders. The angle of contact measurement has been carried out to evaluate the wettability of the products. The measurement of conversion ratio has been done by sieving the products. The real particle motion has also been visualized with transparent vessel of the mixer and characterized by PIV method.

4.1 Morphology

It is quite important to realise the morphological analysis in order to know what exactly happens to the particles. In this research work, the SEM, and particle size analyse by means of laser diffraction methods have been used

4.1.1 Scanning Electron Microscopy

The SEM is a common method for visual analysis of the different surfaces. It allows us to observe the surface morphology of the sample with different ambient pressures and in different media (dry & wet). The detail of this apparatus would be shown in **Appendix 2.**

In this study the ESEM type XL30, manufactured by Philips have been used in order to have the visual analysis of the particles before and after treatments. The SEM observations have

been done all the time in samples with 1–20 torrs pressure. The EDX method has also been used in order to have chemical characterization of the surface of the particles.

4.1.2 Particle size distribution (Laser Diffraction Granulometer)

The particle size distribution of the powders was measured by a laser diffraction method using the Mastersizer 2000 from Malvern Instruments Ltd. The equipment uses the diffraction of a laser beam in order to find the particle size distribution of powders between 0.02 μm and 2000 μm range.

The Mastersizer essentially consists in a laser transmitter and a receiver (300 RF lens) unit, detectors, a dry powder feeder (Scirocco 2000) unit with an air venturi in order to control the dispersing air pressure and a cyclone (**Fig. II. 6**).

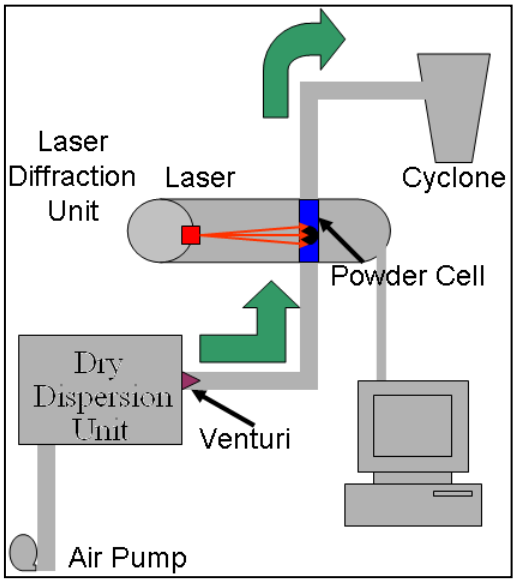

Fig. II. 6 Basic Configuration of Laser Diffraction Granulometer

A representative powder sample is placed in the feeder unit and a vacuum is switched on. The vacuum draws the powder sample into the instrument with chosen dispersing air pressure (up to 4 Bars).

In this apparatus powder de-agglomeration is controlled by adjusting the dispersing air pressure. The variation of the pressure (P) with corresponding air velocity (V) in the venturi can be seen in **Fig. II. 7**. For the dry coating, it can be applied for estimating the bonding force between host and guest particles. That is to say, by measuring the Particle Size Distribution (PSD) at different air pressure, probably we can observe the detachments of guest particle from host particles (Vilela et al. 2006). This study, the air pressures were varied from 0.5 to 3.5 Bar to observe so-called ‘liberation" pressure of each coated particles. The measurements have been done three times each simple to have the average value.

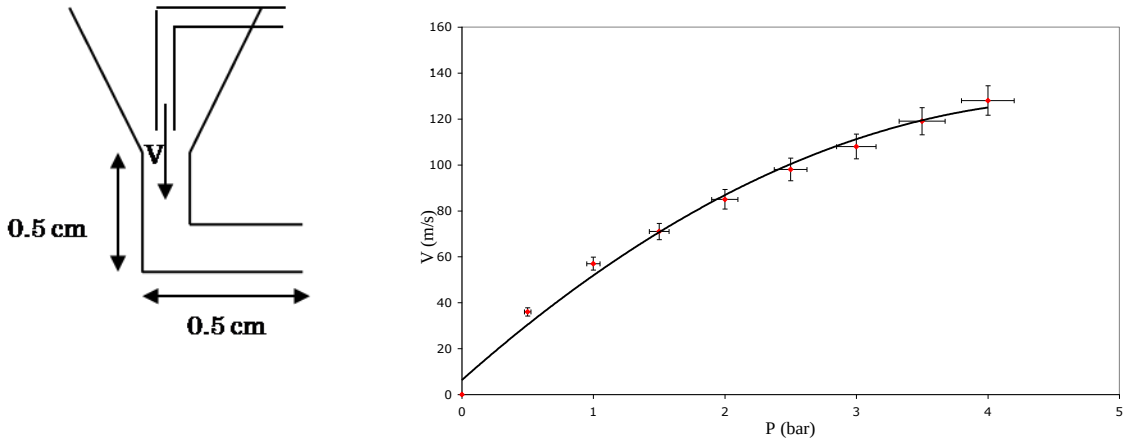

(a) (b)

Fig. II. 7 Air Venturi of the Granulometer : a) Dimensions of the Venturi b) Pressure vs. Corresponding Air Velocity in the Venturi

4.2. Pycnometry

The density of the powders was measured using a helium pycnometer (Accupyc 1330, Micromeritics) which works on the basis of gas displacement. The instrument determines the solid density of solid objects or powders based on the following equation assuming an ideal gas:

$$V_{Pyc} = V_C + \frac{V_a}{1 - \frac{P_1}{P_2}} \qquad \textbf{II. 4}$$

The general principle is that the solid powder sample of unknown volume V_P is placed in a known sample cell volume V_C, and pressurized with helium gas to the desired target pressure P_1. The pycnometer has an internal "added volume" chamber (V_a) which is added to the cell volume by opening a valve between the two chambers. The resulting lower pressure P_2 is then recorded, allowing the calculation of V_{Pyc}. V_a and V_C are known through accurate calibration using the provided calibration spheres. The helium is able to fill all spaces open to the atmosphere, including the pores inside the powder sample. The solid density is calculated from the volume of sample and the known sample mass. The instrument reports an average value from the number of runs specified by the user.

4.3 Flowability (FT-4 Freeman Powder Rheometer)

The FT4 Powder Rheometer is a device that is able to classify powders by their flowability. The aim of this device is to provide an automated testing program that is relatively independent of the operator and rapid measurement. It has a special profile propeller type blade which can be rotated and simultaneously moved axially into a powder cell and axial and rotational forces can be measured (**Fig. II. 8**).

Fig. II. 8 FT-4 FREEMAN powder rheometer

There are different kinds of control variables on both axis such as velocity, force and torque. All powder samples are pre-conditioned using the instrument's conditioning methodology to have a homogeneously packed powder bed. The conditioning blade action gently disturbs the powder bed and creates a uniform, lightly packed test sample that can be readily and consistently reproduced. The conditioning cycle is composed of a traverse of the blade downward towards to the bottom of the powder cell and then a traverse upward. The downward traverse would typically use a 5° positive helix in order that the blade action is more slicing than compacting. The upward traverse would typically use a 5° negative helix that gently lifts the powder and drops it over the blade. In both upward and downward movement of the blade for conditioning the tip speed of the blade is constant and 100 mm/s. This process removes any packing history such as pre-consolidation or excess air (Freeman, 2007).

After the conditioning step, different types of test programs for different rheological

characteristics of powders can be used. In the test programs, the blade moved along a downward helical path, but in the opposite direction, to impose a compaction regime, thereby forcing the power to flow around the blade. In this study, flow rate index FRI program, which includes 4 different test cycles with 4 different blade tip speeds (100 mm/s, 70 mm/s, 40 mm/s, 10 mm/s) has been used in order to characterize the flowability properties of the powders. It allows determining the sensitivity of the powder samples to the stirrer blade speed. The flow rate index values for the powders are calculated by dividing the 11th total energy value to the 8th total energy value. Higher the FRI value, lower the flowability of the particles (Freeman, 2007). A typical total energy according to tip speed graph can be seen in **Fig. II. 9**.

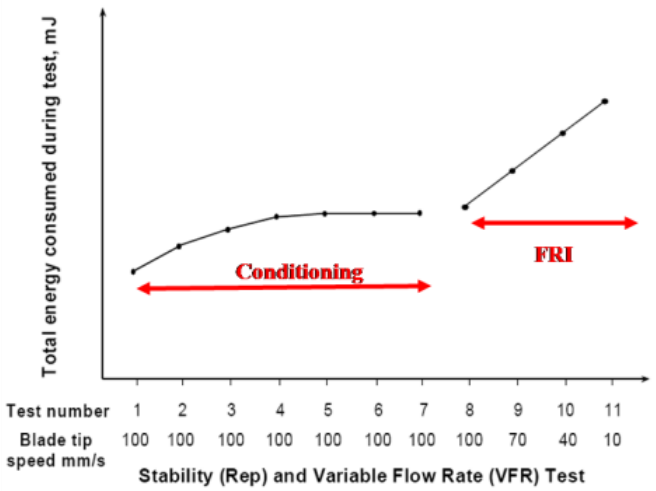

Fig. II. 9 Example of the FT-4 measurement: Total energy as a function of blade speeds

The typical data of the FRI introduced by Freeman is shown in **Fig. II. 10**.

According to the instruction of Freeman, the powder is normally exhibited by very cohesive when the FRI has over a value of 3.0 (**Fig. II. 10 (a)**). The FRI of almost all the powder is characterized from 1.5 to less than 3.0 (**Fig. II. 10 (b)**). When the FRI is given around 1.0, it can be said that the powder is insensitive to the FRI.

Usually those powders have large particle size or are done some surface treatments such as a coating of lubricant. If the powder is pseudo-plastic or Newtonian, that is to say, very free flowing characteristics, the FRI would be given less than 1.0.

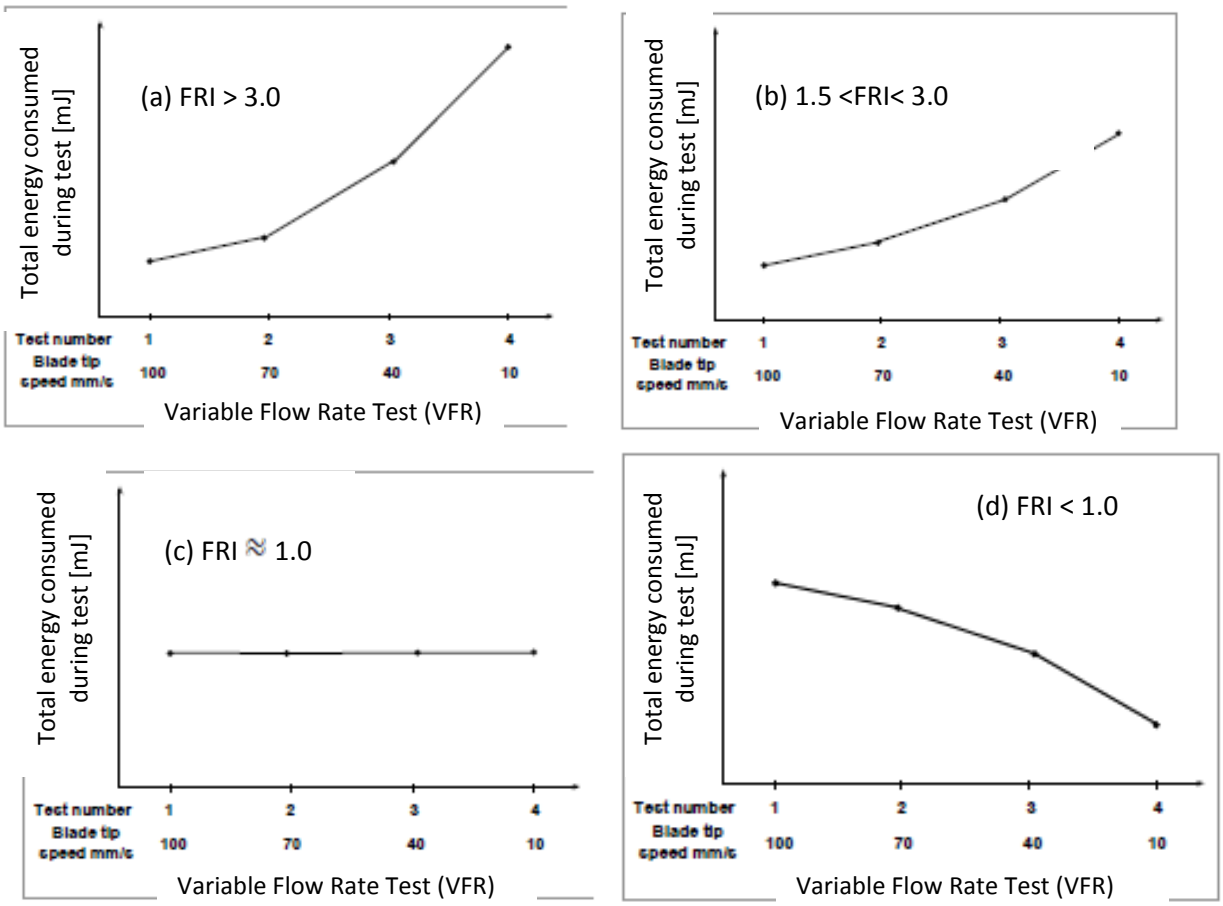

Fig. II. 10 Typical data of FRI

4.4 Wettability (The contact angle measurement)

The contact angle measurement is used to determine the wettability property of a solid by a liquid. Generally, the determination of the contact angle is conducted using the sessile drop method. The liquid is dropped by a micro syringe on the solid and the contact angle between the baseline of the drop and the tangent at the drop boundary is measured. Young formulated a relation between the interfacial tension γ at a point on a three phases contact line (**Fig. II. 11**).

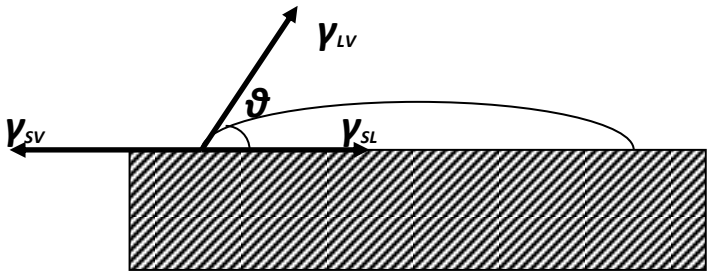

Fig. II. 11 Schematic diagram of the contact angle measurement

The indices 'S' and 'L' stand for solid and liquid, γ_{SL} and γ_{LV} describe the surface tension components of the two phases whereas γ_{SL} represents the interfacial tension between the phases and θ stands for the contact angle corresponding to the angle between vector γ_{SL} and γ_{LV}. Young formulated the relationship between these quantities;

$$\gamma_{LV} * \cos\theta = \gamma_{SV} - \gamma_{SL} \qquad \textbf{II. 5}$$

In contact angle measurements, powder beds have been prepared for each powder sample. A liquid drop of controlled volume (10 µl and around 3 mm diameter) is placed on the powder bed of the particles and then photographed. The contact angle is determined by drawing a tangent to the profile at the point of three-phase contact after the drop profile has been enlarged by image projection.

In this research work, a small 10 µL drop of distilled water is deposited on the surface of a bed of the powder product at room temperature, and the contact angle measured 30 s after the moment the drop is deposited. In addition, to avoid breaking the coating or the particles themselves, the powder bed was not compressed but just patted down with a spatula to give as

homogeneous a flat powder surface as possible. The contact angle measurement was carried out three times on each sample and the average value taken.

4.5 Kinetic study by evaluation of conversion ratio

To estimate how many guest particles attach on the surface of host particles by dry coating treatments with different operation conditions, in other word, the progress of dry coating, the coated particles are sieved. The conversion ratio which could express the progress of dry coating is to be obtained by following protocol (**Fig. II. 12**).

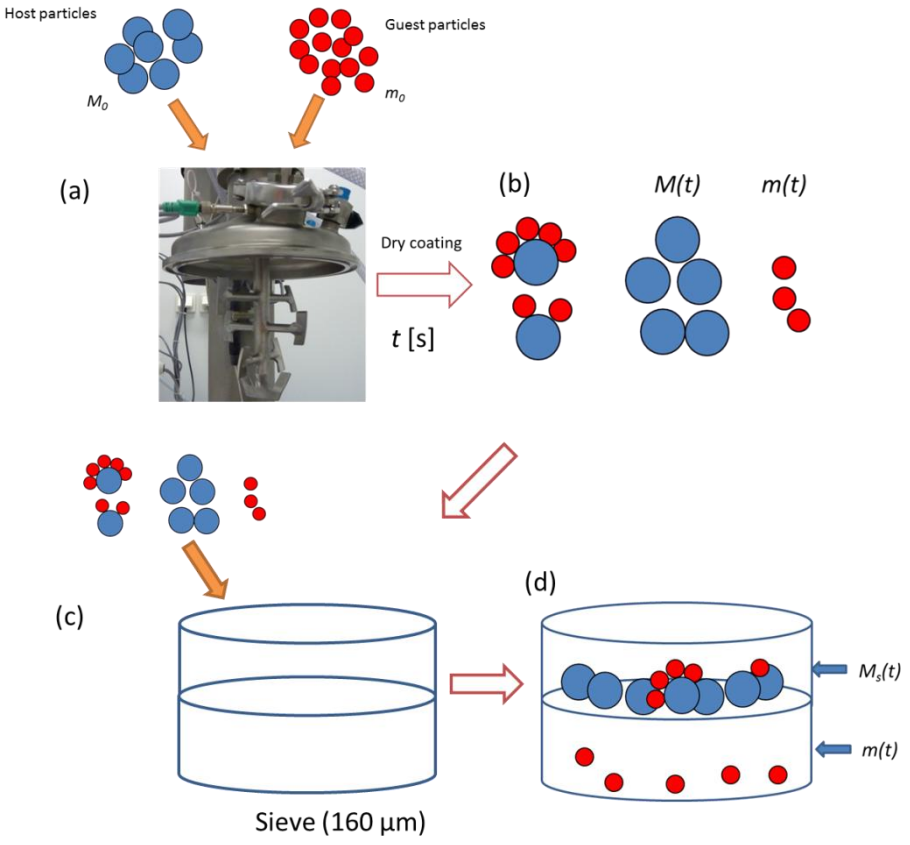

Fig. II. 12 Protocol for measuring the conversion ratio

Fixed quantities of MgSt (mass m_0) and Suglets (mass M_0) are introduced in the mixer, with a mass fraction $w_0 = m_0/(M_0+m_0) = 5$ % (**Fig. II. 12 (a)**). After a mixing time t, in given operating conditions some of the grains of Suglets are coated, with a mass $M_0 - M(t)$, and the

others, with a mass *M(t),* are not coated. Thus some of the guest particles remain as free particles, with a mass *m(t)*, and a mass m_0 - *m(t)* of guest grains are stuck on the surface of host particles to form a coating (**Fig. II. 12 (b)**). We suppose that only a very small quantity of Suglets or MgSt remains attached to the wall or the blades of the mixer, and the powder mixture removed from the mixer is representative of the total volume of the particles (guest and host) introduced in the mixer.

To estimate the effective mass fraction of guest particles coating the host particles, the total volume of the mixture was sieved at 160 µm for 10 min (**Fig. II. 12 (c)**). Neglecting the possibility that guest particles could be liberated by shear or impact forces during the sieving, and neglecting the possibility that host particles could be broken during “mixing", the mass *m(t)* of particles passing through the sieve can be considered to be the amount of guest particles that did not stick to the host particles during the process.

By measuring the mass *m*(*t*) and the mass $M_S(t)$ of the powder that remained on the sieve, the effective mass fraction of MgSt, w_e in the coated product can be estimated, after a time *t* of mixing by **Eq. II.6** (**Fig. II. 12 (d)**):

$$w_e(t) = \frac{m_0 - m(t)}{M_S(t) + m(t)} \; ; \; w_e(t) \sim \frac{m_0 - m(t)}{M_0 + m_0} \qquad \textbf{II. 6}$$

The parameters w_e and m_0 are the mass fraction of the product and the mass of the guest particles introduced into the high shear mixer before mixing.

The comparison of the values w_e and w_0 gives information on the degree of efficiency of the coating process. More precisely, the ratio λ can be regarded as a coating ratio (**Eq. II.7**).

$$\lambda(t) = \frac{w_e}{w_0} \; ; \; \lambda(t) = 1 - \frac{m(t)}{m_0} \qquad \textbf{II. 7}$$

4.6 Real particle motion – Particle Image Velocimetry (PIV)

To obtain the real particles velocity there are two major methods: one is the position emission particle tracking (PEPT), the other is Particle Image Velocimetry (PIV). The advantage of PEPT is that it is able to analyze the velocity of the particle inside of the mixer. However, it is limited the number of particles which can be analyzed, since the only positron emitting tracer particles can be analyzed. Ng et al. (2007) has analysed the particle velocity in the Cyclomix by PEPT, and Hassanpour et al. (2009) showed that the velocity obtained by PEPT agreed with simulated velocity by DEM.

The Particle Image Velocity can only analyze the particle near the transparent vessel. However it can analyze almost unlimited number of particles as long as they are located near the transparent vessel. In this research work, PIV method was carried out in order to analyze as large number of particles as possible. The PIV was developed initially as Laser speckles velocimetry for Young's fringes analysis (Dudderar and Simpkins 1977). In that research the specific characteristics of scattered called 'speckles' was used to allow the measurement of the displacements of the surface of sample subjected to strains. Generally it is used for visualizing the fluid with tracer particles.

However, PIV can also be used to measure the velocity field of the free surface and basal boundary in a granular flow such as those in shaken containers (Lueptow et al. 2005), tumblers (Jain et al. 2002) and avalanches (Pudasaini et al. 2007). This analysis is particularly well-suited for non-transparent media such as sand, gravel, quartz, or other granular materials that are common in geophysics. This PIV approach is called "granular PIV" (Pudasaini et al. 2007).

The set-up for granular PIV differs from the usual PIV setup in that the optical surface structure that is produced by illumination of the surface of the granular flow is already sufficient to detect the motion. In this research work, the PIV analysis was adopted to analysis of both experimental and numerical particle motions.

To visualize the particle motion in the mixer, the transparent acrylate vessel was toll

manufactured by Hosokawa Micron as seen **Fig. II. 13**.

To focus on real motion of the host particles, guest particles were not used in the experiments. The motion of the sample was taken by the high speed camera (FASTCAM SA1.1 Photron LTD) which is able to take over 5000 fps at mega pixel resolution**. Fig II. 13** shows the installation of the high speed camera.

Fig. II. 13 The installation of the apparatus (a) transparent vessel, (b) high speed camera.

The angle of the camera has been inclined at 75^{o} to avoid optical refraction effect (the angle of the vessel is 25^{o}). Finally, the motion of the particles near the transparent part of the chamber was observed for a given rotational speed. The resolution of the images is 1024 × 1024 pixels, and the acquisition frequency is fixed at 2000 Hz. The velocity field of the particles during mixing was measured from the recorded images by Particle Image Velocimetry (PIV) using PIV-lab version 1.131, open-source software.

The analysis field was limited to just around the main rotor in order to avoid the effect of light refraction. The experimental and simulated movements of the particles are observed on a comparable basis, and limited to the particles located just behind the vessel wall. The velocities are measured in a right handed coordinate system, though the rotation direction is clockwise (**Fig. IV. 14**). So, for horizontal velocity, it is expected to have negative values.

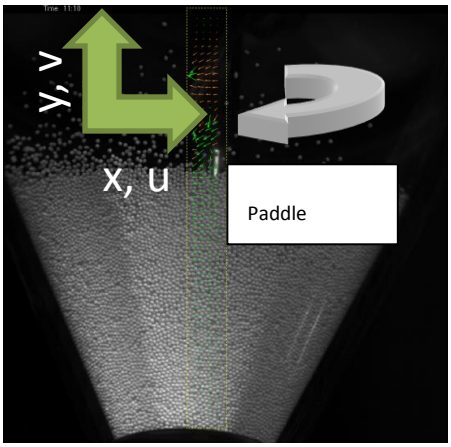

Fig. II. 14 Analysis field of PIV.

The obtained data from PIV were dealt with two aspects: one is velocity field. The other is the horizontal and vertical mean velocity. The velocity filed in which the obtained data (horizontal and vertical velocity of each element) simply plotted along with the horizontal axis is dealt at certain angle of rotation defined as **Fig. II. 15**.

As seen in **Fig. II.15**, 0° is fixed at when the top paddle comes in front of the camera axis, and 90° is fixed at the second paddle comes in front of the camera axis.

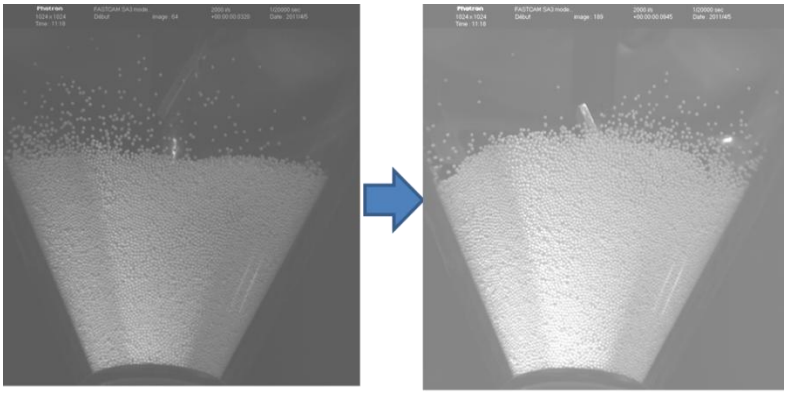

Fig. II. 15 Definition of angle of rotation.

The mean velocity is the value of total sum of either horizontal or vertical velocity of all element divided by the number of elements analyzed at each angle of impeller.

CONCLUSION

In this chapter, the description of dry coating apparatus, materials and characterization methods are given. The various characterization methods for analysing different surface properties (flowability, wettability, surface morphology etc.) can allow us to evaluate the effect of operating condition on dry coating clearly. Especially, the original method to evaluate the conversion ratio, which represents the degree of advancement of dry coating and should be one of the most important parameter, was introduced in this chapter. This method does not require some expensive apparatus to measure and can be applied in any case of dry coating. PIV method is introduced in this chapter. PIV allows us to access the velocity of particles that is generally difficult to obtain.

Chapter III Modelling of the particle motion in the mixer

III. 1. Introduction

First of all, as mentioned in chapter I, many efforts have been made in the development of dry particle coating to enhance the surface modification of powders. However, this technique is not yet in the commercial use. This is because they are still in the try and error state. In other words, it is difficult to predict the optimal process operation for the commercial use or/and to scale up to the industrial scale. There are few researchers that have studied the theoretical approaches for dry coating mechanism so that better understandings of dry coating which is able to optimize the process operation could be obtained. For instance, Mei et al. (Mei et al., 1997) developed an extended Johnson-Kendall-Roberts (JKR) particle model to include the effect of particle coating on the force-displacement relationship due to surface energy and elastic deformation. The method for determining the optimum operating conditions of equipment on dry coating processes based on the energy requirement for immobilizing the guest particles on the surface of host particles was established (Iwasaki et al., 2002). However, it is not yet enough to understand and to propose the universal method to optimize the dry coating. In addition, the theoretical modelling for such process, that is very important to optimize the process or to design new geometry of the coating apparatus, is found to be less comprehensive. Hence, the objective and the motivation of this study are also to understand the dry powder coating by numerical methods.

Meanwhile, computer simulation of dense-phase discrete particle systems was first reported by Cundall and Strack in 1979 (Cundall and Strack, 1979). The scheme developed was termed the ‘Distinct Element Method (DEM)’. This method is analogous to molecular dynamics simulation. However, the discrete element simulation of particles is more complicated because of the non-linear and non-central inter-particle interactions arising from adhesion, friction and presence of viscous fluid. There are different treatments of particle interactions in DEM simulation, for instance, soft spheres and hard spheres models are available. The hard spheres approach assumes that the particles interact by instantaneous collisions. Linear and angular momentum is balanced using collision operators to dissipate energy. Such a

simulation uses a kinematic approach that describes the individual particles by their instantaneous positions and velocities. Hard spheres simulations are mainly concerned with rapid granular flows (Campbell and Brennen, 1985).

In contrast to hard spheres where the collisions are instantaneous, in soft spheres undergo some deformations during collisions and the spheres have a finite contact time. This is generally a better representation of what actually happens during impacts. So the soft spheres method is one of the most common discrete element simulation techniques since it can handle a variety of inter-particle forces. In soft spheres simulation, the interactive forces exerted on each particle are computed as continuous functions of the distance between contiguous particles and are based on physically realistic interaction laws. Even though this approach is computationally intensive, it can provide information on the structure and dynamics of systems including details of position, velocities, forces and energy partitions. During the simulation, the forces acting on each particle in the system are calculated. Newton's second law is then used to determine the resulting accelerations for each particle, which are then integrated in time to find the particle's new state. This procedure is repeated until the end of simulation. In this thesis, this soft sphere method has been used. In this chapter, the principle of the DEM and then the application to the high shear mixer are shown.

III. 2. Modelling of the high shear mixer system

2.1 Designing the apparatus

Fig. III. 1 shows the geometry of the high shear mixer "Cyclomix" modelled for the DEM simulation. This geometry was constructed from the drafting of Hosokawa Micron (producer of this high shear mixer device) shown in **Appendix 1**. This geometry consists in the cylinders for the impellers and a conical shaped chamber. Paddles are made of triangle meshes. The contact detection between particles and cylinders will not be explained in this thesis because it uses only the simple geometric contact detection.

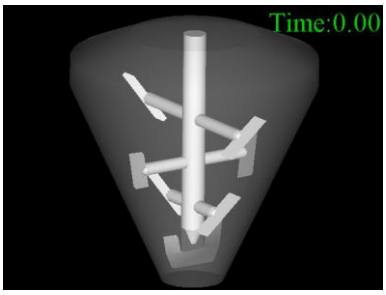

Fig. III. 1 The geometry of the modelled high shear mixer "Cyclomix"

2.2 Performing a numerical experiment

Since the DEM is relatively computationally intensive, which limits either the length (time) of a simulation or the number of particles, in our study the numerical experiments carried out have neither taken into account the real mixing time nor the real particle size due to the computational limitation. . Even though it is not representing exactly the real experiments, it is important to know the information of particle motion inside a mixing chamber, which can hardly be obtained from the experiments, for optimization of operation conditions. Because dry coating is generally done by mechanical forces given by the mixer, information of every single particles, such as normal and shear forces acting on the particles, velocities, kinetic energy and so on are directly related to the dry coating performance. As explained, the

simulations were calculated during a few seconds, which are long enough for particle motion to reach the steady state and the outputs obtained from the simulation are investigated for the dry coating. The image of these numerical approachs is shown in **Fig. III. 2**.

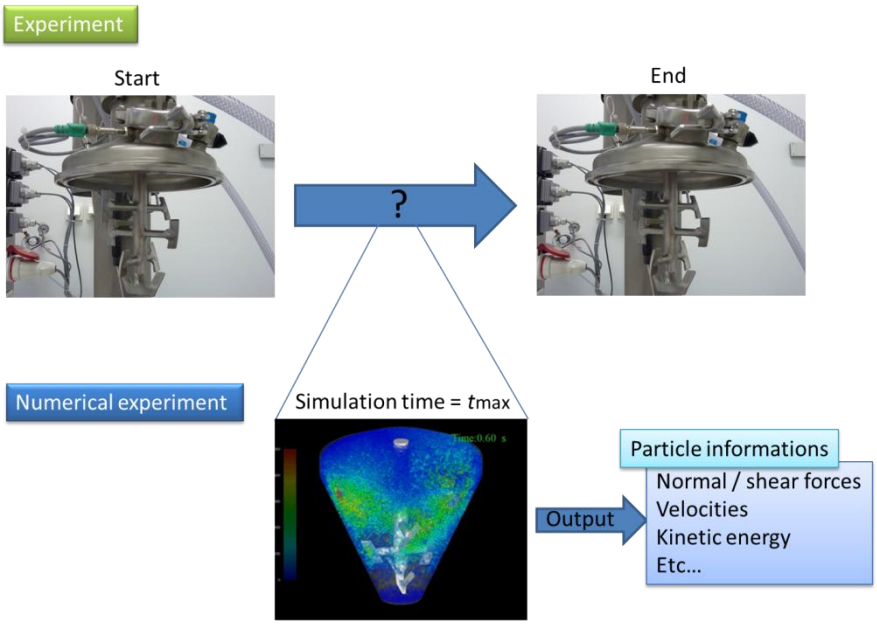

Fig. III. 2 Image of the numerical experiment

The installation of particles is done by the source code developed using Microsoft Visual Basic 2005 as shown in **Fig. III. 3**.

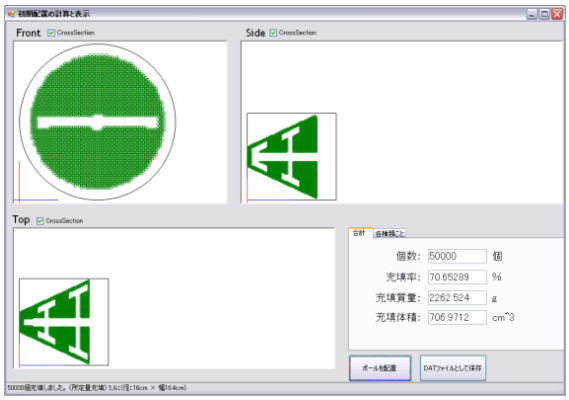

Fig. III. 3 Installation of particles

The host particles were placed in the vessel of the high shear mixer with a hexagonal-close packed structure. Those particles are placed not to have a gap between particle-particle and particle-boundary of a high shear mixer in order to avoid numerical errors.

This initial coordination of particles is given to the main simulation code. The main simulation is done using a Fortran 90 coded program based on the source code developed by Saito Lab (IMRAM of Tohoku University). The Compiler is the Intel Fortran Complier 11.1. The interest of the simulation of the particle motion in a high shear mixer is to understand the effect of the operating conditions such as rotational speed of the impellers ω, filling ratio *J* and particle size. The number of the particles *N* required to the calculation is obtained by the following equation. As explained in Chapter II, the total volume of the sample can be obtained at given filling ratio, then supposing all the particles are ideal spheres, of uniform size. The volume of each particle is $\frac{4}{3}\pi r^3$, where *r* is the radius of each particle, and the number of particles in the system will be given by:

$$N = \frac{V_p}{\left(\frac{4}{3}\pi r^3\right)} \qquad \textbf{III. 1}$$

Where V_p is the total volume of particles.

III. 3 Principle of DEM simulation

The application of DEM to a high shear mixer system has been introduced in previous section. In this section, the principle of DEM method will be shown.

In general, the DEM simulation proceeds as following procedure (**Fig. III. 4**).

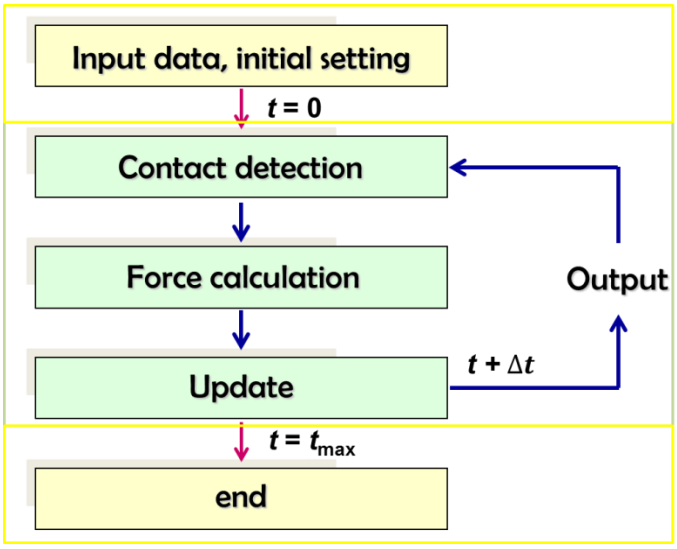

Fig. III.4 Procedure of DEM simulation

Input data and initial settings are done by the source code of Visual Basic as explained above. The data of initial settings is given to the main simulation code and then the simulation starts. The procedure of DEM is firstly, to detect all the collision happening in the system, secondly to calculate the interaction forces. Finally from the derived forces acting on each particle are applied to calculate the accelerations, velocities and coordination of every single particle according to the Newton's second law of motion at each time step. This procedure continues until the simulation time reaches the defined time. The method of each procedure would be explained in this section.

3.1 Spatial partitioning (contact detection)

Handling the high level of discreteness of granular systems, which is further emphasized by practically always "hard" contact interactions, makes discrete element simulations algorithmically complex. Finding the element pairs which are "close" to each other is the most challenging part of the computation. Solving this purely geometrical problem, which is mostly independent of the way the interactions are calculated, should not affect the outcome of the simulations. It is only a mean to increase their efficiency. Indeed, the overall power of a discrete element simulation program depends very much on building – as fast as possible – a sufficiently tight set of possibly interacting element pairs and applying the interaction model only on these pairs. In practice, it makes no sense to find the tightest set of such element pairs because the condition whether they are interacting or not is inevitably tested once more when the interactions are calculated. In fact, one could also consider all the possible pairs and let the interaction model select those that are really interacting and neglect the others. This naive $O(N^2)$ method (where N is the number of participating elements, and N^2 the number of tests necessary in each time step of contact detection) is very inefficient even for relatively small systems. Below, we present some algorithms, which can improve the speed of interaction calculation to $O(N\log(N))$. For a two-dimensional system of disks that interact only when they come into contact, the geometric constructions used by these algorithms are outlined in **Fig. III. 1**. Probably the simplest way to find particles, which are close to each other, is to divide the space into uniform cells of a given size and "assign" each particle to the cell in which its center point is located (see **Fig. III. 5 (a)**). Then the possible interacting particles are found by checking the neighboring cells. Because of its simplicity, this method is widely used in distinct element simulations. If the particles and the cells have more or less the same size and thus in average each cell contains one single particle, this uniform grid gives a solution close to optimum. However, if there are both very small and very large particles in the simulated system, then this becomes less efficient. In case of a fine grid, having a cell size close to the size of the smallest particle, not only the adjacent cells but also second or higher

order neighbors are to be considered. In a region where the particles are predominantly small, this is needless and a waste of time. If we consider a coarse grid, having a cell size close to the size of the largest particle, then a grid cell can contain many small particles. In a region where the size of the particles is again predominantly small, the large majority of the particles in one cell is not in contact with any particle in the adjacent cells. Consequently, applying the contact model between these particles is again no more than a waste of CPU time.

The problems above mentioned are solved by using an adaptive cell size (Müller 1996, Hoffmann 2006). Starting from a sufficiently large box, containing all the particles, the space is divided into smaller boxes. Each box, which contains more than one particle, is further divided into even smaller boxes. The procedure is repeated until each box contains no more than one particle. This leads to a hierarchical structure. At least on the highest level, this should accommodate the shape of the simulated system (see **Fig. III. 5 (b)**). Neighboring particles are found by considering nodes that are hierarchically close to each other. This method is more efficient than a uniform grid only when the particles have a wide size distribution. Then in this research, the hierarchical grid method is adopted.

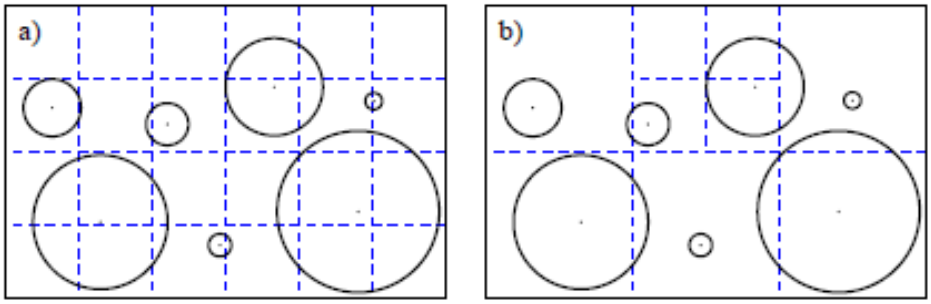

Fig. III. 5 Geometric constructs used to speed up the detection of interacting element pairs : (a) fixed grid, (b) hierarchical grid

3.2 Model for inter-particle forces

In the reality, a particle can undergo translational and rotational motion, depending on the forces and torques acting on it. This may come from interactions with neighbouring particles, confining walls or paddles and with a surrounding fluid (air). The motion of particles is affected not only by the forces and torques originated from neighbouring particles and vicinal fluid, but also by the fluids coming far away from the contact points considered (drag force). The complexity of such a process has defied any attempt to model this problem analytically. Even for the numerical approach, proper assumptions have to be made in order that this problem can be solved effectively without an excess requirement for computer memory or expensive iterative procedure. It has been established that if a time-step is chosen to be less than a critical value, these forces and torques can be determined from the interactions between the particles and their immediate neighbours (Cudall and Strack 1979, Xu and Yu 1997). The interaction caused by fluid (drag force) has been ignored in the present work that deals with low-viscosity fluid (air). The long-range forces, such as Van der Waals and electrostatic forces have been also ignored to shorten the calculation time. Hence, only the contact force caused by particle-particle and particle-wall contacts has been taken into account.

When two particles are close one to each other, the condition of contact between a sphere i (radius r_i) and a sphere j (radius r_j) is given by **Eq.(III. 2),** where R_{ij} is the distance between the centers.

$$r_i + r_j \geq R_{ij} \qquad \textbf{III. 2}$$

When contact events happen, occurring forces and momentums between two particles can be shown such as **Fig. III. 6**.

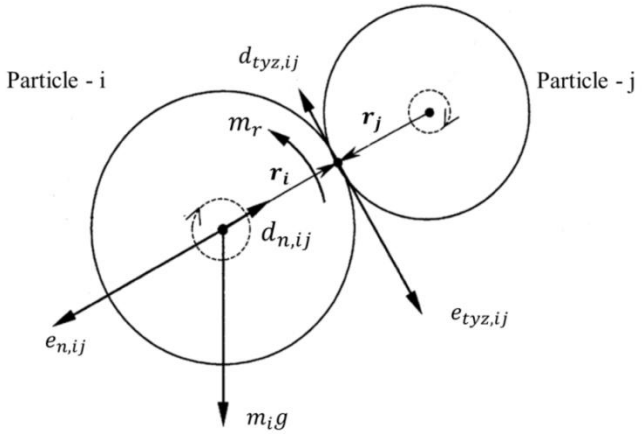

Fig. III. 6 Two dimensional illustration of the forces acting on particle *i* in contact with particle *j*

The inter-particle force acting at the contact point, $\boldsymbol{F_{ij}}$ is decomposed into the normal force $f_{\mathrm{n,ij}}$ and tangential forces $f_{\mathrm{ty,ij}}$, $f_{\mathrm{tz,ij.}}$ This force $\boldsymbol{F_{ij}}$ can be expressed by the equation:

$$\boldsymbol{F_{ij}} = \boldsymbol{e}_{\mathrm{ij}} + \boldsymbol{d}_{\mathrm{ij}} \qquad \textbf{III. 3}$$

Taking into account the elastic force, $\boldsymbol{e}_{\mathrm{ij}} = \begin{bmatrix} e_{\mathrm{n,ij}} \\ e_{\mathrm{ty,ij}} \\ e_{\mathrm{tz,ij}} \end{bmatrix}$ and the viscous damping force $\boldsymbol{d}_{\mathrm{ij}} = \begin{bmatrix} d_{\mathrm{n,ij}} \\ d_{\mathrm{ty,ij}} \\ d_{\mathrm{tz,ij}} \end{bmatrix}$.

The subscripts n and t represent the normal and the tangential components.

To obtain the elastic and viscous damping force, the simulation model shown in **Fig. III. 7** has been used. This simulation model consists of the spring and viscous dashpot approach to express elastic and viscous damping force respectively. A slider is also implemented in the tangential component of the contact force to consider the frictional interaction.

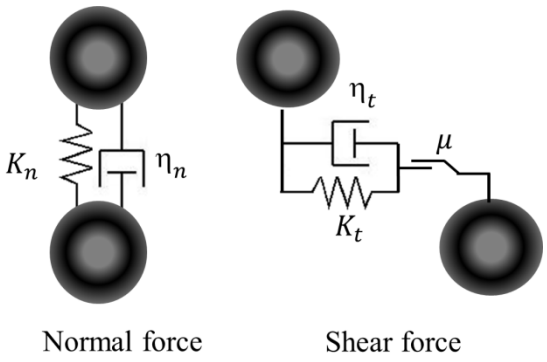

Fig. III. 7 The simulation model of inter-particle force between two particles

From this model, the elastic force $\boldsymbol{e}_{\mathrm{ij}}$ and the viscous damping force $\boldsymbol{d}_{\mathrm{ij}}$ are expressed by **Eq. III. 4**.

$$\boldsymbol{e_{ij}} = \begin{pmatrix} K_n \Delta u_n \\ K_t \Delta u_{ty} \\ K_t \Delta u_{tz} \end{pmatrix}, \boldsymbol{d_{ij}} = \begin{pmatrix} \eta_n \dfrac{\Delta u_n}{\Delta t} \\ \eta_t \dfrac{\Delta u_{ty}}{\Delta t} \\ \eta_t \dfrac{\Delta u_{tz}}{\Delta t} \end{pmatrix} \qquad \textbf{III. 4}$$

Where, K and η mean the spring and the damping coefficients. Δt represents the timestep in the simulation. Δu_{n}, Δu_{ty} and Δu_{tz} are the relative displacements between centres of two particles for normal and tangential components as shown in **Fig. III. 8**.

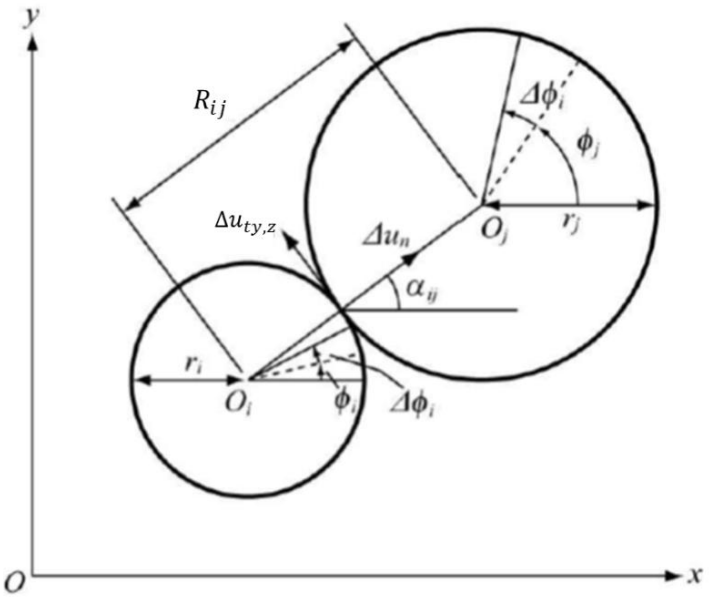

Fig. III. 8 Illustration of displacements in two dimensions.

In the shear direction, to take the effect of friction into account, the following condition equation (**Eq. III. 5**) is added into **Eq. III. 4** that can also be considered as a sliding condition, according to the Coulomb's law of friction.

If $e_{\mathrm{t,ij}} = \sqrt{{e_{\mathrm{ty,ij}}}^2 + {e_{\mathrm{tz,ij}}}^2} > \mu e_{\mathrm{n,ij}}$ then,

$$e_{\mathrm{ty,ij}} = \mu e_{\mathrm{n,ij}} \frac{e_{\mathrm{ty,ij}}}{e_{\mathrm{t,ij}}}, d_{\mathrm{ty,ij}} = 0, e_{\mathrm{tz,ij}} = \mu e_{\mathrm{n,ij}} \frac{e_{\mathrm{tz,ij}}}{e_{\mathrm{t,ij}}}, d_{\mathrm{tz,ij}} = 0 \qquad \textbf{III. 5}$$

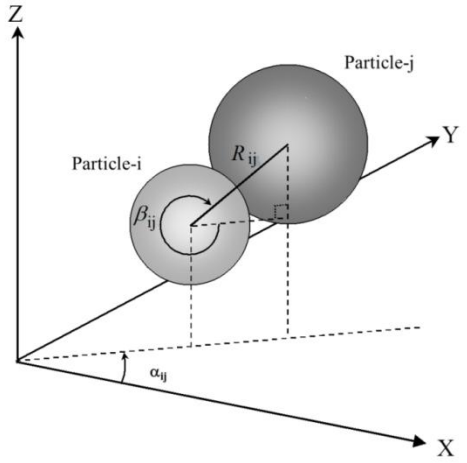

Fig. III. 9 Contact angles between two particles

From these models, the net forces acting on the particle *i* are now to be obtained.

These inter-particle forces are required to be converted into x-, y-, z coordinates by using the coordinate transform matrix of rotation in order to get the net force acting on the particle *i*, when the angles of contact of two particles are defined as **Fig. III. 9**. Finally, the net force acting on the particle *i*, in *x*-, *y*- and *z*-coordinates $\boldsymbol{F}_{\mathrm{xyz,i}} = \begin{bmatrix} f_{x,i} \\ f_{y,i} \\ f_{z,i} \end{bmatrix}$ is given by **Eq. III. 6**.

$$\boldsymbol{F_{xyz,i}} = \sum_{j}^{k_i} \begin{pmatrix} \cos\alpha_{\mathrm{ij}} & -\sin\alpha_{\mathrm{ij}} & 0 \\ \sin\alpha_{\mathrm{ij}} & \cos\alpha_{\mathrm{ij}} & 0 \\ 0 & 0 & 1 \end{pmatrix} \begin{pmatrix} \cos\beta_{\mathrm{ij}} & 0 & \sin\beta_{\mathrm{ij}} \\ 0 & 1 & 0 \\ -\sin\beta_{\mathrm{ij}} & 0 & \cos\beta_{\mathrm{ij}} \end{pmatrix} \boldsymbol{F_{ij}} + M_i \boldsymbol{g} \qquad \textbf{III. 6}$$

Where $M_{\mathrm{i}}\mathbf{g}$ is the gravitational force. The force acting on the particle *i* is expressed as the sum of the inter-particle forces over k_{i} particles in contact with particle *i*. The shear forces act at the contact point between particle *i* and *j* rather than at the particle centre and it must generate the momentum $\boldsymbol{m_{xyz,i}} = \begin{bmatrix} m_{x,i} \\ m_{y,i} \\ m_{z,i} \end{bmatrix}$, causing the particle *i* to rotate. The net momentum acting on particle *i* can be expressed also by being converted into the x- y- z- coordinates and accumulating each momentum caused by k_{i} particles in contact with particle *i* (**Eq. III. 7**).

$$\boldsymbol{m_{xyz,i}} = r_i \sum_{j}^{k_i} \begin{pmatrix} 0 & \cos\alpha_{\mathrm{ij}}\sin\beta_{\mathrm{ij}} & \sin\alpha_{\mathrm{ij}} \\ 0 & \sin\alpha_{\mathrm{ij}}\sin\beta_{\mathrm{ij}} & -\cos\alpha_{\mathrm{ij}} \\ 0 & \cos\beta_{\mathrm{ij}} & 0 \end{pmatrix} \boldsymbol{F_{ij}} \qquad \textbf{III. 7}$$

The relative rotation between contacting spheres or between a sphere and a wall in contact

should produce a rolling resistance (**Fig. III. 6**), due to the resulting elastic hysteresis loss or time-dependent deformation (Tabor 1952, Tabor 1955). For the modelling of this physical phenomenon, there have been a few equations proposed (Brilliantov and Poschel 1998, Greenwood et al. 1960).

In this research work, the model proposed by Kawaguchi et al (1993) has been chosen. The rotational resistance momentum, $\boldsymbol{m_r}$ is defined as a function of rotational friction μ_r and the stress acting on the contact area created by two particles in contact such as:

$$\boldsymbol{m}_r = -\frac{3}{8}\mu_r a f_{n,ij}\frac{\boldsymbol{\varphi_i}/\Delta t}{|\boldsymbol{\varphi_i}/\Delta t|} \qquad \textbf{III. 8}$$

Where a is the radius of contact area, $\boldsymbol{\varphi_i}$ is the angular displacements of x-, y- and z-coordinates of the particle i as shown in **Fig. III. 8**.

Finally, the net force and momentum acting on the particle i are considered..

3.3 Properties of particles

From the above section, all the force and momentum acting on the particle was described from the simulation model shown in **Fig. III.7**. Then, it is required to have the value of spring coefficients (K_n and K_s) and dumping coefficients (η_n and η_t), to execute numerical experiments. In this research work, the spring coefficient were based on the Thornton and Yin's model without adhesion (Thornton et al., 1991) as described in **Eqs.(III. 9, 10, 11, 12).**

$$K_n = 2E^* a \qquad \textbf{III. 9}$$

$$K_t = 8G^* a \qquad \textbf{III. 10}$$

$$\frac{1}{E^*} = \frac{1-\nu_i^{\,2}}{E_i} + \frac{1-\nu_j^{\,2}}{E_j} \qquad \textbf{III. 11}$$

$$\frac{1}{G^*} = \frac{2(1+\nu_i)(2-\nu_i)}{E_i} + \frac{2(1+\nu_j)(2-\nu_j)}{E_j} \qquad \textbf{III. 12}$$

Where, E and ν denote the Young's modulus and the Poisson's ratio of particle, respectively. a means a radius of a circular area of a contact. Thus, the non-linear value of the spring coefficient has been introduced in this simulation.

From the equation of motion in the system of spring and dashpot, the damping coefficient is expressed by **Eqs. (III. 13)** and **(III. 14),** where m^* is the average mass of a particle, as shown in **Eq. (III. 15)**.

$$\eta_n = 2\gamma\sqrt{m^* K_n} \quad \textbf{III. 13}$$

$$\eta_t = 2\gamma\sqrt{m^* K_t} \quad \textbf{III. 14}$$

$$\frac{1}{m^*} = \frac{1}{m_i} + \frac{1}{m_j} \quad \textbf{III. 15}$$

Where, γ can be obtained from the coefficient of restitution of Newton (ratio of velocities after and before the collision) e (Kawaguchi et al. 1992). This relationship between γ and coefficient of restitution e (**Eq. III. 16**) can be derived from solving the equation of motion in the spring-dashpot system (Kawaguchi et al. 1992).

$$\gamma = -\frac{\ln e}{\sqrt{\pi^2 + \ln^2 e}} \quad \textbf{III. 16}$$

3.4 Updating the particle coordination

The normal and the shear forces, as well as the momentum acting on a particle from all contacts, are discussed and obtained from previous sections, and then the accelerations of each particle can be calculated by the following equations (Newton's second law of motion).

$$\left[\frac{d^2\boldsymbol{u}_i}{dt^2}\right]_t = \frac{\left[\boldsymbol{F}_{xyz,i}\right]_t}{m_i} \quad \textbf{III. 17}$$

$$\left[\frac{d^2\boldsymbol{\varphi}_i}{dt^2}\right]_t = \frac{\left[\boldsymbol{M}_{xyz,i} + \boldsymbol{M}_r\right]_t}{I_i} \quad \textbf{III. 18}$$

Where, $\boldsymbol{u}_i = \begin{bmatrix}\Delta x_i \\ \Delta y_i \\ \Delta z_i\end{bmatrix}$ is defined as the displacement of particle i in x- y- and z- coordinates and $\boldsymbol{\varphi}_i$ is the angular displacements of x-, y- and z-coordinates of the particle i as illustrated in **Fig. III.10**. I_i is moment of inertia of the particle i.

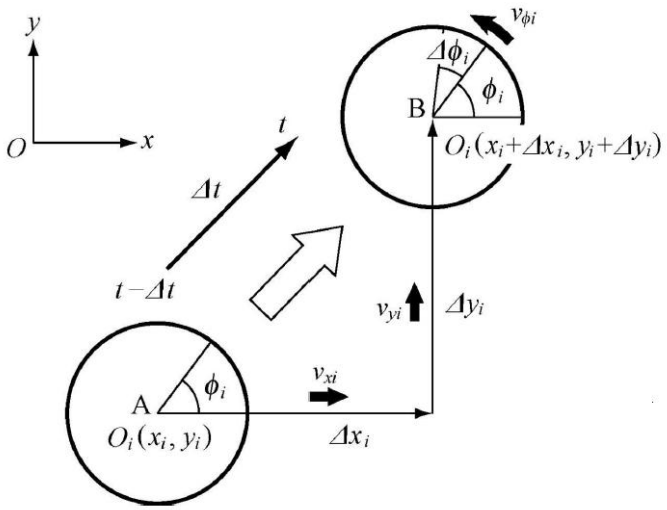

Fig. III. 10 Two dimensional illustration of displacements of particle *i*.

The translational and the angular velocities of *i*-th particle for *x*-, *y*- and *z*- components are given by integrating of Eqs.(**III. 18**) and (**III. 19**) by Δt.

$$\left[\frac{d\boldsymbol{u}_i}{dt}\right]_t = \left[\frac{d\boldsymbol{u}_i}{dt}\right]_{t-\Delta t} + \left[\frac{d^2\boldsymbol{u}_i}{dt^2}\right]_t \Delta t \qquad \textbf{III. 19}$$

$$\left[\frac{d\boldsymbol{\varphi}_i}{dt}\right]_t = \left[\frac{d\boldsymbol{\varphi}_i}{dt}\right]_{t-\Delta t} + \left[\frac{d^2\boldsymbol{\varphi}_i}{dt^2}\right]_t \Delta t \qquad \textbf{III. 20}$$

Finally, the incremental translational and angular displacement of *i*-th particle for *x*-, *y*- and *z*- components are given by Verlet's Leap-Frog method. Verlet's Leap-Frog Method is a numerical method used to integrate Newton's equations of motion, invented by the French physicist Verlet (1967). Because of its simplicity as well as accuracy, Verlet's Leap-Frog method is the most popular and the most widely used integration scheme in discrete element simulation. Compare to other integration methods such as the Predictor-Corrector method or the Runge-Kutta method which are highly accurate but time consuming and Euler's method which is computationally efficient but presenting a low accuracy (Rapaport 2004, Thijssen 1999), Verlet's Leap-Frog method appears as a good compromise, because it is both sufficiently accurate and computationally efficient. Verlet's Leap-Frog method is originally developed for Molecular Dynamics simulations (Rapaport 2004, Thijssen 1999), calculate the displacement in an intermediate state, such as:

$$[\Delta\boldsymbol{u_i}]_t = [\Delta\boldsymbol{u_i}]_{t-\Delta t} + \left[\frac{d\boldsymbol{u}_i}{dt}\right]_t \Delta t \qquad \textbf{III. 21}$$

$$[\Delta \boldsymbol{\varphi_i}]_t = [\Delta \boldsymbol{\varphi_i}]_{t-\Delta t} + \left[\frac{d\boldsymbol{\varphi}_i}{dt}\right]_t \Delta t \qquad \textbf{III. 22}$$

The acceleration, the velocity and the displacement for every particle are updated by these equations at every time step, Δt.

To have the stability of calculation and to have accurate results, the timestep is required to be small enough. However, if it is too small, it can raise not only an increase of calculation time but also an accumulation of numerical rounding errors. Thus, timestep has to be chosen at proper value (so-called critical timestep). The critical timestep is related to the ratio of spring coefficient to particle mass since the timestep should not be longer than the half of duration of oscillation time of the spring dashpot system t_c as show in **Eq. III. 23**.

$$t_c = \pi \sqrt{\frac{m}{K_n}} \qquad \textbf{III. 23}$$

Kawaguchi et al. (1992) has investigated the stability of calculation by using the time step, which is the value of t_c devided by several natural number,l. It is found that when the number l is over 5, the calculation is stabilized. According to this finding, time-step in this research work was decided to use timestep at the value described in **Eq. III. 24**

$$\Delta t \leq \frac{\pi}{5} \sqrt{\frac{m}{K_n}} \qquad \textbf{III. 24}$$

Conclusion

This chapter is mainly focused on the algorithms and calculation techniques used in our computational investigation concerning the particle motion in a high shear mixer, which is going to be presented in the Chapter V.

In our numerical study, DEM method has been applied and introduced.

The geometry of a high shear mixer has been constructed as well as the installation method.

Then the principle of the DEM has been studied and applied into the system of a high shear mixer.

Chapter IV Experimental results

IV. 1 Introduction

As discussed in previous chapters, it is very complicated and important to understand the effect of operating conditions on the dry coating process performance. This chapter shows the results of experimental work performed in order to understand the effect of operating conditions. The dry coating experiments carried out using a high shear mixer, Cyclomix with several operating conditions such as rotational speed, filling ratio and particle size. The evolution of properties of coated particles such as flowability and wettability was measured. The surface of the coated particles was observed. The particle size distribution has also been measured and the conversion ratio of the coated particles has been estimated.

IV. 2 Preliminary study

2.1 Agitation of Suglets

Only Suglets particles have been treated in the Cyclomix at different rotational speeds and operating times. The purpose of this study is to understand clearly the behaviour of the Suglets with different operating conditions. Especially, it is important to know how breakage, attrition or erosion could occur. The melting of the surface may also occur as a result of the heat caused by the friction of each particle, even if the temperature of a mixing chamber can be controlled by the cooling jacket.

The degradation of the host particle should be avoided to have a good quality of dry coating products. In addition a morphological study such as surface observation and particle size distribution analysis has been carried out in order to decide suitable operation conditions for dry coating.

2.1.1 Operating conditions

Following the purpose of this study, the rotational speed range was chosen from 1000 rpm to 3000 rpm. The operating time varied from 60 s to 1800 s, which is relatively long in comparison with previous works (Ouabbas 2008, Otles 2008). The temperature of the cooling jacked was fixed at 16 ^{o}C. The filling ratio was also fixed at 60 %, corresponding to 462 g in mass of Suglets particles. The operating conditions are summarized in **Table IV. 1**.

Table IV. 1 Operating conditions

Device	Rotational speed [rpm]	Operating time [s]	Filling ratio [%]
Cyclomix	1000 - 3000	60 – 1800	60

2.1.2 Particle size

The series of figures (**Fig**. **IV. 1 -5**) shows particle size distributions (PSD) with different rotation speeds. All the PSDs were measured at 3.5 bar of air pressure. At 1000 rpm, the particle size distribution does not change significantly even after 1800 s operation (**Fig. IV.1**). In addition, compare to the PSD of raw Suglets measured at 0.5 bar (**Fig. II. 2**), the PSD of raw Suglets measured at 3.5 bar has a small population ranging from 7 µm to 100 µm. This suggests that the attrition of the surface occurs from the high pressure at 3.5 bar. Consequently, the treated particles have almost the same PSD as that of raw Suglets. It indicates that there was no major breakage or fragmentation happening during the operation. At 1500 rpm, the PSDs also show a slight difference from those of 1000 rpm.

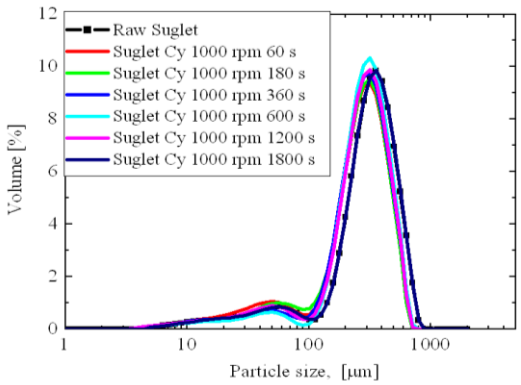

Fig. IV. 1 PSDs in volume of the particles treated at 1000 rpm after each operating time. Air pressure of 3.5 bar

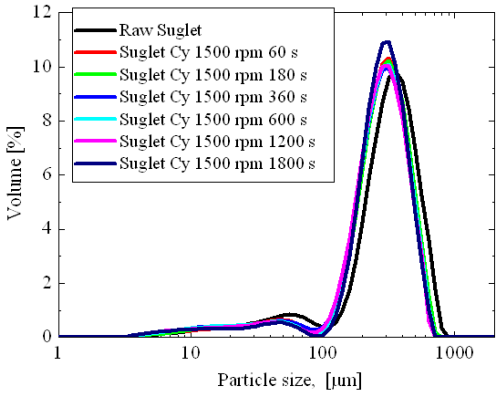

Fig. IV. 2 PSDs in volume of the particles treated at 1500 rpm after each operating time. Air pressure of 3.5 bar

Fig. IV. 3 shows the PSDs of treated particles at different operating time and at 2000 rpm. On the contrary to the PSDs of the 1000 and 1500 rpm, the difference from the raw Suglets is observed. Especially, at relatively long operating time, such as 1200 s and 1800 s of operation, the small population seen around the sub-micron scale (6 -10 µm) is higher than that of raw material. It could be because attrition or erosion happens during the operation. At 2500 rpm, the significant change after 1800 s of operation is observed (**Fig. IV. 4**). It is suggested that not only the attrition or fragmentation, but also the major breakage of the Suglets occur particularly for long operating time at 2500 rpm.

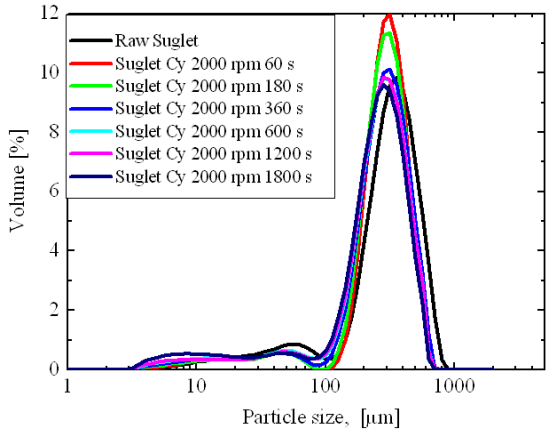

Fig. IV. 3 PSDs in volume of the particles treated at 2000 rpm after each operating time. Air pressure of 3.5 bar

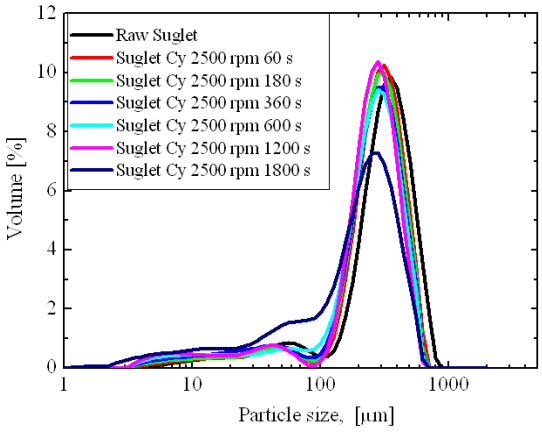

Fig. IV. 4 PSDs in volume of the particles treated at 2500 rpm after each operating time. Air pressure of 3.5 bar

At 3000 rpm, the PSDs differ remarkably from those of the other rotational speeds (**Fig. IV. 5**).

Even after 60 s of operation, the small population of sub-micron size is increasing. For long operating time such as 600 s and 1200 s, PSDs exhibit strangely populations, which are bigger than 1000 µm. It indicates that at higher rotational speed like 3000 rpm, excess forces given to the particles cause the fragmentation and breakage even in the short time operation, and then agglomeration of the fragments of particles.

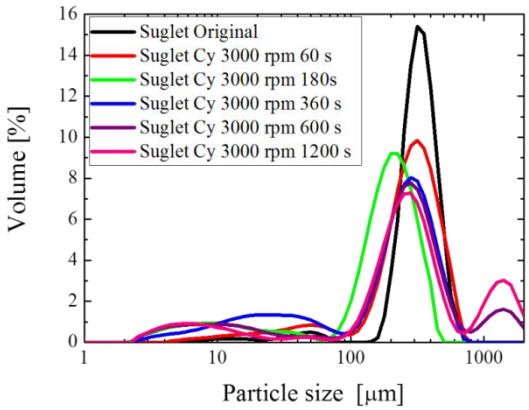

Fig. IV. 5 PSDs in volume of the particles treated at 3000 rpm after each operating time. Air pressure of 3.5 bar

The evolution of the normalized median diameter ($d_{t,50}$/ $d_{0,50}$) of the treated particles at different rotational speed as a function of operating time is shown in **Fig. IV. 6**.

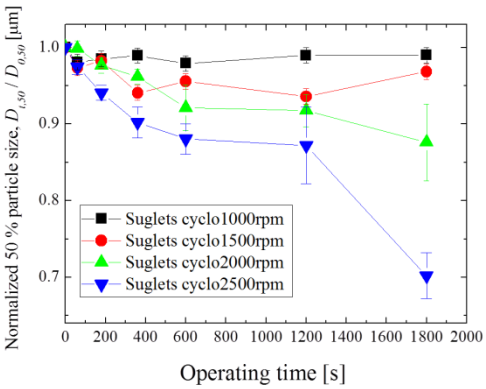

Fig. IV. 6 Normalized median diameter ($d_{t,50}$/ $d_{0,50}$) as a function of operating time at each rotational speed

The median diameter decreases with an increase in the operating time and also the rotational speeds. Particles treated at 1000 and 1500 rpm maintain their original median diameters, even

though a little decrease is observed. It can be said that even for low rotational speeds, the attrition or fragmentation of the surface occurs but without major breakage of the particles. Higher rotational speeds (2000 – 2500 rpm) can break particles, thus the median diameter decreases significantly. Especially, at 2500 rpm, the median diameter decreases until below 0.7. It is obviously not suitable for the dry coating process.

2.1.3 Surface Observation

The treated particles at different rotational speeds and at 600 s and 1800 s have been observed by SEM. **Fig. IV. 7** shows the SEM images of the treated particles at 1000 rpm and 600 s with different magnitudes. Though PSDs results show that there is little difference from the raw Suglets, the SEM image shows a big difference from that of raw Suglets (**Fig. II. 1**).

There is no major breakage or cracks of the Suglets observed. However, small particles attached on the surface of Suglets are observed, which is not observed from the raw Suglets (**Fig. IV. 7 (a)**). Since this work has been done with only the Suglets, it is obvious that those small particles are formed by the result of the fragmentation of Suglets. Surface of the treated particles is also quite different from the raw Suglets (**Fig. IV. 7 (b)**), it seems to have smoothed surface with small particles sticking. From these observations one can conclude that the attrition or abrasion of the surface occurred during the operation, and then those small fragments were attached on the surface of the particles.

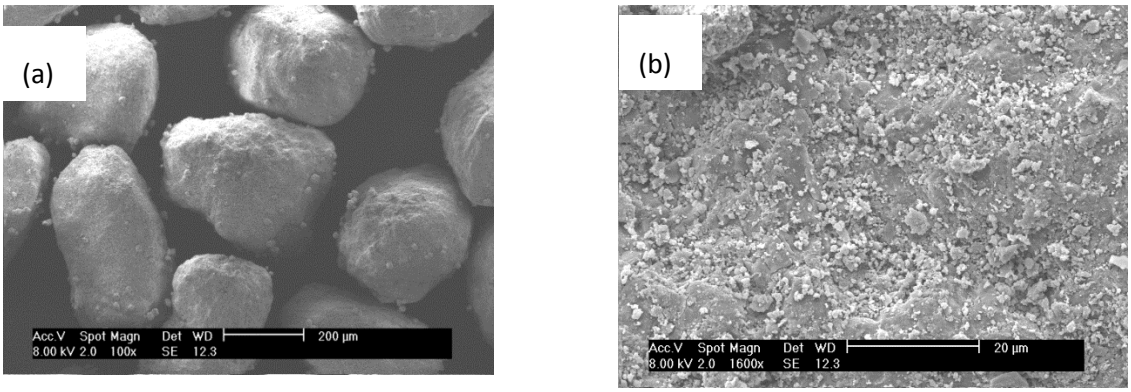

Fig. IV. 7 SEM images of the treated particles at 1000 rpm and 600 s with different magnitude : (a) × 100, (b) × 1600

Fig. IV. 8 shows the SEM images of treated particles at each rotational speed and at 600 s and 1800 s operating time. Along with the increase of rotational speeds, the quantity of the small fragments increases, especially for the treated particles at 3000 rpm. Degradation of the Suglets particles is so crucial that it is obviously not convenient to conduct the dry coating process at this rotational speed.

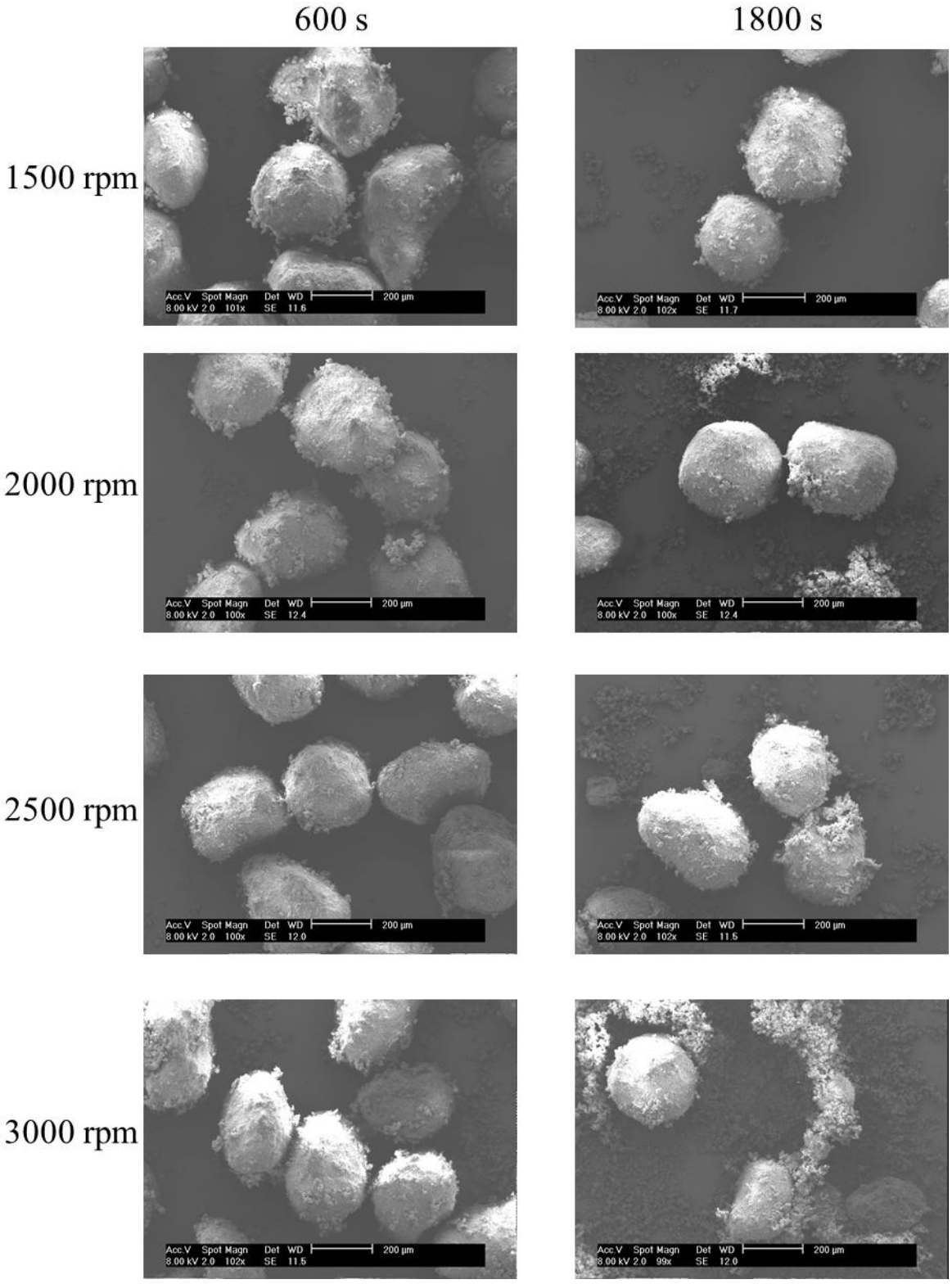

Fig. IV. 8 SEM images of treated particles at each rotational speeds and at 600 s and 1800 s of operating time

2.2 Summary

From the morphological analysis (PSD and SEM), it can be summarized as below.

(1) Even for 1000 rpm, the attrition or abrasion occurs, and then the small fragments are generated. However, PSD does not change significantly. It means probably that the quantity of fragments is relatively small or might be generated by granulometry treatment by the air pressure of the PSD measurement.

(2) Some of those small fragments are agglomerated and attached on the surface of Suglets.

(3) Over 2000 rpm, the median size reduction is put in evidence. Hence those rotational speeds are not suitable for the dry coating operation.

From those findings, the dry coating operation conditions were decided as shown in **Table IV. 2**.

Table IV.2 Suitable operating conditions for dry coating using Cyclomix

Rotational speed [rpm]	1min	3min	6min	10min	20min	30min
1000	○	○	○	○	○	○
1500	○	○	○	○	○	○
2000	○	○	×	×	×	×
2500	×	×	×	×	×	×
3000	×	×	×	×	×	×

IV. 3 Dry coating of Suglets with MgSt

The dry coating of a model couple, Suglets and MgSt for host / guest particles respectively, has been carried out using a high shear mixer "Cyclomix". The interest of this study is to understand how the operating conditions such as rotational speed, operating time and filling ratio affect the dry coating performance. To do so, the coating experiments with several operating conditions have been done. The properties of coated particles have been characterized by different methods.

3.1 Effect of operating time and rotational speed

The objective of this study is to understand the effect of operating time and rotational speed on the dry particle coating and consequently, modification of the surface properties of host particles (Suglets). Hence, the morphological analysis (PSD, SEM, Pycno-density) and properties analysis, flowability and wettability tests were done.

3.1.1 Operating conditions

To understand the effect of rotational speed, the experiments have been done at different rotational speeds (500 – 1500 rpm) and operating times (60 – 1800 s). The filling ratio and mass fraction of MgSt have been fixed to focus on the effect of those operating conditions. The filling ratio was chosen to 60 % (462 g of Suglets). The mass fraction of MgSt was 5 % obtained from the experimental model shown in **Eq. II. 2**. The temperature of the chamber was fixed at 18 ^{o}C by the cooling jacket. The operating conditions are summarized in **Table IV. 3**.

Table IV. 3 Operating conditions

Device	Rotational speed [rpm]	Operating time [s]	Filling ratio [%]	Mass fraction [%]
Cyclomix	500 -1500	60 – 1800	60	5.0

3.1.2 SEM observations

The SEM images of the coated particles with different rotational speeds and operating time are shown in **Fig. IV. 9**. At 500 rpm, we can observe that the amount of free small particles which are probably MgSt, decreases with an increase of operating time. It suggests that dry coating proceeds along with operating time. On the contrary at 1000 rpm and 1500 rpm, the free particles of MgSt are not observed even at the beginning of the operation (60 s). Almost all the MgSt particles might already be attached on the surface of Suglets.

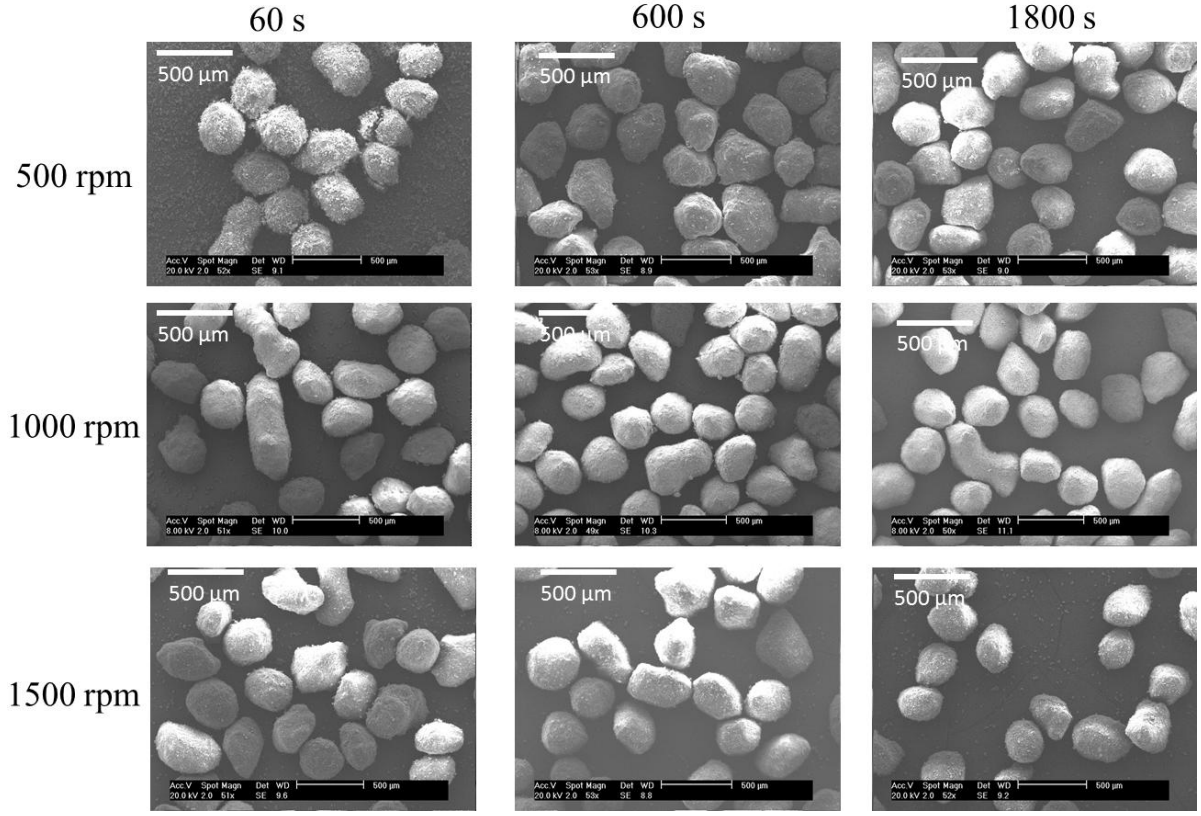

Fig. IV. 9 SEM images of coated particles with different rotational speeds and operating times.

The SEM images of the particles surface after the dry coating operation are shown in **Fig. IV. 10**. For the coated particle mixed at 500 rpm during 60 s, it seems that almost the entire surface of the host particle is discretely covered by MgSt.

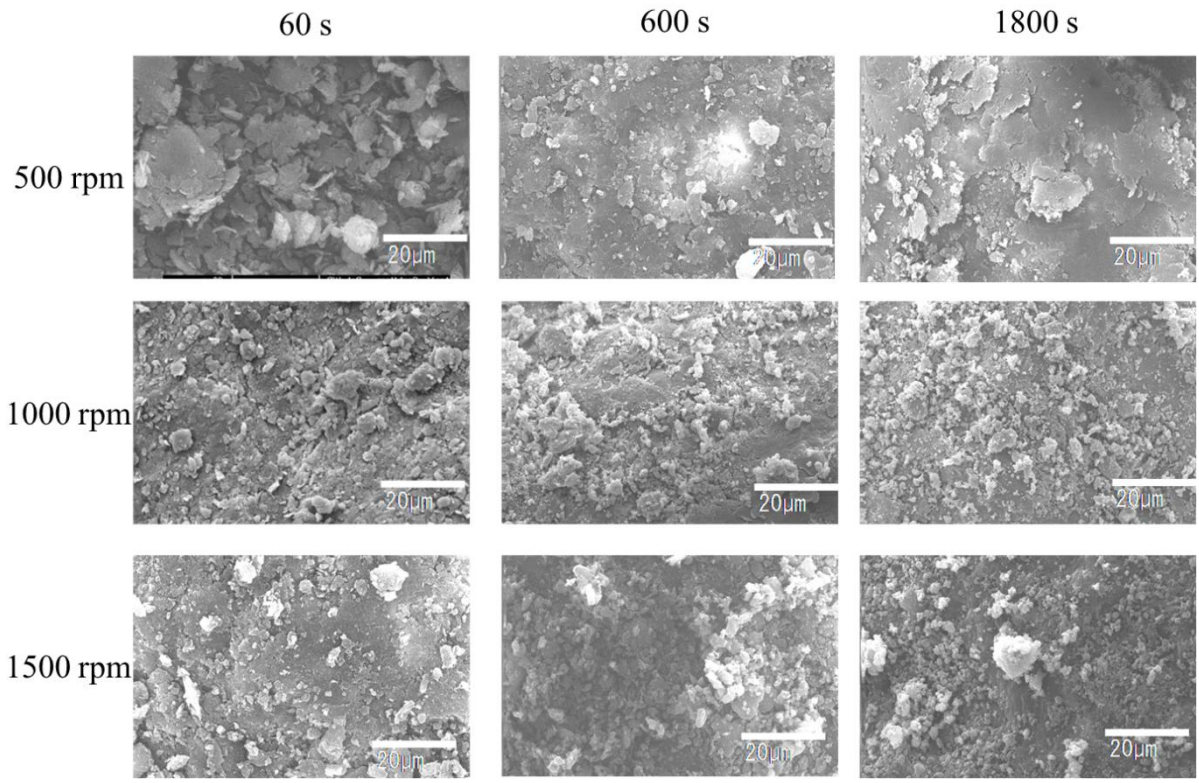

Fig. IV. 10 SEM images of the surface of coated particles with different rotational speeds and operating times.

Moreover, the surface seems to become smoother when the operating time increases. This could be explained as follows: MgSt particles that had stuck to the surface of host particle were beat out to a film-like or flat shape by shear forces or impactions during high shear mixing and smeared firmly on the surface of host particle, since MgSt is well-known as a lamellar and soft material (Galdwall 1974). The dry coating progressed to a continuous coating. As for the coated particles mixed at 1000 rpm during 60 s, the surface seems to be rougher than that at 500 rpm operation. After 600 and 1800 s operations, those surfaces seem to present some aggregates on them, which are similar to the surface of treated particle without presence of the MgSt particles (**Fig. IV.7**). During the operation, firstly host particles could have been abraded by mechanical solicitations, and then some separated fragments of host particles could have been agglomerated. Finally those agglomerates can be attached to the surface of the host particles. Therefore, the surface would be a mixture of the host particles fragments and MgSt particles. As for the coated product at 1500 rpm operation

during 60 s, the surface seems to be similar to that of 1800 s and 500 rpm. That is to say, this coated particle achieves a continuous coating only after a 60 s mixing. After 600 s and 1800 s operations at 1500 rpm, the mixture surace seems to be similar to the surface of mixture after the same times at a 1000 rpm operation. Then, it can be concluded that at high rotation speed, host particles could be abraded by high shear mixing, and this may reduce the efficiency of the dry coating.

To verify if MgSt particles are attached on the surface of Suglets, EDX analysis of the Mg element was also carried out. In **Fig. IV. 11**, yellow spots indicate the presence of Mg element. Those yellow spots represent well the shape of the particles, in other words, MgSt particles covers almost all the surface of the host particles. Then, it is confirmed that the MgSt particles are well attached on the surface, the dry coating is successfully performed by these treatments.

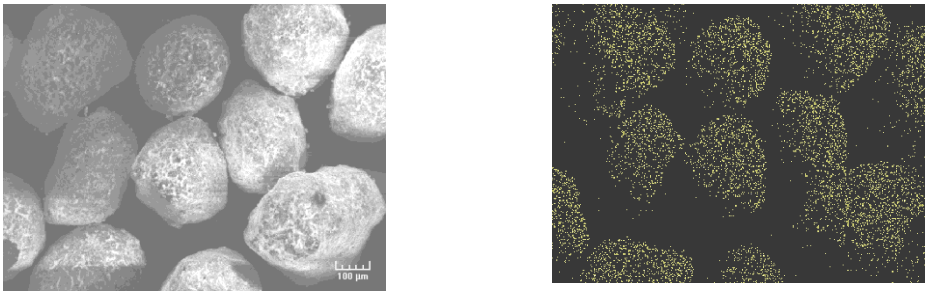

Fig. IV. 11 EDX analysis of the coated particles with 500 rpm and 600 s.

3.1.3 Particle size distribution analysis

Fig. IV. 12 shows the number distributions obtained by a Malvern Mastersizer dry feed system with 0.5 bar air pressure. It can be seen that all the peaks are located around 250 µm not far from the median diameter of the Suglets. There is neither a dispersion of MgSt nor small fragments of Suglets observed.

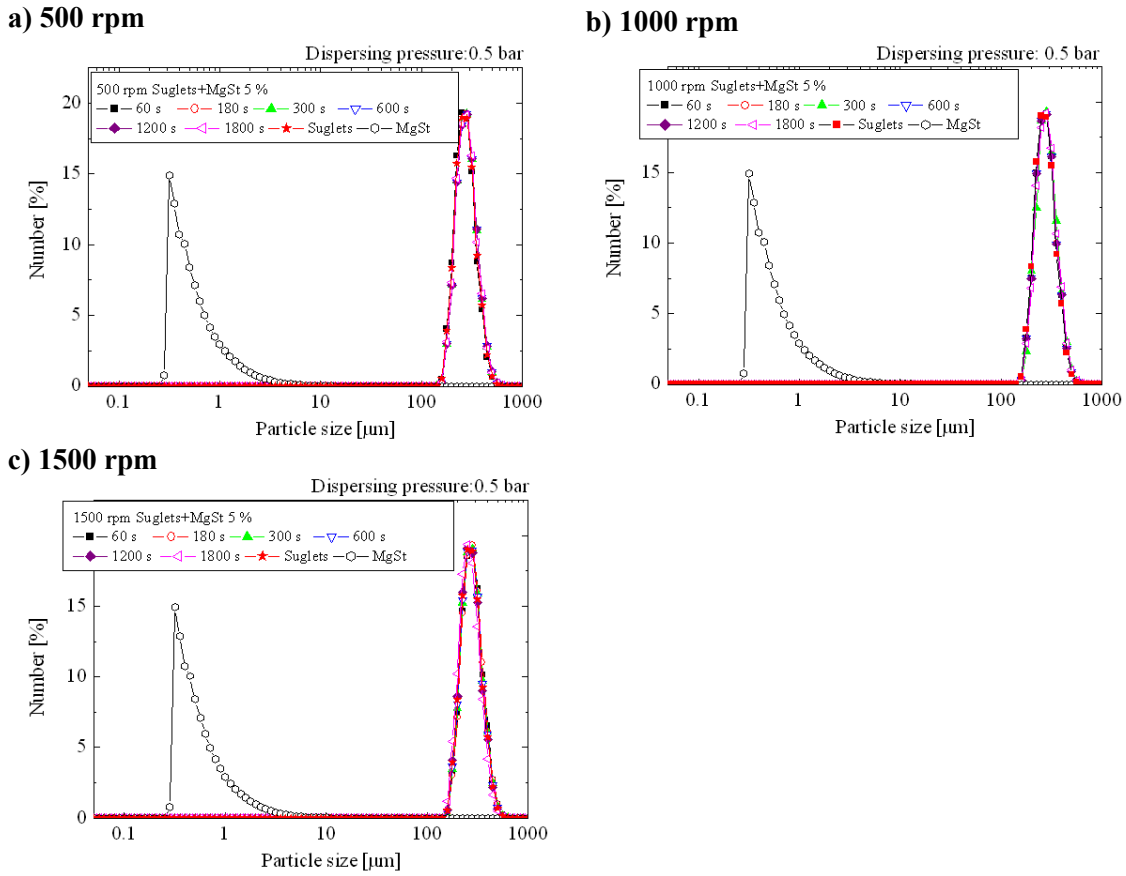

Fig. IV. 12 Particle size distribution in volume of coated particle at each operating time and (a) 500 rpm, (b) 1000 rpm, (1500 rpm) at 0.5 bar

It is suggested that those small particles, either MgSt or fragments are attached firmly enough to resist against the air pressure having an effect of separating from the host particles. The volume distribution at 0.5 bar were omitted to show since it presents exactly the same tendency as that in number distribution.

Fig. IV. 13 shows the volume distribution obtained with 2.5 bar air pressure at each rotational speeds.

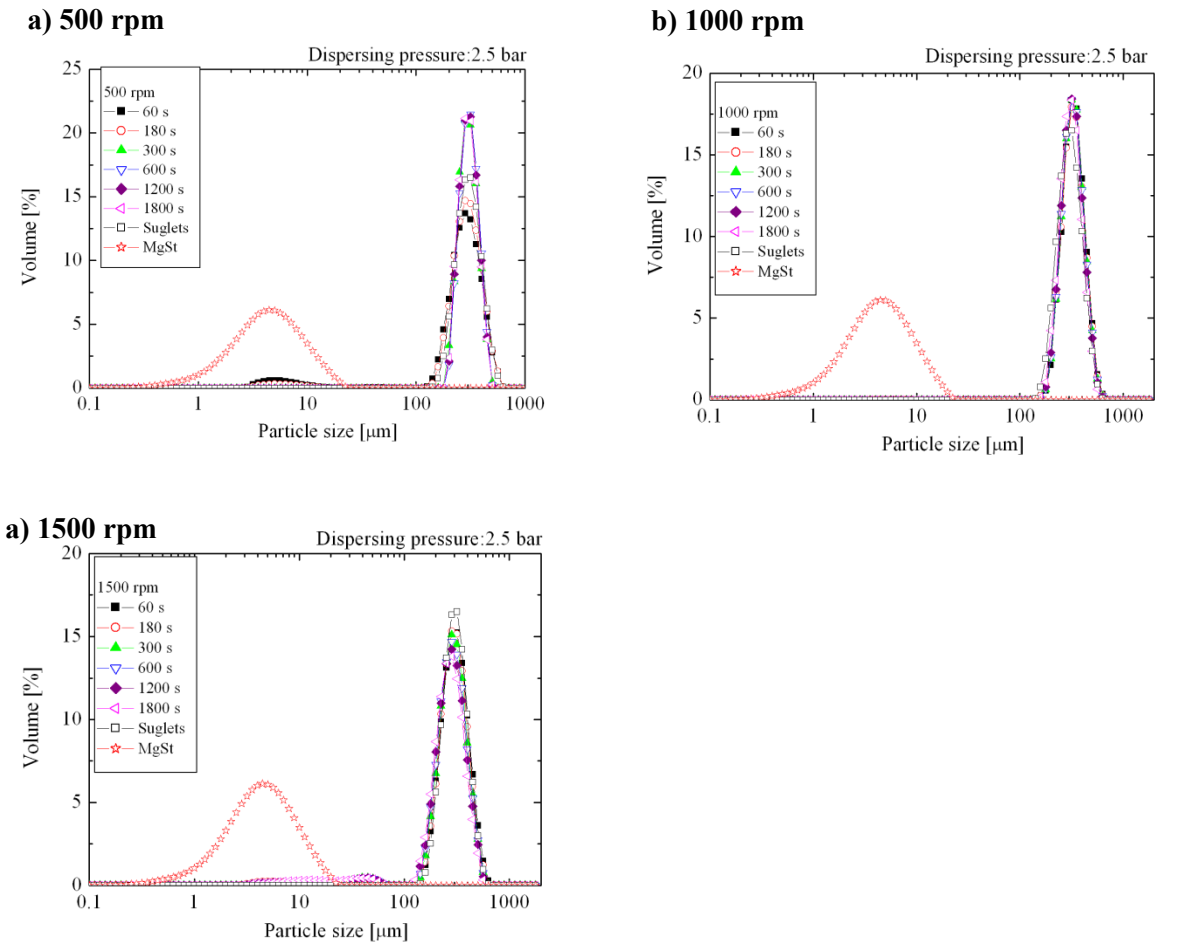

Fig. IV. 13 Particle size distribution in volume of coated particle at each operating time and (a) 500 rpm, (b) 1000 rpm, (1500 rpm) at 2.5 bar

At 500 rpm the majority of the PSD of coated particles shows the same population as that of Suglets. However, there are small populations of the products obtained from 60 s and 180 s treatments which are similar to the population of MgSt. This indicates that there is a small release of MgSt particles from Suglets surface due to the air pressure (**Fig. IV. 13 (a)**).

At 1000 rpm, on the other hand, there is no remarkable change observed (**Fig. IV. 13 (b)**). It is understandable, since the observation of SEM as well as preliminary study in previous section shows that both abrasion and coating of MgSt happens. However, those small particles are attached firmly on the surface. At 1500 rpm, there also can be seen smaller peaks around 60 µm. These peaks might be the broken or abraded Suglets. There are the populations from 2 to 60 µm. Those are probably both separated MgSt and small fragments of aggregates of Suglets (**Fig. IV. 13 (c)**).

The number distribution would show these tendencies clearer. **Fig. IV. 14** shows the number distributions obtained with a 2.5 bar air pressure.

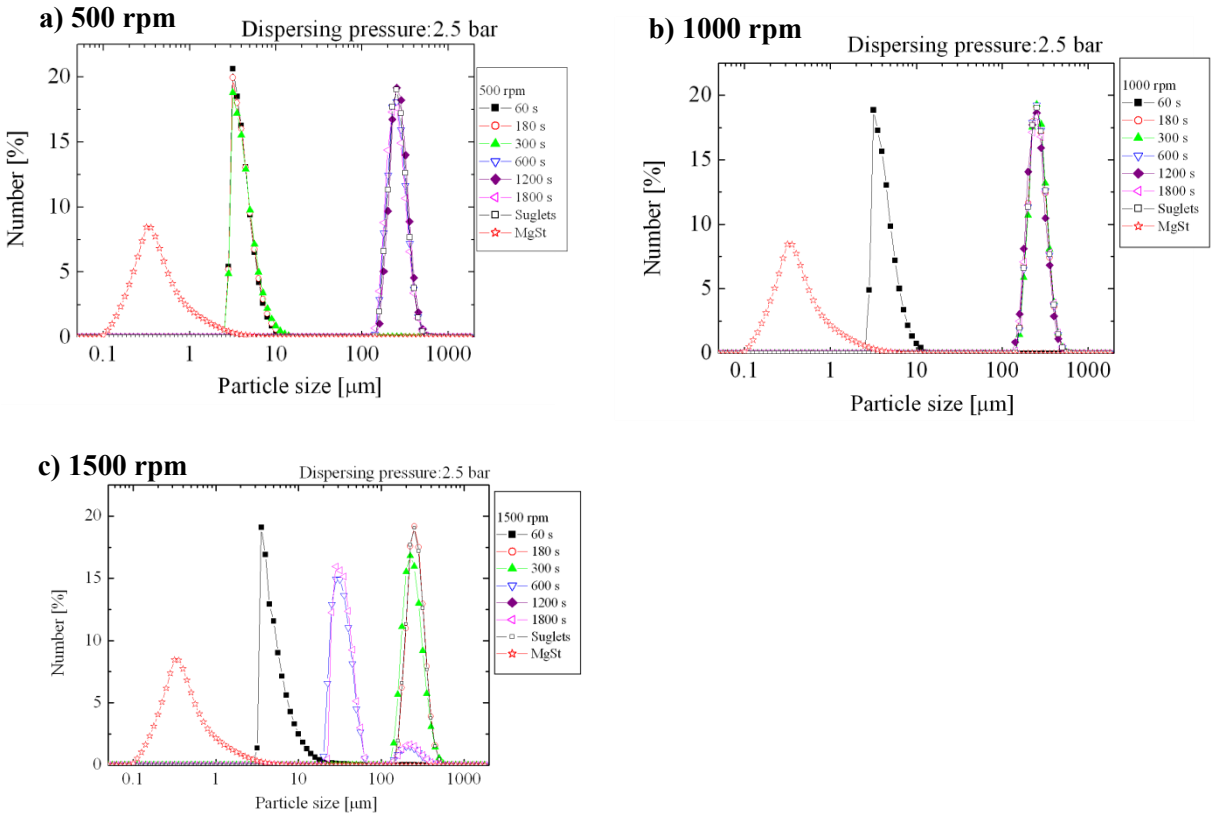

Fig. IV. 14 Particle size distribution in number of coated particle at each operating time and (a) 500 rpm, (b) 1000 rpm, (c) 1500 rpm at 2.5 bar

At 500 rpm, the populations of the products obtained from 60s and 180 s are found around 7-8 μm, which are not fully corresponding to that of free MgSt (**Fig. IV. 14 (a)**). Two possible explanations can be proposed for this result. One is those populations are not that of MgSt but that of fragments of Suglets. The other is those populations are from released MgSt, however, the difference from free MgSt was caused by the deformation or agglomeration of MgSt particles during the coating operation. Since the others products treated at much longer time remain the population of Suglets, the latter explanation is more reasonable. At 1000 rpm, almost all the populations of products remain that of Suglets except the product of 60 s operation (**Fig. IV. 14 (b)**). This tendency indicates that 1000 rpm operation gives stronger adhesion between host and guest particles than that of 500 rpm. At 1500 rpm, a different

tendency was observed (**Fig. IV. 14 (c)**). The products obtained after 600 s and 1800s have populations around 60 μm. Considering that this is a high speed operation, those populations should be corresponding to the fragments of Suglets which occurred in the coating operation. From the preliminary study, the fragmentation of Suglets obviously occurs at lower rotational speed (1000 rpm), however the amount of fragments generated are much less than in the 1500 rpm experiments, and probably those fragments are firmly attached on the surface, then they were not detected by the PSD analysis at 2.5 bar. On the contrary, at 1500 rpm, those fragments are somehow attached on the surface as indicated by PSD at 0.5 bar (**Fig. IV. 12**). However, the amount of fragments is so important that there are some fragments whose bond forces are not strong enough to remain attached on the surface under 2.5 bar of air pressure, even though a 1500 rpm operation would give stronger bond forces to the small particles.

3.1.4 Flowability

First of all, the flowability of the raw materials, Suglets and MgSt were measured with the FT-4 powder rheometer from Freeman. **Fig. IV. 15** shows the results of those pure materials.

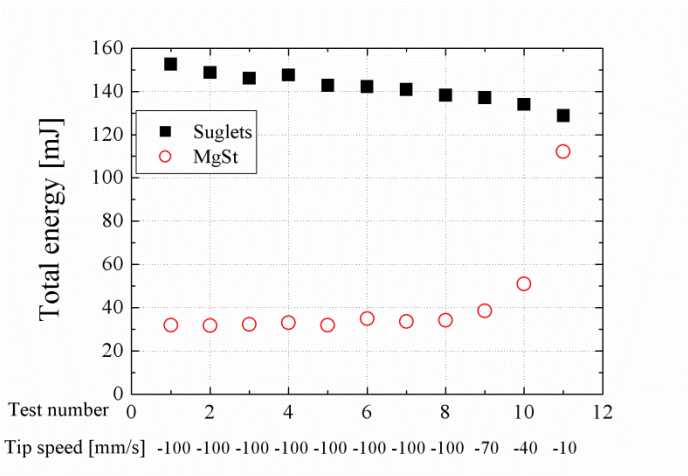

Fig. IV. 15 FT-4 results of raw Suglets and MgSt

From this result, three indexes can be obtained. These are BFE (Basic Flowability Energy) which is related to the porosity of bulk and density of powders, SI (Stability Index) corresponding the stability of powder under flow and FRI (Flow Rate Index). The obtained values are summarized in **Table IV. 4**.

Table IV. 4 The values of raw materials obtained from FT-4

Values	Suglets	MgSt
BFE [mJ]	139.2	35.2
SI	0.99	0.96
FRI	0.88	3.11

FRI is the most important and significant value to describe the flow property of powder as introduced in Chapter II. A high FRI value corresponds to cohesive powders. The FRI of Suglets is much smaller than that of MgSt. It is quite understandable since Suglets is a granular material and MgSt is well-known as a highly cohesive powder. In addition, Otles (2008) showed that FRI is well correlated to the Carr index as well as the Hausner Ratio. Then The FRI is defined as the index to determine the flowability in this study.

Fig. IV. 16 shows the variation of FRI as a function of operating time at each rotational speed. The initial value of FRI is that of host particle.

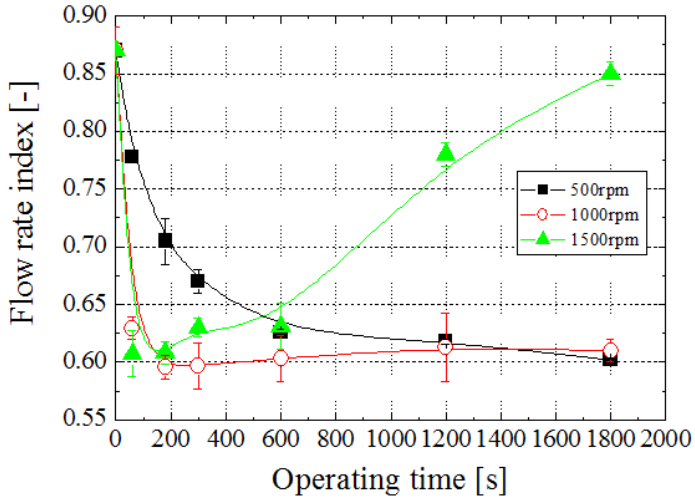

Fig. IV. 16 Flow Rate Index (FRI) as a function of operating time.

At 500 rpm, FRI decreases with an increase in the operating time. In other word, the flowability of the coated particles is improved for longer operation times. This result agrees with the SEM observation of the products at 500 rpm, since the surfaces of the host particle are immediately covered by the guest particles and the surface of the coated particles became smoother as the operating time increased. The coating of the guest particle as well as this transformation of the surface condition (from discrete to continuous coating) could help the particles to have a better flowability. As for 1000 rpm, FRI decreases with an increase in the operation time more rapidly than that of 500 rpm up to 300 s, and then it became stable. It indicates that the coating and deformation of the surface were finished at about 300 s. Then no more mixing can contribute to improve the flowability. At 1500 rpm, the FRI decreases rapidly with an increase in the operation time up to just 60 s, and the FRI starts to increase. The decrease of FRI marks a better flowability due to the attachment of MgSt particles to the host ones and surface deformation as already explained above. The increase might be attributed to the fragmentations of the host particles, which were observed by the SEM,

submitted to the high shear stress and impaction during particle-particle and particle to the wall/impeller interactions. To verify if the flowability is improved without presence of MgSt, the change of flowability of raw Suglets treated by a high shear mixer at 500 rpm was measured (**Fig. IV. 17**). The FRI increases with an increase of operating time, which is an opposite tendency with respect to the results of coated particles. It is probably because of degradation of the surface of host particles. It is confirmed that MgSt plays a great role for improving the flowability.

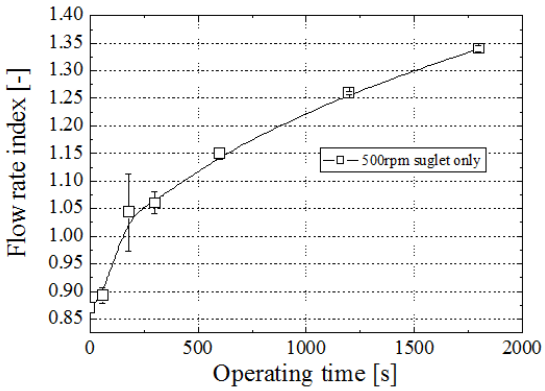

Fig. IV. 17 FRI of treated raw Suglets with a high shear mixer at 500 rpm as a function of operating time.

3.1.5 Wettability

The water drop test has been carried out to analyze the wettability of the products. **Fig. IV. 18** shows that the images of the water drop test for raw Suglets™ and for the product mixed at 1000 rpm during 60 s. As it can be seen, the water drop was absorbed as soon as it was dropped on the powder bed of the raw Suglets™ due to its high hydrophilic property. On the other hand, the water drop on the product remains even after 30 s. The 60 s operation at 1000 rpm is sufficient to change the surface property from hydrophilic to hydrophobic.

(a) (b)

Fig. IV. 18 Snapshots of the angle of contacts (a) raw Suglets (b) coated particle with 1000 rpm and 60 s treatment.

The angle of contact in this measurement is also affected by the porosity of bulk powder bed, inducing penetration of the water into the pores due to the capillary action since the powder beds of the samples are not compressed. So, it is not the absolute value of the contact angle of those samples. Nevertheless, the interest of this study is to evaluate the changes in the wetting behavior by the dry coating with the various operating conditions, so the absolute values of the contact angle is not really necessary. In addition, since the PSDs of the coated particles do not remarkably change, the porosity of the powder bed should not be much different. Then the effect of the capillary action would not change much amongst the coated particles with different operating condition. The changes of the wetting behavior can be observed fairly enough by this measurement.

Fig. IV. 19 shows the contact angle of the products 30s after the water drop on the surface as a function of operation time.

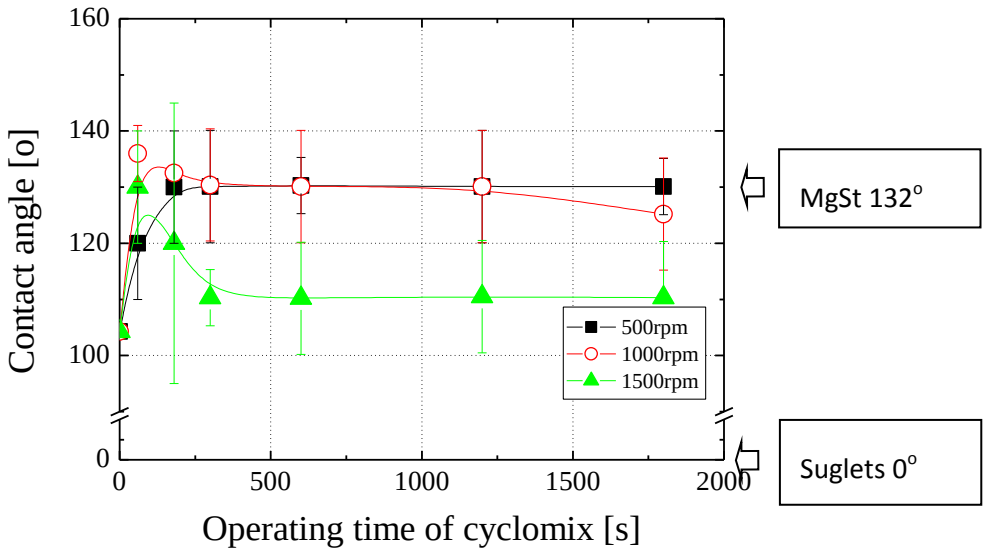

Fig. IV. 19 Contact angle as a function of operating time at different rotational speeds

The initial value (t = 0 s of operating time) in this figure is calculated from the assumption that the contact angle θ (t = *0*) of the product at certain operation time t is proportional to the surface fraction (1-S_H) of guest particles (**Eq. IV. 1**), when the host and guest particle are just introduced (though not mixed nor coated) at beginning. In this equation we must take θ_H =*0* for highly hydrophilic particles like Suglets.

The surface fraction of the initial, S_{H0} could be given by **Eq. IV. 2**:

$$\theta(t) = S_H\,\theta_H + (1 - S_H)\,\theta_I \qquad \textbf{IV. 1}$$

$$S_{H0} = \frac{{k_H}^2}{4C_{2D}(k_H + 1)^2 + {k_H}^2} \qquad \textbf{IV. 2}$$

This expression can be obtained by writing that the surface fraction of host particles in the initial state is the ratio of the area of the sphere passing through the points of contact between host and guest particles (radius $R_I + R_H$) and the effective area occupied by an guest particle at the surface of host's one ($\pi R_I^2/C_{2D}$).

Since the contact angle of a host particle θ_H and that of a guest particle θ_I are 0° and 132° respectively, the theoretical value derived from **Eq. IV. 1** of the contact angle for the initial mixture θ (0) is found to be 104°. We can notice that the physical meaning for t = 0 corresponds to a state where the two kinds of grains are present without any coating.

As it can be seen in **Fig. IV. 19**, at 500 rpm, the contact angle increases with an increase of

operating time until 300 s, and then it seems to become stable and the value is almost the same as that of MgSt, which indicates that the surface of the host particle is almost covered by the MgSt after 600 s of operation. At 1000 rpm, the contact angle increases more rapidly than that of 500 rpm for t= 60 s. However, the contact angle decreases slightly with the operation time after reaching the maximum. That might be because of the agglomerates of host particles fragments attached on the surface as already explained. At 1500 rpm, it also increases until 60 s, then after that, it starts to decrease with the operating time with more remarkable rapidity. For the same reasons, since the mechanical forces applied to the particles should be stronger than that of 1000 rpm, this tendency proceeded faster. However once, the angle of contact decreases, it reaches stable again around the initial value obtained from **Eq. IV. 1**. This behaviour is unclear since the surface fraction of host particles is increased because of generation of fragments.

3.1.6 Pycnometry density

Fig. IV. 20 shows the evolution of the pycnometry density with the operating time. Initial points of those curves are the density of Suglets™. At 500 rpm, the pycnometry density decreases with an increase in operating time, and finally it reaches about 1.47 g/cm^3. Even if the dry coating identically proceeds, that is to say, if all the guest particles are attached to the host particles, the density would only reach about 1.55 g/cm^3 calculated by the following equation since density of host and guest particles are 1.58 and 1.12 g/cm^3, respectively.

$$\boldsymbol{\rho_{ideal} = \frac{1}{\frac{1 - w_0}{\rho_H} + \frac{w_0}{\rho_I}}} \qquad \textbf{IV. 3}$$

Where, ρ and w_0 represent the density and the mass fraction of guest particles introduced into a mixer.

So, there must be another reason for the coated particles to have a smaller value than the ideal density. As it has been discussed in the SEM observation, the dry coating starts from the discrete coating. It proceeds to the continuous coating. When the film coating was being made, probably the film of magnesium stearate covered the rough surface and opened pores of host particles. As a result, the closed porosity of the coated particles could increase and the

pycnometry density could have decreased. At 1000 rpm, the density decreases more rapidly than that of 500 rpm. Because of high rotational speed, coating and making the covering of open pore proceeds faster than low rotational speed. After certain time of operation, it seems to reach the asymptote state. It is indicated that almost all the guest particles stick to the host particles or wall the mixer and no free guest particle remains. At 1500 rpm, once the pycnometry density decreases, however, it immediately starts to increase. That might be because firstly the voids of host particles is generated by the film-like coating, and then excess mixing force brake that void structure. Overall, these tendencies of the change in density are similar to those of flowability.

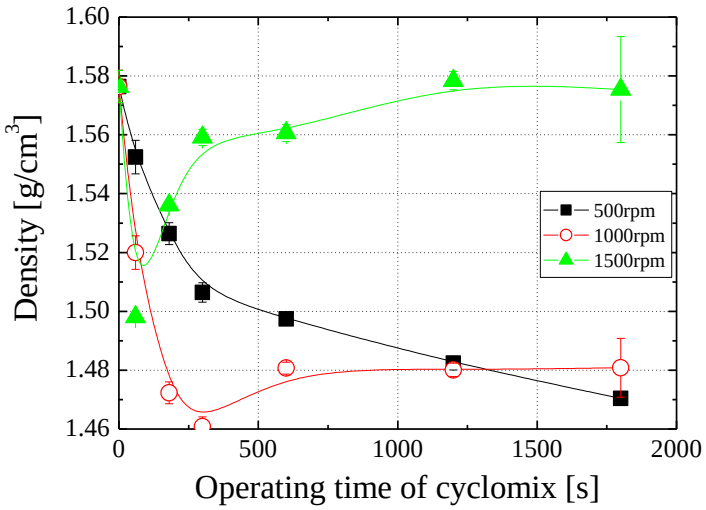

Fig. IV. 20 Measured density as a function of operating time at different rotational speeds

3.2 Partial conclusions

In this study, a dry coating process has been carried out by using a high shear mixer, for the purpose of coating Suglets™ by magnesium stearate. Different operating conditions, especially rotational speed and operating time, have been used and it was shown that they were playing a role on the mixture properties. The main following results have been achieved:

1) The surface morphology of the coated particles indicates that, at first, the guest particles are distributed as discrete particles on the surface of the host particles. Then, as processing time increases, the guest particles fixed on the host particles are deformed by mechanical action such as shear and impact forces, and the coating changes from being in the form of discrete particles to become a film-like coating. At high rotational speeds, these phenomena proceed rapidly, rearrangements of the superficial grains occur so that a somewhat continuous film-like coating is obtained, even at short processing times. PSD results at low air pressure confirm that the guest particles are well attached to the host particles. High pressure PSD measurement indicated that at high rotational speed, especially, 1500 rpm, the fragmentation of the host particles occurs. Those fragments of host particles could be agglomerated and re-attached on the host particles.

2) The flowability becomes better when the operation time is longer, not only because of the coating of guest particles but also because the transition from discrete coating to film coating contributes to the flowability improvement. However it gets worse when the fragmentation of host particles occurs.

3) The wettability rapidly changed from hydrophilic to hydrophobic even at 1000 rpm during 60 s. The contact angle increases with operating time and rotational speed. However, the wettability again starts to decrease when the aggregates of host particle fragments attach on the surface.

4) The pycnometry density measurements reveal the transition from discrete coating to film coating: when the film formation undergoes, internal closed pores appear in the coated grain. The excess treatment makes attrition or breakage of the film, the close pores become open, and the pycnometry density starts to increase.

All these characteristics evolutions can allow us to propose the following evolution of the system during mixing (**Fig. IV. 21**).

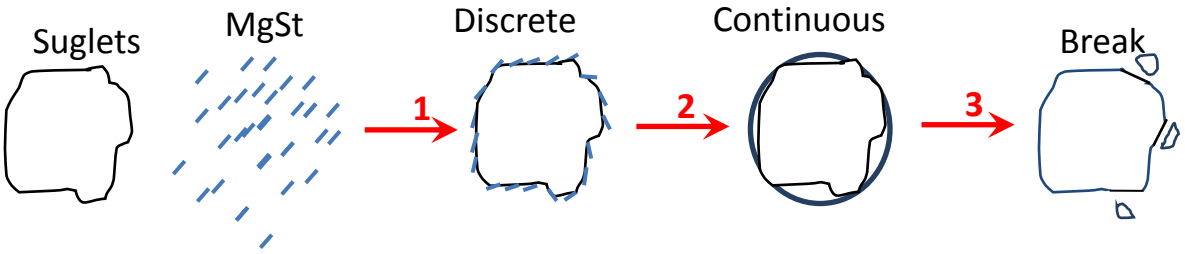

Fig. IV. 21 System evolution during the dry coating process

The first step (1) is a discrete coating that rapidly occurs and the density decreases, the wettability goes up to 132° and the FRI decreases also. The second step (2) is a continuous film formation. As a consequence, the wettability is still the same but the density decreases to a certain value (1.47 g/cm^{-3}) and is constant when all the grains are continuously coated with internal porosity. The FRI is also constant. This "pseudo-steady state" is reached for coating conditions such as 1000 rpm for 60s to 600s of mixing. For rougher treatments (at 1500 rpm) the step (3) occurs, the breakage of coated particles also shown by laser granulometry induce the increase of density and also of FRI. As shown in **Fig. IV. 21**, we can imagine that this breakage may open the coating film and generate "free" Suglets™ surfaces responsible for the drop of wettability form 132° to 110°. This is also shown in the increase of density up to the value of an ideal mixture.

3.3 Effect of filling ratio

The effect of operating time and rotational speed has been investigated in the previous section. Then the interest of this section is to know the effect of the filling ratio. As the filling ratio of the sample affects the particle motion, this operation condition would have an influence on the dry coating performance even though this influence would be smaller than that of the rotational speed or operating time.

3.3.1 Operating conditions

The operating conditions were then chosen to test several filling ratios from 20 % to 60 %. Operating time decrease to 600 s, since even the short time operating can have a good coating as investigated in previous study. The rotational speeds vary from 250 – 1500 rpm, namely 250 rpm is added to this study since even the operation at 500 rpm showed a quite good coating as well. The temperature of the chamber was also fixed at 16 ^{o}C. The mass fraction of guest particles is also fixed at 5.0 %. The operating condition is summarized in **Table IV. 5**.

Table IV. 5 Operating conditions

Device	Rotational speed [rpm]	Operating time [s]	Filling ratio [%]	Mass fraction [%]
Cyclomix	250 -1500	30 – 600	20,40,60	5.0

3.3.2 SEM observations

Fig. IV. 22 shows the SEM picture and its EDX analysis of coated particle at a filling ratio J = 20 %, operating time t = 180 s and ω = 250 rpm.

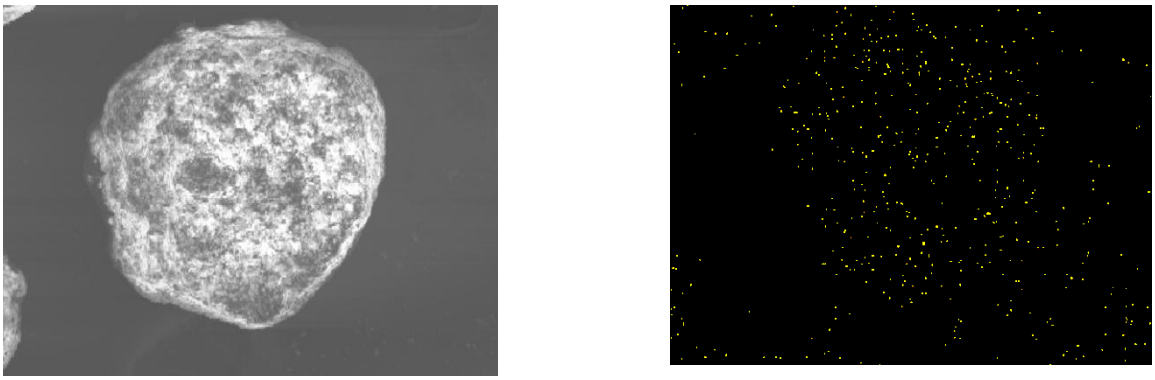

Fig. IV. 22 EDX analysis of the coated particles with a filling ratio J = 20 %, operating time t = 180 s and ω = 250 rpm.

MgSt indicated as yellow spots vaguely represents the shape of the particle. It can be said that the 250 rpm operating speed is not sufficient to coat the Suglets with MgSt during the short time as 180 s. To make clear the effect of the filling ratio, the SEM picture and EDX analysis of coated particles, filling ratio J = 60 %, operating time t = 180 s and ω = 250 rpm are shown in **Fig. IV. 23**. MgSt is scattered homogeneously in the picture. It can hardly be said that coating is successfully done. By comparing **Fig. IV. 22** and **23**, one can say that they are slightly different. The coated particles at lower filling ratios seem to have more MgSt on their surface than that at higher filling ratios. This suggests that at a lower filling ratio proceeds the coating faster than a higher ratio.

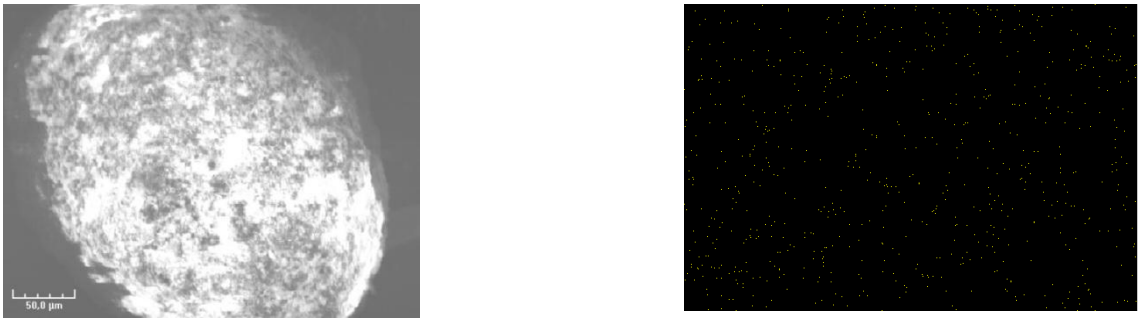

Fig. IV. 23 EDX analysis of the coated particles with a filling ratio J = 60 %, operating time t = 180 s and ω = 250 rpm.

Fig. IV. 24 shows the SEM picture and its EDX analysis of coated particle at a filling ratio J = 60 %, operating time t = 180 s and ω = 500 rpm.

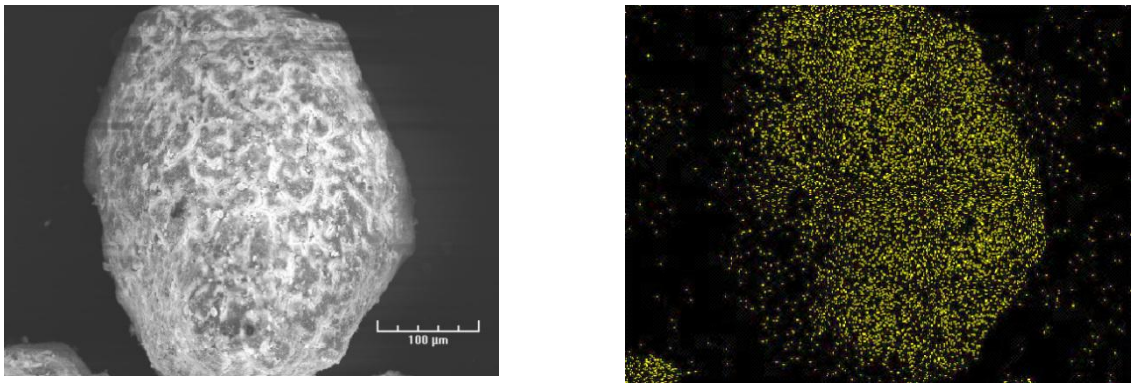

Fig. IV. 24 EDX analysis of the coated particles with a filling ratio J = 60 %, operating time t = 180 s and ω = 500 rpm.

Comparing the other two coated particles at a lower rotational speed, this particle is obviously coated with MgSt since the yellow spots indicate well the shape of the particle. Those results suggest that the effect of rotational speed is much bigger than that of filling ratio.

3.3.3 PSD analysis

Fig. IV. 25 shows the PSD of coated particles in volume with a filling ratio J = 20 % and different rotational speeds. The air pressure was 0.5 bar. The population of coated particles does not change from the population of raw Suglets particles. It is concluded that there is neither separation of MgSt nor fragment of Suglets. The other filling ratios (J = 40 % and 60 %) have same tendency as the J = 20 %. So the effect of filling ratio is not observed from this experiment.

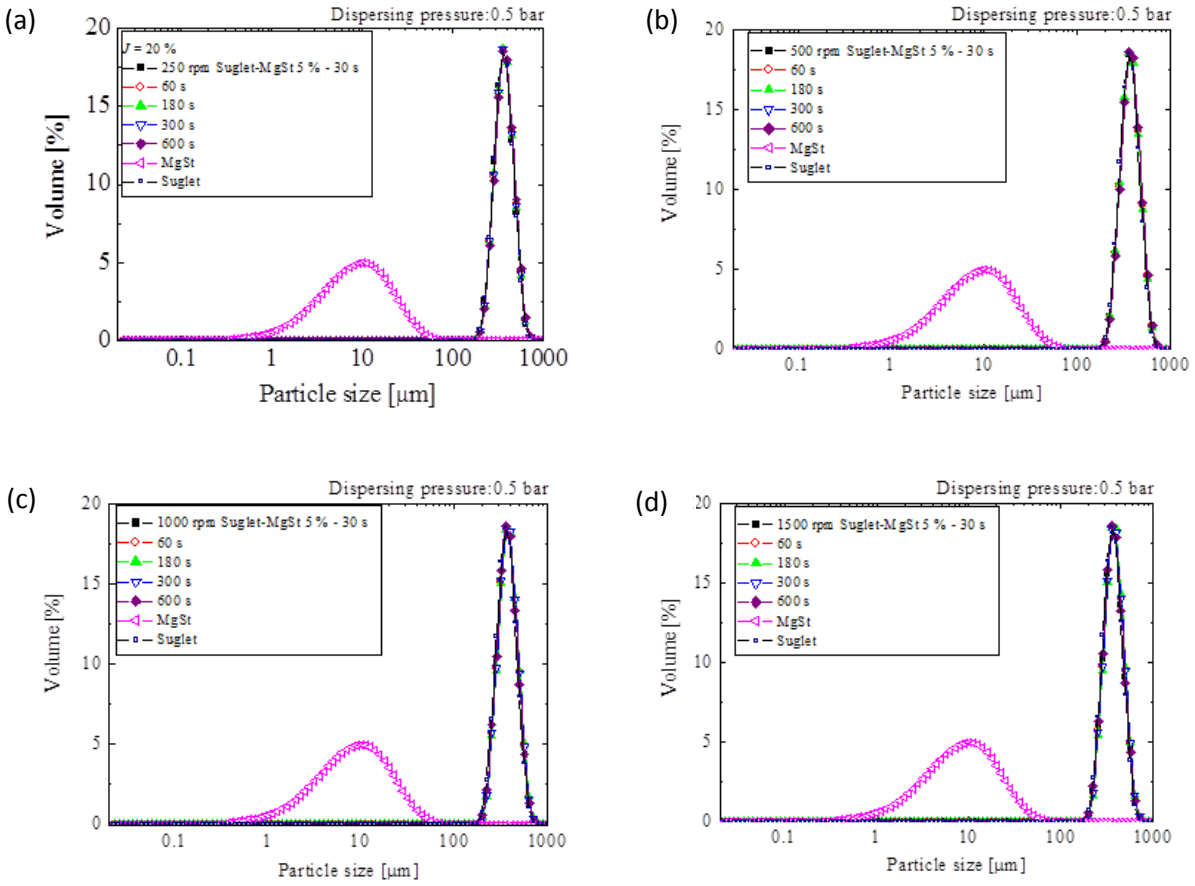

Fig. IV. 25 Particle size distribution in volume of coated particle at each operating time and (a) 250 rpm, (b) 500 rpm, (c) 1000 rpm, (d) 1500 rpm at 0.5 bar

For higher air pressures, the populations of coated particles change. **Fig. IV. 26** shows the PSD in volume of coated particles with filling ratio J = 20 % and different rotational speeds. The air pressure was 3.5 bar. The PSD of coated particles can be divided into 3 populations. One is around 250 µm, which should be the coated particles itself. Another one is around 60 µm which is probably the fragments of Suglets or agglomerates of MgSt and Suglets. The last

one is around 5 µm, it can be estimated as the MgSt extracted from the coated surface of the Suglets. The first one is probably the population of coated particles themselves, however the others remain unclear.

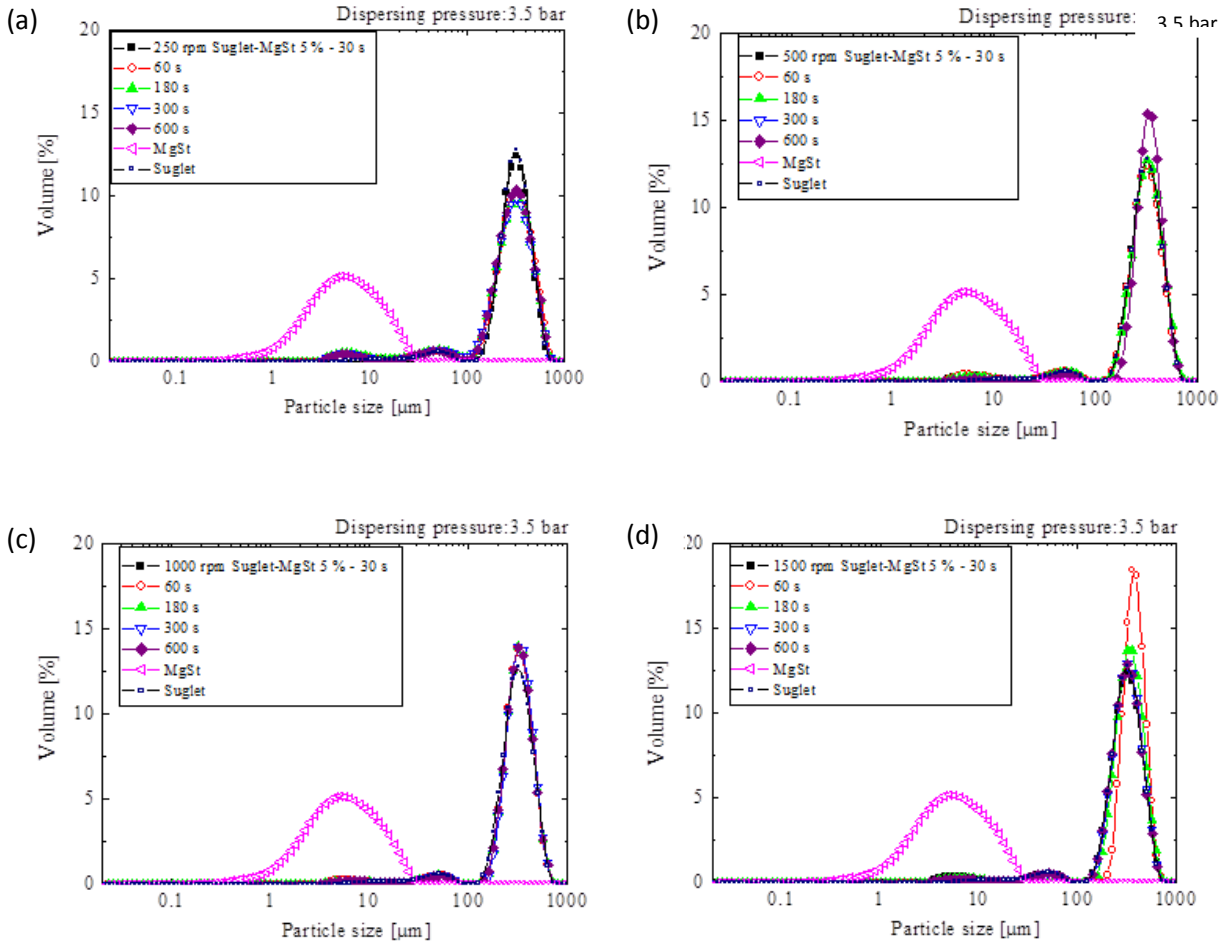

Fig. IV. 26 Particle size distribution in volume of coated particle at each operating time, filling ratio J = 20 % and (a) 250 rpm, (b) 500 rpm, (c) 1000 rpm, (d) 1500 rpm at 3.5 bar

To identify those populations remaining unclear, the same PSDs but in greater magnitude ranging from 0 µm to 100 µm is shown in **Fig. IV. 27**. For the smaller population around 5 µm, it is observed that there is a difference of peak height between the population of Suglets and coated particles. The gap is most likely caused by the separation of MgSt otherwise, the small fragments of Suglets generated by the dry coating treatment. However, considering the changes between the different rotational speeds, these gaps are surely from the separated MgSt particles. For example, the gap of the results of 250 rpm (**Fig. IV. 27 (a)**) is much larger than that of 500 rpm especially (**Fig. IV. 27 (b)**). If those gaps are caused by the fragments of

Suglets, the PSDs of higher rotational speed should have larger gaps. Since the gaps became smaller along with the rotational speed, it is logical to estimate that those gaps come from the separated MgSt particles. Since higher rotational speeds can attach MgSt particles on the surface of Suglets, those gaps decrease with the rotational speed. Concerning the populations around 60 µm, there are little difference between Suglets and coated particles. Then it is clear that those particles are small fragments of Suglets broken during the PSD measurements due to the high air pressure.

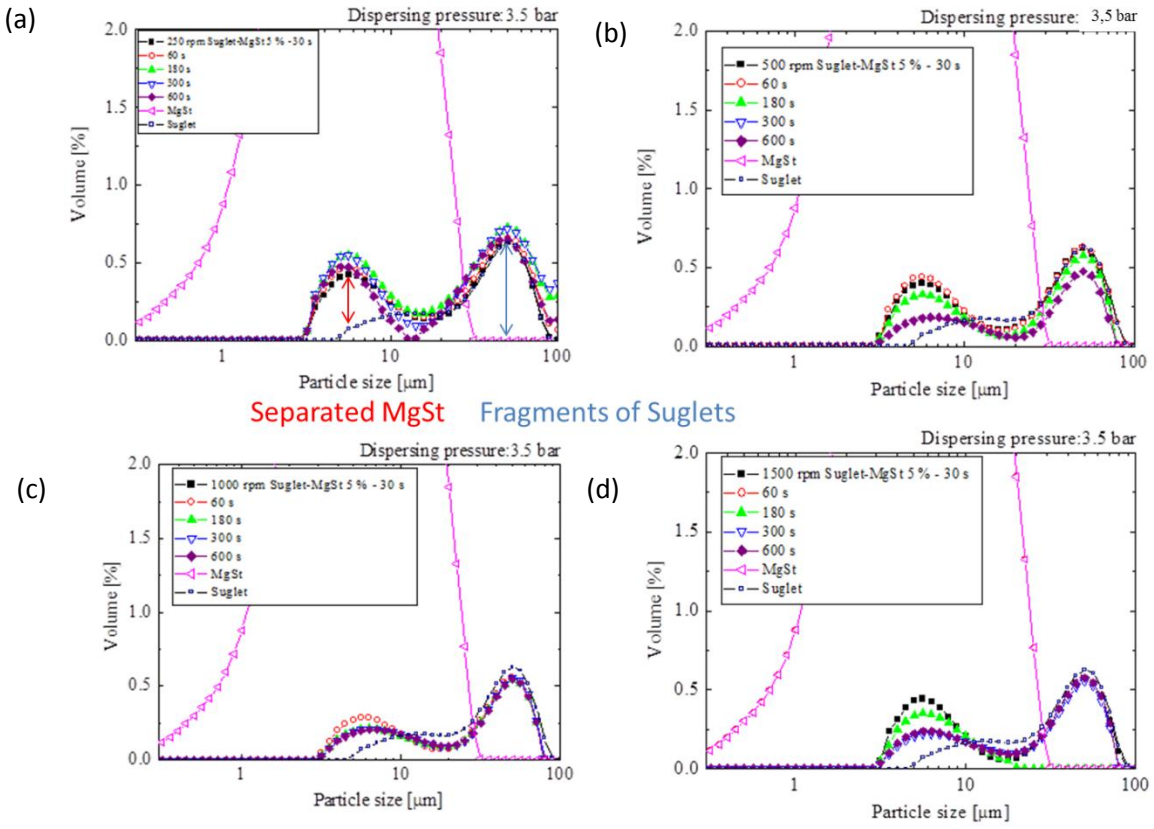

Fig. IV. 27 Particle size distribution in volume of coated particle at each operating time, filling ratio J = 20 % and (a) 250 rpm, (b) 500 rpm, (c) 1000 rpm, (d) 1500 rpm at 3.5 bar in grater magnitude.

At 250 rpm (**Fig. IV. 27 (a)**), the gaps of coated particles with different operating time do not differ a lot. It is suggested that at 250 rpm, the coating anyway proceeds, however those bond forces are not strong enough to resist to the high air pressure even at 600 s of operating time. At 500 rpm (**Fig. IV. 27 (b)**), on the contrary, the gaps are smaller than that of 250 rpm, as explained. In addition, the gaps get smaller with the operating time. It is confirmed that the

operating time plays a role to attach the MgSt particles on surface of Suglets firmly. At 1000 rpm (**Fig. IV. 27 (c)**), almost all the coated particles present a small gap. So, even the short time operation can have a firm coating at 1000 rpm. At 1500 rpm (**Fig. IV. 27 (d)**), it has almost same population as 1000 rpm except 30 s and 180 s, it is unclear the reason why this results were achieved.

Fig. IV. 28 shows the PSD in volume of coated particles with a filling ratio J = 60 % and different rotational speeds for a comparison purpose. Those figures also focus on the range from 0 to 100 µm since from the global scale, there is a little difference.

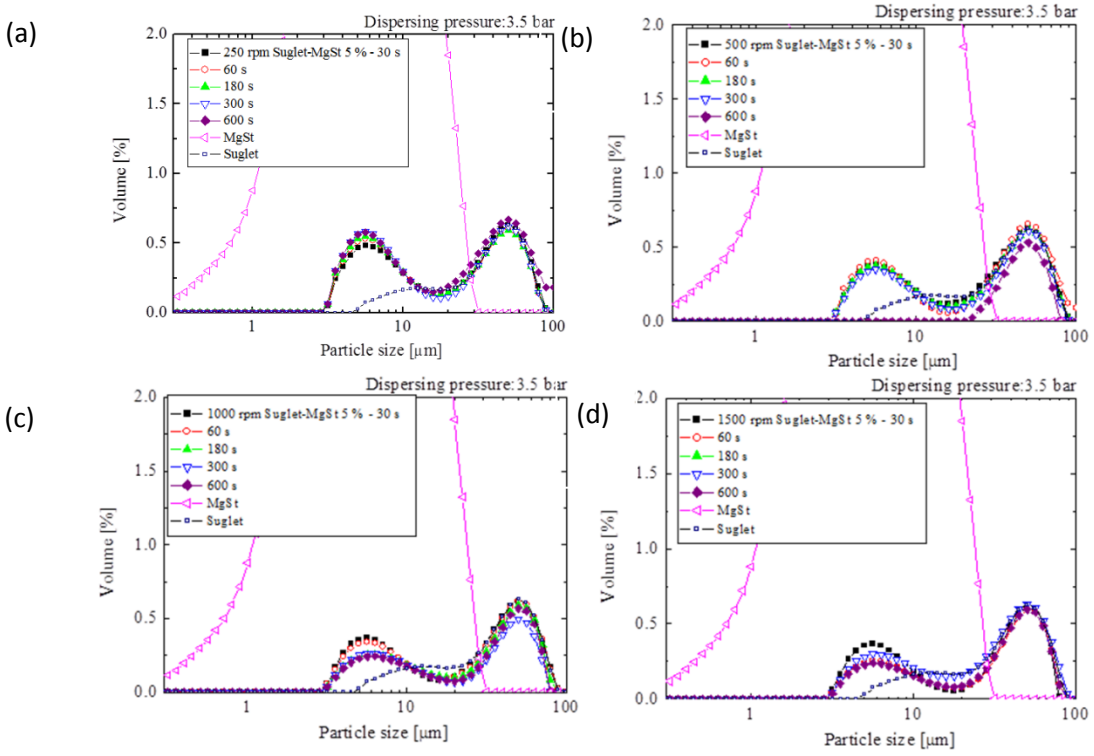

Fig. IV. 28 Particle size distribution in volume of coated particle at each operating time, filling ratio J = 60 % and (a) 250 rpm, (b) 500 rpm, (c) 1000 rpm, (d) 1500 rpm at 3.5 bar in greater magnitude.

The gaps are getting smaller with an increase in the rotational speeds. Comparing the results for J = 20 % (**Fig. IV. 27**), the gaps are slightly larger in general. It indicates that the total volume of guest particles detached from the surface of host particles and dispersed is much larger, that is to say, the coating at higher filling ratios proceeds slower than the coating at lower filling ratios.

3.3.4 Flowability

Flowability of powders can be affected by several physical properties of particles, such as their size, shape, surface roughness and texture. In this work, it is assumed that changes in the surface texture of the particles by coating MgSt could influence flowability by functioning as a lubricant. **Fig. IV. 29 (a)** and **(b)** presents the Flow Rate Index (FRI) as a function of operating time t at different speeds of rotation of the mixer ω and at filling ratios J = 20 % (a), 60 % (b). The initial value of FRI is that of the uncoated host particles.

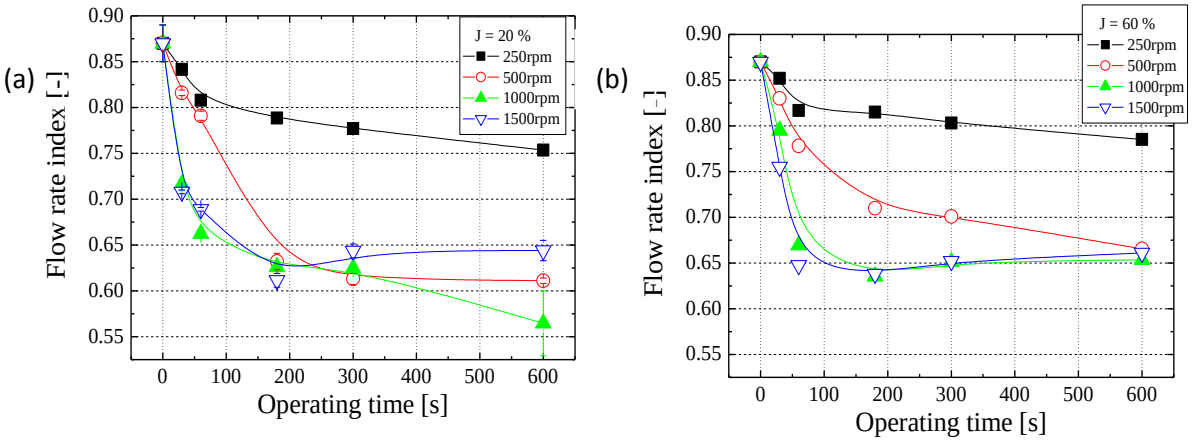

Fig. IV. 29 Dependence of the Flow Rate index (FRI) on the operating time *t,* and on the different rotational speeds ω for different filling ratios (a) J = 20 %, (b) 60%.

In **Fig. IV. 29 (a)**, at 250 rpm, the FRI decreases with an increase in the processing time due to coating by MgSt. However, the FRI at 250 rpm decreases very slowly compared to that obtained for other rotational speeds. This could be because the coating process is slower than at higher speeds. At 500 rpm, FRI decreases also with an increase in the processing time. In other words, the flowability of the coated particles improves with increasing processing time. At 1000 rpm, the FRI decreases with an increase in the processing time more rapidly than at 500 rpm. At 1500 rpm, the FRI decreases with an increase in the processing time up to 180 s, and then it increases slightly. This could be attributed to an increase in the roughness of the surface of the coated particles, due to fragmentation of the host particles, giving an over-coating with some small fragments sticking to the surface of the host particles. **Fig. IV. 29 (a)**,

at J = 60 %, the same behavior is observed as at J = 20 %. However, the FRI decreases more slowly than that of J = 20 % even though the difference is rather small perhaps due to the fact that at higher filling ratios less mechanical energy given to each particle. FRIs at 40% are not given since they gave the same tendencies.

3.3.5 Wettability

The sessile water drop test has been carried out to analyze the wettability of the products.

Fig. IV. 30 (a) and **(b)** shows the contact angle measured 30 s after the water drop is placed on the powder surface for different processing times t, different speeds of rotation ω, and at a filling ratio of J = 20 % (a), and J= 60 % (b).

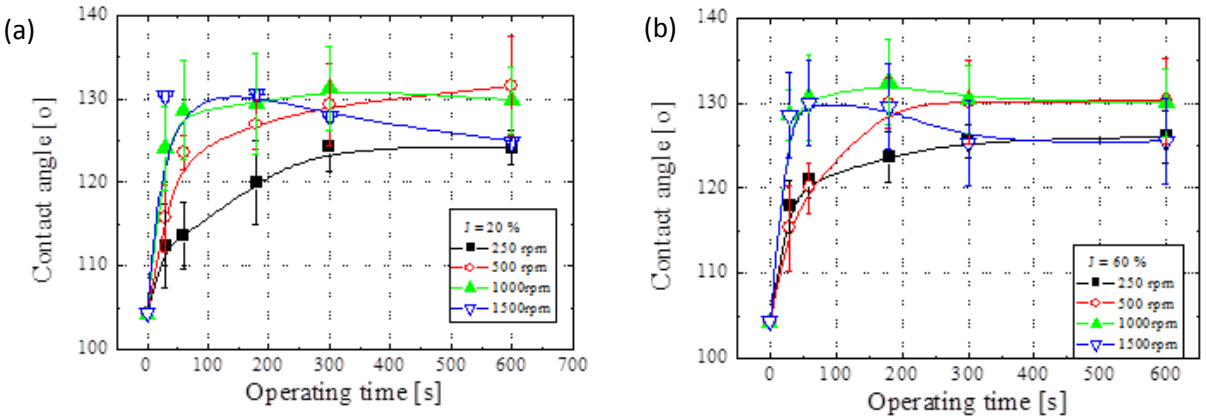

Fig. IV. 30 Dependence of the contact angle on the operating time t, and on the different rotational speeds ω for different filling ratios (a) J = 20 %, (b) 60%.

In **Fig. IV. 30 (a)**, at 250 rpm, the contact angle increases with an increase of processing times. From the assumption above, the surface fraction of the coated material will also increase. In other words, the coating process proceeds as a function of the processing time; at 500 rpm, it increases more rapidly than at 250 rpm. At 1000 rpm, θ (t) increases with time and is asymptote to the θ_1 of guest particles. In **Fig. IV. 30 (b)**, it is observed that these curves have almost the same general tendency as that of **Fig. IV. 30 (a)** thus, the product contact angle is not sensitive to the filling ratio of a high shear mixer. These results have also been confirmed for J = 40%. To summarize, all the coated particles have a contact angle greater than 90°, and the wettability of the coated particles goes from hydrophilic to hydrophobic

even with the smallest processing time and the lowest speed of rotation of the mixer. Regarding wettability, this indicates that this mixer has a good efficiency for coating particles where the particle size ratio between host and guest particles is high enough so that Van Der Waals forces are sufficient enough to firmly coat the guest particles on the host particles.

3.4 Partial conclusion

Investigations on the effects of the operating parameters when using the Cyclomix mixer to achieve dry particle-particle coating has been carried out using model powders: Suglets as a host particles and MgSt as guest particles. The coated particles produced were characterized for flowability, wettability and mass fraction of guest particles forming the coating. The results of the influence of filling ratio are summarized below.

1) The wettability is not sensitive to the filling ratio.

2) The filling ratio is not a significant factor in coating performance.

3.5 Effect of particle size

So far, the effect of rotational speed, operating time and filling ratio of the sample has been investigated. In this section, the aim is to understand the effect of the host particle size. For this reason, larger particles of Suglets ($d50$ = 1000 µm) and the same MgSt product has been used for host / guest particles respectively. It is easy to estimate that the interaction forces applied on the contact area of host and guest particles increase along with the increase of the size, and then the firm attachment of guest particles on the surface of a host particle can be obtained more often. In addition, as reported by Yang et al. (2005), the coating strength between the particles increases with increasing particle size ratio. It is expected to have better coating with an increase in size ratio.

3.5.1 Operating conditions

For this purpose, the Suglets with the median diameter of 1000 µm have been used for the sequence of experiments. The rotational speed varied from 250 to 1000 rpm and the several operating time from 30 to 600 s were used. The mass fraction of MgSt is calculated to be 1.2 % according to the model introduced in Chapter II and used in this study. The filling ratio of the sample is fixed at 60 %. The temperature in the chamber is also fixed at 16 ^{o}C. The operating condition is summarized in **Table IV. 6.**

Table IV. 6 Operating conditions

Device	Rotational speed [rpm]	Operating time [s]	Filling ratio [%]	Mass fraction [%]
Cyclomix	250 -1000	30 – 600	60	1.2

3.5.2 PSD analysis

Fig. IV. 31 shows the PSD of coated particles with different rotational speeds in volume. The air pressure is 3.5 bar. Overall, those PSD have two populations, one is around 1000 µm which is obviously from the Suglets particles themselves. The other one is around 120 µm. It

can be estimated that the latter populations would be either the fragments of Suglets or the separated MgSt particles from the surface of host particles. However, considering the size, it can be hardly thought that those populations are from separated MgSt particles. Even though there is a possibility that the MgSt particles agglomerate during operations, these agglomerates would not grow up until 120 μm.

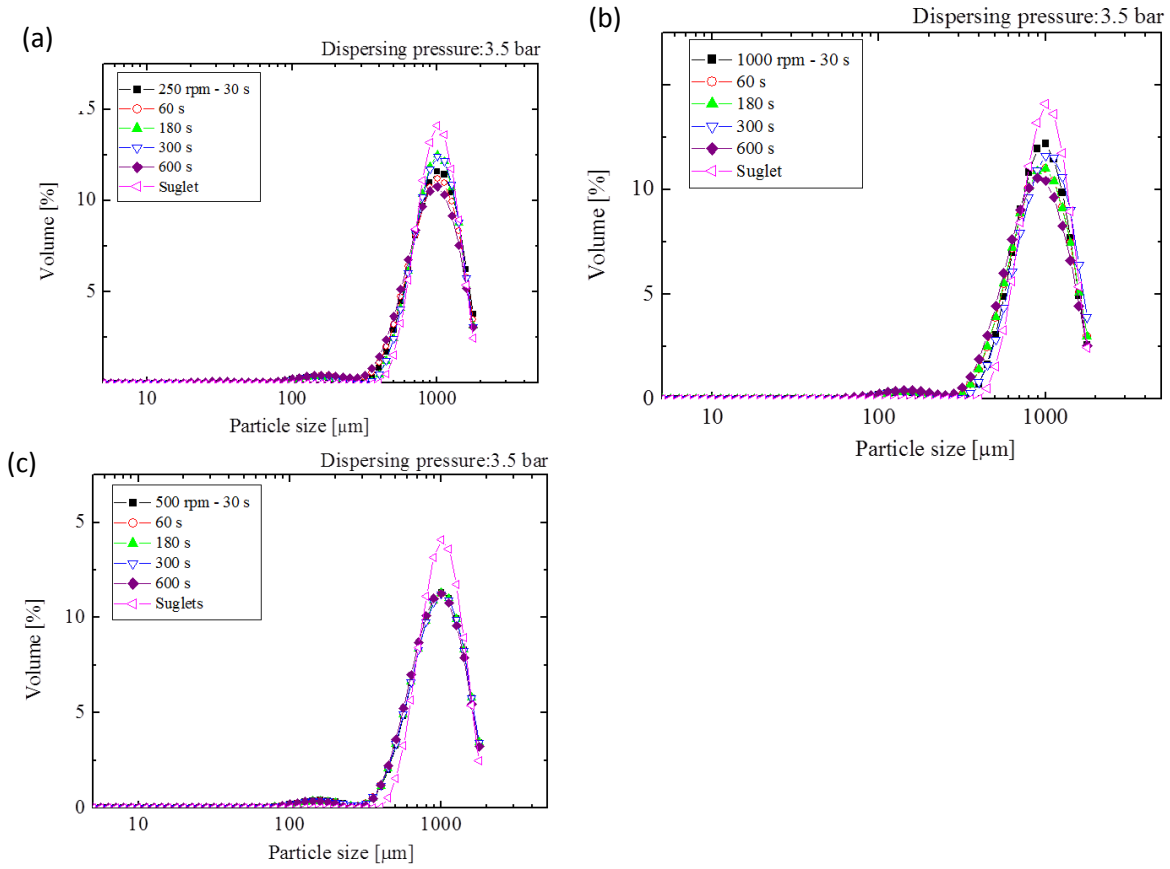

Fig. IV. 31 Particle size distribution in volume of coated particle at each operating time, filling ratio J = 60 % and each rotational speed (a) 250 rpm, (b) 500 rpm, (c) 1000 rpm at 3.5 bar

So those populations should be constituted of the fragments of Suglets particles caused by the high air pressure of the PSD measurement. Consequently, there is no smaller population observed in those figures. It is suggested that there are no separation of MgSt particles due to the air pressure. So, it can be said that the adhesive forces between guest particles attached on the surface and host particles are stronger than that of smaller host particles. For instance, in

Fig. IV. 27, it is confirmed that there is no separation of MgSt particles at same air pressure which causes the separation of the coated particles composed of Suglets with 250 μm and MgSt. These results indicate that bigger host particles could achieve firmer coating.

3.5.2 Flowability

Fig. IV. 32 shows the variation of FRI as a function of operating time at each rotational speed. The initial value of FRI is that of host particle. In general, the FRI of each coated particles decreases with an increase in operating time. It indicates that the coating of MgSt particles on Suglets particles has been successfully done since to achieve improved flowability. At 250 rpm, FRI decreases almost as rapidly as for the other higher rotational speed and around 300 s, it seems to reach the asymptotic state. By comparing the results of smaller host particles (**Fig. IV.29 (b)**) treated exactly with the same operating conditions (except particles size ratio), one can see that the FRI decreases much more rapidly. In other words, the coating proceeds faster than smaller host particles. It seems to be because the impact forces applied on the contact point between host and guest particles increase with an increase of size ratio.

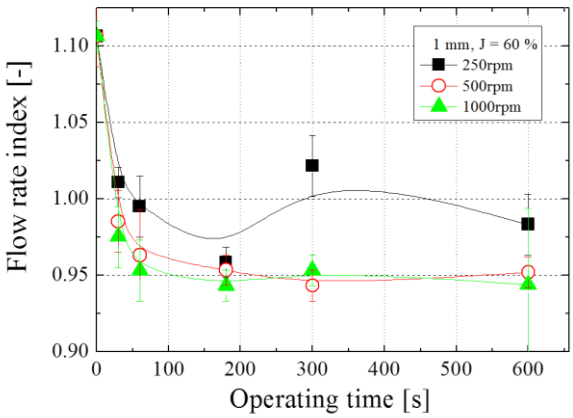

Fig. IV. 32 Variation of FRI as a function of operating time at each rotational speed.

As for 500 and 1000 rpm, FRI decreases with an increase in operating time up to 180 s and then it reaches an asymptotic state. However, there is little difference between the two

rotational speeds. This result indicates that over 500 rpm, the impact forces given by the rotating mixer are high enough to attach almost all the MgSt particles on the surface of host particles rapidly as well as the deformation of MgSt particles to have the film-like coating.

3.5.3 Wettability

The variation of contact angles of coated particles with different rotational speeds is shown in **Fig. IV. 33**. The initial point calculated as seen previously (**Eq. IV. 1**), is equal to 104^{o}. The contact angles increase very rapidly and it reaches a plateau. Compared to the results of smaller particles (**Fig. IV. 30 (b)**), the difference is very large. It can be due to exactly the same reason as the evolution of flowability, that is to say, due to the difference of impact forces given to the host and guest particles. In fact, it is not really comparable to the results of smaller host particles since the capillary forces should be different due to the difference in the porosity of the bulk powder bed. At least, it is obvious that the surface coating and modification proceed very rapidly, in comparison with surface modification observed in experiments with smaller host particles.

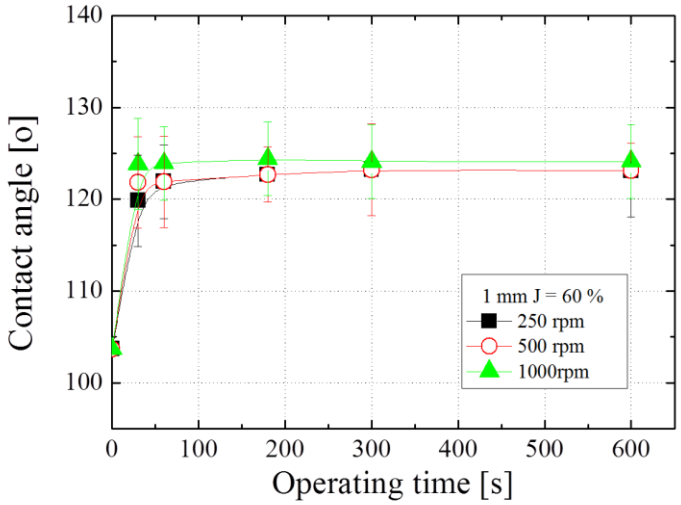

Fig. IV. 33 The variation of contact angles of coated particles with different rotational speeds.

3.6 Partial conclusion

The dry coating with several operating conditions using Suglets whose median diameter is 1 mm and MgSt for host / guest particles respectively has been done. The results are summarized below.

1) PSD analysis shows that there was no separation of MgSt particles from the surface of host particles even at 3.5 bar of air pressure. It is indicated that the coating of bigger particles seems to have stronger adhesive forces than that of smaller particles.

2) The flowability of coated particles was improved rapidly and it reaches an asymptotic state. Compare to the results of smaller host particles, it is clear that the flowability of bigger host particle was improved faster. It indicates that the coating as well as the deformation of MgSt particles on the surface, which gives film-like coating, proceeds faster than smaller host particles. It is because the impact forces applied on the contact point between host and guest particles increase with an increase of size ratio.

3) The wettability of coated particles was improved also rapidly compare to the results of smaller particles. It is confirmed that the coating of bigger particles advances faster than that of smaller one.

In conclusion, all the characteristics of the coated particles indicate that coating proceeds much faster than that of smaller host particles. In addition, the effect of rotational speeds as well as the coating time is not remarkable compare to experiments with smaller host particles. The impact forces given by the rotating mixer are sufficiently high enough to attach almost all the MgSt particles on the surface of host particles rapidly. The deformation of MgSt particles to become a film-like coating is also a quick step coating; so, the particle size plays a very important role in dry coating.

IV. 4 Kinetic study by evaluation of conversion ratio

So far the evolution of surface properties such as flowability and wettability by dry coating has been investigated. The questions still remaining are how many guest particle stick to the host particles and if there is some relationship the amount of guest particles attached and those surface properties. The conversion ratio as introduced Chapter II, has been measured and the efficiency of the dry coating has been estimated.

4.1 Suglets 250 µm

The conversion ratio of dry coating has been measured by sieving the coated particles (See Chapter II). This ratio allows us to keep track of progress of dry coating, which is important to evaluate the efficiency of the operating conditions.

Fig. IV. 34 presents the variation of the conversion ratio λ(t) of the coating process as a function of processing time *t* at different rotational speeds *ω*, and for two filling ratios *J* = 20 % **(a)**, 60 % **(b)**.

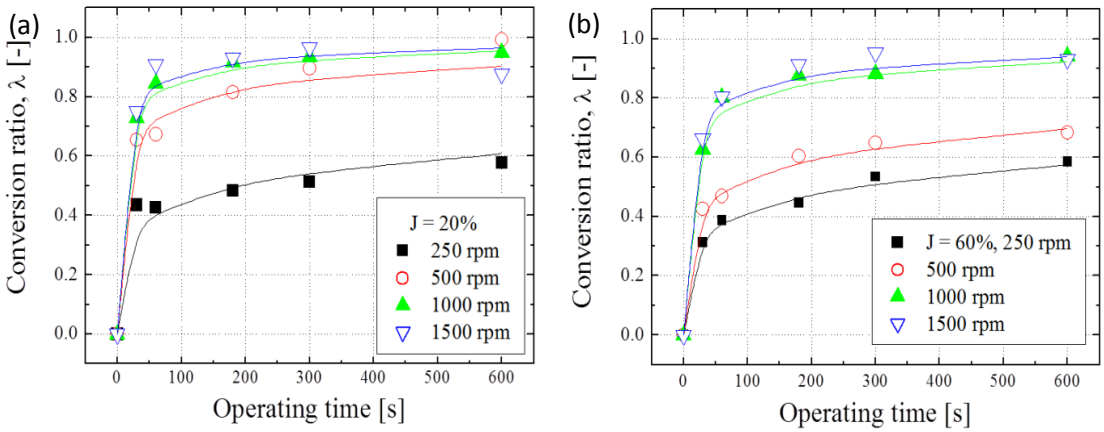

Fig. IV. 34 Dependence of the conversion ratio on the operating time t and on the rotational speed *ω* for different filling ratios (a) J = 20 %, (b) 60%.

In general, the conversion ratio increases with an increase of processing time. The higher the speed of rotation the faster the conversion ratio increases. Higher rotation speeds of the mixer provide more energy to coat the host particles. The influence of the filling ratio is not observed clearly, however at smaller filling ratios the conversion ratio increases more rapidly. For J = 40 %, analogous curves were observed, hence it was omitted to show.

All the data plotted in **Fig. IV. 34** indicate that the conversion ratio increases exponentially with an increase in processing time up to the asymptotic value of 1.0, the coating obtained when almost all the guest particles stick to the host particles. Those behaviors are similar to the first-order reaction in chemical kinetics. Hence the conversion ratio obtained at certain processing time $\lambda(t)$ can be expressed by an empirical exponential equation with one parameter K_c given in **Eq. IV. 4**.

$$\lambda(t) = 1 - e^{-k_c t^a} \qquad \textbf{IV. 4}$$

The index number a is given by the empirical method as shown in **Fig. IV. 32**.

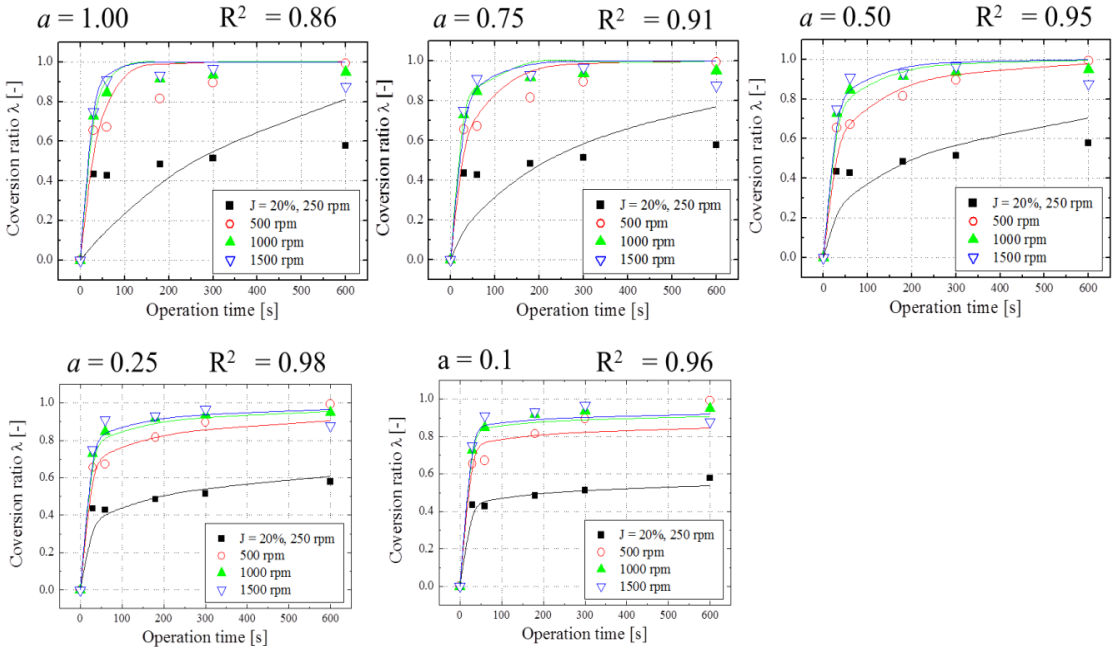

Fig. IV. 35 Fitting curves with different index a on the conversion ratio of coated particles at filling ratio J = 20 %.

The index *a* is obtained from the Non-linear least square method with trying several values from 0.1 to 1. As seen in **Fig. IV. 35**, the best correlation coefficient R^2 was given when the index *a* is 0.25. So, the index *a* is determined at 0.25. This index should be dependent on the experimental system such as, temperature and humidity in the mixing chamber, the materials, particle size and size ratio of host and guest particles.

The parameter K_c was obtained by the nonlinear least square fitting of the curves as shown also in **Fig. IV. 34** with obtained index a = 0.25. The parameter K_c depends on the operating condition such as rotational speed, filling ratio.

It can be concluded that this empirical equation is able to express the conversion ratio. So, the parameter K_c represents the ability of the mixer to achieve a coating, and it shall be called the coating rate constant from now on.

The K_c *value* obtained by comparing experiments and empirical modeling has been plotted in **Fig. IV. 36**.

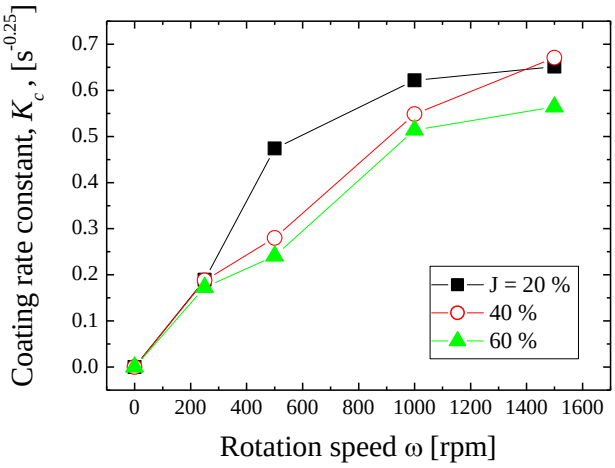

Fig. IV. 36 Coating rate constant K_c as a function of rotational speed.

K_c increases with an increase in rotational speed, however it does not seem to vary linearly. In particular, at higher speeds from 1000 to 1500 rpm, the coating rate constant K_c does not increase very much. This indicates that there is an optimum rotational speed for coating the host particles and if an excess energy is given, it does not contribute to improving the coating but leads to heat dissipation, attrition and erosion due to too rapid particle flow. The constant

K_c is representing the efficiency of the operating conditions on dry coating.

The mixture composition is related to the particle physical properties. If there is a relation between the conversion ratio and the coated product properties, then the product properties can be predicted. Furthermore, determining the conversion ratio does not require special equipment and is simply determined by measuring masses after sieving.

Fig. IV. 37 shows the relation between FRI, the value corresponding to flowability and the conversion ratio λ. It is observed that even though the plotted points are widely spread, the FRI is linearly proportional to the conversion ratio. The flowability depends not only on the conversion ratio but also on the shape and angularity of the particles, which explains why the plotted points are scattered around the line.

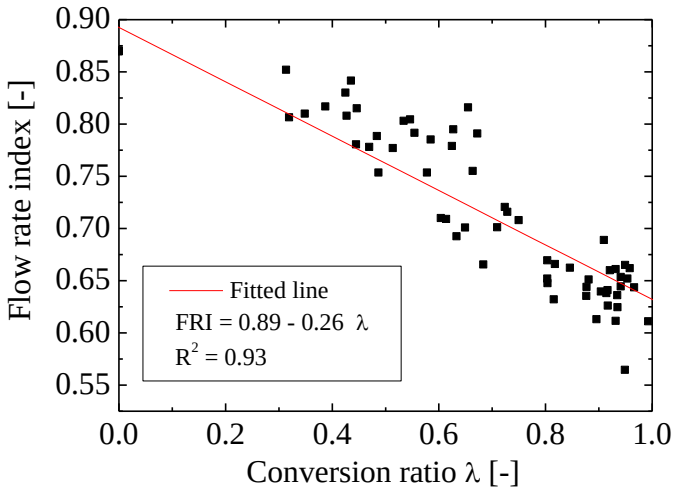

Fig. IV. 37 Relationship between the conversion ratio and the FRI - fitted line.

Fig. IV. 38 presents a linear relation between the contact angle and the conversion ratio λ.

The plotted points are seen to be more widely scattered than that of flowability data. One possible reason is the powder bed used to determine the contact angle was not compressed and thus the surface was not perfectly uniform, thus inducing experimental errors even though the contact angle was measured at 3 different locations on each sample to alleviate this problem.

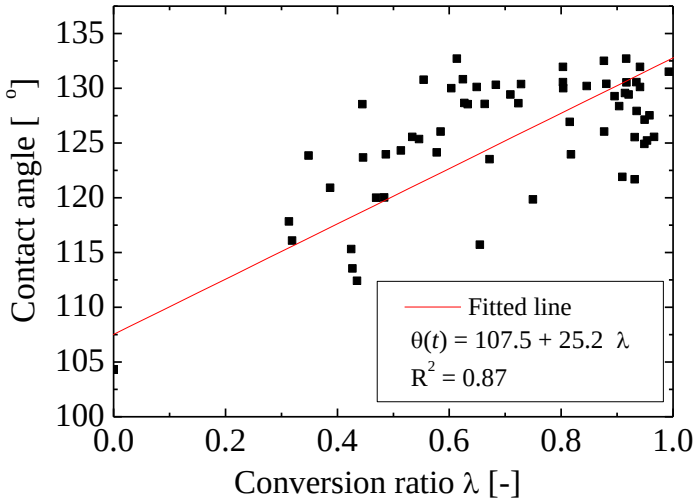

Fig. IV. 38 Relationship between the conversion ratio and the contact angle θ - fitted line.

The physical state of the surface, characterized for example by the porosity of the surface, is a significant factor in determining the contact angle.

To summarize, there seems to be a linear relationship between the physical properties of the coated particles and the conversion ratio.

4.2 Suglets 1 mm

Conversion ratio of Suglets 1 mm coated with MgSt has been measured. **Fig. IV. 39** shows the conversion ratio as a function of operating time at each rotational speed. In general, the conversion ratios of each rotational speed increase rapidly up to 60 s and they seem to reach an asymptotic state. Comparing **Fig. IV. 34 (b)** in which the experiments have been done exactly in the same operating conditions (except host particles size), an increase of the conversion ratio, in other words, a progress of dry coating is remarkably high. It is obviously because of particle size: the particle size ratio of host / guest particles plays an important role in dry coating.

At 500 and 1000 rpm, there were few particles having passed through the sieve. It was almost impossible to collect them and measure the mass of them. So, in the **Fig. IV. 39**, those are plotted to 1.0 of conversion ratio. Probably, it is possible to approximate the behaviour of

conversion ratio by proposed model as shown in **Eq. IV. 4**. However, to do so, it is required to observe this behaviour in microscopic small scale of duration of coating since coating proceeds so rapidly.

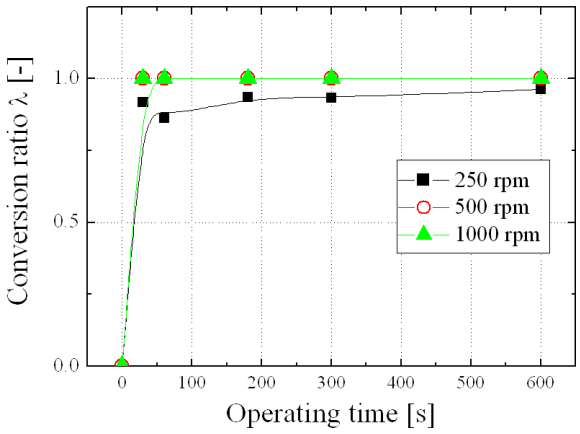

Fig. IV. 39 Variation of the conversion ratio of coated particles with different rotational speeds.

4.3 Partial conclusion

The conversion ratio increases exponentially to reach an asymptotic value around the value for an ideal coating. This behavior has been fitted by an exponential model with one variable parameter defined as K_c. The fitted curved represents the conversion ratio.

It is found that the properties of the coated particles can be predicted by the conversion ratio at a given time in the coating process. The linear relation between the conversion ratio and the product properties can be quantified by a model involving a coating rate constant K_c, which can be used to optimize dry coating processes to give desired properties of coated particles.

Because of the size ratio of host / guest particles, the conversion ratio increases also more rapid than that of smaller host particles.

Conclusion

In this chapter, the results of variation of surface properties of coated particles with various operating conditions have been shown. As a result, it is found that the rotational speed as well as the operating time has a great influence on the dry coating. These results also allow us to estimate that the evolution of dry coating can be classified into two cases (**Fig. IV. 40**).

If a low rotational speed is applied in the dry coating, firstly the discrete coating is made rapidly, and with longer operating times, MgSt particles on the surface of host particles are smeared and deformed into flat and coating proceeds to a continuous state (**Fig. IV. 10**). This behaviour of MgSt on the surface makes internal closed pores on the surface, which causes the decrease of pycnometry density (**Fig. IV. 20**).

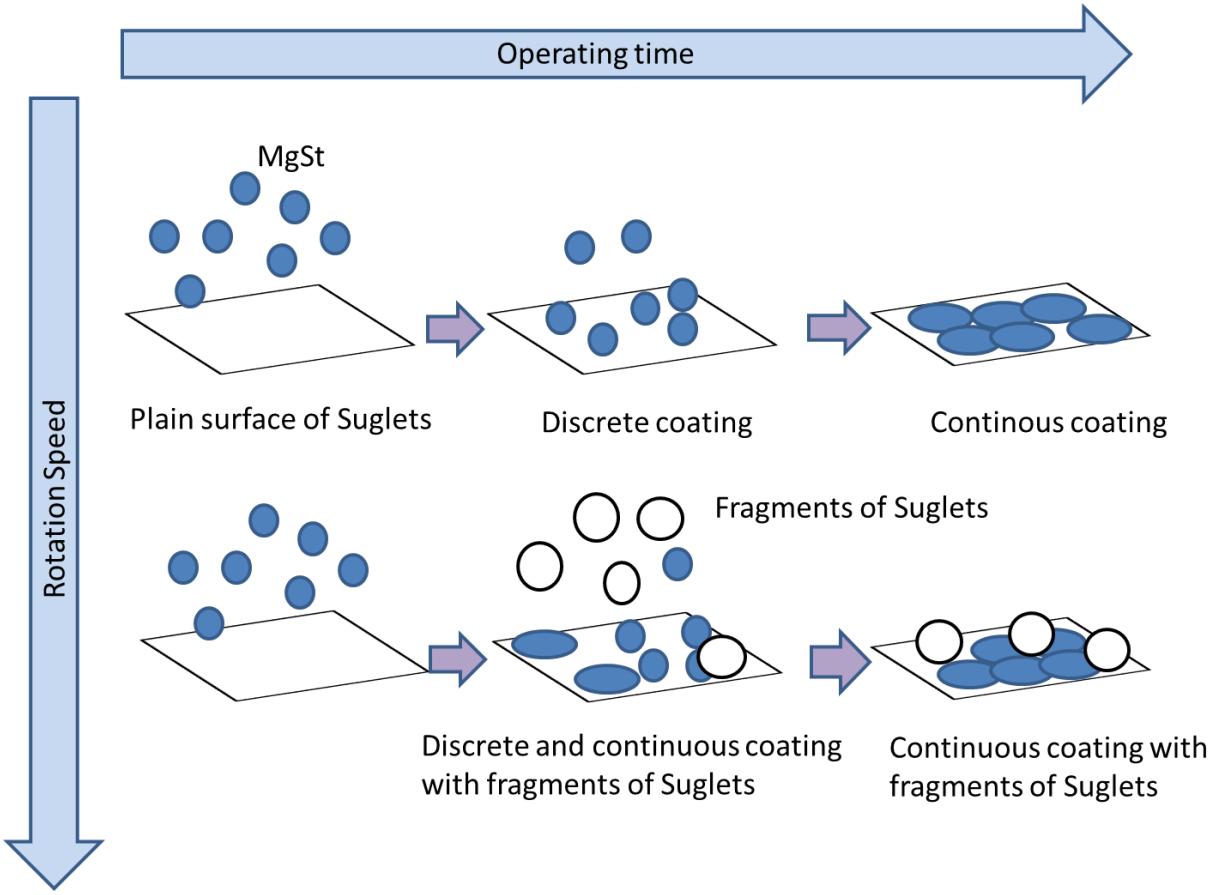

Fig. IV. 41 Progress of dry coating under effect of rotation speed and operating time

If a high rotational speed is applied in the dry coating, either a discrete or continuous coating occurs rapidly. However, fragments of Suglets also occur in the meantime as shown in (**Fig**

IV. 14 (c)). They attach on the surface of the Suglets particles. That makes the surface properties worse again as seen in (**Fig IV. 19** and **20**).
Finally, it is essential to choose the suitable operating time and rotational speed to have coated particles with a good quality.

For the effect of filling ratio, it is found that this operating condition has less effect on the dry coating than the rotational speed and operating time. However for operating conditions at small filling ratio, the coating proceeds slightly faster than at higher filling ratio.guest

For the effect of particle size, all the characteristics of the coated particles indicate that coating proceeds much faster than that of smaller host particles. In addition, the effect of rotational speeds as well as the coating time is not remarkable compare to smaller host particles. The impact forces given by the rotating mixer are sufficiently high to attach almost all the MgSt particle on the surface of host particles rapidly as well as to ensure the deformation of MgSt particles to form the film-like coating. As a result, there is little difference. So, the particle size plays a very important role in dry coating.

In the kinetic study, the conversion ratio of the coated particle has been measured. It is found that the evolution of conversion ratio with operating time has some similar tendency to follow a first order reaction in chemical kinetics. Then this evolution is approximated described by an empirical exponential model with one variable parameter K_c.
It is found that the properties of the coated particles can be predicted by the conversion ratio at a given time in the coating process since there are linear relations found between them (**Fig. IV. 37** and **38**). The linear relations between the conversion ratio and the product properties can be quantified by a model involving a coating rate constant K_c, which can be used to optimize dry coating processes to give desired properties of coated particles.

In conclusion, an investigation of the effect of operating condition on dry coating has been done. It made clear that those dependences on the dry coating. The numerical results will be compared to those dependences and shown in Chapter V.

Chapter V Numerical results

V. 1 Introduction

In this chapter, the numerical studies of dry particle coating process in a high shear mixer have been dealt. The work presented in this chapter is the analysis of the velocity field of the numerical and real particle motion. The real particle motion has been taken by the high speed camera and transparent vessel. Both numerical and experimental velocity fields have been obtained from the PIV method. The second objective is to calculate several values such as collision frequency, force distribution, rotating kinetic energy, impact energy and so on, in order to understand the behaviour of particles in a high shear mixer system under different operating conditions (rotational speed, filling ratio, and particle size). To shorten the calculation time, only the motion of host particles is focused since guest particles are so small that they may not be able to affect the motion of the host particles. The third objective of this chapter is to simulate in the dry coating process the attachments of guest particles on host particles.

Simulation parameters for a system of host particles only

Some among the most important physical conditions and simulation conditions are shown in **Table V. 1**.

Table V. 1 Physical (a, b, c) and simulation (d to g) conditions

Young's modulus (a)	E [GPa]	4.5
Poisson's ratio (b)	[-]	0.30
Density (c)	[kg/m^3]	1600
Coefficient of friction (d)	[-]	0.7
Coefficient of restitution (e)	[-]	0.3
Time step (f)	Δt [µs]	2.0
Total simulation time (g)	T [s]	3.0

The total simulation time is chosen by the stability of the number of collisions at each time step (that is to say, the value is not cumulative.). **Fig. V. 1** shows the number of collisions particle-particle or particle-wall (conical wall or paddles) as a function of simulation time, for a rotational speed of 100 rpm, a particle size 1 mm and a filling ratio

60 %. The number of collisions, until 1.0 s of the simulation seems to be unstable. After 1.0 s, it is seen reaching a steady state. So it was decided to calculate for 3 s, so that the particles collisions would sufficiently reach a steady state. It is assumed that the configuration of the mixture should be also in a state not far from a steady state after 3 s.

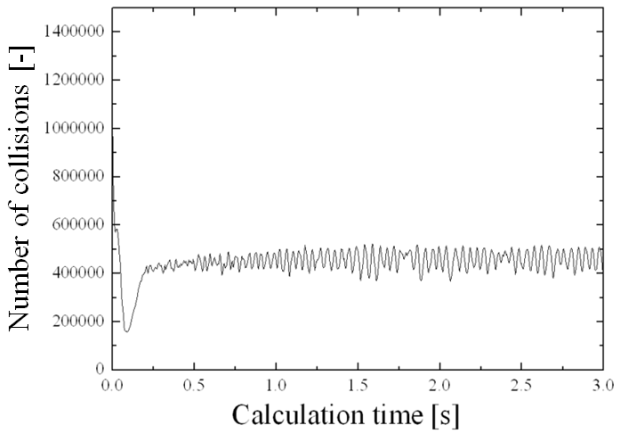

Fig. V. 1 The number of collisions as a function of calculation time.

V. 2 Velocity analysis of real and simulated particle motion by PIV

AS introduced chapter II, PEPT is limited the number of particles which can be analyzed, since the only positron emitting tracer particles can be analyzed. Hassanpour et al. (2009) has analyzed the particle velocity by PEPT, and velocity obtained agreed with simulated velocity. The Particle Image Velocity can only analyze the particle near the transparent vessel. However it can analyze almost unlimited number of particles as long as they are located near the transparent vessel. In this research work, PIV method was carried out in order to analyze as large number of particles as possible.

Both numerical and experimental velocity fields have been obtained from the PIV method. Of course from the simulation, the exact calculated values of velocity can be obtained. However to compare the experiment and numerical particle motion in the same conditions, both are analysed by the PIV and with the same analysis field. The height of the impellers is shown in

Fig. V. 2. The impellers are named impeller N^{o} 1 to 3 in the order of height as shown in **Fig. V. 2**.

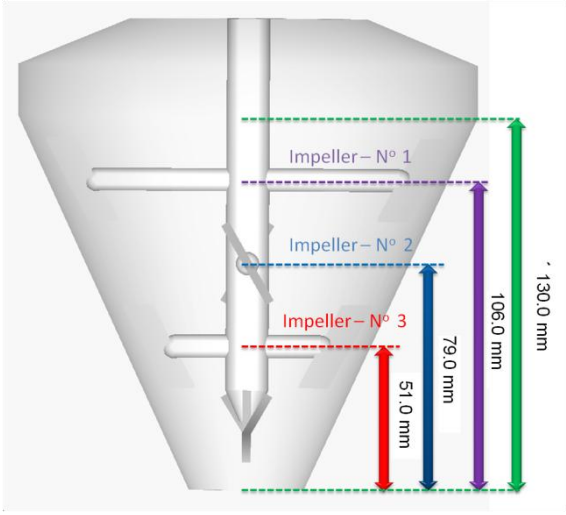

Fig. V. 2 Schematic diagram of the high shear mixer.

2.1 Comparison of velocity vector fields between experiment and simulation

Fig.V. 3 shows the images of particle motion acquired in a high shear mixer from a high speed camera, at a rotational speed of 250 rpm. The apparent volume of the particles introduced into mixer is 200 cm^{3}, and the porosity of the bulk is about 53 %. The estimated number of particles is 191000. The rotation angle of the rotor, 0^{0} was defined as the reference angle for this study. This angle corresponds to the position where the highest impeller is located just in the camera axis. Then for 90^{o}, the second highest impeller comes in front of the camera axis, because each impeller is shifted from 90^{o}. It can be observed how the impellers agitate the particles. A powder bed seems to stay just around the midst of the impeller N^{o} 2. The particles near the impeller N^{o} 2 are scattered by its rotation.

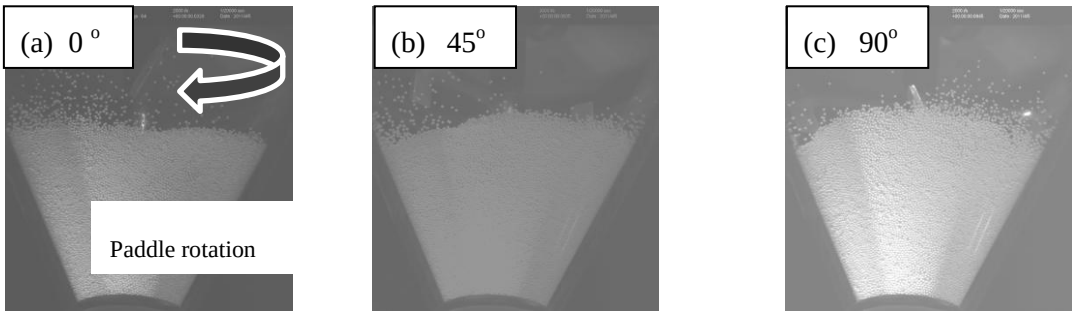

Fig. V. 3 Particle motion taken by a high speed camera at (a) 0° , (b) 45°, (c) 90°.

Fig. V. 4 shows the particles motion in the high shear mixer obtained from the simulation work under the same conditions of experiment (particle diameter: 1 mm, volume of sample introduced: 200 cm^3 (porosity of the bulk is 53 %.), number of the particles: 190986, rotation speed of the mixer: 250 rpm). The height of the powder bed seems to be almost the same as the experimental one. In these figures, the behavior of the simulated particles is quite similar to the experimental one. Though, in the simulation, there are less scattered particles observed than in experiments when the the impeller N° 2 is in the camera axis.

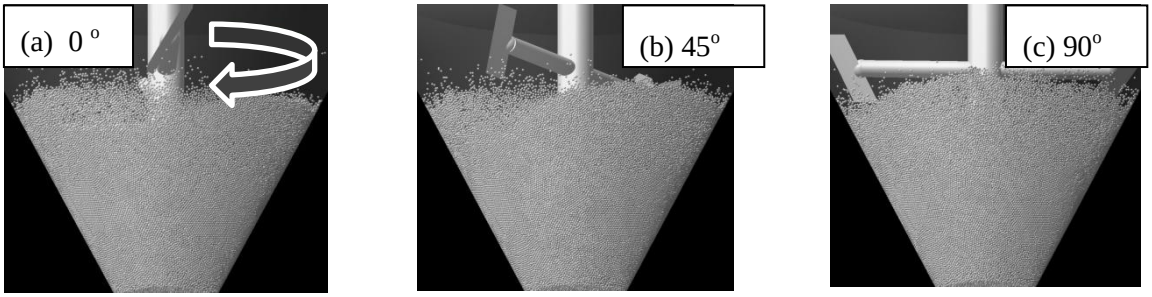

Fig. V. 4 Particles motion obtained from the simulation at (a) 0° , (b) 45°, (c) 90°.

To get a more quantitative validation, the velocity vectors field of both experiment and simulation has been analyzed by PIV. The analysis field was limited to just around the main rotor in order to avoid the effect of light refraction. The experimental and simulated movements of the particles are observed on a comparable basis, and limited to the particles located just behind the vessel wall. The velocities are measured in a right handed coordinate system, though the rotation direction is clockwise (**Fig. V. 5**). So, for horizontal velocity, it is

expected to have negative values.

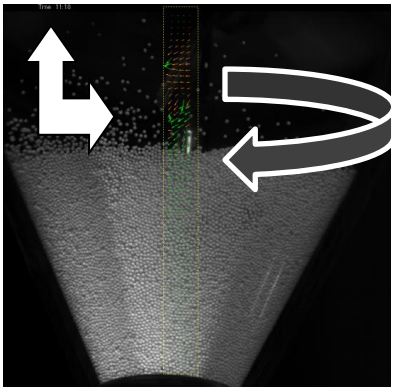

Fig. V. 5 Analysis field of PIV.

Since this mixer possesses a conical symmetry, only the velocity vectors fields at rotation angles 0^o and 90^o were processed, after a transitory period of 100 impeller rotations. The modules of horizontal and vertical velocity vectors in the simulation and the experiment at 0^o are shown in **Fig. V. 6** (a) and (b) respectively. In **Fig. V. 6** (a), there is an increase in horizontal velocity of particles located at the height of 0.03 m in both experimental and simulation fields (near the bottom of the mixer). That is obviously the effect of the impeller N^o 3 (height: 0.051 m, see **Fig. V. 2**) in front of the analysis field at this rotation angle. Both fields are very similar even though there is a small gap between the simulation and the experiment. In **Fig. V. 6** (b), the effect of the third impeller is found in both fields.

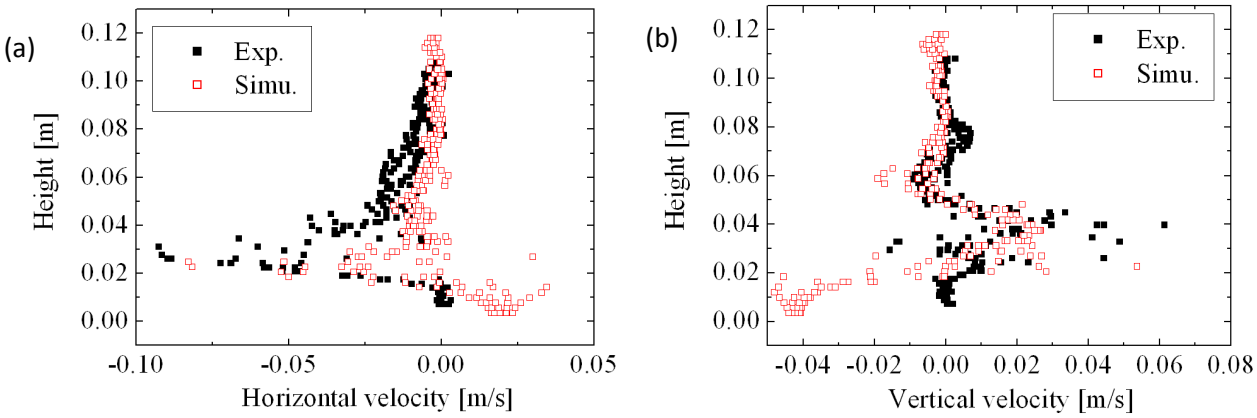

Fig. V. 6 The horizontal (a) and vertical (b) velocity modulus for simulated and real motion at 0^o.

Fig. V. 7 shows the modulus of horizontal (a) and vertical (b) velocity vectors in the simulation and the experiment at 90°. Since the impeller N° 2 (height: 0.079 m, see **Fig. V. 2**) is just in front of analysis field, its effect is found in vertical velocity vectors of simulation and experiment. In the horizontal velocity vectors of the simulation, the effect of second impeller does not appear as much as that in experiment. Even though there are some gaps, a certain similarity between experiment and simulation can be noticed.

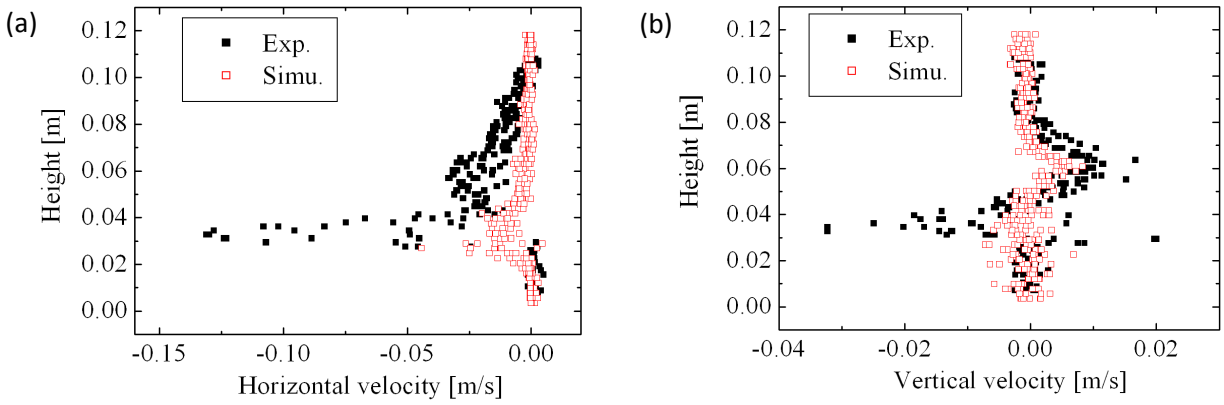

Fig. V. 7 The horizontal (a) and vertical (b) velocity modulus for simulated and real motion at 90°.

From the investigation of velocity vectors field at 0 ° and 90°, it is confirmed that the simulation can fairly represents the real motion in the different locations of the high shear mixer.

2.2 Comparison of mean velocity between experiment and simulation

Fig. V. 8 shows the relation between the mean velocity in experiment and simulation. The mean velocity is defined as the sum of all the velocities achieved by PIV divided by the number of elements analyzed. Concerning the horizontal mean velocities, (**Fig. V. 8** (a)), the experimental one shows a strong dependence of velocities on the angle of impellers such as 90° and 270 °.

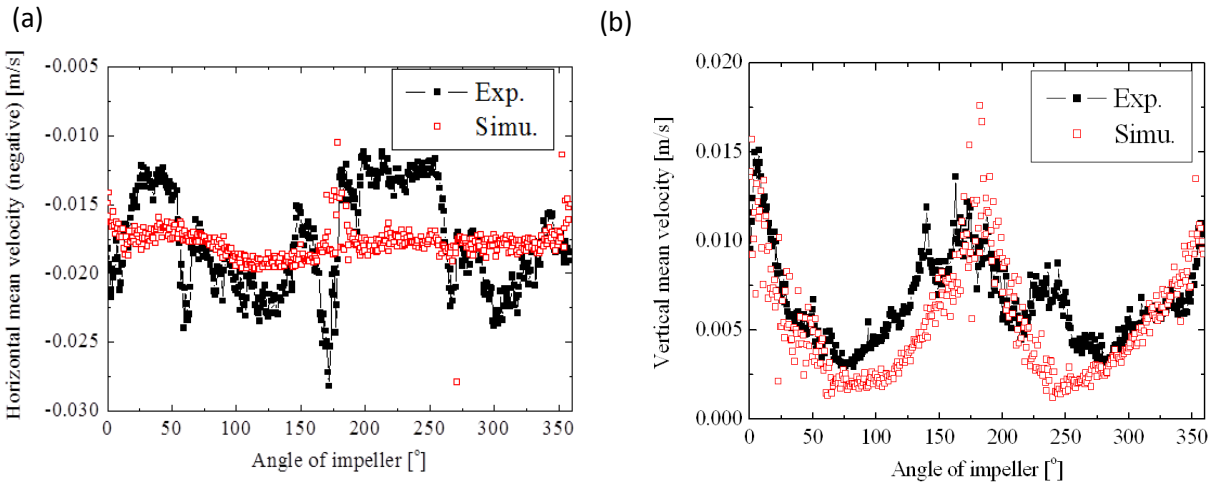

Fig. V. 8 Relations between the mean velocities as a function of the angle of impeller in vertical (a), horizontal (b) axis.

On the contrary, the simulated one shows little dependence. Probably, it is because the difference of initial position between experiment and simulation that is to say, in experiment, the particles are introduced from the input and filled with gravity. On the contrary, in the simulation it is arranged hexagonagal structure. As a result, even after they reach the steady state, they behave differently. So, the collisions simulated between particles and the impeller were weaker than in the real system in the horizontal direction. At least, the simulation has succeeded in representing certain parts of experimental ones. For the vertical mean velocity (**Fig. V. 8** (b)), it is found that both are strongly affected by the impeller position. A close agreement between simulation and experiment is found. From the mean velocity analysis, it can be said that the simulation has a good enough validity to give the information about the dry coating efficiency in a high shear mixer.

V. 3 Simulation of motion of host particles in a high shear mixer

Numerical experiments with different operation conditions such as rotational speed ω, filling ratio J and particle size have been carried out in order to understand the effect of those operating parameters. Outputs of the simulation are aimed to compare the experimental results shown in previous chapter, particularly to find the parameters which are corresponding to the coating rate constant so that the efficiency of the operating condition on the dry coating can be predicted. If there were certain correlationships between experiment and simulation, it would be a great step for optimization of operating conditions of dry coating. The operating conditions are summarized in **Table V. 2**.

Table V. 2 Operating conditions

Rotational speed ω [rpm]	Particle size [mm]	Filling ratio J [%]
100, 500, 1000, 1500, 2000, 2500, 3000	1, 2, 3	20, 40, 60, 70, 80

3.1 Velocity and motion analysis

The particle motion, as well as the velocity of each particle has been analyzed from the snapshots of the simulations with different operating conditions. The color shows the normalized dimensionless velocity which is calculated by the following equation.

$$v_{\text{normalized}} = \frac{v_i}{\omega \cdot \sqrt{({x_i}^2 - {x_c}^2) + ({y_i}^2 - {y_c}^2)}} \qquad \textbf{V. 1}$$

Where, v_i is the velocity of i th particle, x_i, y_i are the x- y coordinates of the i th particle. x_c, y_c are the coordinates of the rotating axis. ω is the rotational speed (rd s^{-1}) of a high shear mixer. For example, when the particle in contact with the rotating paddle and its normalized velocity is close to 1.0 (red), it indicates the particle has same velocity as that of paddle. In other word, if the particle moves efficiently, its color is close to red. The blue color corresponds to a small value.

3.1.1 Effect of the rotational speed

Fig. V. 9 shows the normalized velocity of a particle in color at each rotational speed: (a) 100 rpm, (b) 500 rpm, (c) 1000 rpm and (d) 3000 rpm in bird and top viewes. The particle size is 2 mm and the filling ratio 60 %.

For 100 rpm (**Fig. V. 9 (a)**) the particle bed stays under the highest impellers. Particles around second highest impeller present higher velocities. At 500 rpm (**Fig. V. 9 (b)**), the powder bed rises over the highest impellers,unlike 100 rpm. The particles around the bottom can be seen from the top view. The particles are forced to go to the upper side of the mixer as well as to the side wall. It makes a vertical hole around the rotating axis. One can see also that the particles around the paddles have a higher velocity, which is almost red. At 1000 rpm (**Fig. V. 9 (c)**), the powder bed rises even more than 500 rpm and the hole around the rotating axis is smaller. This indicates that even more and more particles are going up to the upper side. The distribution of normalized velocity shows that for the particles around the wall, the velocities are relatively lower than for the other lower rotational speeds. It is suggested that the efficiency of the mixing could be lowered as well. At 3000 rpm (**Fig. V. 9 (d)**), too many particles go up to the upperside, so the middle part of mixer can be seen (rotating axis and impellers are able to be seen from bird view.). The majority of the particles stays either upper or in the bottom part of the chamber. Since the gap between the lowest paddle and the conical wall is large, the particles staying in the bottom part have lower velocities. Also, the particles which can been seen from the bird view as well as the top view have a relatively low velocity (low efficiency).

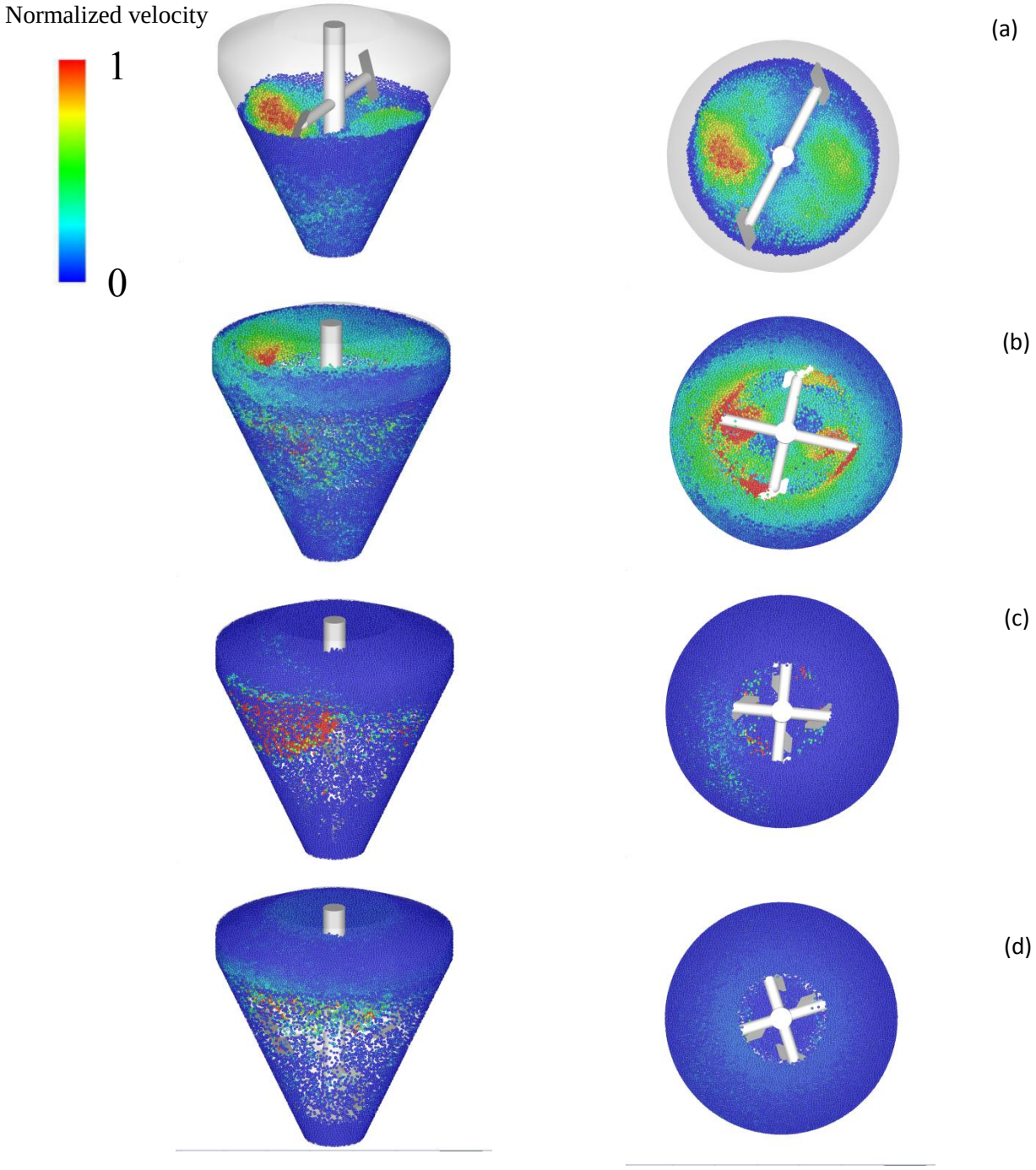

Fig. V. 9 Normalized velocity of particle in color at each rotational speed: (a) 100 rpm, (b) 500 rpm, (c) 1000 rpm and (d) 3000 rpm, particle size 2 mm, filling ratio $J = 60$ %

Fig.V. 10 shows the normalized velocity of a particle in color at each rotational speed: (a) 100 rpm, (b) 500 rpm, (c) 1000 rpm and (d) 3000 rpm in cross section viewes. In the cross section, the particle motion is revealed clearer, at low rotational speed (100 rpm), particle bed stays below the top impeller, and particles around paddle have relatively high normalizewd velocity. At 500 rpm, powder bed reaches top of the chamber, and at 1000 rpm, most of the particle go to the upper side. Finally at 3000 rpm, the particles stay either upperside or bottom, and there are few particles around middle part of the chamber.

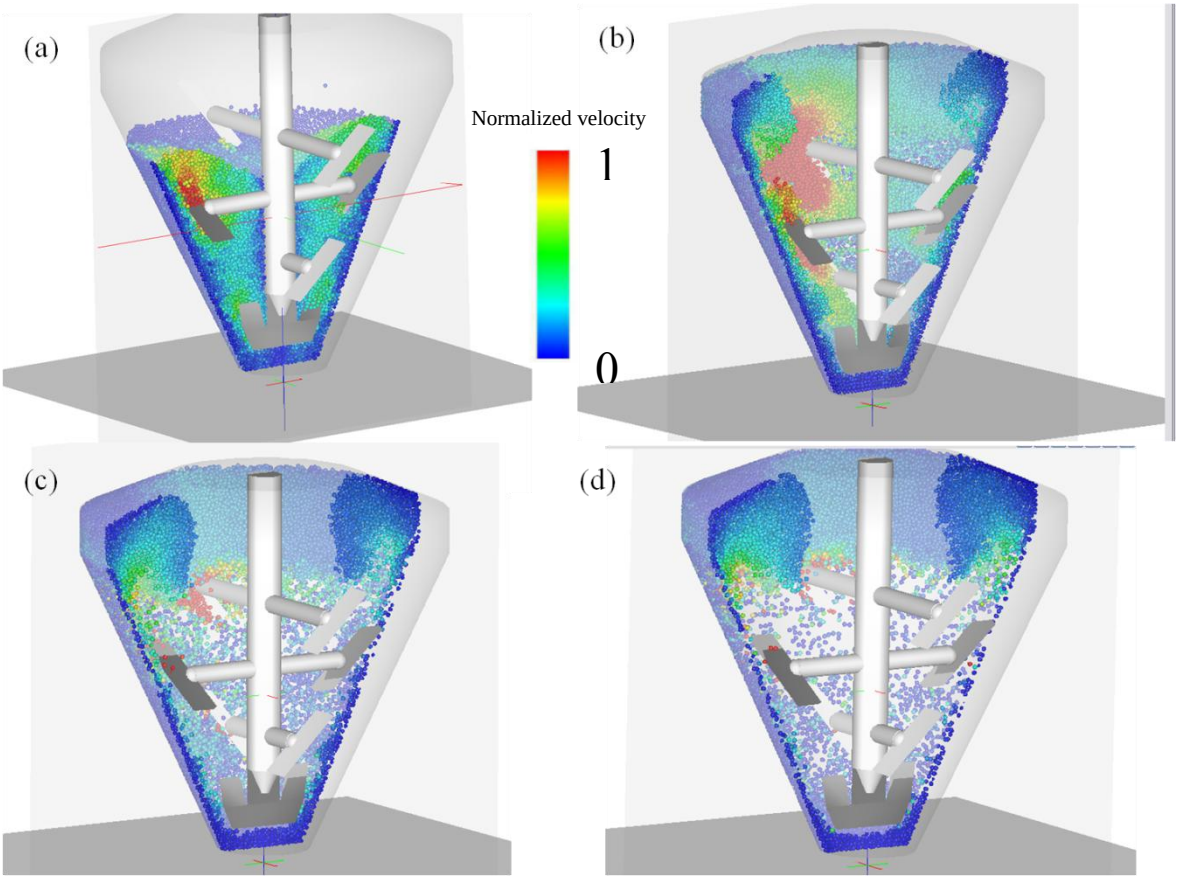

Fig. V. 10 Normalized velocity of particle in color at each rotational speed: (a) 100 rpm, (b) 500 rpm, (c) 1000 rpm and (d) 3000 rpm, particle size 2 mm, filling ratio J = 60 % in cross section.

3.1.2 Effect of particle size

Fig. V. 11 shows the normalized velocity of particle in color for each particle size : (a) 3 mm , (b) 1 mm in bird and top viewes. The rotational speed is 1000 rpm and the filling ratio 60 %.

For particles of 3 mm (**Fig. V. 11 (a)**), compared to the result for 2 mm particles (**Fig. V. 9**

(b)), the normalized velocity tends to increase. It is probably because the gap between the paddle and the conical wall is about 2 mm. So for diameters of 3 mm, all the particles around paddles are hit by the paddles, meanwhile particles of 2 mm can escape from the paddles. Also, From the top view, the hole around a rotating axis is smaller than for 2 mm particles. For particles of 1 mm (**Fig. V. 11 (b)**), a different tendency is observed. Particulary, from the top view, the impellers are clearly seen, so a smaller number of particles go up to the upper side. In addition, there are a lot of particles staying along the side wall. As explained, it is probably because of the gap between the paddles and side wall, many particles escaped from being hit by the paddles and do not go to the upper side of chamber.

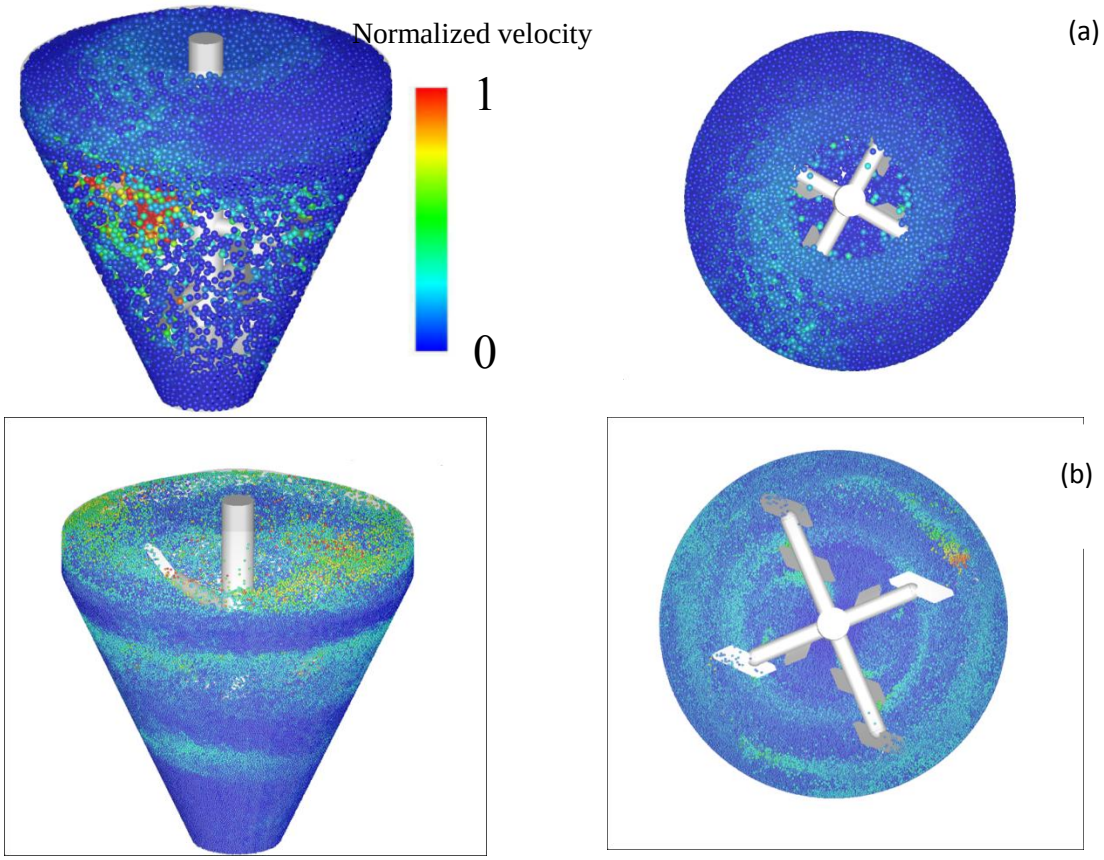

Fig. V. 11 Normalized velocities of particles in color for each particle size: (a) 3 mm , (b) 1 mm, and for a rotational speed, 1000 rpm, and a filling ratio J = 60 %.

3.1.3 Effect of filling ratio

Fig. V. 12 shows normalized velocity of particle in color at each filling ratio : (a) 20 %, (b) 60 % in bird and top viewes. Rotational speed is 1000 rpm and particle size is 2 mm.

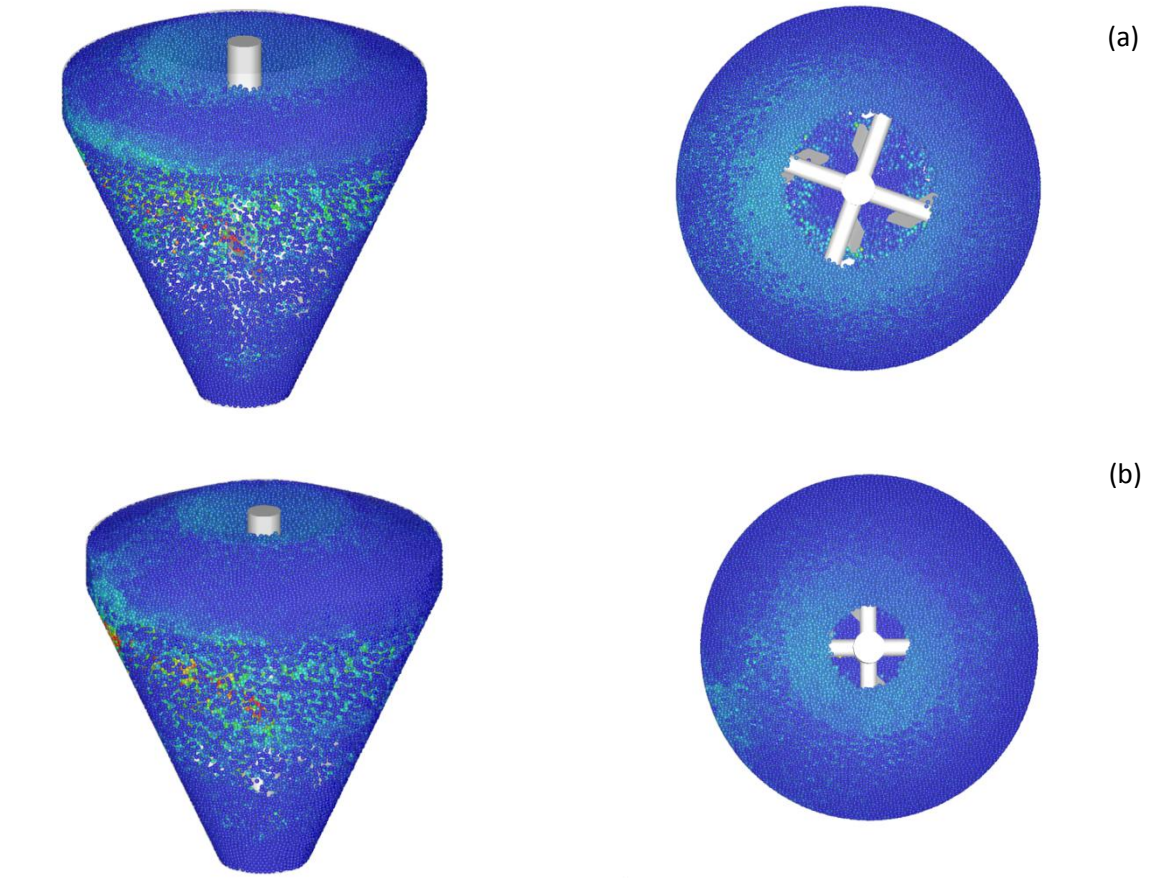

Fig. V. 12 Normalized velocity of particle in color at each filling ratio: (a) 20 % (b) 80 %, particle diameter is 2 mm and rotational speed is 1000 rpm.

Comparing the different filling ratio (**Fig. V. 9 (c)** , **Fig. V. 12 (a)**, **Fig. V. 12 (b)**), the velocity distributions are very similar. It is indicated that the filling ratio exhibits a quite small influence in a high shear mixer. However, from the top view, the fewer the filling ratio is, the larger the hole around the rotating axis becomes. Since less particles were introduced into the chamber at lower filling ratio, less particles are going up to the upper side of the mixing chamber.

3.2 Force distribution

In this section, all the collisions happening during the numerical experiments has been recorded and plotted into the histogram of the number of collisions in order to understand how the operating conditions affect the particle collisions. The collision force is defined as the maximum normal inter-particle force during each collision. It is obvious that the inter-particle interaction as well as the magnitude of the impact of particles inside the system is the key index to the dry coating process occurring in a high shear mixer.

3.2.1 Effect of the rotational speed

Fig. V. 13 shows that the distribution of the colliding forces of the particles at each rotational speed. Particle size is 2 mm and filling ratio is 60 %.

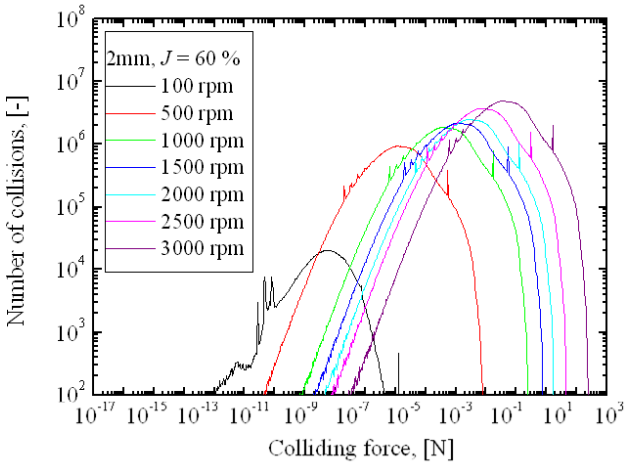

Fig. V. 13 Colliding force distribution at each rotational speed, for a 3 s simulation. Particle diameter:2 mm, filling ratio: 60 %.

The magnitude of the forces range from 10^{-8} to 10^{2} N. The peak height increases with an increase in the rotational speed. In the same time, the maximum forces increase too. This result indicates that the colliding forces increase with an increase in the rotational speed. Those tendencies agree qualitatively with those observed in the experimental results: the coating rate constant increases with the rotational speed. However, since the breakage or

attrition of the particles was not considered, it cannot represent the degradation of the dry coating. If the breaking force of the host particles is reached, the degradation can be predicted since the force information at every single contact event can be obtained.

3.2.2 Effect of particle size

Fig. V. 14 shows the distribution of the colliding forces of the particles for each particle size. The rotational speed is 1000 rpm and filling ratio is 60 %. The peak height decreases with an increase in particle size since a smaller number of particles was introduced. On the contrary, the force population shifts to the right side (bigger force) when the particle size increases. Since this figure is in the log scale, it might show a quite high dependence on the particle size. This is one reason why the dry coating proceeds rapidly for big sized particles even for lower rotational speeds, which was shown in Chapter IV.

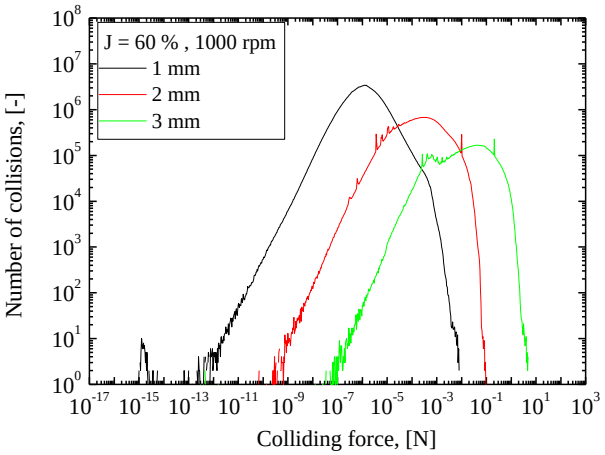

Fig. V. 14 Dependence of the colliding force distribution on the particle size.
Time: 3 s; rotational speed: 1000 rpm; filling ratio: 60 %.

3.2.3 Effect of filling ratio

Fig. V. 15 shows that the distribution of the colliding forces of the particles at each filling ratio. The particle size is 2 mm, and the rotational speed 1000 rpm.

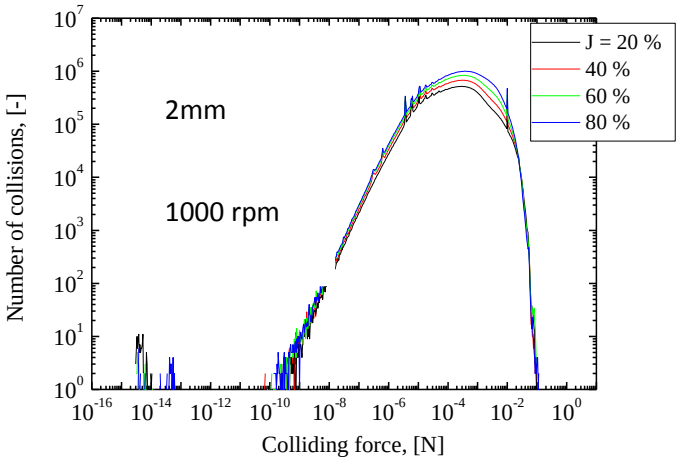

Fig. V. 15 Colliding force distribution at each filling ratio. Rotational speed:1000 rpm, particle size: 2 mm.

The height of the peak increases slightly with an increase in the filling ratio. It is simply because the number of particles introduced into the mixer is higher. Compare with the rotational speed, the effect of the filling ratio is smaller. The force ranges do not change with the filling ratio. The collision forces does not seem to be sensitive to the filling ratio .

3.3 Collision frequency per particle

The collision frequency is obtained in order to understand how active are the interactions of a particle in the system for different operating conditions. The collision frequency f is given by dividing the accumulative number of collisions during the simulation N_c by the number of particles N, and the total simulation time, T. Thus, the collision frequency per particle can be expressed by:

$$f = \frac{N_c}{N \cdot T} \qquad \textbf{V. 2}$$

It is representing the average number of contact events of each particle during a unit time (1 s). Of course it is expected that the larger this value is, the more efficient the dry coating is. It is obvious that the collision frequency of the particle in the system is a quite important factor for the dry coating.

3.3.1 Effect of particle size

Fig. V. 16 shows the evolution of the collision frequency as a function of the rotational speed at each particle size. The filling ratio is fixed at 60 %. In general, collision frequency is around order of 10^3 s^{-1}. The collision frequency increases with the rotational speed. However around over 1500 rpm, it seems to reach an asymptote, becausefor too high rotational speeds, the particles tend to go to the upper side of the chamber. This phenomenon can decrease the particle interactions as discused in section 3.1.

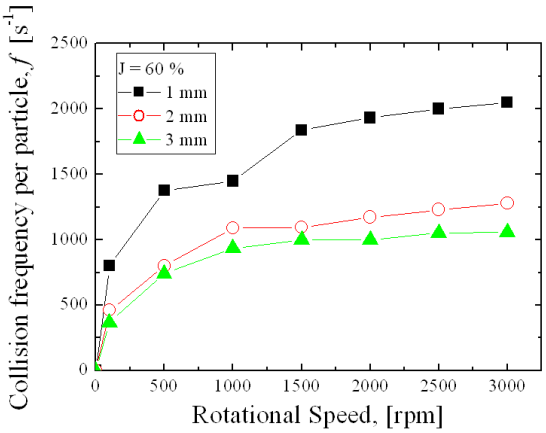

Fig. V. 16 collision frequency as a function of rotational speed at each particle size at filling ratio $J = 60$ %

This tendency is quite similar to that presented by the coating rate constant as a function of the rotational speed of a high shear mixer. However, looking at the effect of particles size, the collision frequency increases with a decrease of particle size. This result is quite logic since as the filling ratio is fixed, a larger number of smaller sized particles are introduced in the system . This result could be consisered as in opposition with the experiments showing that the dry coating proceeds faster at bigger particle size.

One must take into account that for bigger particles, the collisions imply more energy, and each collision has a better probability to yield a good adhesion betwen small anf big particles.

Then, it can be said that, to have a good coating performance, a high collision frequency is recommended but is not a sufficient condition. Since probably a firm attachement of guest particle on a host particle requires not only the contact but also a certain colliding force.

3.3.2 Effect of filling ratio

Fig. V. 17 shows the collision frequency as a function of rotational speed at each particle size. It increases with an increase in the filling ratio.

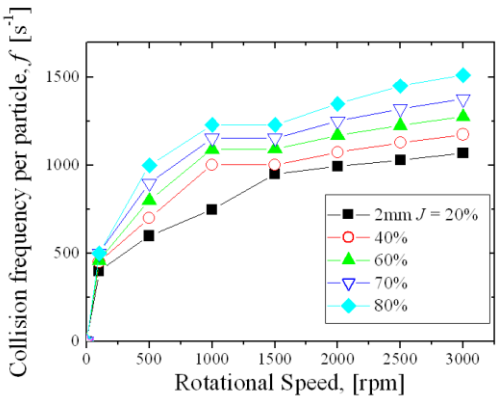

Fig. V. 17 collision frequency as a function of rotational speed at each particle size at filling ratio J = 60 %

This tendency is similar to that of the coating ratio constant. Since a larger number of particles were introduced into the system in higher filling ratio, it is a logical result. However compared to the effect of the particle size, the collision frequency is not seen to be sensitive to the filling ratio.

3.4 Translational kinetic energy

In the particle motion, there are two major energies. One is translational kinetic energy, the other is rotational kinetic energy. Those kinetic energies probably provide the valuable information for the dry coating. The translational kinetic energy is given by the following equation.

$$E_t = \frac{1}{2} \cdot \frac{\sum_{i=1}^{N} m_i {v_{ip}}^2}{N} \qquad \textbf{V. 3}$$

Where, m is mass of particle and v is the velocity of particles.

3.4.1 Effect of particle size

Fig. V. 18 shows the translational kinetic energy as a function of the rotational speed of a high shear mixer at each particle size.

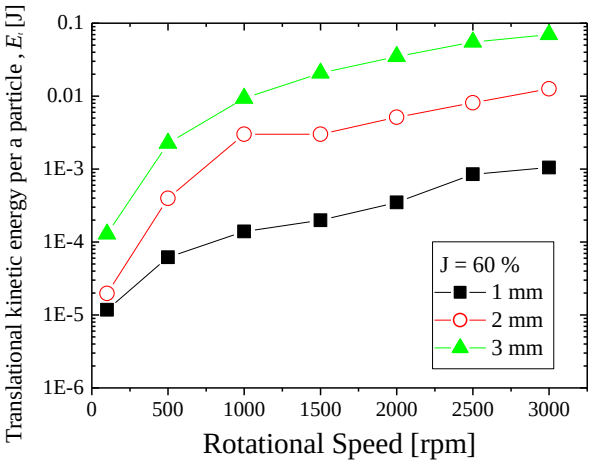

Fig. V. 18 Translational kinetic energy as a function of rotational speed at each particle size. Filling ratio is fixed at 60 %

To see the difference between the particle size clearly, this energy is plotted in log scale. The translational kinetic energy increases with an increase in rotational speed and particle size. It is probably because of the mass of each particle, which varies with third power of radius of particles.

3.4.2 Effect of filling ratio

Fig. V. 19 shows the translational kinetic energy as a function of the rotational speed of a high shear mixer at each filling ratio. In general, the translational kinetic energy seems to increase with square of rotational speed of a high shear mixer. This result is quite logical since the translational velocity of the particles should increase with rotational speed of a high shear mixer.

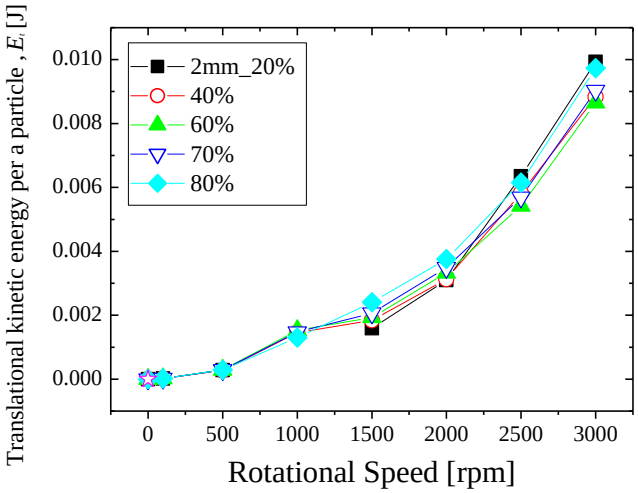

Fig. V. 19 Translational kinetic energy as a function of rotational speed at each filling ratio

The difference between filling ratio is quite small compare to the effect of particle size as well as the rotational speed of a high shear mixer. Hence it can be said that the effect of filling ratio is not influential to this value. This tendency agrees with the experimental finding.

3.5 Rotational kinetic energy

There are many papers in literature reporting that one of the most important factor of the granulation is the rotational kinetic energy of the particles (Kano et al. 2001, Kano et al. 2005, Kano et al 2006, Soda et al. 2009, Mujmdar 2003). Since granulation and dry coating are very similar techniques, the rotating kinetic energy of the particles is expected to correspond to the dry coating efficiency.

Then in this work, the rotational kinetic energy per particle is given by the following equation.

$$E_R = \frac{1}{2} \cdot \frac{\sum_{i=1}^{N} I_i {\omega_{ip}}^2}{N} \qquad \textbf{V. 4}$$

Where I is the moment of inertia and ω_{ip} is the angular velocity of the i th particle.

3.5.1 Effect of particle size

Fig. V. 20 shows the rotational kinetic energy as a function of the rotational speed of a high shear mixer at each particle size.

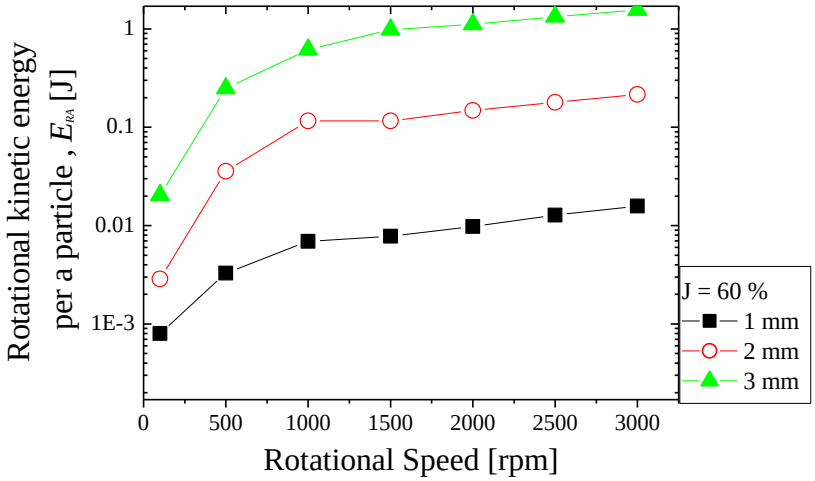

Fig. V. 20 Rotational kinetic energy as a function of rotational speed at each particle size. Filling ratio is fixed at 60 %

The rotational kinetic energy increases with an increase in the particle size. Especially the difference between 3 mm and 2 mm is quite significant. Since the moment of inertia of sphere is given by $\frac{8}{15}\pi\rho r^5$, so this value is basically proportional to the radius of the particle and plays a big role in the value of rotational kinetic energy.

3.5.2 Effect of filling ratio

The rotational kinetic energy as a function of rotational speed of a high shear mixer at each filling ratio is shown in **Fig. V. 21**. In general, the rotational kinetic energy seems to be proportional to the rotational speed. It does not match the behavior of the coating rate constant which increases with an increase of rotational speed, but it reaches an asymptote (or pseudo-steady state).

It increases with an increase of the filling ratio except 40 %, however the difference between filling ratio is quite small compare to the effect of particle size as well as the rotational speed of a high shear mixer.

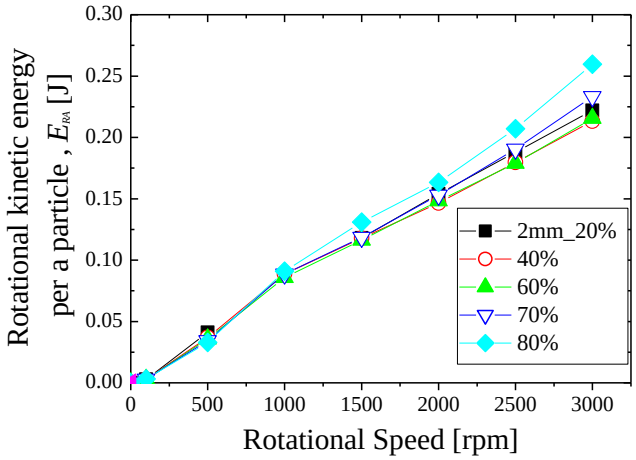

Fig. V. 21 The rotational kinetic energy as a function of rotational speed of a high shear mixer at each particle filling ratio

As discussed in section 3.1, the particle motion does not change significantly with the filling ratio; rotational kinetic energy could correspond to that. The experimental results show that the dry coating is not affected by the filling ratio. This tendency agrees qualitatively with the experiments.

Comparing with translational kinetic energy, the value of rotational kinetic energy is over 10 times bigger than the value of translational energy. It can be said that the rotational kinetics of the particles are dominant in a high shear mixer system.

3.6 Rotational velocity of particle

As discussed in previous section, the rotational kinetic energy of a particle in a mixer may be a quite important factor of the dry coating. However, the behavior of the rotational kinetic energy shows that it does not agree with the coating rate constants. The rotational kinetic energy seems to be proportional to the rotational speed for a high shear mixer. Meanwhile, the coating rate constant does not.

The rotational superficial velocity of particle has been also calculated. The rotational superficial velocity of the particles is accumulated rotational distance of every single particle during the simulation as shown in **Fig. V. 22**, divided by number of particle and calculation time. This value is defined as rotational superficial velocity of particles. The interest of this notion stays in the fact that the shear stress occurring during a collision is mainly related to the relative rotational velocity of the two particles at the contact point. This has a crucial effect on the breaking of agglomerates in cohesive powders, and to improve the efficiency of dry coating.

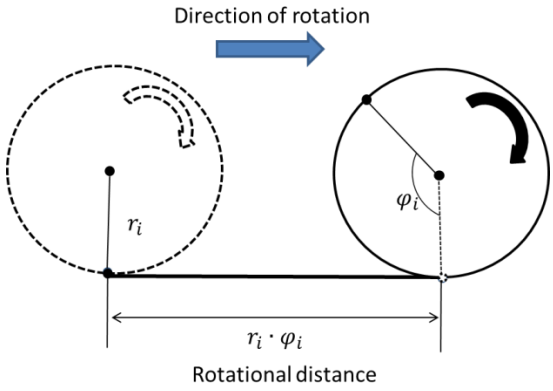

Fig. V. 22 Illustration of the rotational distance of a particle: the initial position of the particle is shown in left and the final position after the simulation time at right.

The rotational superficial velocity of a particle can be expressed in **Eq. V. 5**.

$$v_R = \frac{\sum_{i=1}^{N} r_i \cdot \varphi_i}{N \cdot T} \qquad \textbf{V. 5}$$

Where, φ_i is angular displacement of the *i* th particle during the time *T* of calculation

3.6.1 Effect of particle size

Fig. V. 23 shows the rotational distance of particle as a function of rotational speed of a high shear mixer at each particle size.

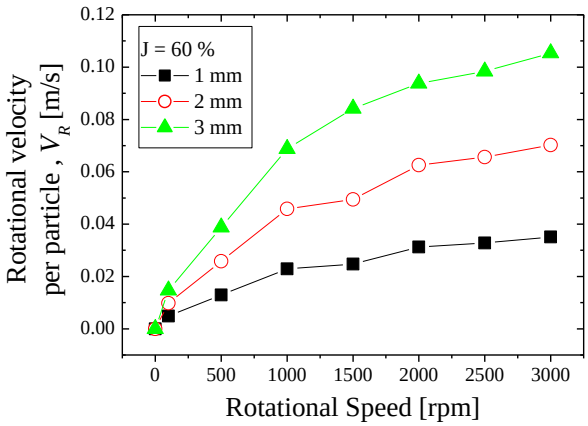

Fig. V. 23 The rotational superficial velocity of particle as a function of rotational speed of a high shear mixer at each particle size. The filling ratio is fixed at 60 %.

The filling ratio is fixed at 60 %. It increases with an increase of rotational distance of a high shear mixer and particle size. This tendency qualitatively agrees with the behavior of the coating rate constant measured in previous section.

3.6.2 Effect of the filling ratio

Fig. V. 24 shows the rotational velocity of a particle as a function of the rotational speed of a high shear mixer at each filling ratio (particle size:2 mm). It decreases when increasing the filling ratio.

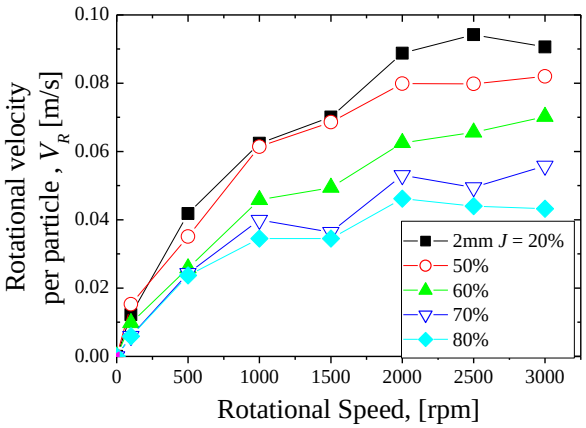

Fig. V. 24 The rotational velocity of particle as a function of the rotational speed of a high shear mixer at each filling ratio. The particle size is fixed at 2 mm.

As mentioned in section 3.1, a larger number of particles go to the upper side of the mixer where a particle moves relatively smoothly at higher filling ratios. As a result, the value of rotational velocity of a particle tends to be smaller at the higher filling ratio. This result agrees qualitatively with the behavior of the coating rate constant that also decreases with an increase of the filling ratio, as seen below.

3.7 Correlation

Fig. V. 25 shows the influence of the rotation speed of the rotor on the coating rate constant (b), which is already shown in **Fig. IV. 33**. The dependence for experiments (a) and for calculation (b) are quite similar.

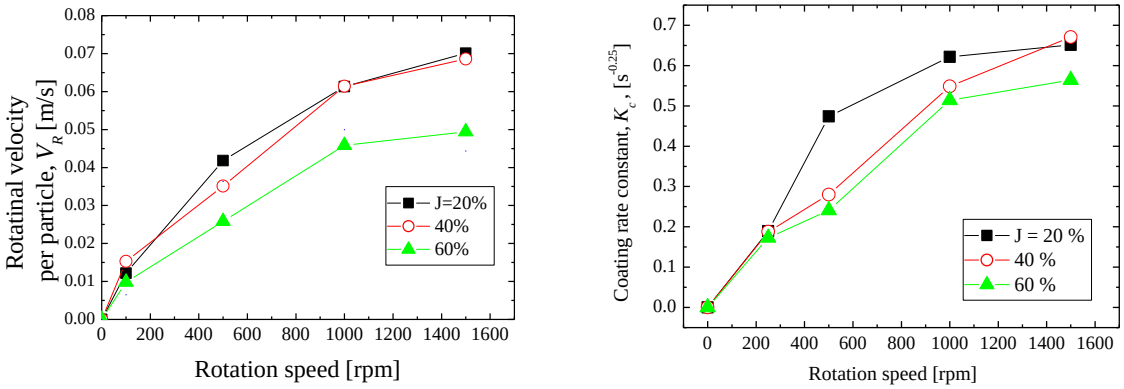

Fig. V. 25 The result of rotational velocity of particles limited to have only the same condition as experiment (a) and the result of coating rate constant (b)

Hence, a linear relation between rotational distance of particle and the coating rate constant can be derived (**Fig. V. 26)**.

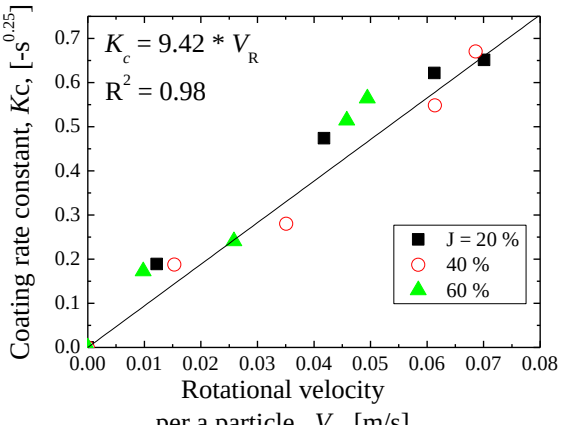

Fig. V. 26 Relationship between rotational velocity of particle and coating rate constant

The linear correlation between the rotational distance of particle and coating rate constant would be useful for predicting the coating rate constant.

V. 4 Simulation of motion of host and invited particles in a high shear mixer

From the previous section, the motion of the host particle has been focused and investigated. In this chapter, the motion of the guest particles has also been taken into account in order to get the better understandings of dry coating. For the first part of this section, the mixing without considering the adhesion of the host – guest particle has been done. The last part of this section presents the adhesion based on simple model has been applied.

4.1 Simulation of host and guest particles without adhesion

The simulations have been performed in order to know the effect of rotational speed on the mixing of host and guest particles. The rotational speed varies from 250 to 1500 rpm. The filling ratio of samples is fixed at 40 % and 20 % for host and guest particles, respectively. Simulation time is also fixed at 3.0 s. Particle size is also fixed at 3 mm and 1 mm for host and guest particles respectively. The physical parameter used for the host and guest particles are summarized in **Table V. 3**. Initially the invited particles are located over the powder bed of host particles (as seen in **Fig. V. 27 (a)**)

Table V. 3 Physical conditions of host and guest particles

material		host	guest
Young's modulus	E [GPa]	4.5	2.2
Poisson's ratio	[-]	0.30	0.30
Density	[kg/m^3]	1600	1120
Coefficient of restitution	[-]	0.3	0.0
Radius	[mm]	3	1
Number of particles	[-]	14 148	190 986
Total simulation time	T [s]	3.0	

4.1.1 Snapshots

Fig. V. 27 shows the snapshots for different mixing times at 1500 rpm. Since the guest particles (yellow particles) are initially positioned over the host particles (in blue) (**Fig. V. 27 (a)**), at the beginning of the mixing, the majority of the guest particles go to the upper side of a mixer according to the impeller effect (**Fig. V. 27 (a) then (b)**). After this period, a part of guest particles are seen to be near to the side wall, compared to host particles, probably because guest particles can escape from the rotating paddles since they are smaller.

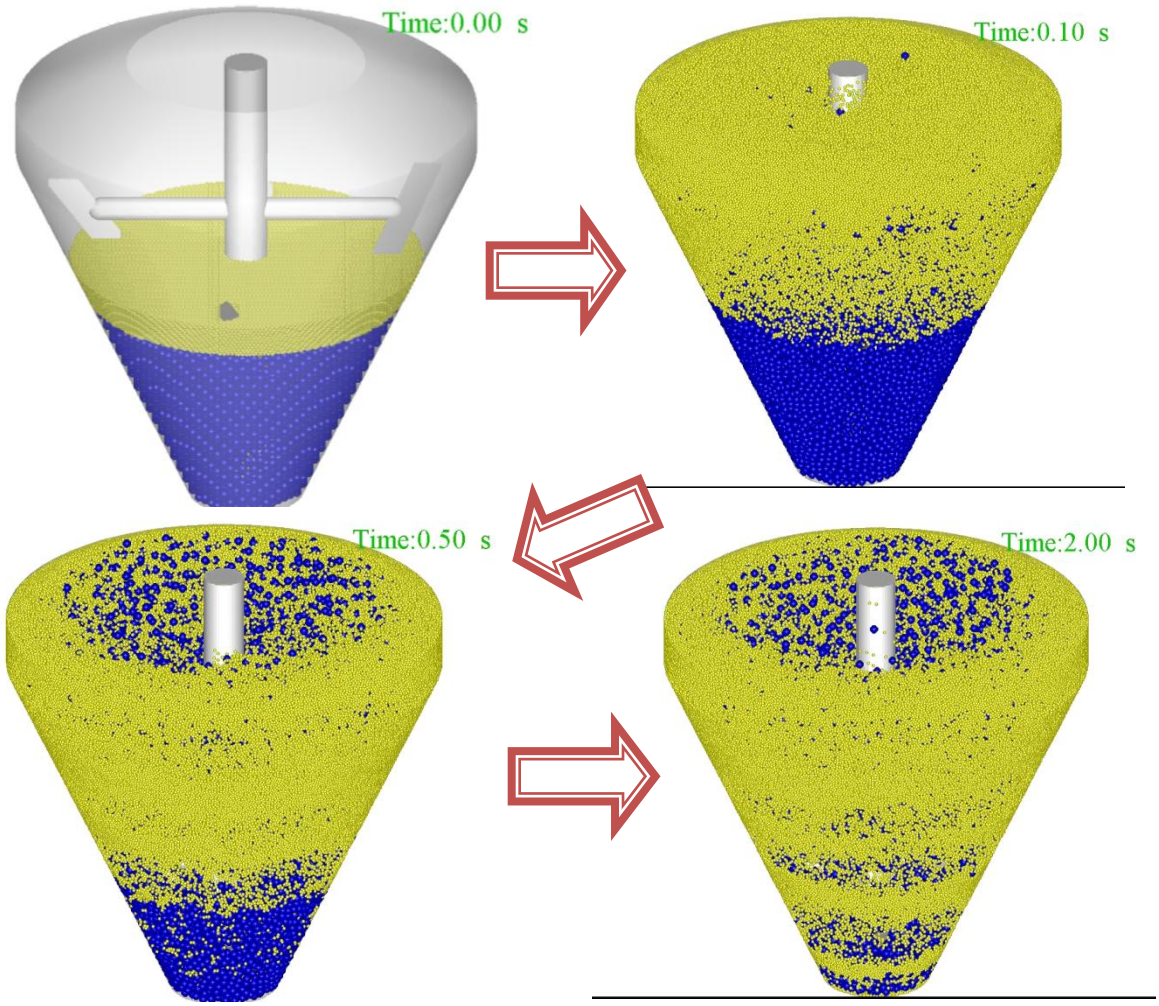

Fig. V. 27 The snapshots of variety of the mixing time at 1500 rpm: (a) upside left, to (d) downside right. Big host particles in blue, small guest particles in yellow.

The guest particles go to the bottom part of the mixer along the side wall (**Fig. V. 27 (c)**), and little by little reach the bottom (**Fig. V. 27 (d)**).

To observe the inside of the mixing chamber, the cross sections of the mixing chamber at each rotational speed are shown in **Fig. V. 28** (Guest in Blue and host in Red). At 250 rpm the guest particles are located around the surface of the powder bed and rotating axis (**Fig. V. 28 (a)**).

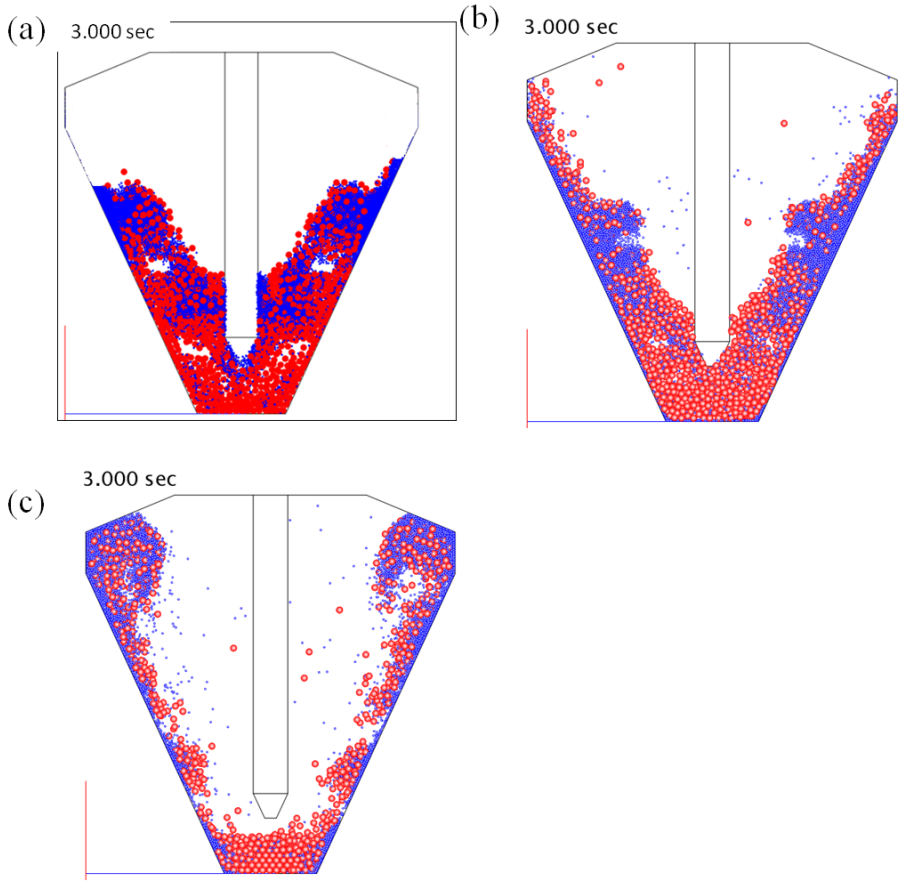

Fig. V. 28 Cross section of the mixing chamber at each rotating speed: (a) 250 rpm, (b) 500 rpm, (c) 1500 rpm, T= 3s (host in red and guest in blue).

At higher rotational speeds, 500 rpm, the guest particles are located along the side wall (**Fig. V. 28 (b)**). It is suggested that the dry coating occurs in this region. At 1500 rpm the guest particles are evenly located around the side wall and especially there are a lot of guest particles seen at the upper part of the mixer (**Fig. V. 28 (c)**). Since the guest particles are smaller and lighter than the host particles, they are likely to go upper side.

4.1.2 Collision analysis

Fig. V. 29 shows Collision frequency as a function of simulation time: (a) collision between host – host particles, (b) host – guest particles.

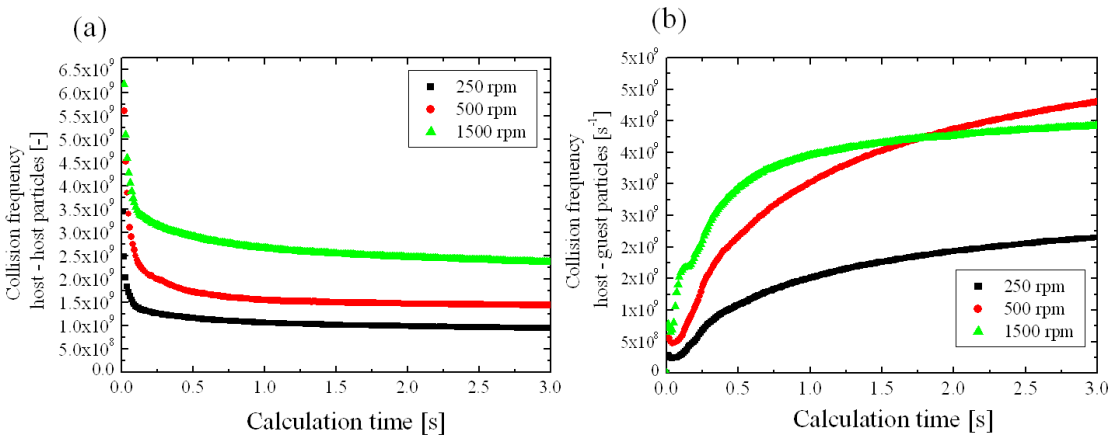

Fig. V. 29 Dependence of the collision frequency (host-host or host-guest) on the mixing time

The collision frequency between host-host particles increases with an increase in rotational speed. It is clear that at higher rotational speeds, the interactions among particles are more active. However, for the collisions between host-guest particles, unexpectedly the collision frequency at 500 rpm overtakes the one at 1500 rpm. Probably at 1500 rpm, too much guest particles go up to the upper side and then the interaction between host – guest particle could be reduced.

4.2 Simulation of host and guest particles with adhesion

The particle motion of host and guest particles without adhesion has been investigated in the previous section. Hereafter, the simulation considering the adhesion of guest particles on the host particles has been carried out based on a simple model: as soon as a guest particle touches a host particle, this guest particle remains attached definitively on the host particles, and no separation will be further considered. The simulation condition is the same as shown in **Table V. 3**. To observe the effect of rotational speed, the rotational speed varies from 250 to 1500 rpm. The host and guest filling ratios are fixed at 40 % and 20 % for host and guest particles respectively whereas the filling ratio is 60 %. The particle size is also fixed at 3 mm and 1 mm for host and guest particles respectively. In this model, the multilayer is allowed to occur, that is to say, unlimited number of guest particles can be attached on the same host particle.

4.2.1 Snapshot

Fig. V. 30 shows the snapshots of simulation with two rotational speeds: (a) 250 rpm, (b) 1500 rpm

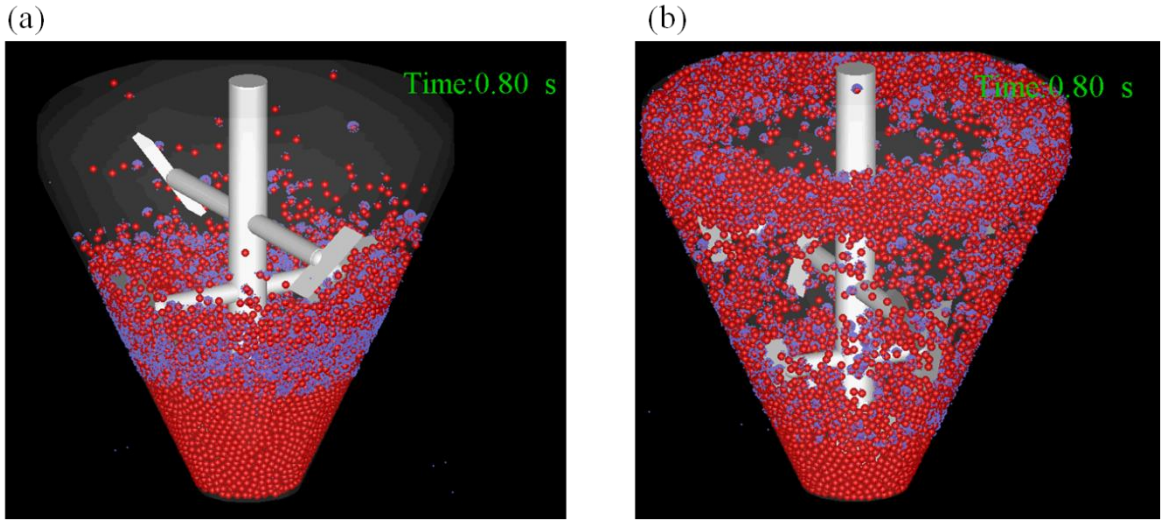

Fig. V. 30 The snapshots of simulation at two rotational speeds: (a) 250 rpm, (b) 1500 rpm

At 250 rpm, almost all guest particles are attached on the surface at 0.8 s of simulation time.

The host particles located on the bottom part of the mixer seem to remain unattached. At 1500 rpm, free guest particles are also not seen from the snapshot. The host particles attached can be seen everywhere in the chamber except in the bottom part of chamber. This is probably because the tip speed of the lowest paddle is so low that the host particles initially located at bottom cannot go up and meet the guest particles, since initially the invited particles are located over the powder bed of host particles.

4.2.2 Collision analysis

The number of guest particles attached on surface of host particles as a function of simulation time is shown in **Fig. V. 31 (a)**. **Fig. V. 31 (b)** shows the same figure but different scale in order to see the difference clearly. It should be noted that this number is the number of guest particle 'newly' attached at the certain simulation time. So if it reaches 0, it indicates that there are no free guest particles left in the system.

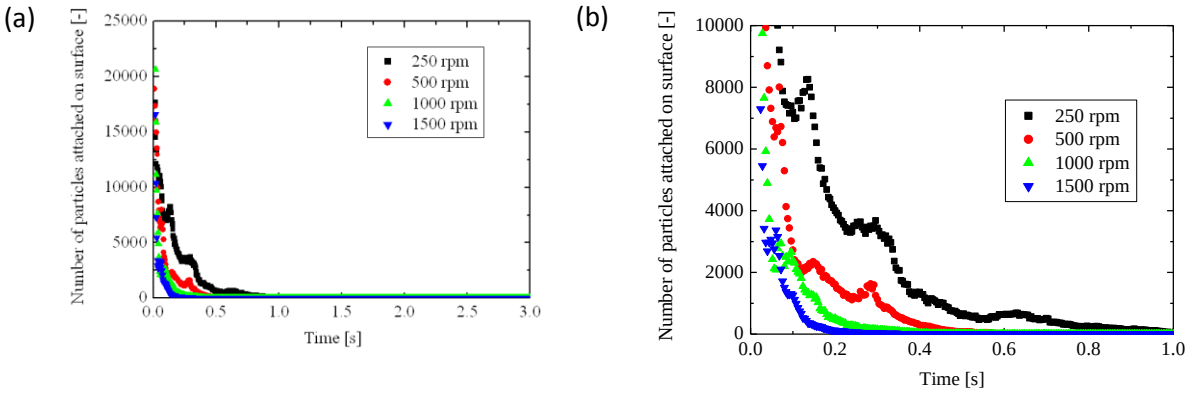

Fig. V. 31 The number of guest particles attached on surface of host particles as a function of simulation time. Number of initial guest particles: 200 000

At the beginning of the simulation, a great number of guest particles attach very rapidly.

All the simulations show that after a simulation time of around 1.0 s, all the guest particles are attached on the surface of host particles. This time can be reduced drastically by increasing the rotation speed. So it can be said that higher interactions between host and guest particles occur at higher rotational speeds. This tendency agrees qualitatively with the experimental

results.

Fig. V. 32 shows the histogram of the number of guest particles attached on the surface at each rotational speed.

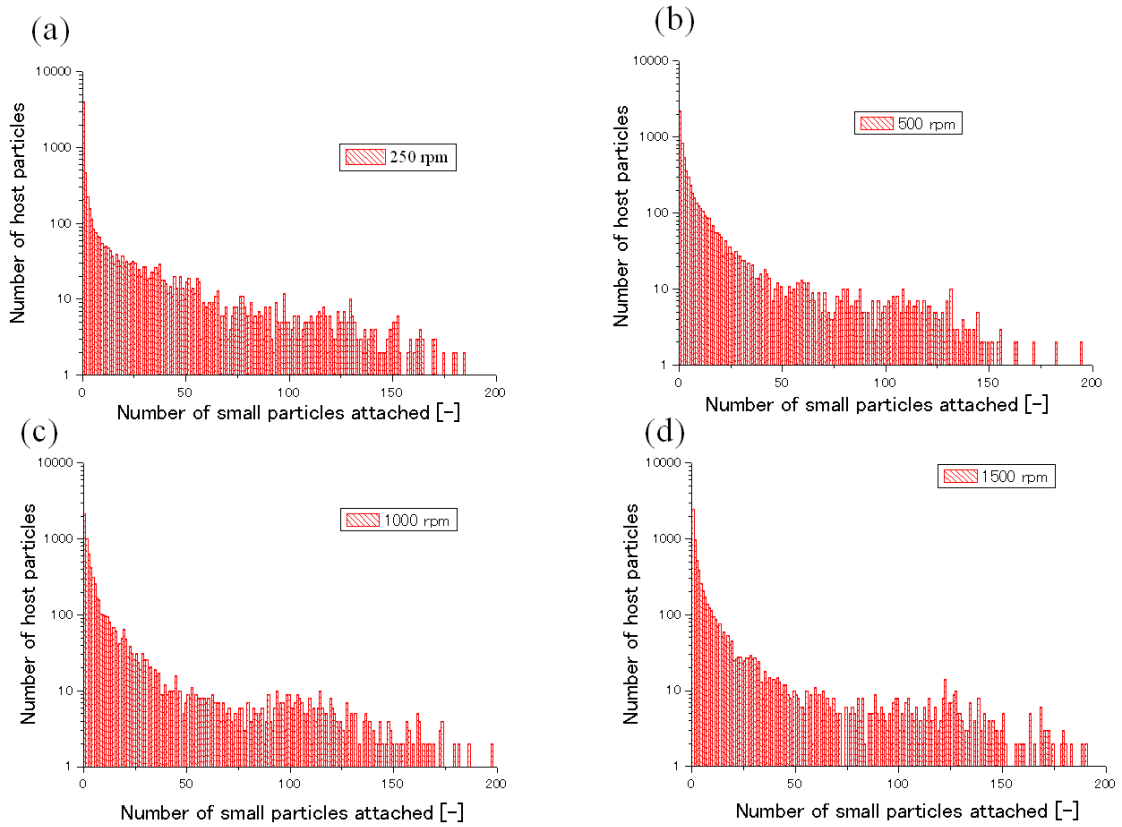

Fig. V. 32 Histograms of the number of guest particles attached on the surface at each rotational speed: (a) 250 rpm, (b) 500 rpm, (c) 1000 rpm, (d) 1500 rpm.

Except for 250 rpm, the histograms at each rotational speed have similar tendency. At 250 rpm, there is a larger number of host particles having no guest particle on their surface.

Conclusion

In this chapter, firstly, the motion of host and guest particles in a high shear mixer has been observed and the velocities quantified by a PIV method. The motion has also been simulated by DEM. Both motions were analyzed by the PIV method and compared. The validation of the simulation work was discussed.

Secondly, the numerical simulation of the motion of host particles has been carried out in order to understand the effects of operating conditions (rotational speeds, filling ratio and particle size) on the interactions between particles or between the walls and the particles, and how these conditions should affect the performance of the dry coating.

Thirdly, the numerical simulation of the motion of host and guest particles has been undertaken and investigated the behavior and the state of the mixture with or without adhesion between a guest particle and a host particle.

From those approaches, the findings were obtained and summarized below:

(1) The velocity of the particles simulated by the DEM is consistent with that measured experimentally, even though there are some differences between them. Especially, the vertical components of particles velocity from experiment and numerical motions present a good agreement. It can be concluded that the simulated particle motion can represent sufficiently the real particle motion. It confirms the applicability of the proposed method for simulating the particles motions in the dry coating process.

(2) The numerical simulation revealed that the height of the powder bed in the mixing chamber rises with rotational speeds, and it reaches the upper part of the chamber at high rotational speed over 500 rpm. However, the normalized velocities tend to have lower values at higher rotational speeds. It is indicated that the efficiency of mixing could get lower when the rotational speeds are increased.

The effect of particle size seems to be very significant from the motion observations.

Especially, the power bed of 1 mm diameter particles is located relatively lower than the other bigger particles. It is suggested that the gap between the side wall and rotating paddles plays an important role in the motion of the particles.
The particle motion does not seem to be sensitive to the filling ratio.

(3) The force distributions in the dynamic mixture of particles show that the colliding forces increase with an increase in the rotational speed as well as the frequency of collisions. Those tendencies agree qualitatively with experimental results showing that the coating rate constant increases with the rotational speed. The colliding forces increase with an increase in particle size. On the contrary, the number of collisions decreases with the particle size. The effect of particle size is quite remarkable. The force distribution does not change very much with a change of filling ratio.

(4) The cumulative parameters which could be related to the dry coating have been calculated. The collision frequency shows that it increases with a decrease of particle size and an increase of the filling ratio. The rotational kinetic energy presents a great dependence on the particle size, however little dependence on the filling ratio.
Rotational velocity of particle is affected by both particle size and filling ratio.

(5) Comparing the behavior of rotational distance obtained from numerical method and the coating rate constant obtained from experimental approach, it is found a linear relationship. From this correlation, it would be possible to predict the coating rate constant from this numerical approach.

(6) Simulations of host and guest particles without considering adhesion show that the guest particles tend to go near the side wall since they are smaller than the host particles. The dry coating could be taken place along the side wall since there are more interactions between host and invited particles.

(7) From simulation of host and guest particles with adhesion based on a simple model of immediate attachment when a guest-host collision occurs, the attachment of guest particles onto the host particles proceeds very rapidly (t< 1 s). This rate increases with an increase of rotational speed, which agrees qualitatively with experimental results. However, regarding the histogram of the number of guest particles onto the surface of host particles, the guest particles are quite heterogeneously attached on particular host particles (probably the host particles positioned initially the place neighboring the powder bed of guest particles). That is far from the experimental evidence that host particles are almost homogeneously coated. This is because the particle size ratio was not corresponding to the real experiment. To represent well the real phenomenon, it is required to simulate the real particle ratio and to consider the model based on the physical adhesion forces, such as JKR adhesion force or Van der Waals forces.

In conclusion, this approach requires further developments for better understandings of dry coating. However, it is clear that the numerical experiments of particle motion can give precious information to understand the dry coating in a high shear mixer. Thus, this numerical approach has a large possibility for establishing the new optimization method of the dry coating process as well as the scale-up the coating device and proposing new efficient designs of dry coating devices.

Conclusions and perspectives

In this study experimental and numerical investigations on dry coating have been done.

For the experimental part, the aim was focused on revealing the effect of operating conditions on dry coating using a commercial high shear mixer called 'Cyclomix'.

Firstly the effect of the rotational speed as well as the treatment time has been observed for mixtures of Suglets (S) with a median diameter 250 μm and Magnesium Stearate (MgSt) of median diameter 5μm at a fixed mass fraction of guest particles (MgSt).

Secondly the effect of the filling ratio has been studied using same material couple.

Finally the effect of the particle size has been investigated using the bigger host particles, Suglets with median diameter 1 mm and same MgSt powders.

For the numerical part of this study, the DEM Method has been chosen to simulate the motion of particles in a high shear mixer.

First, the motion of an assembly of Suglets has been created and analyzed by an optical method (Particle Image Velocimetry). Both experimental and simulated motions were analyzed by the PIV method and compared. The validation of the simulation work was discussed in terms of horizontal and vertical particle velocities.

Secondly, the numerical simulation of the motion of host particles has been carried out in order to understand the dependence of the interactions between particles upon the operating conditions (rotational speeds, filling ratio and particle size) which should affect the performance of the dry coating.

Thirdly, the numerical simulation of the motion of host and guest particles has been undertaken. The behavior of the mixture was investigated in two cases: with or without adhesion of guest particles on a host particle.

Experiments

It was found that the rotational speed as well as the operating time have a great influence on the dry coating. Applying a low rotational speed into the dry coating process, firstly the discrete coating is made rapidly, and with longer operating times, MgSt particles on the

surface of host particles are smeared and deformed into flat and coating proceeds to a continuous coating.

This deformation of MgSt on the surface makes internal closed pores on the surface, which causes a decrease of pycnometry density.

When the coating time goes on, the flowability as well as the wettability of the resulting mixture are improved. If a high rotational speed is applied to the system, coating proceeds rapidly. From the industrial point of view, it would be more efficient. However, there are also the risks of fragmentation of Suglets particles occurring in the same time. Those fragments could attach on the surface of the Suglets particles, as seen on the SEM picture of coated particles at high rotational speed: the picture showed that there were agglomeration of small fragments on the surface of host particles. The PSD analysis confirmed that at low air pressure, the guest particles are well attached to the host particles. High pressure PSD measurements revealed that the guest particles, attached on coated particles at low rotational speed, are separated from the host particles because of high energy impacts generated at high air pressure. At high rotational speed, the pressure at which separation occurs is increasing, that is to say bond forces between host and guest particles increase, however, over certain rotational speeds (such as 1500 rpm), PSD analysis proved that there are fragments of the host particles. That makes the surface properties worse again. The flowability, wettability and pycnometry analysis indicated also this degradation of the surface properties.

For the effect of filling ratio, it was found that this operating condition has a poor effect on the dry coating with respect to the rotational speed and operating time. However for operating conditions at smaller filling ratios, the coating proceeds slightly faster than at higher filling ratios. From the industrial point of view, it should be recommended to use a higher filling ratio which is of course able to get a higher productivity, since the filling ratio is not sensitive to the coating efficiency.

For the effect of particle size, all the characteristics of the coated particles indicate that coating proceeds much faster than that of smaller host particles. In addition, the effect of

rotational speeds as well as the coating time is not remarkable compare to smaller host particles. The impact forces given by the rotating mixer are sufficiently high to attach almost all the MgSt particles on the surface of host particles rapidly as well as to ensure the deformation of MgSt particles to form the film-like coating even at a low rotation speed (250 rpm). It is probably because the collision forces happening between the particles get stronger when the particle size is coarsen since the mass of the host particles also increases with the particle size. Thus, the particle size plays a very important role in dry coating.

In the kinetic study, the conversion ratio of the coated particle has been measured by a new method based on the sieving technique. It is found that the evolution of the conversion ratio with operating time has some similar tendency to follow a first order reaction in chemical kinetics. Then this evolution is approximately described by an empirical exponential model with one variable parameter K_c. It is found that the properties of the coated particles can be predicted by the conversion ratio at a given time in the coating process since there are linear relations found between them. The linear relations between the mass fraction of invited particles on the surfaces of the host particles and the product properties can be quantified by a model involving a coating rate constant K_c, which can be used to optimize dry coating processes to give desired properties of coated particles.

Numerical Results

From the PIV analysis, the velocity of the particles simulated by the DEM is consistent with that measured experimentally, even though there are some differences between them. Especially, the vertical components of particles velocity from experiment and numerical motions exhibit a fairly good agreement. It can be concluded that the simulated particle motion can represent adequately with a sufficient precision the real particle motion. It confirms the applicability of the proposed method for simulating the particles motions in the dry coating. This methodology should contribute to a better estimation of the evolution of the dry particle coating efficiency. The numerical simulation revealed that the height of powder bed in the mixing chamber rises with rotational speeds, and it may reach the upper part of the

chamber at high rotational speed (over 500 rpm). However, the normalized velocities tend to have lower values at higher rotational speeds. It is indicated that the efficiency of mixing could be lowered for high rotational speeds.

The effect of particle size seems to be very significant from the motion observation. Especially, the power bed of 1mm particles is located relatively lower than the other bigger particles. It is suggested that the gap between the side wall and rotating paddles plays an important role in the motion of the particles. The particle motion seems not to be sensitive to the filling ratio. Forces distribution diagrams show that the colliding forces increase with an increase in the rotational speed as well as the number of collisions. Those tendencies agree qualitatively with experimental results showing that the coating rate constant increases with the rotational speed. The colliding forces increase with an increase in particle size. On the contrary, the number of collisions decreases with the particle size. The effect of particle size is quite remarkable. The force distribution does not change much when changing the filling ratio. The cumulative parameters which could be related to the dry coating have been calculated. The collision frequency curves show that collisions increase with a decrease of the particle size and with an increase of the filling ratio, respectively. The rotational kinetic energy presents a great dependence on the particle size, but little dependence on the filling ratio. The rotational velocity is affected by the particle size and the filling ratio. Comparing the behavior of rotational velocity obtained from numerical method and the coating rate constant obtained from experimental approach, it is found that they have a good linear relationship. From this relationship, it would be possible to predict the coating rate constant from this numerical approach. In simulation of host and guest particles without considering adhesion, the guest particles tend to go near the side wall since they are smaller than the host particles. The dry coating could be taking place along the side wall since there are more interactions between host and invited particles.

Simulation of host and guest particle with adhesion has been carried out on the basis of a simple model: the attachment is effective as soon as a host-guest particle collision was made. The attachment of guest particles onto the host particles proceeds very rapidly. This rate

increases with an increase of rotational speed which agrees qualitatively with experimental results. However, regarding the histogram of the number of guest particles onto the surface of host particles, the distribution of guest particles attached on particular host particles is very large (probably the host particles positioned initially the place neighboring the powder bed of guest particles). That is far from the experimental evidence that host particles are almost homogeneously coated. This approach requires further development for better understandings of dry coating. However, it is clear that the numerical experiments of particle motion can give valuable information to understand dry coating in high shear mixer from data which are not easy to obtain from the experiment.

Thus, this numerical approach has a large possibility for establishing the new optimization method of the dry coting process as well as the scale-up the coating device and proposing new efficient designs of dry coating devices.

Perspectives

In this study, some governing laws for dry coating have been obtained in various operating conditions.

However, the materials used in this research work were only Suglets and MgSt. By using different materials, cohesive or not, the dry coating would behave differently. The governing laws which can also be applied to any material couple, particle shape and particles size would be needed for further development of optimization for dry coating processes. To do so, microscopic and physic-chemical study would be needed, for example the analysis and modeling of bond forces between host and guest particles that was already proposed by Thomas (Thomas et al. 2009).

For the modeling, the number of particles and calculation time are also limited. Thus the conditions of numerical simulation are not completely the same as the ones in real dry coating experiments. To increase the computational efficiency so that more realistic simulations can be done, the optimization of programs is required. Parallel computing techniques such as Message Passing Interface (MPI), General-Purpose computing on GPU (GPGPU) should be applied to the simulation. For example, Open Multiprocessing (OpenMP) has already been implemented into our program.

To simulate the dry coating, the model based on the bond forces such as JFK adhesive forces or Van Der Waals forces that cause the attachment of guest particles on host particles could be considered. By doing this, probably more realistic dry coating simulation might be obtained.

References

Adams M. J. and V. Perchard
The cohesive forces between particles with interstitial fluid, *Institution of Chemical Engineering Symposium Series*. **91**, 147-160 (1985)

Alonso M., M. Satoh and K. Myanami
Mechanism of the combined coating - mechanofusion processing of powders, *Powder Technology*, **59**, 42-52 (1989 a)

Alonso M., M. Satoh and K. Myanami
Kinetic of fines transfer among carriers in powder coating, *Powder Technology*, **59**, 217-224 (1989 b)

Asmar B. N., P. A. Langston, A. J. Matchett and J. K. Walters
Validation tests on a distinct element model of vibrating cohesive particle systems, *Computers & Chemical Engineering*, **26**, 785-802 (2002)

Bannister P. and N. Harnby
A colorimetric technique for assessing the mixture quality if fine particle mixtures, *Powder Technology*, **36**, 275-270 (1983)

Brilliantov N. V. and T. Poeschel
Rolling friction of a soft sphere on a hard plane, *Europhysics. Letters*, **42**, 511 (1998)

Campbell C. S. and C. E. Brennen
Computer simulation of granular shear flows, *Journal of Fluid Mechanics*, **151**, 167-188 (1985)

Cleary P. W. and M. L. Sawley
DEM modelling of industrial granular flows: 3D case studies and the effect of particle shape on hopper discharge, *Applied Mathematical Modelling*, **26**, 89-111 (2002)

Coowanitwong N., C. Y. Wu , M. Cai, M. Ruthkosky, J. Rogers and L. Feng
Surface modification of Al_2O_3 fiber with binary nanoparticles using a dry-mechanical coating technique, *Journal of Nanoparticles Research*, **5**, 247-258 (2003)

Cundall P. A. and O. D. L. Strack
A discrete numerical model for granular assemblies, *Geotechnique* , **29**, 47-65 (1979)

Dave R., W. Chen, A. Mujumdar, W. Wang and R. Pfeffer
Numerical simulation of dry particle coating processes by discrete element method, *Advanced powder Technology*, **14**, 449-470 (2003)

Dudderar T. D. and P. G. Simpkins
Laser speckle photography in a fluid medium, *Nature*, **270**, 45-47 (1977)

Egermann H. and N. A. Orr
Ordered mixtures-Interactive mixtures, *Powder Technolgy*, **36**, 117-118 (1983)

Fisher R. A.
On the capillary forces in an ideal soil: correction of formulae given by W.B. Haines, *Journal of Agricultural Science*, **16**, 493-505 (1926)

Freeman R.
Measuring the flow properties of consolidated, conditioned and aerated powders-A comparative study using a powder rheometer and a rotational shear cell, *Powder Technology*, **174**, 25-33 (2007)

Fröberg J. C., O. J. Rojas and P. M. Claesson
Surface forces and measuring techniques, *International Journal of Mineral Processing*, **56**, 1-30 (1999)

Galet L., Y. Ouabbas, A. Chamayou, P. Grosseau, M. Baron and G. Thomas
Surface analysis of silica gel particles after mechanical dry coating with magnesium stearate, *Kona*, **28**, 209-218 (2010)

Gera D., M. Gautam, Y. Tsuji, T. Kawaguchi and T. Tanaka
Computer simulation of bubbles in large-particle fluidized beds, *Powder Technology*, **98**, 38-47 (1998)

Goldman A. J., R. G. Cox and H. Brenner
Slow viscous motion of a sphere parallel to a plan wall I. Motion through a quiescent fluid, *Chemical Engineering Science*, **22**, 637–651 (1967)

Greenwood J. A., H. Minshall and D. Tabor
Hysteresis losses in rolling and sliding friction, *Proceedings of the Royal Society of London A*, **259**, 480-507 (1960)

Guerin, E., P.Tchoreloff, B. Leclerc, D. Tanguy, M. Deleuil and G. Couarraze
Rheological characterization of pharmaceutical powders using tap testing, shear cell and mercury porosimeter, *International Journal of Pharmaceutics*, **189**, 91–103 (1999)

Hamaker H. C.
The London-Van der Waals attraction between spherical particles, *Physica IV*, **10**, 1059-1072 (1937)

Han X., C. Ghoroi, D. To, Y. Chen and R. N. Davé
Simultaneous micronization and surface modification for improvement of flow and dissolution of drug particles, *International Journal of Pharmaceutics*, **423**, 213-225 (2012)

Hersey J. A.
Ordered mixing: a new concept in powder mixing, *Powder Technology*, **11**, 41-44 (1975)

Hersey J. A.
Preparation properties ordered mixtures, *Australian Journal of Pharmaceutical Sciences*, **6**, 29-31 (1977)

Hassanour A., C. C. Kwan, B. H. Rahmanian, Y. L. Ding, S. J. Antony, X. D. Jia and M. Ghadiri
Effect of granulation scale-up on the strength of granules, *Powder Technology*, **189**, 304-312 (2009)

Hoffmann R.
DEM simulations of toner particles with an O(N log N) hierarchical tree code algorithm, *Granular Matter*, **8**, 151-157 (2006)

Honda H., K. Ono , T. Ishizaka, T. Matsuno and M. Katano
Surface modification of powders by the high speed impact treatment method, *Journal of the Society of Powder Technology Japan*, **24**, 593-599 (1987)

Honda H., T. Matsuno and M. Koishi
Preparation of composite and encapsulated powder particles by dry impact blending, *International Journal of Chemistry and Biotechnology*, **9**, 21 (1991)

Honda H., M. Kimura, F. Honda, T. Matsuno and M. Koishi
Preparation of monolayer particle coated powder by the dry impact blending process utilizing mechanochemical treatment, *Colloids and Surfaces A: Physicochemical and Engineering Aspects*, **82**, 117-128 (1994)

Honda H., M. Kimura, F. Honda, T. Matsuno and M. Koishi
Preparation of composite and encapsulated powder particles by dry impact blending, *Journal of the Society of Powder Technology Japan*, **25**, 597-602 (1998)

Ishizaka T., H. Honda, Y. Kikuchi, K. Ono, T. Katano and M. Koishi
Preparation drug diluent hybrid powder by dry processing, *Journal of Pharmacy and Pharmacology*, **41**, 361-368 (1989)

Iwasaki T., M. Satoh and T. Ito
Determination of optimum operating conditions based on energy requirement for particle coating in a dry process, *Powder Technology*, **123**, 105-113 (2001)

Jain, N., J. M. Ottino and R. M. Lueptow
An experimental study of the flowing granular layer in a rotating tumbler, *Physics of Fluid*, **14** 572–582 (2002)

Jallo, L. J., Y. Chen, J. Bowen, F. Etzler and R. N. Dave
Prediction of interparticle adhesion force from surface energy and surface roughness, *Journal of Adhesion Science and* Technology, **18**, 367–384 (2011)

Jiang Y., S. Matsusaka, H. Hiroaki and T. Yokoyama
Evaluation of Flowability of Composite Particles and Powder Mixtures by a Vibrating Capillary Method, *Journal of Chemical Engineering of Japan*, **39**, 14-21 (2006)

Kangwantrakool S. and K. Shinohara
Preparation of new WC-Co/TiC-Al_2O_3 composite materials with mechanically coated particles, *Journal of Chemical Engineering of Japan*, **34**, 1486-1492 (2001)

Kangwantrakool S. and K. Shinohara
Hot hardness of WC-Co/TiC-Al_2O_3 composite materials, *Journal of Chemical Engineering of Japan*, **35**, 893-899 (2002)

Kangwantrakool S. and K. Shinohara
Sintering behaviour of mechanically coated WC-Co/TiC-Al_2O_3 particles by high speed rotational impact blending, *International Journal of Refractory Metals & Hard Materials*, **21**, 171-182 (2003)

Kano J.
Ryushi houni yoru funtai simulaton ni kansuru kenkyu (in Japanese), Ph.D. Thesis, Doshisha University (1996)

Kano J., N. Chujo and F. Saito
A method for simulating three dimensional motion of balls under presence of powder in a tumbling mill, *Advanced powder technology*, **8**, 39-51 (1997)

Kano J., Q. Zhang, F. Saito, M. Baron and A. Nzihou
Synthesis of Hydroxyapatite with the Mechanochemical Treatment Products of PVC and CaO, *Process Safety and Environmental Protection*, **84**, 309-312 (2006)

Kawaguchi T., T. Tanaka and Y. Tsuji
Lagrangian simulation of Fluidized bed, *Transactions of the Japan Society of Mechanical Engineers. Series B,* **58**, 2119-2125 (1992)

Kawaguch T., A. Miyoshi, T. Tanaka and Y. Tsuji
Discrete particle simulation of Two-dimensional fluidized bed, *Powder Technology*, **77**, 79-87 (1993)

Kawashima N., K. Soetanto, K. Watanabe, K. Ono and T. Matsuno
The surface characteristics of the sintered body of hydroxyapatite-zirconia composite particles, *Colloid and Surface B: Biointerfaces*, **10**, 23-27 (1997)

Krupp H.
Particle adhesion theory and experiment, *Advances in Colloid and Interface Science*, **1**, 111-239 (1967)

Kuo H. P., P. C. Knight, D. J. Parker, Y. Tsuji, M. J. Adams and J. P. K. Seville
The Influence of DEM Simulation Parameters on the Particle Behaviour in a V-mixer, *Chemical Engineering Science*, **57**, 3621-3638 (2002)

Kwan C. C., Ding Y., Williams R. A. and Ghadiri M.
Effects of operating parameters of high shear granulator on the evolved properties and structure of calcium carbonate granules, *Particulate Systems Analysis*, Stratford-upon-Avon, U.K. (2005)

Lecoq O., L. Galet and A. Chamayou
High energy dry coating mixing: elements on velocities, temperatures and melting, *Advanced Powder Technology*, **22**, 184–189 (2011)

Lefebvre G., L. Galet and A. Chamayou
Dry coating of talc particles with fumed silica: Influence of the silica concentration on the wettability and dispersibility of the composite particles, *Powder Technology*, **208**, 372-377 (2011 a)

Lefebvre G., L. Galet and A. Chamayou
Dry coating of talc particles: Effect of material and process modifications on their wettability and Dispersibility, *American Institute of Chemical Engineers*, **57**, 79-86 (2011 b)

Lerk C. F., G. K. Bolhuis, A. J. Smallenbroek and K. Zuurman
Interaction of tablet disintegrants and magnesium stearate during mixing II: effect on dissolution rate, *Pharmaceutica Acta Helvetiae*, **57**, 282-286 (1982)

Lian G., C. Thornton and M. J. Adams
Discrete particle simulation of agglomerate impact coalescence, *Chemical Engineering Science*, **53**, 3381-3391 (1998)

Lindberg, N., M. Palsson, A. Pihl, A. Freeman, T. Freeman, H. Zetzener and G. Enstad
Flowability measurements of pharmaceutical powder mixtures with poor flow using five different techniques, *Drug Development and Industrial Pharmacy*, **30**, 785–791 (2004)

Liu D. and P.V. Kamat
Electrochemically active nanocrystalline SnO2 films. Surface modification with thiazine and oxazine dye aggregates, *Journal of The Electrochemical Society*, **142,** 835-839 (1995)

Lueptow R. M., A. Akonur and T. Shinbrot
PIV for granular flows, *Experiment and Fluid*, **28**, 183–186 (2000)

Masson S. and J. Martinez
Effect of particle mechanical properties on silo flow and stresses from distinct element simulations, *Powder Technology*, **109**, 164-178 (2000)

Matchett A. J., T. Yanagida, Y. Okudaira and S. Kobayashi
Vibrating powder beds: a comparison of experimental and Distinct Element method simulated data, *Powder Technology*, **107**, 13-30 (2000)

Mei R., H. Shang, J. F. Klausner and E. Kallman
A contact mode for the effect of particle coating on improving the flowability of cohesive powders, *Kona*, **15**, 132-141 (1997)

Mio H., A. Shimosaka, Y. Shirakawa and J. Hidaka
Cell optimization of fast contact detection in the discrete element method algorithm, *Advanced powder technology*, **18**, 441-453 (2007)

Mizukami K., T. Ito, S. Saeki, Q. Zhang, F. Saito and H. Ryu
Computer Simulation Study on the Interaction Between a PVC Model Molecule and Ca(OH)2 Excited Under Mechanical Force, *Chemical Engineering Research and Design*, **82**, 1112-1116 (2004)

Moreno R., M. Ghadiri and S.J. Antony
Impact fracture of composite and homogeneous nanoagglomerate, *Powder Technology*, **130**, 132-137 (2003)

Muguruma Y., T. Tanaka and Y. Tsuji
Numerical simulation of particulate flow with liquid bridge between particles (simulation of centrifugal tumbling granulator), *Powder Technology*, **109**, 49-57 (2000)

Mullarney M. P., L. E. Beach, R. N. Davé, B. A. Langdon, M. Polizzi and D. O. Blackwood
Applying dry powder coatings to pharmaceutical powders using a comil for improving powder flow and bulk density, *Powder Technology*, **212**, 397–402 (2011)

Müller D.
Techniques informatiques efficacies pour la simulation de milieux granulaires par des méthodes d'élément distincts, PhD Thesis, Ecole Polytechnique Fédérale de Lausanne, 1996

Mujumdar A., D. Wei, R. N. Davé., R. Pfeffer and C. Y. Wu
Improvement of humidity resistance of magnesium powder using dry particle coating, *Powder Technology*, **140**, 86-97 (2004)

Naito M., M. Yoshikawa, T. Tanaka and A. Kondo
Analysis powder composite process by mechanical method, *Kona*, **11**, 229-234 (1993)

Nase S. T., W. L. Vargas, A. A. Abatan and J. J. McCarthy
Discrete characterization tools for cohesive granular material, *Powder Technology*, **116**. 214–223 (2001)

Ng B. H., C. C. Kwan, Y.L. Ding, M. Ghadiri and X. F. Fan
Solid motion of calcium carbonate particles in a high shear mixer granulator: A comparison between dry and wet conditions, *Powder Technology*, **177**, 1-11 (2007)

Ng B. H., C. C. Kwan, Y.L. Ding, M. Ghadiri, X .F. Fan and D. J. Park
Granular flow fields in vertical high shear mixer granulators, *American Institute of Chemical Engineers*, **54**, 415-426 (2008)

Ng B. H., Y. L. Ding and M. Ghadiri
Modelling of dense and complex granular flow in high shear mixer granulator- A CFD approach, *Chemical Engineering Science*, **64**, 3622-3632 (2009)

Ouabbas Y., J. Dodds, L. Galet, A. Chamayou and M. Baron
Particle-particle coating in a cyclomix impact mixer, *Powder Technology*, **189**, 245-252 (2009 a)

Ouabbas Y., A. Chamayou, L. Galet, M. Baron, G. Thomas, P. Grosseau and B. Guilhot
Surface modification of silica particles by dry coating: characterization and powder ageing, *Powder Technology*, **190**, 200-209 (2009 b)

Otles S
Modification of surface properties of biopowders by dry particle coating, Ph.D. Thesis, Ecole des Mines d'Albi-Charmaux (2008)

Otles S., O. Lecoq and J. A. Dodds
Dry particle high coating of biopowders: An energy approach, *Powder Technology*, **208**, 378-382 (2011)

Pudasaini S. P., K. Hutter, S. S. Hsiau, S. C. Tai, Y. Wang and R. Katzenbach
Rapid Flow of Dry Granular Materials down Inclined Chutes Impinging on Rigid Walls, *Physics of Fluid*, **19**, 053302 – 053302 -17 (2007)

Pfeffer R., R. N. Dave , W.Dongguang and M. Ramlakhan
Synthesis of engineered particulates with tailored properties using dry particle coating, *Powder Technology*, **117**, 40-67 (2001)

Pieper W. and C. Mattern
Optimization of taste masking pharmaceutical compounds by hybridization technique, *Powder Handling and Processing*, **16**, 136-138 (2004)

Podzeck F. J. M. Newton and M. B. James
The influence of constant and changing relative humidity of the air on the auto adhesion force between pharmaceutical powder particles, *International Journal of Pharmaceutics*, **145**, 221-229 (1996)

Podczeck F., J. M. Newton and M. B. James
Variation in the adhesion force between a drug and carrier particles as a result of changes in the relative humidity of the air, *International Journal of Pharmaceutics*, **149**, 151-160 (1997)

Rahmanian N., M. Ghadiri and Y. L. Ding
Effect of scale operation on granule strength in high shear granulators, *Chemical Engineering Science*, **63**, 915-923 (2008 a)

Rahmanian N., M. Ghadiri, X. Jia and F. Stepanek
Characterisation of granule structure and strength made in a high shear granulator, *Powder Technology*, **192**,184-194 (2009)

Rahmanian N., A. Naji and M. Ghadiri
Effect of process parameters on granules properties produced in a high shear mixer, *Chemical Engineering Research and Design*, **89**, 512-518 (2011)

Ramlakhan M., C. Y. Wu, S. Watano, R. N. Dave and R. Pfeffer
Dry particle coating using magnetically assisted impaction coating: modification of surface properties and optimization of system and operating parameter, *Powder Technology*, **112**, 137-148 (2000)

Rapaport D.C.
The art of molecular dynamics simulation, *Chambridge University Press*, 2nd edition, (2004)

Seville J. P. K, U. Tuzun and R. Clift
Processing of particulate solids, Brian Blackie Academic & Professional (1997)

Singh R. K., A. Ata., J. F. Gerald, L. Rabinovich and W. Hendrickson
Dry coating method using magnetically assisted impaction in a randomly turbulent fluidized bed, *Kona*, **15**, 121-131 (1997)

Staniforth J. N.
Ordered mixing or spontaneous granulation?, *Powder Technology*, **45**, 73-77 (1985)

Sreejith P. S. and B. K. A. Ngoi
Dry machining: Machining of the future, *Journal of Materials Processing Technology*, **101**, 287-291 (2000)

Tabor D.
The mechanism of rolling friction, *Philosophical Magazine*, **43**, 1055-1059 (1952)

Tabor D.
The mechanism of rolling friction 2: The elastic range, *Proceedings of the Royal Society of London A,* **229**, 198-220 (1955)

Thiel W. J., L. T. Nguyen and P. L. Stephenson
Fluidized bed granulation of ordered powder mixture reduces the potential for ordered segregation, *Powder Technology*, **34**, 75-80 (1982)

Thijssen J. M.
Computational Physics, chapter Molecular dynamics simulations, *Cambridge University Press*, 175-241 (1999)

Thornton. C and K. K. Yin
Impact of elastic spheres with and without adhesion, *Powder Technology,* **65**, 153-156 (1991)

Thomas G., Y. Ouabbas, P. Grosseau, M. Baron, A. Chamayou and L. Galet
Modeling the mean interaction forces between powder particles. Application to silica gel-magnesium stearate mixtures, *Applied surface science*, **255**, 7500-7507 (2009)

Verlet L.
Computer experiments on classical fluid. I. thermodynamical properties of Lennard-Jones molecules, *Physical Review*, **159**, 98-103 (1967)

Vilela A., L. Concepcion, P. Accart, A. Chamayou, M. Baron and J.A. Dodds
Evolution of the mechanical resistance of powder-powder coating by modulated dry feed particle size analysis, *Particle and Particle System Characterization*, **23**,127-132 (2006)

Visser J.
Particle adhesion and removal, P*articulate Sciences and Technology*, **13**, 169-196 (1995)

Watanabe T., I. Ohno, N. Wakiyama, A. Kusai and M. Senna
Stabilization of amorphous indomethacine by co-grinding in a ternary mixture, *International Journal of Pharmaceutics*, **241**, 103-111 (2002)

Watanabe T., S. Hasegawa, N. Wakiyama, K. Akita and M. Senna
Comparison between polyvinylpyrrolidone and silica nanoparticles as carriers for indomethacine in a solid dispersion, *International Journal of Pharmaceutics*, **250**, 283-286 (2003)

Watano, S., R. Pfeffer, R.N. Davé and W. Dunphy
Dry particle coating by a newly developed rotating fluidized bed coater, *Advanced Technologies for Particle Processing: AIChE Conference,* **Vol. I**, 598-565, (1998)

Watano S., Y.Imada, K. Miyanami, C. Y. Wu, R. N. Davé, R. Pfeffer and T. Yoshida
Surface modification of food fiber by dry particle coating, *Journal of Chemical Engineering of Japan*, **33**, 848-854, (2000)

Yang J., A. Sliva, A. Banerjee, R. N. Davé and R. Pfeffer
Dry particle coating for improving the flowability of cohesive powders, *Powder Technology,* **158**, 21–33 (2005)

Yang R. Y., R. P. Zou and A.B. Yu
Microdynamic analysis of particle flow in a horizontal rotating drum, *Powder Technology*, **130**, 138-146 (2003)

Yeung C. C. and J. A. Hersey
Ordered powder mixing course fine particulate systems, *Powder Technology*, **22**, 127-131 (1977)

Yip C. W. and J. A. Hersey
Perfect powder mixtures, *Powder Technology*, **16**, 189-192 (1977)

Yokoyama, T., K. Urayama, M. Naito, M. Kato and T. Yokoyama
The Angmill Mechanofusion System and Its Applications, *Kona*, **5**, 59–68 (1987)

Yuu S., T. Umekage and Y. Johno
Numerical simulation of air and particle motions in bubbling fluidized bed of small particles, *Powder Technology*, **110**, 158-168 (2000)

Xu B. H. and A. B. Yu
Numerical simulation of the gas-solid flow in a fluidized bed by combining discrete particle method with computational fluid dynamics, *Chemical Engineering Science*, **52**, 2785-2809 (1997)

Zhou Q., L.Q. I. Larson, P. J. Stewart and D. A. V. Morton
Effect of mechanical dry particle coating on the improvement of powder flowability for lactose monohydrate: A model cohesive pharmaceutical powder, *Powder Technology*, **207**, 414-421 (2011)

Zhu K., R. B. H. Tan, W. K. Ng, S. Shen, Q. Zhou and P. W. S. Hang
Analysis of the influence of relative humidity on the moisture sorption of particles and the aerosolization process in a dry powder inhaler, *Journal of Aerosol Science,* **39**, 510-524 (2008)

Appendices

Appendix 1

Geometry of Cyclomix high shear mixer

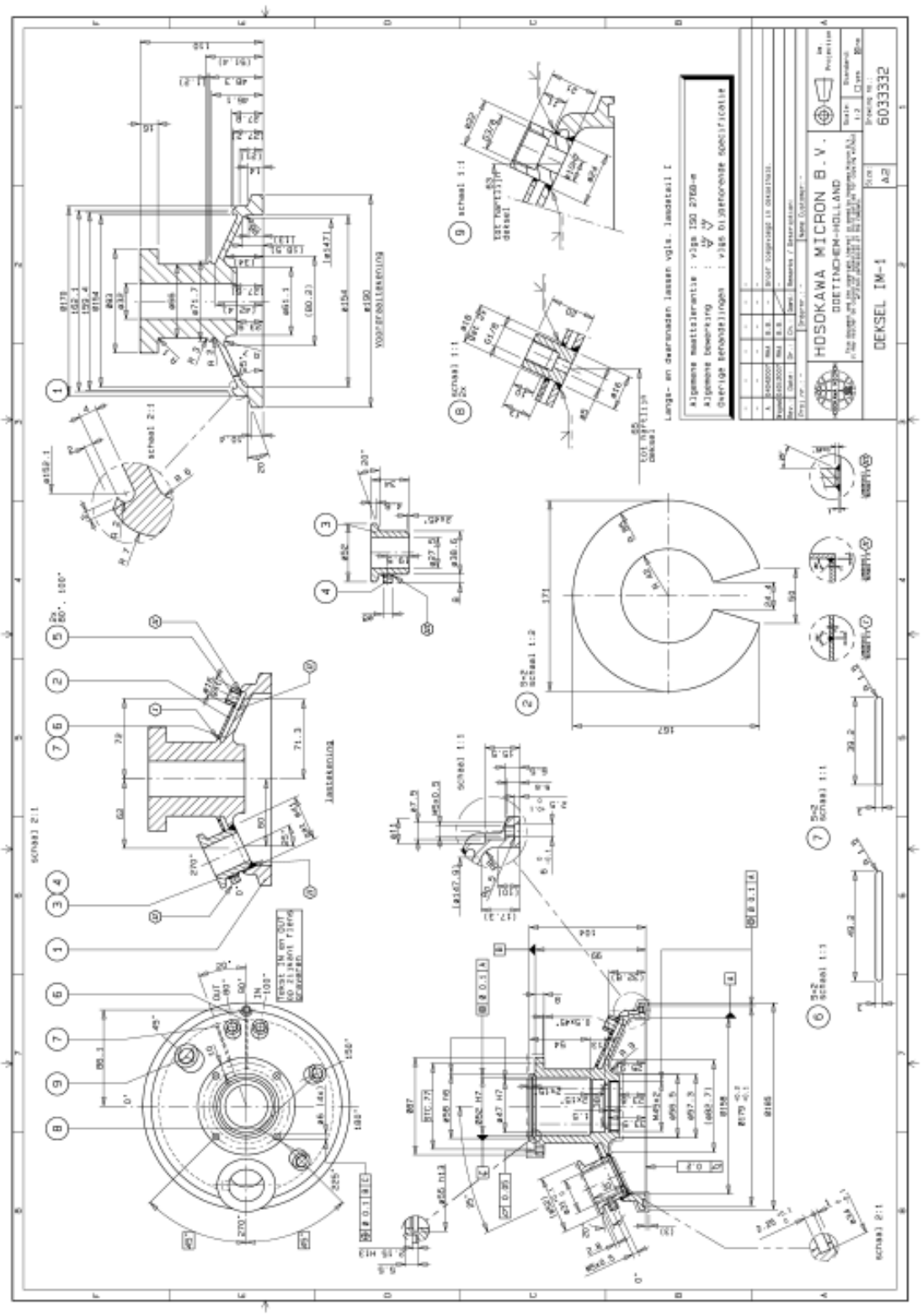

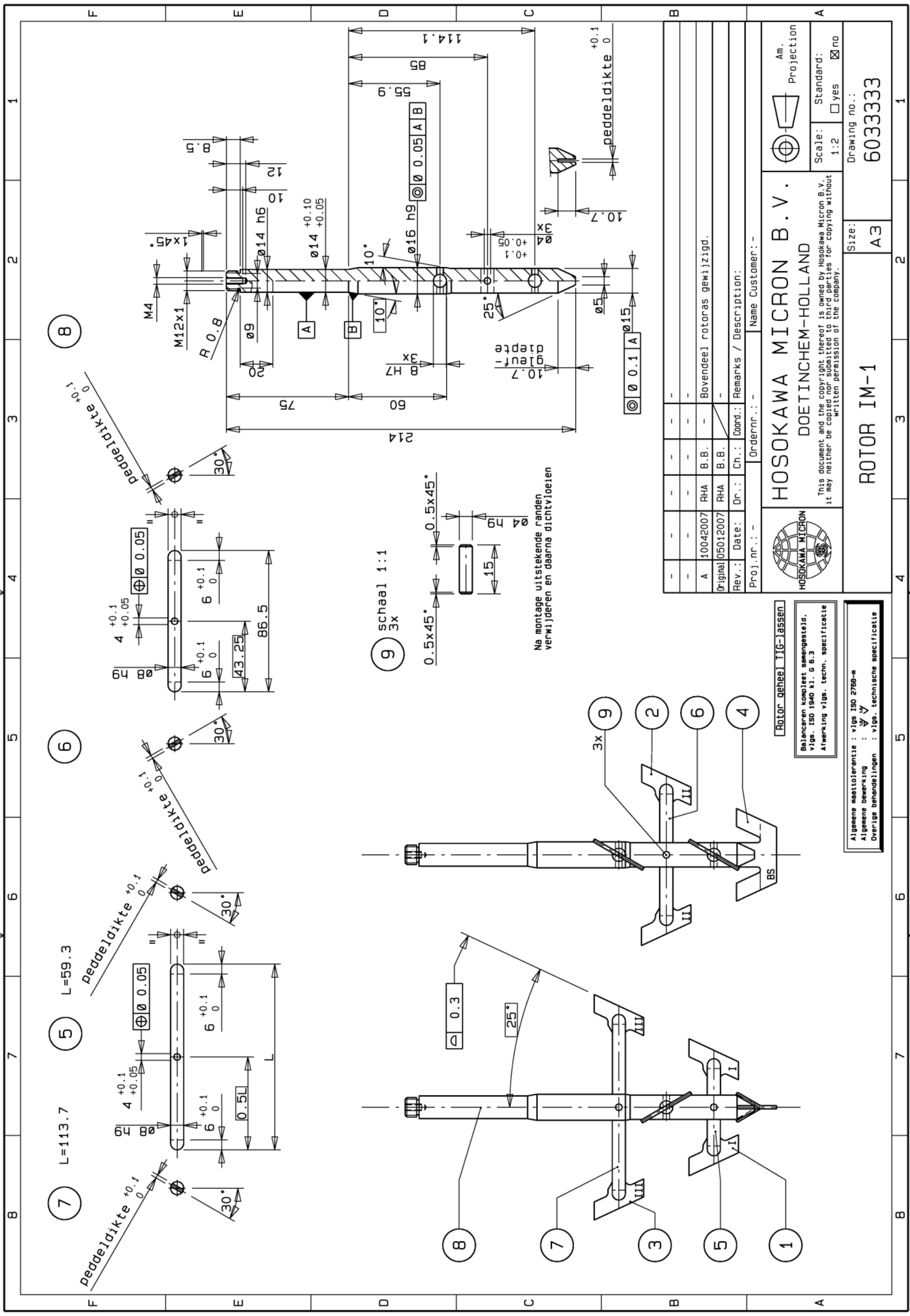
HOSOKAWA MICRON B.V.
DOETINCHEM-HOLLAND
ROTOR IM-1
Drawing no.: 6033333
Size: A3
Scale: 1:2
Rotor geheel TIG-lassen
schaal 1:1
Bovendeel rotoras gewijzigd.
peddeldikte
L=113.7
L=59.3

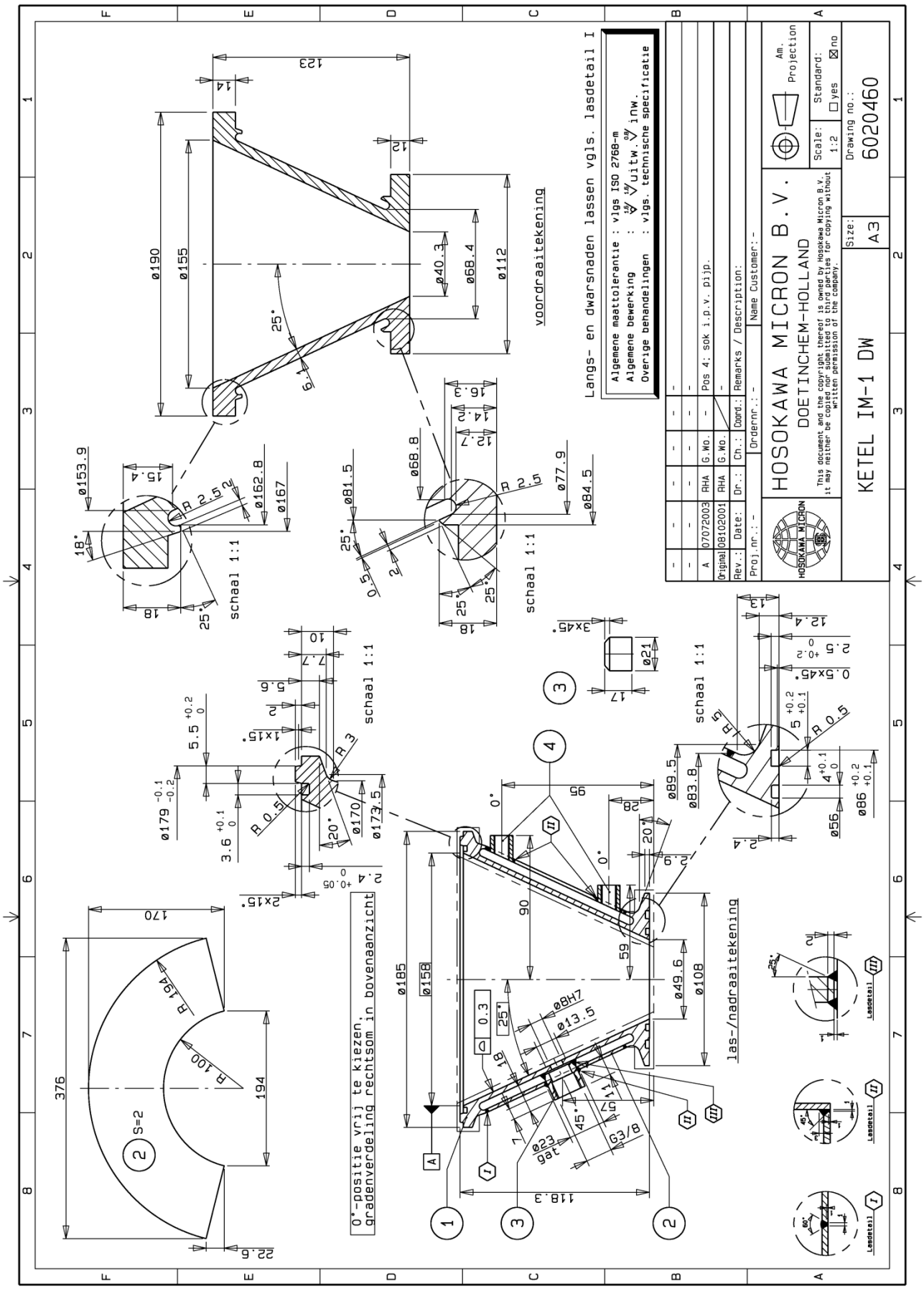
KETEL IM-1 DW
HOSOKAWA MICRON B.V.
DOETINCHEM-HOLLAND
Drawing no.: 6020460
Size: A3
Scale: 1:2
Standard: ☒no ☐yes
Am. Projection
Langs- en dwarsnaden lassen vgls. lasdetail I
Algemene maattolerantie : vlgs ISO 2768-m
Algemene bewerking : vlgs. technische specificatie
Overige behandelingen : vlgs. technische specificatie
voordraaitekening
schaal 1:1
0°-positie vrij te kiezen, gradenverdeling rechtsom in bovenaanzicht
las-/nadraaitekening
Lasdetail I
Lasdetail II
Lasdetail III

Appendix 2

Scanning Electronic Microscopy

SEM (Scanning Electronic Microsconsists) is composed of an electron column that creates a beam of electrons; a sample chamber, where the electron beam interacts with the sample; detectors, that monitor a variety of signals resulting from the beam–sample interaction; and a viewing system that constructs an image from the signal (**Fig. A 1**).

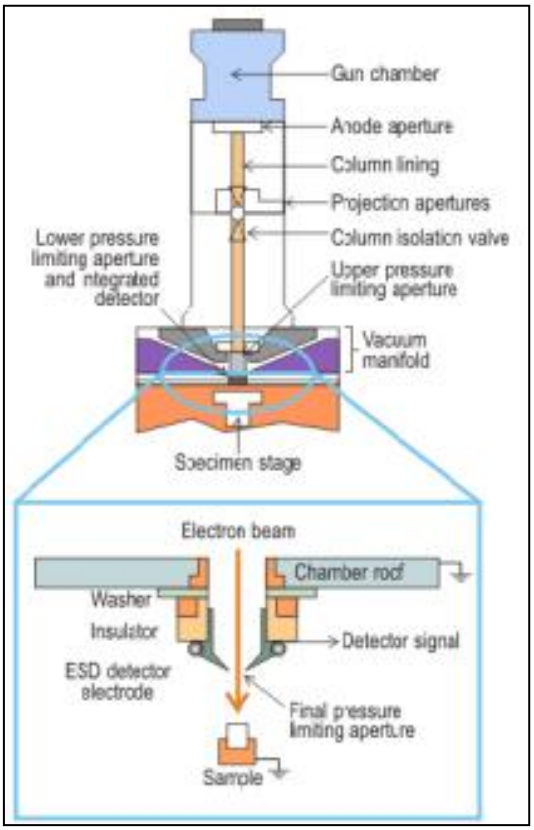

Fig. A. 1 Schematic diagram of SEM

An electron gun at the top of the column generates the electron beam. In the gun, an electrostatic field directs electrons, emitted from a very small region on the surface of an electrode, through a small spot called the crossover. The gun then accelerates the electrons down the column toward the sample with energies typically ranging from a few hundred to tens of thousands of electron volts.

The electrons emerge from the gun as a divergent beam. A series of magnetic lenses and apertures in the column finds and focuses the beam into a de-magnified image of the crossover. Near the bottom of the column a set of scan coils deflects the beam in a scanning

pattern over the sample surface. The final lens focuses the beam into the smallest possible spot on the sample surface.

The beam exits from the column into the sample chamber. The chamber incorporates a stage for manipulating the sample, a door for inserting and removing the sample and access ports for mounting various signal detectors and other accessories. As the beam electrons penetrate the sample, they give up energy, which is emitted from the sample in a variety of ways. There are two major ways of emission:

Secondary Electrons (SE) are sample atom electrons that have been ejected by interactions with the primary electrons of the beam. They generally have very low energy (by convention less than fifty electron volts). Because of their low energy they can escape only from a very shallow region at the sample surface. As a result they offer the best imaging resolution. Contrast in a secondary electron image comes primarily from sample topography. More of the volume of interaction is close to the sample surface, and therefore more secondary electrons can escape, for a point at the top of a peak than for a point at the bottom of a valley. Peaks are bright and valleys are dark. This makes the interpretation of secondary images very intuitive as they look the same as the corresponding visual image would look.

Backscattered Electrons (BSE) are primarily beam electrons that have been scattered back out of the sample by elastic collisions with the nuclei of sample atoms. They have high energy, ranging (by convention) from fifty electron volts up to the accelerating voltage of the beam. Their higher energy results in a larger specific volume of interaction and degrades the resolution of backscattered electron images. Contrast in backscattered images comes primarily from point to point differences in the average atomic number of the sample. High atomic number nuclei backscatter more electrons and create bright areas in the image. Backscattered images are not as easy to interpret, but properly interpreted, can provide important information about sample composition. Each emission mode is potentially a signal from which to create an image.

SEM also allows us to have elemental analysis or chemical characterization of a sample by **Energy dispersive X-ray spectrometer (EDX) technique**. As a type of spectroscopy, it

relies on the investigation of a sample through interactions between electromagnetic radiation and material analyzing x-rays emitted by the matter in response to being hit with charged particles. Its characterization capabilities are due in large part to the fundamental principle that each element has a unique atomic structure allowing x-rays that are characteristic of an element's atomic structure to be identified uniquely from each other.

Résume étendu

Etude numérique et expérimentale de l'enrobage en voie sèche dans un mélangeur à haut cisaillement

Résumé étendu de Thèse de Akira SATO [a,b]

Encadrants : SERRIS Eric[a], GROSSEAU Philippe[a], THOMAS Gérard[a*]
CHAMAYOU Alain[b], GALET Laurence[b], BARON Michel[b*]

[a]Ecole Nationale Supérieure des Mines de Saint Etienne
LPMG-FRE CNRS3312, 158 cours Fauriel, 42023 Saint-Etienne, France
[b]Ecole des Mines d'Albi Carmaux, Centre Rapsodee
FRE CNRS 3213, Université de Toulouse, Campus Jarlard, 81013 Albi, France

1. Introduction

L'enrobage en voie sèche est une technologie relativement nouvelle pour modifier des propriétés de particules. Dans un tel procédé, des petites particles (particules invitées) se collent sur la surface de particules plus grandes (particules hôtes) par des actions mécaniques comme des cisaillements et des forces d'impact. Il intéresse divers domaines industriels, car il n'utilise aucun solvant organique, et ce procédé économique est compatible avec les contraintes environnementales. Il y a de nombreuses publications sur la production de particules composites par l'enrobage (Alonso et al. 1989, Watano et al. 2000, Ouabbas et al. 2009a). Par contre, il y moins d'études trouvées sur l'optimisation du procédé (Iwasaki et al. 2002) et sur l'analyse de ce procédé de façon théorique (Thomas et al. 2009).

La méthode des éléments discrets (DEM) est une des méthodes numériques les plus utilisées pour analyser le comportement de particules solides. Elle a été appliquée dans de nombreux domaines avec succès(Clearly et al. 2002, Kano et al. 1997, Sato et al. 2010).

Le but de notre etude est de comprendre l'effet de paramètres du procédé d'enrobage (comme la durée d'opération, la vitesse de rotation et le taux de remplissage de produit dans le cyclomix) sur l'enrobage. Les analyses des propriétés des produits finaux, comme la coulabilité et la mouillabilité, l'estimation de la composition des produits et de l'écoulement des particules ont été effectuées. La simulation numérique a été

conduite par la DEM pour mieux comprendre les phénomènes apparaissant lors du mélangeage, afin d'optimiser le procédé.

2. Matériaux et méthode

2.1 Matériaux

Les matériaux choisis sont, pour les particules hôtes les Suglets, et pour les particules invitées le stéarate de magnésium (StMg). Les propriétés des deux matériaux sont montrées dans le Table 1. Les Suglets, produits de NP pharm (Colorcon INC.) sont des granules sphériques constitués principalement de sucre, avec une forte tendance hydrophile. Ce matériau est normalement utilisé en formulation comme excipient pour les capsules et les comprimés. Ces particules sont utilisées dans les technologies de contrôle et de libération de principe actif en pharmacie. Les Suglets sont cristallisées et sphériques. Le diamètre médian en volume, D_{50} vaut environ 250 μm. Pour les particules invitées, le stéarate de magnésium (StMg) a été choisi. Cette poudre est très cohésive et de nature hydrophobe, insoluble dans l'eau, et utilisée largement dans la formulation pharmaceutique comme lubrifiant. Le D_{50} vaut environ 5 μm.

Table 1. Propriétés des particules choisies

Matériaux	D_{50} [μm]	Masse volumique (pycnomètre Hélium) [kg/m3]	Attractivité /eau
Suglets	250	1580	hydrophile
StMg	5	1120	hydrophobe

2.2 Procédé d'enrobage

Le Cyclomix, un mélangeur à haut cisaillement fourni par la société Hosokawa Micron B.V., a été choisi pour effectuer l'enrobage en voie sèche. Cet appareil est essentiellement composé d'une chambre de mélange fixe, verticale et de forme conique,

équipée d'un axe tournant à grande vitesse ω, avec des pales se déplaçant le long de la paroi. Le Cyclomix a déjà été utilisé avec succès pour faire l'enrobage en voie sèche (Ouabbas et al. 2009b). Supposant que les particules invitées et hôtes ont des tailles homogènes, et que toutes les particules sont de forme sphérique, la fraction massique pour former une monocouche sur la surface des particules hôtes, *w* peut être obtenue par l'équation suivante avec le rapport de taille de particules hôte et invitée, K_H (Thomas et al. 2009) :

$$w = \frac{4C_{2D}(k_H + 1)^2}{4C_{2D}(k_H + 1)^2 + \frac{\rho_H}{\rho_I}{k_H}^3} \quad (1)$$

$$k_H = \frac{R_H}{R_I} \quad (2)$$

Où C_{2D} est la compacité surfacique (à 2 dimensions) de particules invitées sur la surface de particules hôtes, et ρ_H et ρ_I sont des masses volumiques des grains de particules hôtes et invitées, et R_H et R_I sont les rayons de particules hôtes et invitées. Nous supposons que C_{2D} est la compacité de la structure hexagonale à 2D, soit C_{2D}=0.906. Alors la fraction massique *w* pour une monocouche est estimée à 5.0 %. Pour observer l'effet des conditions opératoires, la fraction massique a été fixée à cette valeur. La vitesse de rotation ω varie de 250 à 1500 tr/min et la durée d'opération est de 30 s à 600 s. Le taux de remplissage J du Cyclomix (rapport du volume apparent de grains solides, introduits de façon non tassée dans l'appareil, au volume du Cyclomix) est de 20 à 60% (162 g – 486 g de Suglets).

Table 2. Conditions opératoires

Appareil	Vitesse de rotation [tr/min]	Durée d'opération [s]	Remplissage [%]	Fraction massique de StMg [%]
Cyclomix	250 – 1500	30 – 600	20 – 60	5

2.3 La coulabilité

Pour vérifier la modification de propriétés de surface, plusieurs techniques ont été utilisées. Le Freeman Technology Powder Rheometer (FT-4) a été choisi pour analyser la coulabilité des produits. Cet appareil peut mesurer l'indice de coulabilité (flow rate index (FRI)) qui présente des variations en sens contraire de la coulabilité de la poudre : Une valeur FRI élevée signifie que la poudre est très cohésive, très peu coulable.

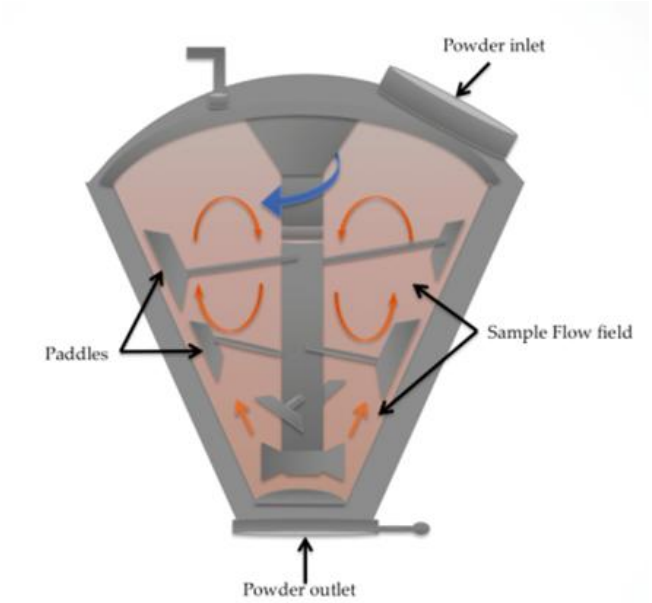

Figure 2. Schéma du Cyclomix, mélangeur à haut taux de cisaillement

2.4 La mouillabilité

Dans notre étude, une goutte d'eau de 10 µl a été déposée sur la surface du lit de poudres, et l'angle de contact a été mesuré après 30 s de dépôt d'une goutte. En plus, pour éviter de casser des particules enrobées, le lit de poudre n'a pas été compressé, mais juste déposé avec une spatule, et aplati à la spatule pour donner une surface de poudre plus homogène et la plus plate possible. La mesure de l'angle de contact a été effectuée trois fois sur chaque échantillon et la valeur moyenne a été utilisée.

2.5 Etude cinétique par l'estimation du rapport de conversion

Le tamisage de produit a été utilisé pour estimer la fraction massique de StMg enrobé après passage au mélangeur. Après le traitement d'enrobage, le mélange des trois types

de produits (StMg seul, Suglet seul, et Suglet enrobé) est passé au tamis de 160 µm pendant 10 min. Nous avons mesuré la masse *m* de particules passant le tamis : c'est celle des particules invitées ne se collant pas sur la surface des particules hôtes après l'enrobage, ou celles dont les forces d'adhésion ne seraient pas suffisamment grandes pour résister aux forces de cisaillement mises en jeu lors du tamisage (ce dernier cas est négligé). Une fois m connue, la fraction massique w_e du produit StMg après mélange restant sur la surface des particules hôtes peut être estimée en pourcentage par l'équation suivante :

$$w_e = \frac{m_{ini} - m}{M + m} \times 100 \quad (3)$$

Où w_e est la fraction massique du produit estimé, *M* est la masse de particules qui restent au-dessus du tamis, et m_{ini} est la masse de particules invitées introduites dans le mélangeur. La comparaison des valeurs w_e and w donne l'information sur le dégré d'efficacité du procédé d'enrobage. Plus précisément, le ratio λ peut être considéré comme le degré d'avancement de la réaction de création d'un mélange ordonné, ou encore le rapport d'enrobage (eq. (4)).

$$\lambda(t) = \frac{w_e}{w_0} \quad (4)$$

3. Modélisation du mouvement de particules dans le mélangeur par DEM

Pour observer l'écoulement des particules dans le Cyclomix, la modélisation DEM, développée par le Laboratoire du Professeur Saito (Saito et Kano) à l'université de Tohoku, Japon, a été appliquée dans notre étude. Au début, les particules hôtes ont été déposées dans le récipient symbolisant le bol du Cyclomix en couches successives de structure hexagonale. Pour obtenir le mouvement de particules réelles à la paroi du récipient de mélange, une caméra rapide avec un récipient transparent a été utilisée. Les particules choisies sont des grains de « Suglets » à base de saccharose, de 1 mm de diamètre (+- 100 µm). Les mouvements de particules sont filmés, et les caractéristiques des deux vecteurs, vitesse tangentielle et vitesse verticale, sont évaluées par PIV (Particle Image Velocimetry). Le PIV est une méthode optique qui mesure des

déplacements des particules entre deux images cinétiques et des champs des vitesses. Le logiciel PIV-Lab effectue ces mesures pour différentes positions des pales et à différents temps de mélange. Pour estimer l'efficacité de l'enrobage, plusieurs grandeurs peuvent être retenues, et comparées aux données expérimentales : la fréquence de collision, les énergies d'impacts, la distribution des forces de collision. La vitesse de rotation moyenne V_r, présentée dans l'équation eq.(5) et à la figure 3, entre autres, est aussi l'une des valeurs caractéristiques importantes calculée dans notre étude. C'est la vitesse moyennée sur toutes les particules hôtes *N*, lors de la trajectoire parcourue par un point de la surface d'une particule hôte pendant un temps de mélange *T* donné.

$$v_R = \frac{\sum_{i=1}^{N} r_i \cdot \varphi_i}{N \cdot T} \tag{5}$$

Où φ_i est l'angle angulaire de la particule *i pendant T*, r_i est rayon de particule *i* et *N* correspond au nombre de particules dans le mélangeur.

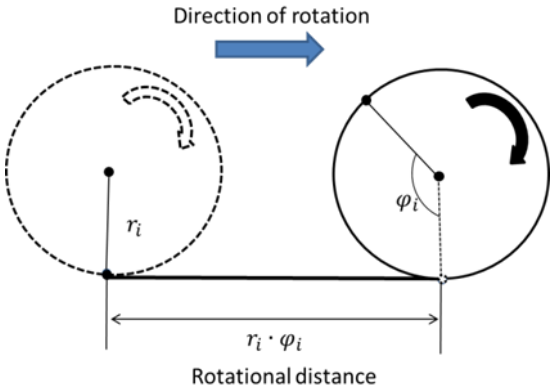

Figure 3. Distance de rotation : à gauche position initiale d'une particule, à droite position finale après un temps T de mélange.

4. Résultats expérimentaux

4.1 La coulabilité

La figure 4 (a,b) présente l'évolution de l'indice de coulabilité (FRI) à chaque remplissage à *J* = 20 % (a), 60 %. En général, le FRI diminue quand on augmente la durée d'opération, c'est à dire que la coulabilité des produits est améliorée quand la

durée d'opération augmente. Le FRI diminue plus vite avec des vitesses de rotation des pales plus élevées. Ceci peut être expliqué par le fait que le mélange, lors d'opérations à vitesse de rotation plus élevée reçoit beaucoup plus d'énergie mécanique, et les pales peuvent ainsi transmettre aux particules des vitesses plus grandes. En conséquent, les interactions entre particules hôtes et invitées sont plus nombreuses. L'enrobage a donc lieu plus rapidement. Comme l'écoulement des particules enrobées est meilleur que celui des particules hôtes, les courbes d'évolution du FRI varient davantage quand la vitesse de rotation augmente. Par ailleurs si nous examinons l'influence du taux de remplissage J, la différence des courbes entre J=20%, J=40 % et J=60 % est assez petite. L'effet du taux de remplissage ne semble pas majeur pour rechercher une amélioration de coulabilité.

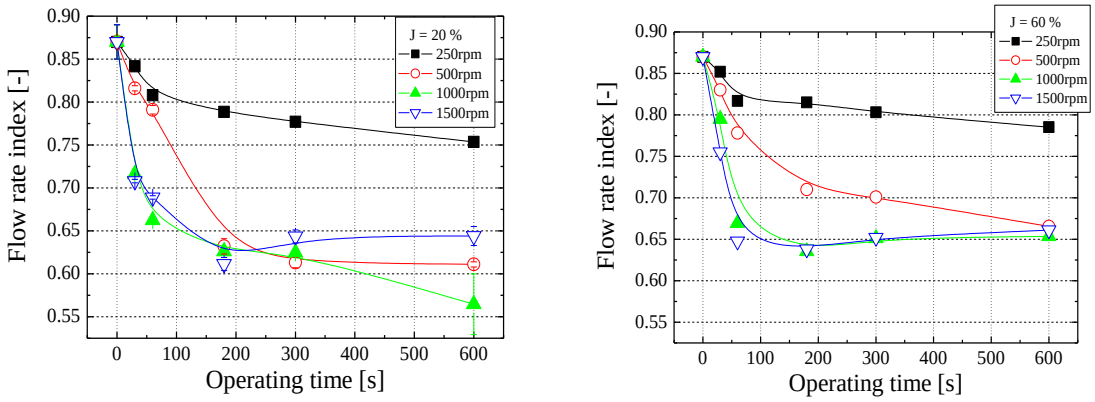

Figure 4. Fonctions Flow Rate index (FRI) versus la durée d'opération t, à différentes vitesses de rotation ω, ετ pour différents taux de remplissage (a) J = 20 %, (b) 60%.

4.2 La mouillabilité

La Figure 5 montre la variation de l'angle de contact des particules enrobées avec la durée d'opération t, à différentes vitesses de rotation ω, et taux de remplissage *J* = 20 % (a), et J=60 % (b).

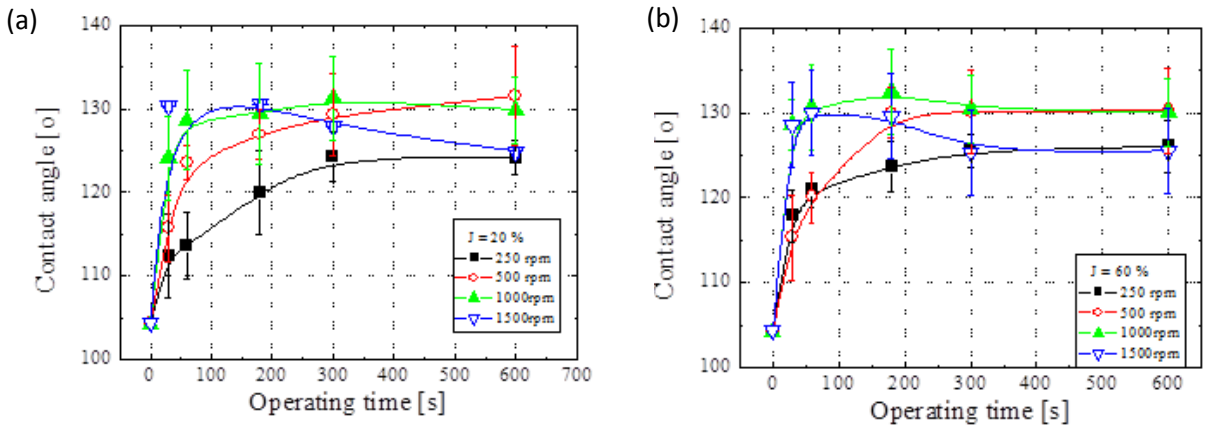

Figure 5. Influence de la durée d'opération t sur l'angle de contact eau-solide, à différentes vitesses de rotation ω, et pour différents taux de remplissage (a) J = 20 %, (b) 60%.

La valeur initiale montrée sur les figures ci-dessus a été calculée à partir de l'hypothèse suivante : on écrit que l'angle de contact θ de la particule enrobée après une durée de l'opération t est proportionnel à la fraction de surface (1-S_H) des particules invitées eq. (6)), quand les particules hôtes et invitées viennent d'être introduites (pas mélangées, ni enduites) initialement dans le système. Dans cette équation, nous allons prendre la valeur $\theta_H=0$ pour les particules très hydrophiles comme les Suglets.

La fraction de surface initiale S_{H0} est donnée par l'eq. (7):

$$\theta(t) = S_H \theta_H + (1 - S_H)\, \theta_I \qquad (6)$$

$$S_{H0} = \frac{{k_H}^2}{4C_{2D}(k_H + 1)^2 + {k_H}^2} \qquad (7)$$

Lorsque l'angle de contact d'une particule hôte θ_H et d'une particule invitée θ_I sont respectivement 0° et 132°, la valeur théorique dérivée de l'équation (6) donnant l'angle de contact pour le mélange initial θ(0) se trouve à 104°. Nous pouvons remarquer que l'état physique à t=0 correspond à un état où les deux types de grains sont présents sans aucun revêtement, avec une probabilité de rencontre avec la goutte liée à leur fraction surfacique.

Dans la Figure 5 (a), à 250 tr./min, l'angle de contact augmente en fonction du temps de traitement. D'après l'hypothèse ci-dessus, la fraction de surface du matériau revêtu va augmenter également. En d'autres termes, le processus de revêtement est fonction du temps de traitement; à 500 tr./min progresse plus rapidement qu'à 250 tr./min. À 1000

tr./min, θ (t) augmente avec le temps et est asymptotique à l' angle θ_I des particules invitées (132°). Dans figure 5 (b), on observe que ces courbes ont presque la même tendance générale que celle de la figure 5 (a) ainsi, l'angle de contact de produit n'est pas sensible au rapport de remplissage d'un mélangeur à haut cisaillement. Ces résultats ont été également confirmés pour J = 40%.

Pour résumer, tous les particules revêtues ont un angle de contact supérieur à 90 °, et la mouillabilité des particules enrobées va de l'hydrophile à l'hydrophobe même avec un petit temps de traitement et une plus basse vitesse de rotation du mélangeur. Concernant la mouillabilité, il est indiqué que ce mélangeur a une bonne efficacité pour les procédés de l'enrobage où le rapport de taille entre les particules hôtes et les particules invitées est suffisamment élevé pour que les forces de Van Der Waals soient suffisamment fortes pour bien enrober les particules invitées sur les particules hôtes.

4.3 Etude cinétique par l'estimation du taux de conversion λ

La figure 6 présente l'évolution de la fraction massique w estimée avec le temps d'opération. La fraction massique augmente avec la durée d'opération, et plus rapidement si la vitesse de rotation est plus élevée. L'influence du taux de remplissage n'est pas claire mais, à moindre remplissage, w augmente un peu plus vite. L'évolution w(t) apparait voisine de celle d'uneexponentielle.

En théorie,on peut supposer qu' elle devrait atteindre la fraction massique idéale (dans notre étude, c'est 5%), mais à cause de la perte de particules invitées qui peuvent se coller sur la paroi ou les lames du mélangeur, elle doit être asymptotique vers la fraction massique idéale. Donc, la fraction massique, $w_e(t)$ divisée par w_0 peut s'exprimer par :

$$\lambda(t) = \left[1 - \exp(-K_c t^{0.25})\right] \quad (8)$$

Où w_0 est la fraction massique idéale, et K_c est défini comme la constante du taux d'enrobage. Cette constante dépend des conditions opératoires : J et ω. Les courbes qui correspondent à eq. (8) sont présentées dans la figure 6. Les courbes sont bien en accord avec les points expérimentaux et tous les coefficients de corrélation R^2 sont supérieurs à 0.98. Donc le taux d'enrobage $\lambda = w_e/w_0$ peut bien s'exprimer par l'eq. (8). Il représente

l'avancement de la « réaction » d'enrobage. L'effet des paramètres opératoires (J, ω) sur l'enrobage peut être quantifié par K_c.

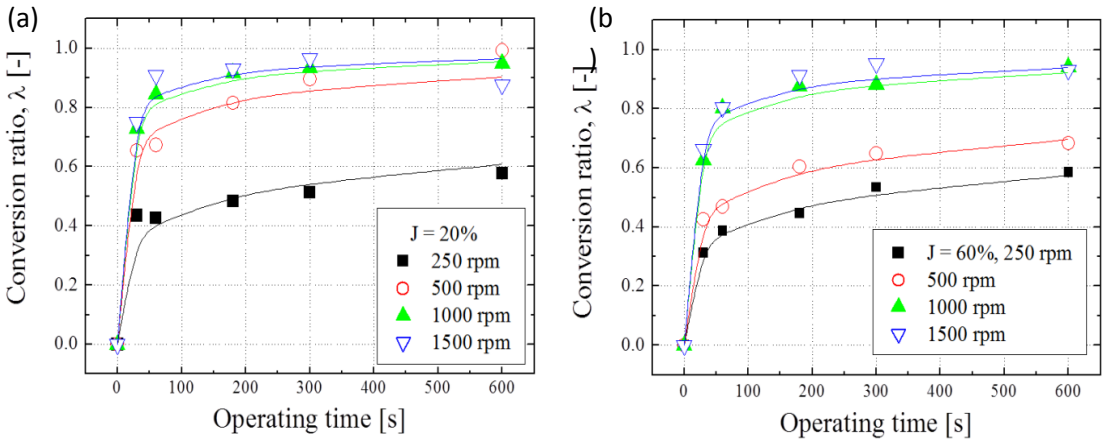

Figure 6 Courbes d'évolution du taux de conversion en fonction de la durée d'opération pour différents taux de remplissage J et différentes vitesses de rotation des pales : (a) J = 20 %, (b) J = 60 %

5 Résultats numériques

5.1 Comparaison de champs des vitesses réel et simulé

La Figure 7 montre des images extraites de films permettant de suivre les mouvements de particules simulés et ceux des « Suglets » à 250 rpm. Même s'il y a une différence de comportement autour des pales, les deux vues semblent cependant en assez bon accord. Ainsi, la validation de cette simulation permet d'envisager, dans un deuxième temps, l'étude de la simulation du comportement des mélanges réels, et de prédire la performance de l'enrobage, à des échelles plus grandes.

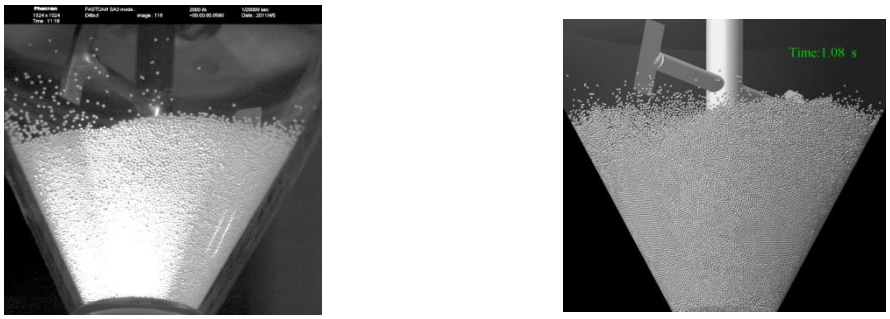

(a) (b)

Figure 7. Comparaison de mouvements de particules
(a) filmés avec un ensemble de grains de sucre « Suglets » de taille 1 mm,
(b) simulés avec des sphères mono-taille de 1 mm de diamètre
vitesse de rotation des pales ω= 250 rpm, taux de remplissage J= 20%, nombre de grains N= 200 000 grains.

La figure 8 montre la relation entre la vitesse moyenne obtenue pendant l'expérience et la simulation. La vitesse moyenne est définie comme la somme de toutes les vitesses obtenues par PIV divisée par le nombre d'éléments analysés. Concernant les vitesses moyennes horizontales (Figure 8 (a)), la valeur expérimentale montre une forte dépendance de vitesses sur l'angle des pales comme 90° et 270 ^{o}.

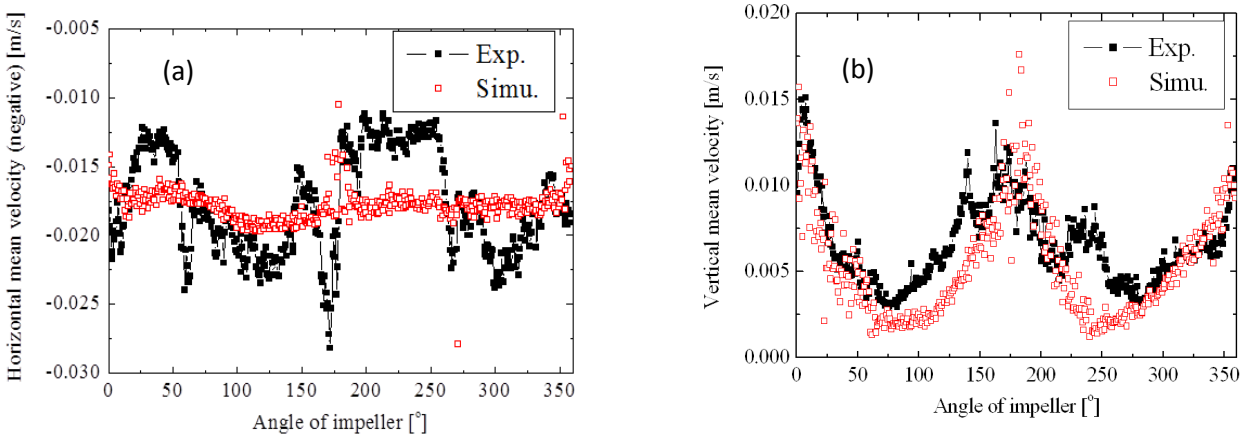

Figure 8 Variation des vitesses moyennes horizontales (a) ou verticales (b) obtenue pendant l'expérience et en simulation.

En revanche, la simulation montre peu de variations. Cela pourrait s'expliquer par le fait que des paramètres physiques des particules, comme le coefficient de restitution, le coefficient de frottement appliqué dans ce modèle peuvent être différents des valeurs réelles. Ainsi, les collisions entre les particules simulées et les pales étaient plus faibles que dans le système réel dans le sens horizontal. Toutefois, la simulation a permis de représenter certaines parties expérimentales. Pour la vitesse verticale moyenne (Figure 8 (b)), il est constaté que les deux méthodes sont fortement affectées par la position du rotor. Une corrélation étroite entre la simulation et l'expérience est observée. A partir de l'analyse de la vitesse moyenne, on peut dire que la simulation a une validité assez bonne pour donner les informations sur l'efficacité de l'enrobage en voie sèche dans un mélangeur à cisaillement élevé.

5.2 Simulation du mouvement de particules hôtes

La Figure 9 représente la vitesse normalisée des particules en couleur correspondant à chaque vitesse de rotation: (a) 100 tr./min, (b) 500 tr./min, (c) 1000 tr./min et (d) 3000 tr./min dans la section transversale. Dans la section transversale, à faible vitesse rotationnelle (100 tr. /min), le lit de poudres reste en dessous de la pale supérieure, et les particules qui sont proches de la pale ont une vitesse normalisée relativement élevée. A 500 tr./min, le lit de poudre atteint le sommet de la chambre, et à 1000 tr./min, la plupart des particules vont se déplacer sur la face supérieure. Enfin à 3000 tr./min, les particules

restent soit sur la partie supérieure ou sur la partie inférieure, et il y a peu de particules autour de la partie médiane de la chambre.

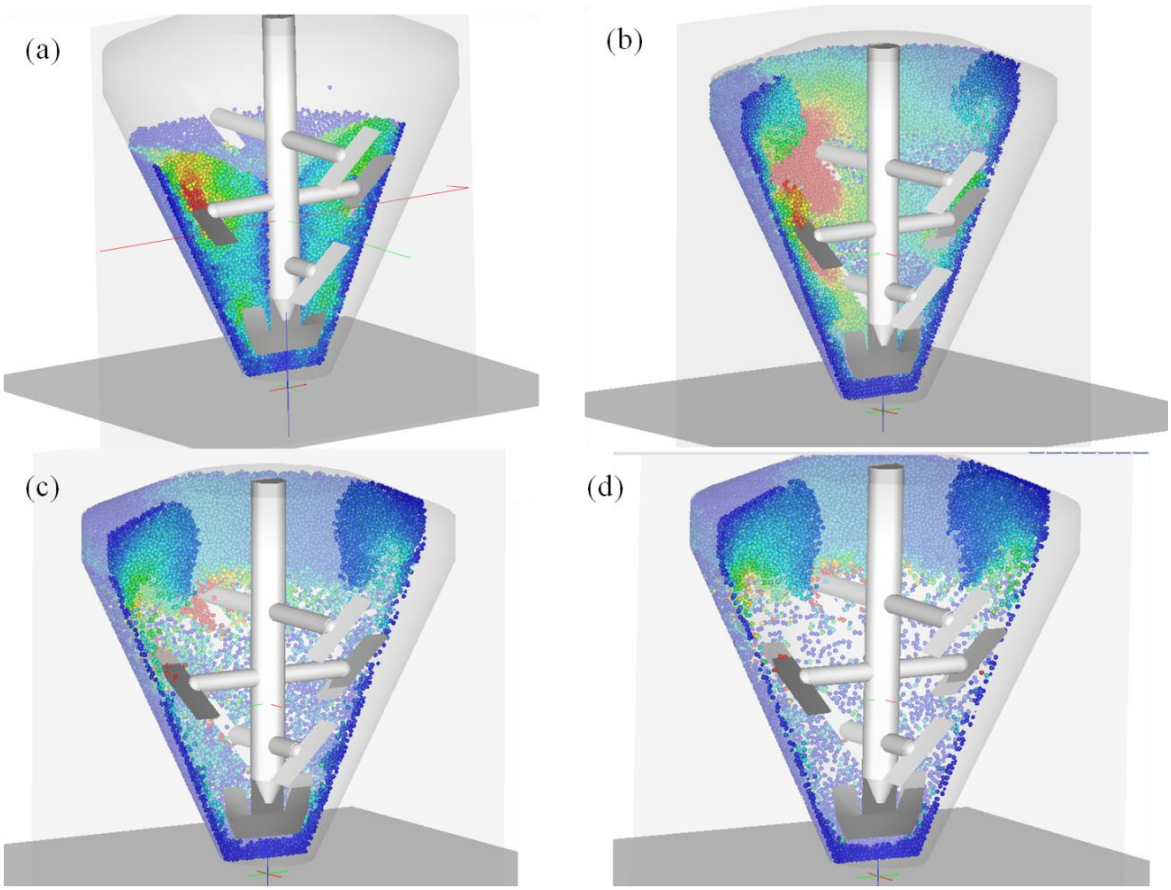

Figure 9 Vitesse normalisée des particules correspondant à chaque vitesse de rotation : (a) 100 tr. /min, (b) 500 tr. /min, (c) 1000 tr. /min et (d) 3000 tr. /min dans la section transversale.

5.3 Comparaison de la vitesse de rotation de particules et la constante du taux d'enrobage

La figure 10 montre la vitesse de rotation moyenne de particule calculée numériquement en fonction de la vitesse de rotation. La vitesse de rotation moyenne de particules augmente avec la vitesse de rotation et semble atteindre un palier. Un plus grand taux de remplissage diminue un peu la vitesse de rotation de particule. L'énergie fournie à chaque particule par le rotor semble diminuer lorsque le taux de remplissage augmente. En effet le nombre de particules est bien plus grand, et chacune des particules recevra moins d'énergie mécanique.

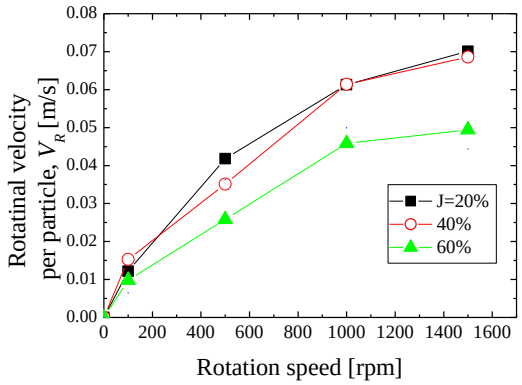

Figure 10 Vitesse de rotation moyenne en fonction de la vitesse de rotation

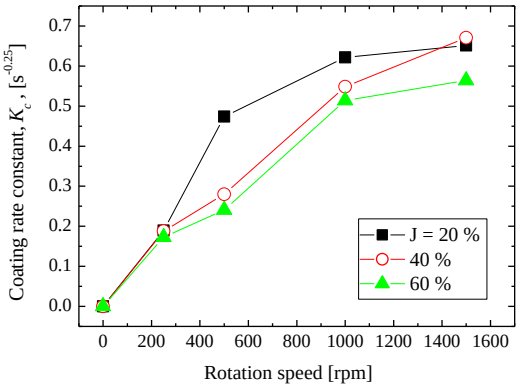

Figure 11 Constante de taux d'enrobage en fonction de la vitesse de rotation

La figure 11 présente la constante du taux d'enrobage K_c en fonction de la vitesse de rotation ω. La figure 10 représente le résultat de la simulation numérique et la figure 11 celui à partir de l'expérience. Les tendances sont très semblables. La figure 12 présente la relation entre la vitesse de rotation moyenne (calculée) et la constante du taux d'enrobage (évaluée à partir de l'expérience). Les points tracés dans la figure 12 peuvent être assez bien corrélés par une droite. Ce résultat, permet d'envisager la prédiction de la constante du taux d'enrobage par la simulation.

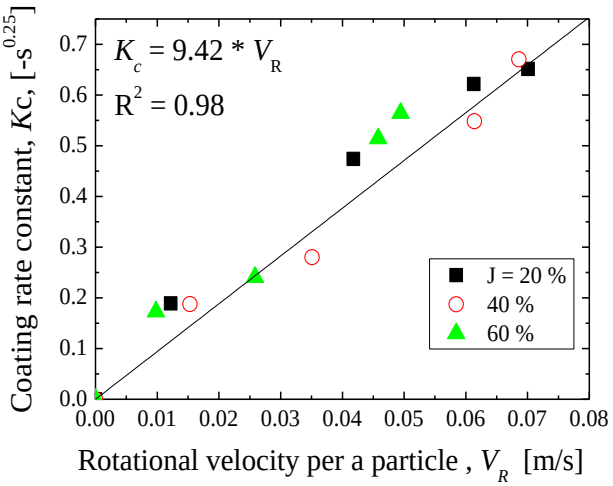

Figure 12 Relation entre la constante du taux d'enrobage et la vitesse de rotation moyenne de particule

6. Conclusion

L'analyse de l'effet des conditions opératoires sur l'enrobage utilisant des Suglets et des StMg comme les particules hôtes et invitées a été effectuée. La simulation de l'écoulement de particules dans le mélangeur a été réalisée par la DEM. En fonction de ces études, quelques points intéressants ont été trouvés.

(1) La coulabilité de produits est améliorée si on augmente la durée d'opération et la vitesse de rotation. Mais le taux de remplissage du mélangeur ne semble pas jouer sur la coulabilité.Le rendement pratique d'enrobage est donc meilleur avec un plus grand remplissage.

(2) Les évolutions des fractions massiques w estimées présentent des tendances très semblables en fonction de chacun des paramètres opératoires.Elles peuvent être approximées par des courbes exponentielles. La constante d'enrobage définie dans les représentations exponentielles, K_c peut être considérée comme une valeur caractéristique pour évaluer l'efficacité de l'enrobage.

(3) La simulation de l'écoulement dans le mélangeur autorise l'observation du mouvement de particules.

(4) La vitesse de rotation de particules et la constante du taux d'enrobage sont bien corrélées. La constante du taux d'enrobage peut être prévue par la simulation.

École Nationale Supérieure des Mines
de Saint-Étienne

NNT : 2012 EMSE 0658

Akira SATO

Numerical and experimental investigation of dry coating in a high shear mixer

Speciality: Chemical Engineering

Keywords: Dry coating, Mixing, Discrete Element Method, Flowability, Wettability, Conversion ratio, Coating rate constant, Cyclomix, Particle Image Velocimetry.

Abstract:

Investigations of the effect of the operating conditions on the dry coating and the motion of particles in a high shear mixer by the DEM simulation have been done. Big Suglets® and small Magnesium Stearate materials have been chosen for the dry coating process. The treatment has been carried out in a Cyclomix, a commercial high shear mixer, at different mixing time, rotational speeds, filling ratio of the samples and particle size ratio to observe the effect of the operating conditions on the dry coating. A conversion ratio has been introduced to quantify the degree of coating and measured thanks to an original sieving method. The properties of the products have been analyzed versus the conversion ratio. The flowability has been improved when increasing the operation time in the mixer. Higher speeds of rotation can improve the flowability more rapidly. However, the flowability doesn't seem to be sensitive to the filling ratio. The curves of conversion ratio versus time exhibit the same kind of variations for different operating conditions. It is possible to approximate this tendency by an exponential function in which a characteristic parameter "coating rate constant" is introduced, linked to the efficiency of the dry coating process, since the conversion ratio shows a linear relation with a flowability index and the wettability angle.

Simulation of the particle motion in the mixer has been carried out by a Discrete Element Method: different parameters characterizing the location, the velocities, and the attachment of the particles have been derived. The velocity fields of the real and simulated particle motions, compared by Particle Image Velocity (PIV), are quite similar, validating the DEM method and allowing the prediction of the coating process.

École Nationale Supérieure des Mines de Saint-Étienne

NNT : 2012 EMSE 0658

Akira SATO

Etude numérique et expérimentale de l'enrobage en voie sèche dans un mélangeur à fort taux de cisaillement

Spécialité: Génie des Procédés

Mots clefs : Enrobage à sec, Méthode par Eléments Discrets, Coulabilité, Mouillage, Taux de conversion, Mélange, Particle Image Velocimetry, Cyclomix.

Résumé :

Dans cette étude, l'intérêt est porté sur l'effet des conditions opératoires sur l'enrobage en voie sèche de grosses particules « hôtes » par de fines particules « invitées » et aussi sur la modélisation de cet enrobage selon la méthode par éléments discrets (DEM) afin de mieux comprendre les phénomènes mis en jeu. Dans ce travail, les matériaux choisis comme particules hôtes sont les Suglets® (des granules sphériques constituées principalement de sucre) et les particules invitées sont en stéarate de magnésium (StMg). Ces deux éléments sont introduits en poudre dans un mélangeur à fort taux de cisaillement, le Cyclomix. Les propriétés du produit final, comme la coulabilité, la mouillabilité et le degré d'avancement du revêtement, ont été caractérisés. La variation de l'indice de coulabilité est étudiée en fonction de la durée de traitement dans le Cyclomix pour diverses vitesses de rotation, taux de remplissage et rapport de taille de particules hôte et invitée. La coulabilité des produits a été améliorée en augmentant la durée du mélange ou la vitesse de rotation, tandis que le taux de remplissage de solide ne semble pas avoir d'importance. Le degré d'avancement présente une tendance semblable pour différentes conditions opératoires. Sa variation est représentée par une loi exponentielle empirique en fonction du temps de mélange, paramétrée par une constante de temps d'enrobage. Cette constante permet d'estimer l'efficacité de l'enrobage puisque le la coulabilité et la mouillabilité dépend linéairement du degré d'avancement.

La simulation des mouvements de particules dans le mélangeur par DEM a permis d'obtenir des informations sur la position, la vitesse des particules, et d'autres paramètres énergétiques, ainsi qu'une estimation du degré de mélange à tout instant.

Les champs de vitesse réelle ou numérique liés aux mouvements de particules, analysés par PIV (Particule Image Velocimetry), sont analogues. La constante d'enrobage dépend linéairement de la vitesse de rotation simulée et peut être ainsi prédite par DEM.